Gene expression analysis of the perinatal heart and the identification of miR-205 as a regulator of cardiomyocyte maturation

Jonathan Weldrick

A thesis submitted in partial fulfillment of the requirements for the
Doctorate in Philosophy degree in Cellular and Molecular Medicine

Cellular and Molecular Medicine
Faculty of Medicine
University of Ottawa

Abstract

Background:

Extensive research has characterized the embryonic development of a four-chambered heart in mammals. After birth, mammalian cardiomyocytes undergo a transition characterized by a final cell cycle with nuclear division (karyokinesis) in the absence of cytoplasmic division (cytokinesis), generating mature binucleated cardiomyocytes. Downregulation of pro-proliferative signaling and epigenetic changes permanently 'lock' cardiomyocytes out of the cell cycle, and nearly all subsequent growth is accomplished via cellular hypertrophy. Before this transition, cardiomyocytes exhibit robust proliferative potential, but afterward are unable to divide.

Rationale & Hypothesis:

Recent evidence suggests that non-coding RNAs influence early neonatal cardiac development and hypertrophy. **We hypothesize that transient expression of regulatory miRNAs may impact the neonatal heart's transition from proliferation to hypertrophy.**

Results:

Cardiac mRNA and miRNA were systematically analyzed using microarrays to identify targets that were transiently and significantly changing after birth. Through our analysis we identified three primary ontogenies significantly changing: metabolism, extracellular matrix remodeling, and cell cycle regulation.

Global analysis of micro-RNA expression patterns during perinatal heart development identified miR-205 as a novel candidate for modulating cardiomyocyte maturation. We observed miR-205 expression undergoing a 20-fold increase from 1-day

postpartum (1D) to 5D, returning to prenatal levels by 10D. It is expressed in cardiomyocytes of the epicardium, the primary location of fetal cardiomyocyte proliferation. MiR-205 targets two important cell cycle regulators: Pten phosphatase of the PI3K/AKT pathway, and Yap1 in the Hippo pathway. Both pathways have proven to be essential for proper heart development. Previous research showed that germline deletion of miR-205 results in death at 5D.

To define its role in the heart, we generated an αMHC-Cre postnatal miR-205 cardiac-specific deletion mouse model. Systematic characterization of miR-205-/- hearts confirmed miR-205's interaction with Pten and Yap1 by western blot and immunohistochemistry. Postnatal miR-205$^{-/-}$ hearts exhibit Hippo pathway dysregulation, increased cardiomyocyte number, more actively cycling cardiomyocytes beyond 7D, and no difference in binucleation.

We also generated a DOX-inducible cardiac-specific miR-205 over-expression mouse model. Perinatal miR-205^{OE} hearts expedited the transitional period, with more cardiomyocytes present at 5D and no difference at 14D. These hearts show increased Hippo signaling immediately after birth, suggesting compensatory mechanisms to ensure sufficient cardiomyocyte number.

Conclusions:

Our data strongly supports miR-205 as a regulator of cardiomyocyte maturation in the neonatal heart, by promoting the neonatal cardiomyocyte transition from hyperplastic to hypertrophic growth. In turn, miR-205's antiproliferative properties originate in part from suppressing the expression of Pten and Yap1.

Acknowledgements

First and foremost, I would also like to acknowledge my co-supervisor, Dr. Lynn Megeney, for providing me with lab space and resources to finish my doctoral project. Your guidance and feedback have proven invaluable to improving my thesis and scientific writing ability.

I would also like to acknowledge my co-supervisor, Dr. Patrick Burgon, for his mentorship throughout my graduate studies. You taught me how to think, plan, and analyze as a scientist. Your guidance has shown me what it means to be a researcher, and how to navigate the world of science.

A special thank you to my Thesis Advisory Committee members: Dr. Jeff Dilworth, Dr. Balwant Tuana, and Dr. Lynn Megeney. The feedback and support provided by this committee was critical for the development and execution of my research project.

I would also like to acknowledge the funding I received from the University of Ottawa Heart Institute Foundation and the Queen Elizabeth II Graduate Scholarship in Science and Technology (QEII-GSST).

I have fond memories of all my fellow lab members over the years: Fawaz Saleh, Dr. Marie-Elodie Cattin, Cassandra Roeske, Anastasia Pimenova, Esther Mak-Washburn, Natasha Bush, Amy Mullin, Natasha Kasulis, Gayashan Tennakoon, Christie Patterson, Shan Dhaliwal, Rishi Gupta, and Zach Verret-Borsos. A special thank you to Esther, Rishi, and Shan for being great friends both in and outside of the lab.

A special acknowledgement must be made for the most important person in my life: Katelynn Rowe. You are the smartest, kindest, and most talented person I have ever

met. I owe more to you than can be said in words. Through my most triumphant moments to my darkest days, you have been by my side helping me navigate through this stage of life. Without you, this would not have been possible. I am truly thankful for everything you have done for me, Colby, Jack, and Lil Miss.

Finally, I would like to thank my friends and family for their love and support. In particular, my mother has been so supportive of me and I could not have done any of this without her.

Table of Contents

Legend

Ago - Argonaute
ANOVA - Analysis of Variance
ASD - Atrial-septal defects
AT - Annealing temperature
AV - Atrioventricular
AVC - Atrioventricular canal
bHLH - Basic helix-loop-helix
Bmp - Bone morphogenic protein
BNP - B-type natriuretic peptide
BP - Base-pair
BSA - Bovine serum albumin
Bvht – Braveheart
β-TrCP – F-box/WD repeat-containing protein 1A
CAF- Cancer-associated fibroblast
CAK - CDK-activating kinase
Camk2d - Calmodulin kinase II-delta
CDK - Cyclin-dependent kinase
CDKI - Cyclin-dependent kinase inhibitor
Chek1 - Checkpoint kinase 1
CM - Cardiomyocyte
CPC - Cardiogenic precursor cell
CREB – cAMP response element-binding protein
Cx - Connexin
DAPI - 4′,6-diamidino-2-phenylindole
DGCR8 - DiGeorge syndrome critical region 8
DNA - Deoxyribonucleic acid
DOX - Doxycycline hyclate
ECM - Extracellular matrix
EDTA - Ethylenediaminetetraacetic acid
EMT - Endothelial-to-mesenchymal
FACS - Flow-assisted cell sorting
FBS - Fetal bovine serum
FDR - False discovery rate
Fendrr - FOXF1 adjacent non-coding developmental regulatory RNA
FGF - Fibroblast growth factor
FHF - First heart field
FIJI - Fiji is just ImageJ
FOG-2 - Friend of GATA 2
GFP - Green fluorescent protein
GO – Gene Ontology
Hdac - Histone deacetylase
Hey2 - Hairy/enhancer-of-split related with YRPW
HUVEC – Human Umbilical vein endothelial cells
IAP - Inhibitor of apoptosis
IDT - Integrated DNA Technologies
IRF – Interferon regulatory factor
Isl1 - Islet1
Klf4 - Kruppel-like factor 4
lncRNA - Long non-coding RNA
LV - Left ventricle
MAPK - p38 mitogen-activated protein kinase
Mef2 - Myocyte enhancer factor
Mesp1 - Mesoderm posterior 1
MHC - Myosin heavy chain
miRNA - Micro-RNA
MMP - Matrix metalleoproteinase
mRNA - Messenger RNA
mTORC - Mammalian target of rapamycin complex
Myh - Myosin heavy chain
ncRNA - Non-coding RNA
NEB - New England Biolabs
Nkx2-5 - NK Homeodomain 2-5
Nppa - Atrial natriuretic factor
Nrg1 - Neuregulin-1
NTC - No-template control
OCT - Optimal cutting temperature
PFA - Paraformaldehyde
pH3 - Phospho-histone 3
PIP3 – phosphatidylinositol-(3,4,5)-triphosphate
piRNA - PIWI-interacting RNA
PKB - Protein kinase B
Pln - Phospholamban
PRC1 - Protein regulator of cytokinesis 1
Pre-miRNA - Precursor micro-RNA
Pri-miRNA - Primary micro-RNA

PTEN - Phosphate and tensin homologue
PVDF - Polyvinylidene difluoride
QEII-GSST - Queen Elizabeth II Graduate Scholarship in Science and Technology
Rb - Retinoblastoma protein
RCF - Relative centrifugal force
RISC - RNA-induced silencing complex
RMA - Robust multi-array average
RNA - Ribonucleic acid
Robo - Roundabout receptor
ROS – Reactive Oxygen Species
ROS: Reactive oxygen species
rRNA - Ribosomal RNA
RT-PCR - Real-time polymerase chain reaction
rtTA - reverse tetracycline transactivator
SAP - SAF-A/B, Acinus, and PIAS\
SDS - Sodium Dodecyl Sulphate
SDS-PAGE - SDS polyacrylamide electrophoresis
SHF - Second heart field
Slit2/3 - Slit homolog 2 and 3
Smpx - Chisel gene
snoRNA - Small nucleolar RNA
SNP - Single nucleotide polymorphism
SRF - Serum response factor
TAC - Transverse aortic constriction
TBS - Tris-buffered saline
TBST - Tris-buffered saline + Tween 20
Tbx - T-box protein family
TCAG - The Center of Applied Genomics
tetO - Tetracycline-ON
tRNA - Transfer RNA
UCSC - University of California Santa Cruz
Uph - Upperhand
UTR - Untranslated Region
VEGF - Vascular endothelial growth factor
VSD - Ventricular-septal defects
WGA - Wheat germ agglutinin
YAP - Yes-associated protein

List of Figures

List of Tables

Chapter 1: Introduction

Understanding the mechanisms that are responsible for cardiac development, regeneration, and disease is an extremely important area of research, as heart disease is one of the most common morbidities and accounts for the most years of life lost worldwide (Lozano et al., 2012). Embryonic development of the heart has been well-studied, with high-resolution day-by-day analysis performed to determine which transcription factors regulate cell-type specification, migration, and differentiation (Bruneau, 2002). After birth, cardiomyocytes permanently exit the cell cycle and the heart primarily grows via hypertrophy of cardiomyocytes. Another primary focus of cardiac research has been to identify potential mechanisms to repair cardiac damage, whether congenital or acquired. This has been problematic due to the remarkable anti-proliferative properties of adult cardiomyocytes (Pasumarthi and Field, 2002). Although significant effort has been devoted to unraveling embryonic heart development and differentiation, how cardiomyocytes transition from a pliable fetal state to fully differentiated adult cells remains poorly understood. This chapter will briefly outline the transcriptional regulation of embryonic heart development and morphogenesis. The perinatal cardiac transition period and the role of non-coding RNAs in regulating cardiomyocyte proliferative capacity will also be discussed.

1.1 Embryonic heart development

The heart is the first organ to form and develop in vertebrates (Zaffran and Frasch, 2002). Embryonic morphogenesis begins with two heart fields: the first of which forms the cardiac crescent and gives rise to the left ventricle, and the second field which gives rise to the right ventricle and atria. The second heart field also contains a number of progenitor cells responsible for continuous proliferation and early cardiac function (Buckingham et al., 2005). The next developmental step is the formation of the heart tube, which elongates by addition of cells from highly divisible progenitor cells adjacent to the heart tube. The second heart field continues to proliferate throughout development and contributes to final heart muscle cell or cardiomyocyte number (Ivanovitch et al., 2017). Lineage tracing covering each stage of heart development showed that both heart fields contribute to heart morphogenesis (Van Vliet et al., 2012). In the heart, the complex interactions of Nkx2-5, Gata4/6, Tbx20, Mef2c, and many other genes have been shown to play critical regulatory roles controlling cardiomyocyte specification and morphogenesis (Bruneau, 2002).

1.1.1 Specification of cardiac progenitors

Mesoderm posterior 1 (*Mesp1*) is a basic helix-loop-helix (bHLH) transcription factor involved in the earliest movements from the primitive streak during gastrulation (Bondue et al., 2008; Saga et al., 2000). *Mesp1* and its homologue *Mesp2* contain the same bHLH motif, and are core components of the embryonic cardiac transcription factor network. The expression of *Mesp1* and *Mesp2* are considered the earliest markers of cardiogenic specification in embryonic development (Kitajima et al., 2000). A subset of

the first cell population expressing *Mesp1* goes on to establish the first heart field (FHF) and the cardiac crescent (Brade et al., 2013; Devine et al., 2014). The FHF proliferates and differentiates first to form the linear heart tube, while a second wave of *Mesp1* expression occurs in the second heart field (SHF) (Buckingham et al., 2005). While the FHF is developing into the linear heart tube, the SHF remains dormant nearby (Buckingham et al., 2005). After the heart tube has been established, the SHF proliferates and differentiates to elongate the heart tube. These SHF progenitors will give rise to the cells that form the right ventricle, inflow/outflow tracts, and the atria (Mjaatvedt et al., 2001; Waldo et al., 2001). The FHF primarily gives rise to the left ventricle with a small contribution to the atria (Brade et al., 2013). Deletion of *Mesp1* has been shown to result in aberrant cardiac development and cardia bifida (Saga et al., 1999). Cardia bifida is the failure of myocardial cells to form a single heart tube from the two heart fields (Compernolle et al., 2003). Double deletion of *Mesp1* and *Mesp2* results in a complete lack of migration and differentiation of cardiomyocytes and other caudal embryonic structures (Kitajima et al., 2000; Saga et al., 1999). These results demonstrate that *Mesp1* and *Mesp2* are essential for early embryonic cardiogenomic specification, proliferation, and differentiation.

The canonical *Wnt/β-catenin* signaling pathway has also been shown to be required for regulation of cell fate specification, proliferation, and differentiation as the embryo develops. This pathway possesses a biphasic role; early in embryogenesis *β-catenin* promotes cardiogenic specification, while later *Wnt1* and *Wnt3a* are secreted from the neural plate to repress cardiogenesis in surrounding tissue and maintain the boundaries of the pre-cardiac mesoderm (Marvin et al., 2001; Schneider and Mercola,

2001; Tzahor and Lassar, 2001; Ueno et al., 2007). The *Wnt* pathway inhibitor Dkk-1 is expressed in the underlying endoderm to counteract the inhibitory *Wnt* signaling (Marvin et al., 2001). Ablation of *β-catenin* signaling results in embryonic death around day 9 due to defects of the right ventricle and outflow tract (Ai et al., 2007; Cohen et al., 2007; Tzahor, 2007). Conversely, constitutively active *β-catenin* signaling resulted in expansion of SHF progenitors which accumulated in the right ventricle and outflow tract (Qyang et al., 2007). Activation of *Wnt/β-catenin* signaling promotes *Isl1* expression (Lin 2007), resulting in increased *Fgf*-family expression (Cohen et al., 2007). In progenitors where *Isl1* is downregulated, *Wnt* signaling inhibits cardiogenesis to promote differentiation (Tzahor, 2007). *Wnt* has also been shown to induce expression of the homeodomain transcription factor *Hex*, which can regulate *Nkx2-5* and *Tbx5* (Foley and Mercola, 2005).

1.1.2 Formation of the linear heart tube and heart looping

After cardiac specification, cardiomyocyte progenitors begin to migrate and rearrange to form the linear heart tube (Ivanovitch et al., 2017). After *Mesp1*, the FHF begins expressing T-box protein family 5 (*Tbx5*) and the NK Homeodomain 2-5 (*Nkx2-5*) proteins (E.G. et al., 2002; Ogura, 2007). *Tbx5* is required for development of the posterior heart, as well as atrial and left ventricular precursors (Bruneau et al., 2001; Ogura, 2007). The SHF begins to express LIM-family homeodomain transcription factor Islet1 (*Isl1*) (Cai et al., 2003). *Isl1*$^{+}$ progenitor cells eventually differentiate into cardiomyocytes and smooth muscle cells of the aorta and pulmonary artery (Moretti et al., 2006). The second heart field also transiently expresses *Prdm1*, *Pitx2*, *Six1*, *Fgf8*, and *Fgf10* before the addition of SHF progenitors to the linear heart tube begins (Kelly, 2012; Vincent et al., 2014; Zaffran et al., 2004). Once this process is initiated, this cohort of genes are downregulated

and the SHF begins expressing *Nkx2-5*, *Gata4*, and *Mef2c* (Verzi et al., 2005; Waldo et al., 2001). Interestingly, these three transcription factors have proven to be the minimum requirement to induce cardiac differentiation from fibroblasts (Ieda et al., 2010; Qian et al., 2012).

Nkx2-5 and *Gata4* are widely expressed throughout the heart tube, while the *Tbx* transcription factors are expressed in specific regions (Hoogaars et al., 2007; Rana et al., 2013). *Nkx2-5* is a transcription factor required for the specification and differentiation of cardiomyocytes by establishing a ventricular gene expression program (Watanabe et al., 2012). *Nkx2-5* is highly conserved in chordates, with the homologous *Nk2*-homeobox containing transcription factor, *tinman*, first being discovered in Drosophila (Azpiazu and Frasch, 1993; Bodmer, 1993). In mice lacking the *Nkx2-5* gene, the heart shows severe dysregulation of myocardial development (Parsons et al., 2007). These hearts do not grow past the earliest stages of heart looping. The T-box (*Tbx*) family of transcription factors is involved in cell-fate specification, differentiation, and organogenesis. The Tbx family contain two highly conserved residues: within their N-terminal domain there is a G residue at position 80 responsible for interaction with the major groove of DNA, and an R residue at position 237 in the C-terminal T-box domain responsible for binding to the minor groove of DNA (Muller and Herrmann, 1997). Of particular importance in amniotic heart development are Tbx2, Tbx3, Tbx5, Tbx20. Tbx5 and Tbx20 interact with Gata4 and Nkx2-5 to promote expression of atrial natriuretic factor (*Nppa*), connexin 40 (*Cx40*) and 43 (*Cx43*), and Chisel (*Smpx*) (Christoffels et al., 2010; Hoogaars et al., 2007; Moorman and Christoffels, 2003). Expression of these effectors promotes the specification of chamber myocardium. *Tbx2* and *Tbx*3 are expressed in the progenitors of the

inflow/outflow tracts and atrioventricular canal (Singh et al., 2012). These 2 factors act in opposition to *Tbx5*, suppressing expression of *Nppa*, *Cx40*, *Cx43*, and *Smpx* to repress chamber specification (Xiang et al., 2016). The opposing effects of *Tbx2*/3 and *Tbx5* creates patterning in the developing heart, and thus distinct populations of cells that give rise to future structures (Bruneau, 2013; Habets et al., 2002).

The *Mef2* family consists of highly conserved transcription factors that contain a MADS-box and regulate the differentiation of all muscle cell types (Potthoff and Olson, 2007). Invertebrates carry only a single *Mef2*, while vertebrates possess four *Mef2* genes (*Mef2a*, *b*, *c*, and *d*) (Desjardins and Naya, 2016). *Mef2b* and *Mef2c* are expressed in the mesoderm at embryonic day 7.5, while *Mef2a* and *Mef2d* are expressed in the linear heart tube between E8 and E8.5 (Edmondson et al., 1994). Of the four vertebrate *Mef2* genes, *Mef2c* is required for the specification of amniote-specific cardiac structures derived from the SHF (Lin et al., 1997). *Mef2c* falls under the control of *Nkx2-5*, *Gata4*, and *Isl1*, and is responsible for upregulating the expression of bHLH family members *Hand1* and *Hand2*, which are also critical cardiogenomic transcription factors (Dodou, 2004; Gottlieb et al., 2002). Embryos lacking *Mef2c* exhibit severe defects in heart looping as well as right ventricle/outflow tract formation (Cai et al., 2003; Lin et al., 1997).

Nkx2-5, *Gata4*, and *Tbx5* are the most studied and well-characterized cardiac transcription factors. These core factors can with each other to regulate cardiac development, forming a complex web of interactions and regulation in cardiac development. An overview of this regulatory network is shown in Figure 1, highlighting the co-regulation and complex interaction of transcriptional factors to control heart development. *Gata4* and *Nkx2-5* physically interact to regulate each others expression

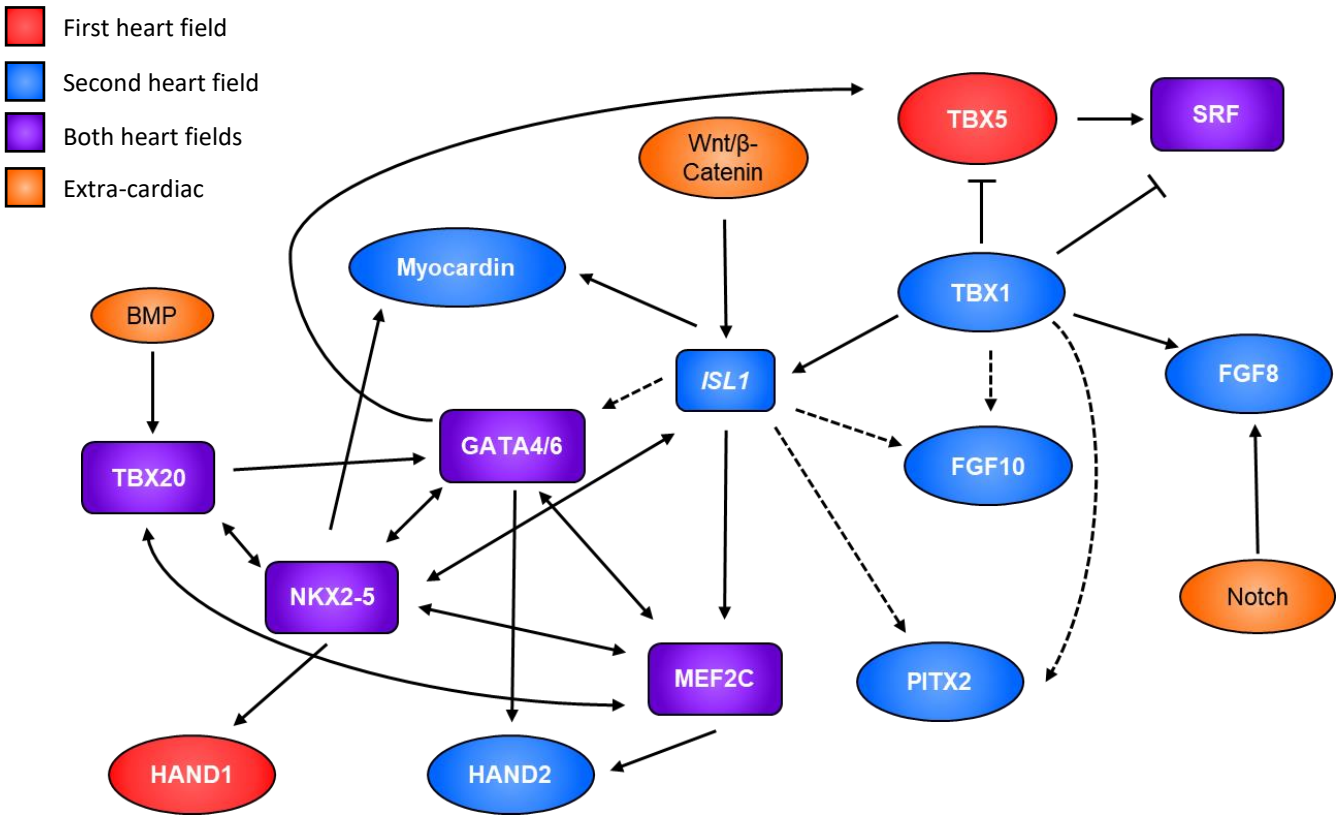

Figure 1. Overview of the transcriptional regulatory network governing embryonic heart development. Transcription factors expressed in the first heart field are shown in red, those expressed in the second heart field are red, while the factors expressed in both fields are purple. Transcription factors involved in cardiac development but not originating from either heart field are shown in orange. Solid lines indicate direct interaction, while dashed lines indicate an indirect/upstream effect.

and promote cardiomyocyte differentiation (Bruneau et al., 2001; Hiroi et al., 2001; Lien et al., 1999). Gene targeting of *Gata4* showed a lack of endodermal differentiation and reduced migration of myocardial progenitors, leading to cardia bifida (Garg et al., 2003; Kuo et al., 2007). Also, Gata4 interaction Nkx2-5 helps regulate Mef2 expression in the second heart field (Dodou, 2004). Gata4 can also interact with Mef2c to activate expression of Nppa, aMHC, and b-type natriuretic peptide (BNP). Gata4 also physically interacts with Tbx5 in the developing heart. In mice that are heterozygous for both Gata4 and Tbx5, embryonic death around 15.5 occurs due to cardiomyocyte hypoplasia, underdeveloped ventricles, and atrial septal defects (Maitra et al., 2009). The interaction between Gata4 and Tbx5 also activate the expression of Cx30.2 required for proper development of the AV node (Munshi et al., 2009). Finally, Tbx5 and Nkx2-5 interact to control gene expression in the progenitors of the cardiac conduction system (Bruneau et al., 2001; Hiroi et al., 2001). Tbx5 also directly interacts with Mef2 in a complex to activate Myh6 expression (Ghosh et al., 2009).

Hand1 and *Hand2* have overlapping and complementary expression patterns in the developing heart (McFadden, 2004). *Hand1* is expressed in specific segments of the linear heart tube that will go on to form the left ventricle (Risebro et al., 2006). Transgenic germ-line *Hand1* deletion mice die at approximately embryonic day 8.5 due to placental and trophoblastic defects (Firulli et al., 1998). Using an αMHC-cre model, it has been shown that mice lacking cardiac-specific *Hand1* are able to survive until the perinatal period, yet they still die of severe congenital heart defects shortly after birth. These hearts exhibited ventricular-septal defects (VSDs), atrioventricular (AV) valve abnormalities, and irregular outflow tract generation (McFadden, 2004). Furthermore, *Hand1* overexpression

mice died embryonically due to interventricular septal defects (McFadden, 2004), suggesting that strict regulation of *Hand1* expression is required for proper cardiogenomic regulation. *Hand2* is expressed throughout the heart tube and continues to be expressed in the cells that will form the right ventricle (Vincentz et al., 2011). Deletion of *Hand2* in mice results in death by embryonic day 10.5 due to reduced right ventricular proliferation and impaired vascular development (Holler et al., 2010).

Myocardin is a member of the SAF-A/B, Acinus, and PIAS (SAP) domain family of nuclear proteins. As a smooth muscle- and cardiac-specific transcriptional cofactor, it is responsible for activation of additional cardiac gene promoters (Du et al., 2003). Myocardin interacts with serum response factor (SRF), another member of the MADS box family, to regulate *Nkx2-5* expression (Wang et al., 2001). *Myocardin*$^{+}$ progenitor cells give rise to the smooth muscle cells present in the coronary vasculature. Expression of a dominant negative mutant version of Myocardin exhibited impaired myocardial cell differentiation, identifying it as another key component of embryonic heart development (Wang et al., 2003).

1.1.3 Cardiac chamber specification and morphogenesis

Once the formation of the heart tube is complete, the pre-programmed gene expression provided by *Tbx5* and and the Iroquois-class homeobox protein *Irx4* allows for wall and chamber specification and morphogenesis (Bao et al., 1999; Bruneau et al., 2001; Mori et al., 2006). *Tbx5* and *Tbx20* both interact with *Nkx2-5* and *Gata4* to promote chamber morphogenesis (Brown et al., 2005). *Bmp2* signaling can control T-box gene family expression early in development, and also helps to establish the conduction system

throughout the cardiac tissue (Prall et al., 2007). Mutations in *Tbx5* results in Holt-Oram syndrome, which involves atrial-septal defects (ASDs), ventricular septal defects (VSDs), and conduction system disarray (Bruneau et al., 2001). Mutations in *Nkx2-5* lead to a similar phenotype, as well as tetralogy of Fallot and Ebstein's tricuspid valve abnormality (Benson et al., 1999). *Tbx*1 has also been shown to be responsible for pre-patterning of the heart tube in preparation for chamber formation. Another gene, *Pitx2* confers "left" identity to cells forming structures on either side of the heart tube (Bruneau, 2002).

Trabeculation of the myocardium results in septation, increased contractility/conductivity, and the establishment of coronary vasculature. *Notch* signaling has been shown to be critical for this process (Abad et al., 2017; Grego-Bessa et al., 2007; Meyer and Birchmeier, 1995). Notch1-Notch4 are type I single-pass membrane-bound transcription factors with large intracellular and extracellular domains. The intracellular domain contains two nuclear localization signals and a DNA transactivation domain. Once activated by ligand binding of Delta4 or Serrate/Jagged protein families *Notch1* is then cleaved by Mib1 to become active, where the intracellular domain translocates to the nucleus (Grego-Bessa et al., 2007; Iso et al., 2003; Kopen, 2002). After migrating to the nucleus and interacting with transcriptional coactivators, cleaved intracellular Notch can drive the expression of *Tbx20*, *Bmp*10, *Hey2*, and neuregulin-1 (*Nrg1*) (Chen, 2004; Grego-Bessa et al., 2007; Zhang et al., 2011). Hairy/enhancer-of-split related with YRPW motif protein 2 (*Hey2*) is another bHLH transcription factor shown to regulate the size of the cardiac progenitor pool during embryogenesis (Gibb et al., 2018). *Nrg1* is an endothelial growth factor that binds to *Erbb4* and promotes the heterodimerization of *Erbb4*/*Erbb2* to promote cell growth and migration (Yarden and

Sliwkowski, 2001). Gene deletion of *Nrg1*, *Erbb2*, and *Erbb4* all result in *in utero* death at approximately embryonic day 10 due to a lack of myocardial trabeculae, reduced contractility, and bradycardia (Chan et al., 2002; Gassmann et al., 1995; Liu et al., 2010; Meyer and Birchmeier, 1995). *Erbb2* also contributes to the formation of cardiomyocyte adhesion to the extracellular matrix and supporting cells of the heart (Lockhart Marie , Wirrig Elaine, Phelps Aimee, 2011; Sanchez-Soria and Camenisch, 2010).

Following chamber formation, there are proliferative centers throughout the heart that contribute to myocardial growth. *Isl1* and *Tbx*1-expressing progenitor cells give rise to cardiomyocytes, endothelial cells, and smooth muscle cells present in the heart (Laugwitz et al., 2007; Zhou et al., 2008). *Irx4* regulates the expression of atrial- and ventricular-specific myosin heavy chain isoforms (Bao et al., 1999). *Tbx*1 is able to delay differentiation by inhibiting bone morphogenic protein (*BMP*) signaling and reducing SRF protein levels (Chen et al., 2009). Also, the expression of various fibroblast growth factors (*FGF*s) is essential for the supporting cells of the heart by promoting angiogenesis and fibroblast proliferation (Lavine et al., 2005).

Fgf8 and *Fgf10* are essential for SHF differentiation, as targeted deletion in the mesoderm resulted in a lack of right ventricle and outflow tract formation (Ilagan et al., 2006; Watanabe et al., 2010). *Bmp*4 activates the homeodomain transcription factor *Msx1* in neural crest cells to repress *Fgf* signaling (Zaffran and Kelly, 2012), thus signaling the transition from proliferation to differentiation in the SHF (Tirosh-Finkel et al., 2010). *Bmp* signaling can also promote differentiation by inhibiting the hedgehog signaling pathway, as well as by activation of microRNA 17-92 cluster which targets *Isl1* and *Tbx*1 (Dyer and Kirby, 2009; Wang et al., 2010). Regulation of the Hedgehog signaling pathway

has been shown to be important for proper cell fate specification and differentiation during embryogenesis (Lavine et al., 2006).

The stages of heart development and the associated transcriptional regulators involved at each timepoint are shown in Figure 2. This figure further demonstrates the multifaceted roles that each transcription factor can play at different developmental stages.

1.1.4 Models of embryonic heart development

Early cardiac development has been well-characterized using methods such as fluorescent lineage tracing in transgenic zebrafish, chickens, and mice (Ivanovitch et al., 2017). While most studies exploring cardiogenesis have been performed using murine models, the first stages of heart development are highly conserved among vertebrates, which provides a rationale to utilize other model systems (Wittig and Münsterberg, 2016). The flexibility of the zebrafish model has served as a means to characterize the earliest stages of cardiac morphogenesis (Bakkers, 2011). Zebrafish undergo early cardiogenic specification via *Nkx2-5*, *Tbx5*, *Hand1*, and *Gata4* to promote the establishment of two heart fields. The progenitors then form an endocardial linear heart tube, which eventually polarizes, loops, and forms chambers, expressing many conserved transcription factors and protein effectors (Bakkers, 2011). Zebrafish are also useful for unbiased whole-genome screens to identify both known and novel genes involved in cardiac development. Additionally, zebrafish embryos are small enough that passive oxygen diffusion can compensate for impaired cardiovascular development.

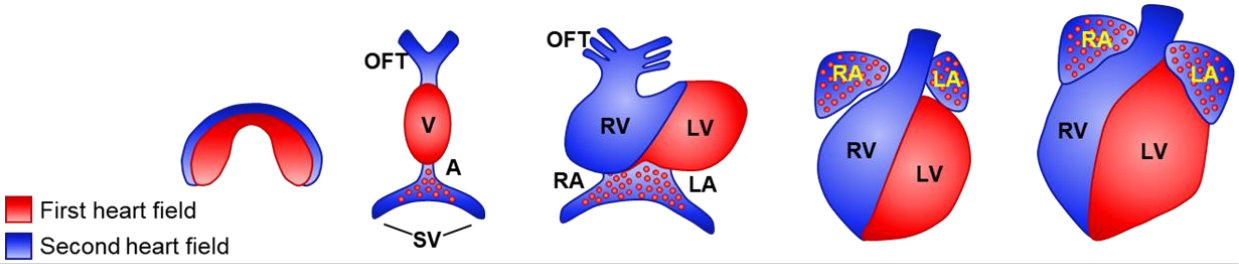

Stage	Cardiac Crescent	Linear Heart Tube	Heart Looping	Chamber morphogenesis	Perinatal Heart
Mouse Age	E7.5	E8	E9 – 12	E10 – 19	E19 – 7D
Regulators	Mesp1/2 Nkx2-5 Isl1 Mef2c Gata4/6 Wnt/β-catenin	Gata4/6 Nkx2-5 Tbx2/3 Tbx5 Tbx20 Mef2c Myocardin SRF Fgf8/10	Gata4/6 Nkx2-5 Tbx5 Tbx20 Mef2C Hand1/2 Irx4 Bmp Pitx2	Gata4/6 Nkx2-5 Tbx5 Pitx2 Tbx1 Notch1 Bmp Nrg1 Erbb2/4 SRF	Cyclins CDKs CDKIs Meis1 Hippo PI3K/Pten/AKT Fgf1 P38 ZEB1/2 E2F C-Myc Hif1α Rb

Figure 2. Regulatory transcription factors at each stage of heart morphogenesis. An illustration of each cardiac development stage is shown above. Embryonic age and key regulators of each stage are displayed below.

(Bakkers, 2011), which allows for in-depth analysis of severe cardiovascular defects brought about by genetic modifications. Zebrafish are also an excellent resource for studying cardiomyocyte division and renewal, as the adult zebrafish heart maintains its proliferative capacity (González-Rosa et al., 2017). Also of note, a functional screen for single nucleotide polymorphisms (SNPs) causing congenital heart defects was carried out in a zebrafish model (Bakkers, 2011). Using these models, researchers were able to identify and confirm novel SNPs in key regulatory genes such as ALK2/3, *Gata4*, *Erbb2*, and EGFR that cause morphogenic defects in the heart.

As a model of vertebrate cardiogenesis, zebrafish have proven to be invaluable in characterizing early cardiac genomic programming, and providing insight into the specific roles of transcription factors involved. As development progresses, however, the zebrafish heart and the amniotic heart diverge in structure and capacity. The fish heart retains a more linear shape, with only one atrium and one ventricle to circulate deoxygenated blood towards the gills. The amniotic heart is composed of four chambers, with one atria and ventricle responsible for collecting and circulating deoxygenated blood to the lungs, and another set of atria and ventricle to collect and pump oxygenated blood to the body.

Chicken embryos have also been utilized to monitor *ex utero* development, allowing easy access to the heart at all stages (Bao et al., 1999; Wittig and Münsterberg, 2016). Many experiments involving lineage tracing and transcription factor patterning have been used to complement studies performed in mice and zebrafish (Wittig and Münsterberg, 2016). The mature chick heart comprises four chambers with a

relatively similar anatomy to mammalian hearts, thus providing great insight into the development of the human heart. Furthermore, the ease of accessibility allows for various *in ovo* manipulations and experiments to be performed, such as dissection, grafting, micro-injections, and labeling (Wittig and Münsterberg, 2016). As such, cardiac valve formation has been extensively studied in chick models (Combs and Yutzey, 2009).

Collectively, these aforementioned studies suggest that embryonic heart development is characterized by a number of well-defined milestones, which include: 1) Specification of cardiogenic progenitors via *Mesp1*, *Nkx2-5* and *Hand1*/2 at gastrulation. 2) Migration and specification of cardiogenic precursor cells (CPCs) to form the two heart fields. 3) Formation of the endocardium via cell migration to the midline. 4) Formation of the myocardial tube and establishment of dorsal/ventral polarization. 5) Looping and ballooning to form distinct atrial and ventricular chambers. 6) Valve formation 7) Conductive system formation and finally 8) Formation of the epicardium.

1.2 Perinatal Heart Development

During fetal development, cardiomyocytes possess high proliferative capacity, and readily multiply to establish a functional heart. At birth, cardiomyocytes undergo a final cycle of karyokinesis in the absence of cytokinesis, and cardiomyocytes lose their proliferative capacity. At the conclusion of binucleation, individual cardiomyocytes and the heart as a whole, switches from hyperplastic to hypertrophic growth. During the first 10 days of life, the size of the mouse heart increases remarkably (Figure 3A). In Figure 3B it is also shown that individual cardiomyocytes drastically increase in size and show much more cellular structure with muscle striation at 10D compared to 3D. This cellular and organ level hypertrophy during early life is physiologic and is scaled to ensure cardiac output matches post-natal growth of the organism.

1.2.1 Cardiac growth in the postnatal heart is characterized by cardiomyocyte bi-nucleation and loss of proliferative capacity.

Shortly after birth, a cardiac transition is characterized by cardiomyocytes undergoing one last round of karyokinesis without subsequent cytokinesis, resulting in two nuclei being present in ~95% of rodent cardiomyocytes (binucleation) (Soonpaa et al., 1996). Each of these nuclei contain a diploid genome. In rodents, the majority of cardiomyocytes are binucleate by 7D (Botting et al., 2012). While in mice up to 95% of cardiomyocytes are binucleated shortly after birth, there is wide variation in binucleation index across species. For instance the binucleation index of cardiomyocytes in humans is reported to be from 25 to 60% (Bergmann et al., 2015a; Botting et al., 2012; Mollova et al., 2013). However, human cardiomyocytes are reported to still contain four copies of the

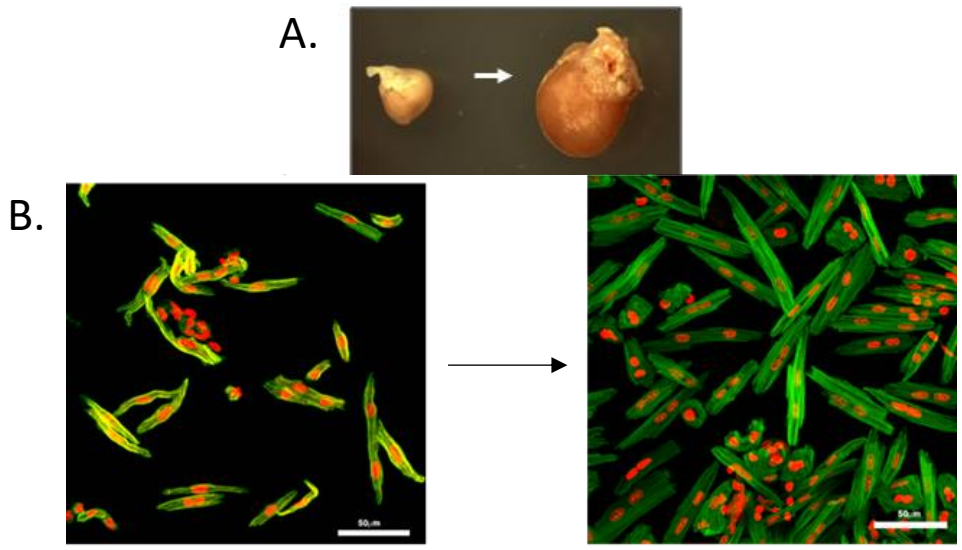

Figure 3. The heart hypertrophies during the neonatal period. A) A 3-day-old (3D) and a 10D mouse heart are displayed side-by-side to demonstrate the amount of cardiac growth which occurs after birth. These two hearts contain a relatively similar number of cardiomyocytes. B) Isolated cardiomyocytes from 3D and 10D mouse hearts to show the significant increase in cardiomyocyte size, organization, and binucleation during the neonatal period.

genome. The mononucleate human cardiomyocyte contains the genome within one tetraploid nucleus instead of two diploid nuclei and are also inhibited from cell cycle re-entry (Mollova et al., 2013). Interestingly, zebrafish cardiomyocytes, which maintain proliferative capacity throughout life, contain a single, diploid nucleus. Adult zebrafish hearts are able to regenerate and heal completely after cardiac injury. Using a modified cre/lox system in which green fluorescent protein (GFP) was expressed via αMHC, researchers showed that cardiomyocytes disassemble and reorganize their sarcomeres before dividing (Karra et al., 2015). Furthermore, they were able to determine that *Gata4* expression marks the subpopulation of cardiomyocytes that can re-enter the cell cycle. Therefore, in zebrafish, re-expression of fetal proliferative genes results in cardiomyocyte re-entry into the cell cycle to replenish cell populations. However, this ability is lost in higher vertebrates such as birds and mammals. *In vitro* stimulation of rat cardiomyocytes with neuregulin-1 NRG-1 caused increased DNA synthesis and allowed for completion of cytokinesis in 0.6% of previously non-dividing mononucleate cardiomyocytes (Bersell et al., 2009). Also, the signaling molecule p38 mitogen-activated protein kinase (p38) has proven to be an inhibitor of cardiomyocyte cytokinesis. Inhibition of p38 *in vitro* increased the rate of successful cytokinesis by nearly 4-fold after stimulation with FGF1 compared to FGF1 alone (Engel et al., 2005). Based on the in vitro rat models and the proliferative capacity of the zebrafish heart, there may a relationship between ploidy and divisibility. However, this remains unclear as there is variation in binucleation index across species, and other multinucleated and/or polyploid cells, such as hepatocytes, skeletal myocytes, and osteoclasts maintain the ability to divide. An illustration showing the neonatal transition of cardiomyocytes is displayed in Figure 4. This graphic emphasizes two distinct

gene programs active in fetal and adult life, and that fetal proliferative gene re-expression can occur in cardiomyopathy conditions. Also highlighted is a neonatal transition program that is responsible for the switch between the fetal and adult phenotypes.

At present, the transitional program responsible for cell cycle arrest and the disjoint between karyokinesis and cytokinesis is not well-characterized, although some genes have been implicated in the process. For example, Anillin is present during G1, S, and G2 phases of mitosis and is localized to the cell cortex where it plays a critical role in cytokinesis by aiding in the formation of the contractile ring necessary for telophase (Brooks et al., 1998). In cardiomyocytes post-birth, Anillin fails to localize to the contractile ring, which results in asymmetric constriction with defective mid-body formation, and failed cytokinesis (Engel et al., 2006). Protein Regulator of Cytokinesis 1 (PRC1) works in conjunction with Anillin to promote cytokinesis during replication. PRC1 expression decreases significantly shortly after birth and is not expressed in adult cardiomyocytes because they do not undergo cytokinesis (Jiang et al., 1998). In the case of cardiomyocyte cell cycle being re-engaged, PRC1 re-expression and proper Anillin localization would be required.

Porrello et al. (2011) showed that a 1-day-old neonatal murine heart injured via surgical resection is able to replenish damaged cardiomyocytes and heal completely (Porrello et al., 2011a). Furthermore, a follow-up study which performed the same injury but also used a *Rosa26-LacZ* reporter locus were able to confirm that the regenerated myocardium is composed of cardiomyocytes that arose from an αMHC-positive lineage (Porrello et al., 2013). This strongly suggests that new cardiomyocytes are being

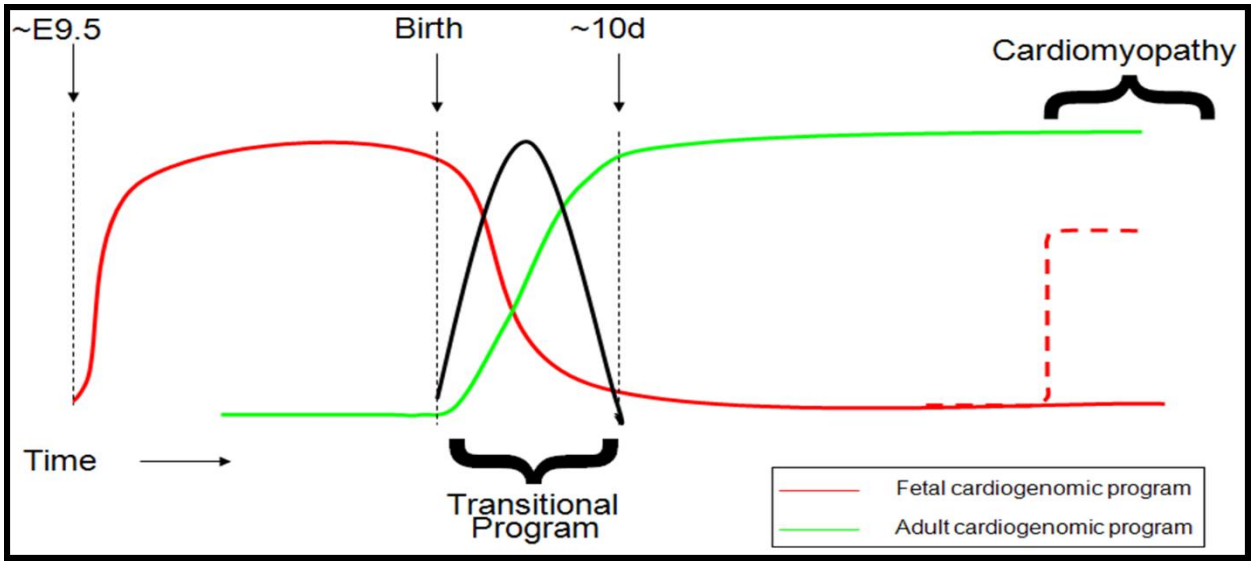

Figure 4. A transitional program is responsible for repressing fetal cardiogenomic programming and allowing the establishment of the adult programming. During gestation, the heart grows via proliferation of cardiomyocytes. Birth triggers the transitional program to inhibit cardiomyocyte proliferation. The adult program enlarges the heart via hypertrophy. In cases of cardiac injury or cardiomyopathy, fetal genes are commonly re-expressed, however no increase in proliferation occurs.

produced from cardiomyocyte replication and not from an intermediate progenitor cell. If the same injury described above is performed on day 7, the cardiomyocytes are unable to divide and replenish, and the heart is permanently damaged with scar formation and decreased functional capacity (Porrello et al., 2011a). This inability to divide anytime after 7 days, especially in adult life, becomes problematic when the heart is injured via myocardial infarction or other disease states that result in loss of cardiomyocytes. Although it has been shown that some fetal genes are reactivated in disease states (Ahuja et al., 2007a), cardiomyocytes are still unable to re-enter the cell cycle to divide and replenish the damaged population.

The epicardium is an epithelial lining of the heart that plays a large role in cardiac development. By secreting retinoic acid and other growth factors, it is able to promote cardiomyocyte proliferation during fetal growth (Lavine et al., 2005). The epicardium is also reported to contribute other cell types to the myocardium, such as fibroblasts and vascular cells (Zhou et al., 2008). In a zebrafish cardiac injury model, the epicardium re-expresses embryonic genes and partially undergoes epithelial-mesenchymal transition to regenerate damaged cardiac tissue (Kikuchi et al., 2011). Furthermore, ablation of the epicardium in zebrafish, which possess the ability to regenerate myocardium, was shown to inhibit cardiomyocyte proliferation and delay heart regeneration (Wang et al., 2015).

In humans, the same loss of proliferative capacity occurs during early life. Using carbon dating, stem cell marker expression, and thymidine-analog cancer treatments, researchers have been able to determine the average turnover rate of cardiomyocytes in humans (Bergmann et al., 2015a). The first decade after birth shows steep decline to

approximately 20% turnover, with a renewal rate of around 1% by age 20. By age 70 this turnover rate is less than 0.5% (Bergmann et al., 2015). Mouse models have shown similar results, and also that there is only a small increase in cardiomyocyte regeneration in the border zone after cardiac injury such as myocardial infarction, with hearts only able to heal by forming a scar (Malliaras et al., 2013). This is in contrast to other muscle cell types, which possess cells able to proliferate in response to injury to regenerate damaged tissue (Laumonier and Menetrey, 2016).

1.2.2 The extracellular matrix must adapt to accommodate post-natal cardiomyocyte cell growth and hypertrophy

Prior to birth, myofibrils within cardiomyocytes are primarily localized to the periphery of the cell (Pilny, 1975). After birth, the myofibril volume of cardiomyocytes increases by 30% and sarcomeres are organized to occupy the entirety of the cytoplasm, resulting in a drastic increase in cardiomyocyte size (Yuan and Braun, 2017). To compensate for the drastic increase in cardiac mass in the first 10 days of life, the heart must undergo significant extracellular matrix remodeling. Since individual cardiomyocytes increase in volume by up to 30% during the neonatal phase, room must be made for these cardiomyocytes to grow.

The primary regulator of ECM remodeling during neonatal heart development are cardiac fibroblasts. These fibroblasts secrete various ECM scaffolding and signaling proteins such as collage, fibronectin, and heparin-binding EGF-like growth factor to support cardiomyocytes (Borg et al., 1984; Ieda et al., 2009). Cardiac fibroblasts must strike a delicate balance between providing enough strength for the heart to pump and

function properly, while also not becoming fibrotic and inflexible (Borg et al., 1981). After birth, the number of cardiac fibroblasts doubles, and the ECM is actively remodeled to tolerate the mechanical stress placed on the ventricles (Krenning et al., 2010). β1-integrin expression by cardiomyocytes is required for proper connection to the ECM, as shown by cardiomyocyte-specific deletion resulting in reduced cardiomyocyte proliferation and impaired ventricular function (Ieda et al., 2009). By one month in murine models, the ECM and heart structure has reached its final “adult” phenotype.

ZEB1 and ZEB2 are transcription factors involved in the TGFβ signaling pathway. Both are responsible for regulating ECM remodeling during fetal development, and are also responsible for the epithelial-to-mesenchymal transition (EMT) phenotype observed in many cancers (Zhao et al., 2005). ZEB1 and ZEB2 have both proven to be critical proteins involved in regulating the degradation and remodeling the extracellular matrix in the heart.

1.3 Regulators of the cardiomyocyte cell cycle

Prior to the final morphologic transition of cardiomyocytes in the early post-natal heart, the expansion of the myocardium is managed by committed progenitor cell populations. Several pathways have been identified that regulate embryonic cardiomyocyte expansion and suppression of these same pathways have been shown to be essential for the transition to hypertrophic growth (Foglia and Poss, 2016). Well-known markers of cell cycle progression, such as the CDK family, MYC, and E2F are downregulated, while p21, p27, and CDK inhibitors are upregulated (Flink et al., 1998; Gilsbach et al., 2014; Greco et al., 2016; Sim et al., 2015a).

After the neonatal transition, the number of cardiomyocytes present nearly dictates the cardiomyocyte endowment for life. Very few new cardiomyocytes are produced throughout postnatal and adult life (Porrello and Olson, 2014). After this transitional event, binucleated cardiomyocytes lose their proliferative capacity and the heart grows primarily via physiologic hypertrophy of cardiomyocytes, in addition to an increase in cardiac fibroblast and endothelial cell populations (Paradis et al., 2014). Based on these findings, many studies have been undertaken to examine whether altered expression of these cell cycle regulatory factors are the key determinant for cardiomyocyte maturation and terminal differentiation.

1.3.1 Cyclins/CDKs in the post-natal heart

Cyclins are a family of proteins responsible for regulating the progression of cells through the cell cycle. Each cyclin involved in division is synthesized and degraded during each cell cycle. The cyclins share a conserved ~150 amino acid region called the ‘cyclin

box' which binds to the N-terminal of their specific cyclin-dependent kinases (CDKs) (Li and Brooks, 1999). CDKs are serine-threonine kinases that become enzymatically active when interacting with cyclins. Cyclins and CDKs interact to form complexes at specific phases of the cell cycle to drive cells through cell cycle checkpoints (Liu and Kipreos, 2000). During the hyperproliferative phase of cardiac growth, cyclin and CDK regulation are extremely important (Kang et al., 1997; McGill and Brooks, 1995).

Cyclins C, D, and E are transient G1 phase proteins responsible for regulating the transition through G1/S phase of the cell cycle. Cyclin C is primarily expressed during G0 and forms a complex with CDK8 to regulate the transition from G0 to G1 by phosphorylating Rb. This complex also controls transcription by regulating RNA polymerase II activity (Julien Sage, 2004). CDK4 and CDK6 form complexes with the 3 Cyclin D-family members (D1, D2, D3) to aid in the regulation of the G1/S transition (Berthet and Kaldis, 2006). The Cyclin D family are considered the most important Cyclins in regulating the G1/S transition (Siddiqi and Sussman, 2014). Cyclin E possesses a similar function but it forms a complex with CDK2 (Woo and Poon, 2003a). This complex can then go on to phosphorylate Rb and regulate E2F activity to regulate cell cycle gene expression. Interestingly, single-deletion mutants of Cyclin D members have no cardiac phenotype, but triple deletion is lethal, partially due to cardiac defects such as ventricle hypoplasia and septal defects (Ciemerych et al., 2002; Siddiqi and Sussman, 2014). Similarly, genetic deletion of CDK2 and CDK4 results in hypophosphorylation of Rb and thus downstream E2F effects with ventricle hypoplasia and wall thinning, and also dilated atria (Berthet and Kaldis, 2006; Berthet et al., 2006). Cyclin E is also an S-phase cyclin, able to mediate accelerated phosphorylation of Rb by interacting with CDK2 (Woo and

Poon, 2003a) . After the G1/S transition, Cyclins C, D, and E are rapidly ubiquitinated and degraded.

Cyclin A is a G2 phase cyclin that also participates in the transition through S and G2 phases of the cell cycle. Cyclin A associates with CDK1 and CDK2 to regulate DNA replication and synthesis (Hu et al., 2001; Neganova and Lako, 2008). Previous studies have reported that the downregulation of Cyclin A correlates with permanent withdrawal of cardiomyocytes from the cell cycle in human and rat hearts (Yoshizumi et al., 1995). Furthermore, overexpression of Cyclin A2 results in increased cardiomyocyte cell cycling (Chaudhry et al., 2004).

Cyclin B is a G2/M phase cyclin responsible for progression through M-phase of the cell cycle. Cyclin B is able to bind CDK1 to control entry into mitosis. The presence of Cyclin B is observed in embryonic cardiomyocytes, but expression is absent in adult cardiomyocytes (Kang et al., 1997). The absence of cyclin B1 results in G2/M cell cycle arrest. Upon birth, Cyclin A, B, D, and E and their corresponding kinases are significantly downregulated (Brooks et al., 1998; Kang et al., 1997; Malumbres et al., 2014; Woo and Poon, 2003a).

In vitro, overexpression of cyclin B1 in isolated adult rat cardiomyocytes was able to increase total cell number by up to 40%, indicating increased proliferative capacity (Bicknell et al., 2004). Another study using transgenic mouse lines overexpressing cyclins D1 and D3 showed increased DNA synthesis in cardiomyocytes and reduced infarct size after coronary artery occlusion (Pasumarthi et al., 2005). Furthermore, cardiomyocyte-specific overexpression of cyclin A2 was shown to increase proliferative capacity of

cardiomyocytes after birth, as assessed by pH3 staining (Chaudhry et al., 2004). Also, kinase assays and pH/ki67 staining show increased actively cycling cells once isolated and cultured. However, this proliferative capacity does not translate *in vivo*. When overexpressed in mice, cyclin D1 increases DNA synthesis and nucleation, but does not cause an increase in cardiomyocyte proliferation (Soonpaa et al., 1997).

Meis1 has also been shown to play a role in cardiomyocyte proliferation. Global deletion of Meis1 resulted in embryonic death by embryonic day 14.5 due to disrupted hematopoiesis, however neonatal cardiac-specific (αMHC) Meis1 repression was shown to increase the proliferative window as shown by increase pH3+, Ki67+, BrdU+ cardiomyocytes. Conversely, overexpression reduced neonatal cardiomyocyte proliferation and inhibited their regenerative ability (Mahmoud et al., 2013). Meis1 is required for transcription activation of p15, p16, and p21, and thus plays an important role in the regulation of cardiomyocyte proliferation.

CDK-Activating Kinases (CAKs) and Cyclin Dependent Kinase Inhibitors (CDKIs) are also extremely important positive and negative regulators of cyclin/CDK activity, respectively, and control progression through the cell cycle. After birth, the upregulation of CDKIs coincides with the downregulation of Cyclins and CDKs (Brooks et al., 1998; Kang et al., 1997; Woo and Poon, 2003a). CDKIs can be categorized into two distinct families that are structurally and functionally separate: The INK4 family (p15, p16, p18, and p190 and the Cip/Kip-family (p21, p27, and p57). The INK4 family block the interaction of Cyclin D and CDK4/CDK6 to inhibit their enzymatic activity (Siddiqi and Sussman, 2014). The Cip/Kip family are selective inhibitors of CDK2's interaction with Cyclin E to inhibit progression through the S-phase (Tane et al., 2014). In addition, they

can inhibit Cyclin A and CDK1 activity to play a broader role in inhibiting mitosis (Tane et al., 2014). P27 and p57 are CKIs which work together to promote cell cycle exit and terminal differentiation of cardiomyocytes (Paradis et al., 2014; Di Stefano et al., 2011). P21 also promotes cell cycle arrest and prevents re-entry into the cell cycle (Abbas and Dutta, 2009). Expression of the Cip/Kip family of CDKIs in undetectable during embryonic heart development and begin to increase during the perinatal transition, with highest expression in adult cardiomyocytes (Ahuja et al., 2007b). Inhibition of these 3 CKIs has been shown to allow rat ventricular cardiomyocytes to re-enter the cell cycle and actively proliferate. This coincided with the re-expression of several fetal genes and the down-regulation of many adult genes, with a concomitant change in cellular morphology (Di Stefano et al., 2011).

1.3.2 Transcriptional control of the cardiomyocyte cell cycle

The term E2F refers to a family of eight transcription factors. While some are responsible for transcriptional activation, others function to inhibit transcription (Siddiqi and Sussman, 2014). Their primary genomic targets are Cyclins/CDKs, DNA damage/repair genes, checkpoint genes, and apoptosis genes (Ren et al., 2002) . Due to the number of family members and overlapping compensatory roles between members, study of individual family member functions has been difficult (Vara et al., 2003)). Specifically, targeted deletion of E2F3 is embryonic lethal due to congestive heart failure, however targeted deletion of other members does not show a phenotype. Conversely, overexpression of E2F1 to 4 increases the rate of S-phase entry in isolated rat cardiomyocytes, while overexpression of E2F1 and 3 induces apoptosis (Timmers et al., 2007; Tsai et al., 2008; Wu et al., 2001). Although the role of each specific E2F member

is not well characterized, the family is considered an essential regulator of cardiomyocyte cell cycle progression.

The myc-family of transcription factors consists of N-myc, L-myc, and C-myc. The myc family functions by interacting with the protein Max. The function of the myc family has primarily been studied in the context of cancer due to their association with increased cellular proliferation (Dang, 2012; Stine et al., 2015). C-myc is able to mediate G1-phase exit by upregulating Cdk4, Cdc25A, and Cyclins A, D1/2, and E, and also by antagonizing the actions of p27 (Dang, 2012; Stine et al., 2015). Targeted deletion of c-myc results in early embryonic death, however it cannot be solely attributed to heart defects as c-myc is important for the development of many other essential organs and tissues (Davis et al., 1993). Transgenic overexpression of c-myc results in hyperplastic ventricles during neonatal development, however this increased proliferation subsides during maturation of cardiomyocytes. Afterward, these hearts display increased hypertrophic growth (Green et al., 1997).

Finally, the HIF1α transcription factor has also been shown to play an important role in regulating cell cycle kinetics. HIF1α is a functional antagonist to c-myc (Koshiji et al., 2004). Transgenic deletion of HIF1α in mice results in cardiac hyperplasticity, leading to obstruction of outflow tracts and functional complications (Kotch et al., 1999). Interestingly, HIF1α also induces vascular endothelial growth factor (VEGF), but these transgenic mice do not exhibit increased angiogenesis along with increased proliferation of cardiomyocytes (Huang et al., 2004).

1.3.3 Pocket Proteins

Three pocket proteins (Rb, p107, and p130) regulate the G1/S-phase transition of the cell cycle by regulating E2F-effectors (Cobrinik, 2005). Embryonic development is characterized by increased Rb expression and low p130 expression. Rb is important for regulating cardiomyocyte cell cycle withdrawal and differentiation. When Rb is dephosphorylated, it can bind to E2F to recruit transcriptional repressors and inhibit the G1/S transition. When phosphorylated by CDK2 and CDK4, Rb cannot bind E2F and allows for the transcription of cell cycle progression genes (Feliers et al., 2002; Ikeda et al., 1996). While deletion of Rb results in embryonic lethality, deletion of both Rb and p130 results in increased heart-weight to body-weight ratio, increased cell number, and increased actively proliferating cardiomyocytes as assessed by BrdU incorporation and pH3 staining (Taneja et al., 2011).

1.3.4 The Hippo Pathway

The Hippo pathway was initially discovered in Drosophila as a pathway regulating organ size (Reddy and Irvine, 2008). This pathway is well-conserved in animals as well and performs a similar function (Halder and Johnson, 2010; Kango-Singh and Singh, 2009). The human orthologs of Hippo are Mst1 and Mst2. When the Hippo pathway is activated, YAP1 and its paralog TAZ are phosphorylated and sequestered in the cytoplasm. When the Hippo pathway is inactive, YAP1 is not phosphorylated and is active in the nucleus where it can regulate genes such as Birc2, Birc5, Cyr6, and Hoxa1 to promote cell proliferation and organ growth (Staley and Irvine, 2012). A schematic of the Hippo signaling pathway is shown in Figure 5. By controlling YAP1 expression, the Hippo

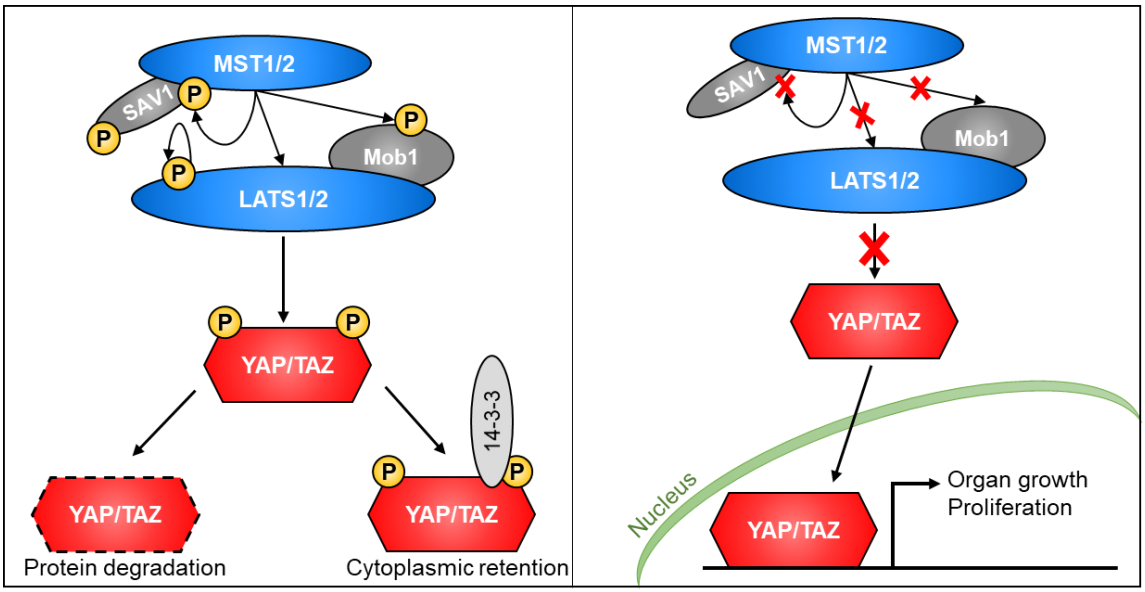

Figure 5. The Hippo pathway is responsible for organ growth and cellular proliferation. When the Hippo pathway is activated (phosphorylated), it results in the phosphorylation of YAP/TAZ. Phosphorylated YAP/TAZ is sequestered in the nucleus and inactive. It is temporarily stored in the cytoplasm or degraded if necessary. When the Hippo pathway is not active (dephosphorylated), YAP/TAZ remains unphosphorylated and active, and migrates to the nucleus to regulate transcription of proliferative genes.

pathway can control cell proliferation and regulate organ size. After birth, the Hippo pathway is activated to inhibit YAP1 activity and stop the proliferation of cardiomyocytes (Wang et al., 2018b).

YAP1 and TAZ have partially redundant functions including cell growth, proliferation, specification, and differentiation (Moya and Halder, 2018). Both can upregulate members of the BCL-2 and inhibitor of apoptosis (IAP)s such as surviving and MCL1. YAP/TAZ are also heavily involved in organ regeneration and tissue repair, where it not only affects proliferation, but cell survival, dedifferentiation, and expansion of stem cells (von Gise et al., 2012). Disruption of the Hippo pathway has previously been shown to induce the expression of *Wnt* signaling and increase cardiomyocyte number in the developing heart (von Gise et al., 2012; Leach et al., 2017; Lin et al., 2014; Singh et al., 2016; Tian et al., 2015; Yang et al., 2018). Overexpression of YAP1 during development results in overgrowth of the liver and heart, and it has also been shown to promote cardiomyocyte proliferation and regeneration after injury (Lin et al., 2014). Hyperactivation of YAP1 in adult mice results in overgrowth of the liver, but not the heart (Terkeltaub et al., 2014). Homozygous deletion of Yap1 results in death at embryonic day 8.5, while Taz deletion mice are viable (Zhao et al., 2010a). Double-deletions of YAP1 and TAZ do not pass the morula stage (Fa-Xing Yu, Bin Zhao, 2016). Cardiac-specific deletion of Yap1 and Taz causes defects in angiogenesis, vascularization, and myocardial hypoplasia (Singh et al., 2016). Cardiac-specific deletion of SAV1, a member of the Hippo pathway, in mice results in an overall reduction in YAP1 phosphorylation and therefore increased YAP1 activity (Heallen et al., 2013). Increased YAP1 transcriptional activation lead to significant cardiomegaly during embryogenesis and neonatal death due to severe

heart defects. Collectively, these observations indicate that YAP1 protein and the Hippo pathway are involved in a delicate balance of generating a heart substantial enough to pump blood and match cardiac growth to whole body maturation but prevent organ overgrowth which would result in impaired function.

1.3.5 The PI3K/PTEN/AKT pathway

The PI3K/PTEN/AKT pathway directly controls cell cycle processes by affecting downstream targets such as cAMP response element-binding protein (CREB), p27, and FOXO (Heineke and Molkentin, 2006; Maillet et al., 2013). PI3K phosphorylates PIP2 into PIP3, which can then go on to phosphorylate and activate AKT. p-AKT then targets and activates mammalian target of rapamycin complex 1 (mTORC1), which interacts with p70-S6 kinase to activate transcription and translation (Manning and Toker, 2017). Phosphatase and tensin homologue (PTEN) is a tumour-suppressor with a wide-range of functions. PTEN works against PI3K using its phosphatase activity to convert PIP3 into PIP2 (Maehama and Dixon, 1998). This downregulates protein synthesis and restrains cell growth (Goberdhan et al., 1999; Myers et al., 1998). Conditional deletion of PTEN has revealed further functions of PTEN in cell-type specification and cardiac muscle contractility (Goberdhan and Wilson, 2003). A schematic of the PI3K/PTEN signaling pathway is shown in Figure 6.

The PI3K/PTEN/AKT pathway is also involved in regulating apoptosis in response to DNA damage (Engelman et al., 2006). Constitutive activation of protein kinase B (PKB) or Akt increases cyclin D molecular half-life (Alao, 2007). Conversely, inhibition of PI3K

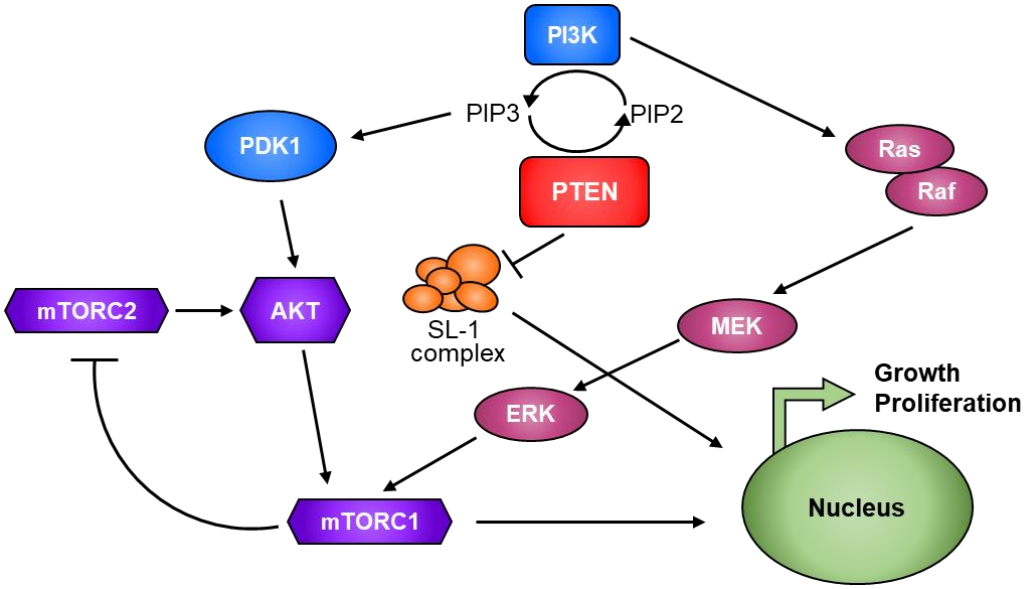

Figure 6. The PTEN/PI3K signaling pathway. PI3K and PTEN regulate PIP2 and PIP3 levels to mediate cell signaling and growth through both the AKT/mTOR and MEK/ERK pathways. PTEN is a negative regulator of cell growth by dephosphorylating PIP3 and inhibiting its pro-proliferative downstream effects. PTEN also negatively regulates the SL1 complex responsible for ribosomal creation and function.

signaling increases cyclin D degradation. CDK2 has also been demonstrated as a target of Akt during cell cycle progression (Maddika et al., 2008). P27 expression is decreased by the PI3K/AKT pathway to promote G2/M progression (Fujita et al., 2002). Overactivation of the PI3K/AKT pathway in neonatal heart results in increased cardiomyocyte number (Beigi et al., 2013). Each regulatory pathway plays an important role in establishing cardiomyocyte endowment and regulating heart size. After birth, these pro-proliferative pathways are repressed, preventing cardiomyocyte cell-cycle re-entry.

1.4 Epigenetic regulation of cardiomyocyte cell cycle

Gene expression profiling (RNA-seq) and genome-wide methylation sequencing has shown dynamic changes in the cardiac methylome during the neonatal period. After birth, there are global epigenetic changes occurring across the genome that accompany the transition from a hyperplastic to a hypertrophic heart. Regulation of DNA methylation plays a critical role in silencing proliferative genes and activating hypertrophic ones. Up to 80% of the changes in the methylome are hypermethylation, resulting in transcriptional repression of replication and developmental pathways (Sim et al., 2015b). Furthermore, inhibition of DNA methylation after birth was shown to reduce cardiomyocyte binucleation and increase proliferative index indicated by phospho-histone 3 (pH3) expression (Paradis et al., 2014).

Epigenetic regulation via histone modification has also been shown to play a role in the neonatal heart transition. Histones in embryonic cardiomyocytes are hyperacetylated (H3K9/14, H3K18, H3K27), but become hypoacetylated shortly after birth, concomitant with cell cycle arrest (Quaife-Ryan et al., 2016; Wamstad et al., 2012; Zhou et al., 2011). Overexpression of *Hdac1* and *Hdac3* decreases global acetylation and supresses cyclin-dependent kinase (CDK) inhibitors, resulting in increased proliferation in 1-day-old (1D) hearts (Trivedi et al., 2008). Inversely, cardiomyocyte-specific deletion of *Hdac3* results in cardiac hypertrophy and metabolic disorder (Montgomery et al., 2008). Global deletion of *Hdac1* in mice results in death by postnatal day 10 due to defects in cell cycle progression, while *Hdac2* global deletion causes unrestricted cardiomyocyte proliferation and death (Lagger et al., 2002; Montgomery et al., 2007). Although cardiomyocyte-specific deletion of either *Hdac1* or *2* show no phenotype, it is notable that

a cardiomyocyte-specific double-deletion results in several heart defects related to cell proliferation (Montgomery et al., 2007).

After birth, inhibitory histone methylation (H3K9me3 and H3K27me3) is present at the promoter of many cell cycle genes in cardiomyocytes (Sdek et al., 2011). H3K9me3 enrichment at E2F-, Rb- and SUV39H1-dependent promoters leads to stable silencing of pro-proliferative genes controlled by these factors. Depletion of *Rb* and *Suv39h1* was also shown to increase cell-cycle gene expression and allow some cell-cycle re-entry in adult cardiomyocytes (Sdek et al., 2011).

Epigenetics evidently play an important role in terms of maintaining the adult cardiomyocyte phenotype by suppressing the fetal growth and development pathways. Also, it has been shown that during cardiac hypertrophy there is a redistribution of methylation back to a neonatal-like pattern (Greco et al., 2016), however cell-cycle re-entry has not been demonstrated.

1.5 The role of non-coding RNAs in heart development

Recently, emerging literature investigating the neonatal heart suggests that non-coding RNAs (ncRNAs) may be a critical driving force behind the transition from fetal to adult cardiomyocytes (Eulalio et al., 2012; Yang et al., 2013). Several types of non-coding RNAs have been shown to be involved in heart development and regeneration, including microRNAs (miRNAs), PIWI-interacting RNAs (piRNAs), transfer RNAs (tRNAs), ribosomal RNA (rRNA), small nuclear RNAs (snoRNAs), and long non-coding RNAs (lncRNAs) (Di Mauro et al., 2018). While the function of certain housekeeping ncRNAs, such as rRNA and tRNA, has been well-established, the function of other ncRNAs are not well studied due to their relatively recent discovery. PiRNAs have been shown to aid in genome stability in the germline by silencing repetitive and transposable elements (Iwasaki et al., 2015).

LncRNAs are >200 bases in length and comprise a majority of the non-coding transcriptome. LncRNAs are distributed throughout the cell nucleus and cytoplasm; they are also subject to post-transcriptional modifications such as splicing, capping, and polyadenylation. The wide variety of functions exerted by lncRNAs is only beginning to be characterized, and several have already been implicated in heart development. The lncRNA Braveheart (Bvht) is involved in the specification of embryonic stem cells into mesodermal progenitors (Klattenhoff et al., 2013). Bvht functions as an epigenetic regulator to reduce the expression of Suz12/PRC2 complex. One function of the Suz12/PRC2 complex normally is to inhibit cardiac-lineage-specific gene expression, and therefore Bvht is an activator of mesodermal-specific genes, including cardiac (Klattenhoff et al., 2013; Rotini et al., 2018).

The lncRNA FOXF1 adjacent non-coding developmental regulatory RNA (Fendrr) has also been identified as a regulator of cardiac specification. Fendrr is involved in differentiation of tissues from the lateral mesoderm, which eventually forms the heart. Loss of Fendrr expression results in increased expression of Nkx2-5 and Gata6, with embryonic death at embryonic day 13.5 due to heart failure (Grote et al., 2013).

Finally, the lncRNA Upperhand (Uph) was recently shown to maintain the super-enhancer signature (H3K27ac) on the upstream regulatory regions of the Hand2 gene. Blockade of Uph transcription inhibited Hand2 expression causing ventricular hypoplasia, outflow defects, and heart failure leading to embryonic death, similar to the effects of transgenic Hand2 deletion in embryos (Anderson et al., 2016).

The importance of regulatory ncRNAs in heart development continues to be proven. Indeed, we have only begun to characterize the role of lncRNAs, while very little is known about piRNAs and snoRNAs. The first type of regulatory ncRNAs to be discovered were miRNAs, and they remain the most well-characterized ncRNA.

1.5.1 MicroRNAs in embryonic heart development

miRNAs are short single-stranded ncRNAs approximately 22 nucleotides in length which target messenger RNA (mRNA) at the post-transcriptional level (Grishok et al., 2001; van Rooij and Olson, 2007). Primarily functioning as negative regulators of gene expression, they are currently the most widely researched ncRNA (Choong et al., 2017). Primary miRNAs (pri-miRNAs) are transcribed from genomic DNA by RNA polymerase II or they are produced as by-products from intronic or exonic regions of mRNA transcripts (Bartel, 2004). Pri-miRNAs are cleaved into ~70 nucleotide precursor miRNAs (pre-

miRNAs) by the RNAse III enzyme Drosha and DiGeorge syndrome critical region 8 (DGCR8) (Bartel, 2004; Tian et al., 2017). The pre-miRNA is then exported from the nucleus via exportin 5 into the cytoplasm (Ha and Kim, 2014; Yi et al., 2003). The protein Dicer is another RNAse III enzyme that cleaves the pre-miRNA into the mature miRNA. One arm of the miRNA is then loaded onto Argonaute (Ago) proteins to form an RNA-induced silencing complex (RISC), while the other arm is degraded. The RISC targets the 3' untranslated region (UTR) of mRNA transcripts by complementary base-pairing to prevent their translation and promote degradation (Ha and Kim, 2014; Di Mauro and Catalucci, 2017). Mature miRNAs can also be packaged into vesicles and exported into the peripheral tissue and blood supply to affect other tissues and cell types (Hunter et al., 2008; Mirra et al., 2015).

miRNAs have proven to be essential for development. Germline deletion of Dicer in mice and zebrafish has proven to be embryonically lethal and prevents development past the gastrulation stage (Bernstein et al., 2003; Wienholds et al., 2003). Furthermore, deletion of Dicer during mouse heart development using Cre-mediated deletion under control of the Nkx2-5 promoter resulted in death due to defective heart morphogenesis (Zhao et al., 2007). Germline deletion of DGCR8 also resulted in proliferation defects, dilated cardiomyopathy and heart failure (Rao et al., 2009). Strong support for the necessity of miRNAs in the neonatal transitional program is provided by Chen et al. (2008). Transgenic postnatal cardiac-specific deletion of Dicer using a Cre-Lox system under control of the αMHC promoter caused neonatal death at day 5 due to aberrant expression of cardiac contractile proteins, sarcomeric disarray, slower heart rates, and reduced fractional shortening (Chen et al., 2008).

Several specific miRNAs have been identified as playing a role in heart development. As mentioned in Chapter 1.1, tightly regulated transcription factor expression is essential for proper cell fate determination, migration, and differentiation of cardiac progenitors. Recent studies in zebrafish have shown that miR-138 is required to establish chamber-specific gene expression patterns (Morton et al., 2008). The zebrafish heart expresses Cspg2, Notch1b, and Tbx2 specifically in the atrioventricular canal (AVC), distinguishing it from the atria and ventricles (Chi et al., 2008; Rutenberg et al., 2006). MiR-138 antagomir treatment resulted in AVC-restricted genes being expressed in atria and ventricles and ventricular cardiomyocytes did not mature (Morton et al., 2008). Future genetic studies in mice will further elucidate the importance of miR-138 in transcription factor patterning in mammalian heart morphogenesis.

miRNA-1 (miR-1) and miR-133 are expressed in cardiac and skeletal muscle beginning at embryonic day 8.5, and have proven to be essential for cardiac development (Cordes et al., 2010; Kwon et al., 2005). In vertebrate hearts, miR-1 (miR-1-1 and miR-1-2) and miR-133 (miR-133a-1, miR-133a-2) are produced as pairs from bicistronic transcripts. MiR-1-1 and miR-133a-2 are produced from the same intergenic region on mouse chromosome 2, while miR-1-2 and miR-133a-1 lie within an intron of Mib1 on chromosome 18 (Chen et al., 2006). MiR-1 and -133 regulate cardiac specification and growth by targeting Hand2 and Cyclin D, and their expression is directly regulated by *Mef2*, *Myocardin*, and SRF (Liu et al., 2008; Zhao et al., 2005). Interestingly, miR-133 has also been shown to target SRF, creating a negative-feedback regulation loop (Chen et al., 2006). Overexpression of miR-1 under control of the βMHC promoter reduces the number of proliferating ventricular cardiomyocytes, with premature exit from the cell cycle

(Zhao et al., 2005). Similarly, exogenous miR-1 introduced to Xenopus embryos caused defective heart development (Chen et al., 2006). In culture, miR-1 promotes myoblast differentiation, while miR-133 promotes proliferation (Chen et al., 2006). The same study was also able to show that miR-1 targets and represses HDAC4. HDAC4 inhibits *Mef2* transcriptional activation, and thus miR-1 enhances expression of *Mef2* targets (Chen et al., 2006). Targeted deletion of miR-1 results in heart malformations, cell cycle dysregulation, and electrophysiological defects. Furthermore, half of the null mice die around embryonic day 15 due to cardiac malfunction and septal defects, likely due to increased Hand2 levels (Zhao et al., 2007). The other half of the mice that survive gestation often die suddenly, usually due to arrhythmias. Surviving hearts also showed increased number of actively dividing cardiomyocytes and cardiac hyperplasia (Zhao et al., 2007).

MiR-133 consists of two genetically identical family members which target Cyclin D2 (Liu et al., 2008). Specific deletion of miR-133a-1 or miR-133a-2 causes no phenotype, however combined deletion results in a reduced embryonic survival rate due to ventricular septal defects (Liu et al., 2008). Mice that survive until birth develop dilated cardiomyopathy and die due to heart failure. Conversely, overexpression of miR-133 resulted in death at embryonic day 13.5, and embryos showed increased Cyclin D2 levels and reduced cardiomyocyte proliferation as assessed by pH3 staining (Liu et al., 2008). *In vitro* overexpression of miR-133 was able to inhibit cardiac hypertrophy (Carè et al., 2007), while the infusion of a miR-133 antagomir into the myocardium caused significant and sustained cardiac hypertrophy. Hypertrophy-related targets of miR-133 include RhoA

and Cdc42, both of which are involved in regulating cardiomyocyte growth (Carè et al., 2007). MiR-133 also targets Nelf-A/WHSC2, a nuclear factor involved in cardiogenesis.

miRNAs -143 and -145 are located on chromosome 18 in mouse and transcribed together as a cluster. Both are expressed in cardiac progenitor cells from embryonic day 7.5 to 16.5. Afterward, they are only expressed in visceral and vascular SMCs (Boettger et al., 2009; Xin et al., 2009). SRF and Myocardin regulate heart morphogenesis and smooth muscle cell gene expression by targeting CArG boxes, which are present and conserved in the upstream enhancer region of miR-143/145 (Cordes et al., 2009). MiR-143 targets Elk1, a SRF cofactor, while miR-145 targets myocardin, Kruppel-like factor 4 (Klf4), and calmodulin kinase II-delta (Camk2d). While primarily being involved in smooth muscle cell proliferation and differentiation in the heart, the latter two genes (Klf4 and Camk2d) have both been characterized as positive regulators of proliferation (Cordes et al., 2009). Genetic deletion of miR-143 or 145 individually, or together causes no obvious phenotype until adulthood. Deficient mice become hypotensive with thinning of the aortic and femoral artery walls, eventually leading to neointimal lesions in old age. Additionally, cardiomyocytes show cytoskeletal disarray and diminished ability to migrate (Boettger et al., 2009; Cheng et al., 2009; Cordes et al., 2009; Xin et al., 2009).

During embryonic development, the primary myosin heavy chain (Myh) gene expressed is the slower-acting βMHC (Myh6). After birth, cardiomyocytes switch to utilizing the αMHC (Myh6) variant which has faster contraction kinetics (Weiss and Leinwand, 1996). Recently, researchers have uncovered the miR-208 family, which is produced from the intronic regions of these two genes. MiR-208a is encoded within Myh6, while miR-208b is encoded within the Myh7 gene. This means that the isotype switch of

Myh expression in the heart results in a miRNA-208 expression switch as well (van Rooij et al., 2009). Furthermore, the miR-208 family has been proven to participate in feedback regulation of their host genes during development and hypertrophy (Callis et al., 2009; van Rooij et al., 2007). Important targets of miR-208a include Gata4 and Cx40, both of which regulate cardiac morphogenesis (Chen and Wang, 2012). Genetic deletion of miR-208a resulted in no immediate phenotype, indicating that it is not essential for embryonic development or cardiac morphogenesis. However, these mice were resistant to stress-induced hypertrophy (Callis et al., 2009; van Rooij et al., 2007). Conversely, overexpression of miR-208a caused increased cardiac hypertrophy, conduction defects, and induction of Myh7 expression (Callis et al., 2009). The role of miR-208b on cardiac development post-birth has not been characterized.

The miR-218 family consists of miR-218a-1, miR-218a-2, and miR-218b, and is highly conserved in vertebrates. The family is found within an intron of slit homolog 2 and 3 (Slit2 and Slit3) and targets Roundabout receptors 1 and 2 (Robo1 and Robo2). Mir-218, Slit2, and Robo are required for proper heart tube formation during embryogenesis (Fish et al., 2011). Tbx5 is another functional target of miR-218 and their expression correlates during development, suggesting miR-218 is involved in cardiac specification and differentiation. Overexpression of Tbx5 and downregulation of miR-218 have similar effects, resulting in heart looping defects and ventricle abnormalities (Chiavacci et al., 2012; Liberatore et al., 2000). Furthermore, downregulation of miR-218-1 can rescue the cardiac defects caused by Tbx5 overexpression (Chiavacci et al., 2012).

The miR-17-92 cluster is a polycistronic gene consisting of 6 miRNAs (miR-17, miR-18a, miR-19a, miR-19b-1, miR-20a, and miR-92-1) processed from the same

transcript (Ota et al., 2004). Due to their regulation of proliferation and differentiation, they have been most widely studied in the context of cancer and are also referred to as Oncomir-1 (He et al., 2005). Recent studies have revealed that the cluster targets the 3'-UTR of Isl1 and Tbx1 to also affect cardiac development. Genetic deletion of the miR-17-92 cluster resulted in failed downregulation of Isl1 and Tbx1 during embryonic development (Wang et al., 2010). After birth, miR-17-92 cluster-deficient mice die during the perinatal period due to lung hypoplasia, thin ventricle walls, and ventricular septal defects (Ventura et al., 2008). In Bmp-deficient mouse embryos, myocardial differentiation is inhibited and there is reduced expression of the miR-17-92 cluster (Wang et al., 2010). Overexpression of the miR-17-92 cluster evokes reduced organ growth and hematopoietic cell differentiation. Also, by directly targeting Isl1 and Tbx1, overexpression the miR-17-92 cluster reduced the number of cardiac progenitors in the second heart field resulting in outflow tract defects (Wang et al., 2010)

1.5.2 MicroRNAs affecting cardiomyocyte proliferation in the perinatal heart

More recently, a connection between miRNAs and the Hippo pathway in heart development has been identified. The miRNA-302-367 cluster consists of 8 co-transcribed polycistronic miRNAs (miR-302a, miR-302a*, miR-302b, miR-302b*, miR302c, miR302c*, miR-302d, and miR-367) (Barroso-delJesus et al., 2008). The cluster is expressed in embryonic stem cells where it acts to maintain a dedifferentiation phenotype and promote cell proliferation. This cluster has also been demonstrated to be expressed in embryonic heart development to regulate cardiomyocyte proliferation. Transgenic cardiac-lineage-specific (Nkx2-5 Cre) deletion of the miR-302-367 cluster caused no obvious phenotype. However, transgenic overexpression had more significant

effects, where overexpression of miR-302-367 in cardiac-lineage specific cells resulted in significant cardiomegaly due to increased cardiomyocyte proliferation (Tian et al., 2015). MiR-302-367 was determined to target the 3' UTR regions of several key regulators of the Hippo pathway: Mst1, Lats2, and Mob1b. Overexpression of miR-302-367 reduced the expression of the Hippo pathway and resulted in increased nuclear-localization of Yap1 (Tian et al., 2015). Mice overexpressing miR-302-367 died by postnatal day 28.

The miR-15 family of genes has also been shown to play a role in neonatal cardiomyocyte maturation by targeting Checkpoint kinase 1 (Chek1) (Porrello et al., 2011a, 2013). Using microarray analysis comparing 1D and 10D hearts, significant upregulation of the miR-15 family was observed. The miR-15 family consists of 6 miRNAs (miR-15a, miR-15b, miR-16-1, miR-16-2, miR-195, and miR-497) which show significant homology and posses identical seed sequences. Between 1D and 10D, miR-195 expression was the most upregulated, although miR-15a, miR-16, and miR-497 expression were also increased (Porrello et al., 2011b). Of three transgenic prenatal-cardiomyocyte-specific (βMHC) overexpression models, two led to perinatal cardiomyopathy and neonatal death. The single viable transgenic line demonstrated a significant reduction in heart weight and died at 5-6 months of age due to slow-onset cardiomyopathy (Porrello et al., 2011b). MiR-15-family loss-of-function using antagomir treatment post-birth resulted in increased pH3+ cardiomyocytes and disorganized sarcomeric structure, although cardiomyocyte size was not affected. Additionally, the authors observed upregulation of Chek1, confirming inhibited expression of this kinase by the miR-15 family. Collectively, these data show that the miR-15 family is the first bona fide miRNA to be implicated in the neonatal cardiomyocyte growth transition.

Novel roles for miRNAs in the heart continue to be discovered and characterized. For example, the miR-130 family includes miR-130a and miR-130b and have been identified as regulators of cardiac development due to repression of the transcriptional co-factor zinc-finger protein friend of GATA 2 (FOG-2). Also, transgenic overexpression of miR-130a causes ventricular hypoplasia and septal defects (Kim et al., 2009). More recently, miR-29a, miR-30a, and miR-141 expression levels were shown to increase dramatically after birth. Antagomir treatment for each of these miRNAs was able to increase the number of cycling cardiomyocytes and increase expression of Cyclin A2 (Zhang et al., 2013). In Figure 7, the same developmental stages and regulators as Figure 2 are shown, however it has been expanded to include the miRNA regulators of each stage.

Here, we have identified a specific miRNA, miR-205, that is expressed and is functionally significant for the fetal-to-adult transitional program. In a previous study, global deletion of miR-205 proved to be neonatal lethal by postnatal day 5 (Farmer et al., 2013). MiR-205 is most abundant in skin stem cells, where it negatively regulates PI(3)K signaling by targeting PTEN to mediate the repression of phospho-Akt and restrict proliferation of skin stem cells (Wang et al., 2013). Due to it's role in the PI3K/Akt pathway, it has also been widely studied in the cancer field, where it is a known tumour suppressor (Zhang et al., 2014). This tumour suppressor role is shared by several other miRNAs that have been shown to inhibit cardiomyocyte proliferation in the neonatal heart (Eulalio et al., 2012).

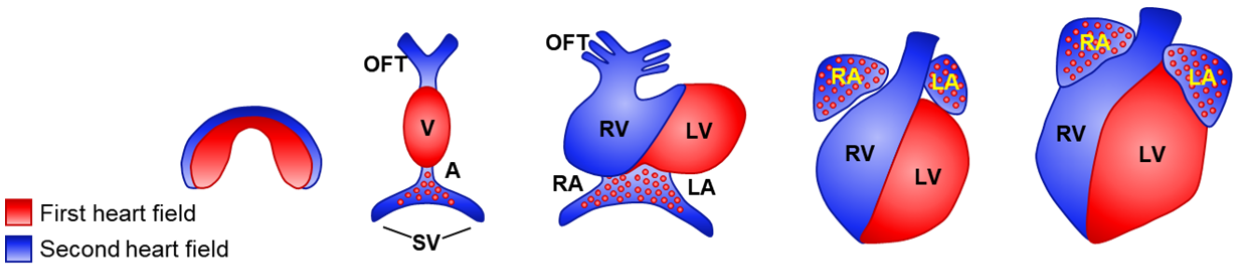

Stage	Cardiac Crescent	Linear Heart Tube	Heart Looping	Chamber morphogenesis	Perinatal Heart
Mouse Age	E7.5	E8	E9 – 12	E10 – 19	E19 – 7D
Regulators	Mesp1/2 Nkx2-5 Isl1 Mef2c Gata4/6 Wnt/β-catenin	Gata4/6 Nkx2-5 Tbx2/3 Tbx5 Tbx20 Mef2c Myocardin SRF Fgf8/10 Hand1/2	Gata4/6 Nkx2-5 Tbx5 Tbx20 Mef2C Hand1/2 Irx4 Bmp Pitx2	Gata4/6 Nkx2-5 Tbx5 Pitx2 Tbx1 Notch1 Bmp Nrg1 Erbb2/4 SRF	Cyclins CDKs CDKIs Meis1 Hippo PI3K/Pten/AKT Fgf1 P38 ZEB1/2 E2F C-Myc Hif1α Rb
Micro-RNAs	miR-138 miR-17-92 miR-302-367	miR-1 miR-17-92 miR-133 miR-138 miR-143 miR-145 miR-208a miR-218 miR-362-367	miR-1 miR-17-92 miR-133 miR-143 miR-145 miR-208a miR-218 miR-362-367	miR-1 miR-17-92 miR-133 miR-143 miR-145 miR-208a miR-362-367	miR-1 miR-15 miR-17-92 miR-29a miR-30a miR-133 miR-141 miR-195 miR-208a → b miR-362-367 miR-497

Figure 7. Regulatory transcription factors at each stage of heart morphogenesis. An illustration of each cardiac development stage is shown above. Embryonic age and key regulators of each stage are displayed below. In addition, the miRNAs involved at each stage are shown below.

Rationale

The complex and interconnected transcription factor networks that govern embryonic heart morphogenesis are well-characterized. After birth, widespread downregulation of pro-proliferative signaling accompanies cardiomyocyte cell cycle withdrawal. Since the discovery of miRNAs, research has identified many critical roles for miRNAs in embryonic heart specification and differentiation. Evidence provided by study of the miR-15 family, miR302-367, and Dicer1 strongly supports miRNAs as mediators of neonatal cardiomyocyte maturation. We reason that a well-orchestrated gene expression and chromatin remodeling event 'locks' cardiomyocytes into a non-proliferative state. Evidently, these genomic remodeling activities are initiated and established during the perinatal heart's transition from hyperplastic to hypertrophic growth. Fully characterizing the transient mRNA/miRNA profile of the neonatal period is critical for a holistic understanding of the transitional process. The fact that micro-RNAs may proceed and promote these reversible epigenetic changes suggests that a therapeutic avenue may exist to reprogram adult cardiomyocytes to restore their proliferative potential.

Hypothesis

We hypothesize that transient expression of regulatory miRNAs may impact the neonatal heart's transition from proliferation to hypertrophy. Where other studies looked at 2 or 3 time-points, our inclusion of 5+ timepoints will identify transient changes occurring during this timeframe. Transiently changing signaling pathways indicate a potential role in the neonatal transition. Further elucidation of these transient effectors will result in new-found regulators of cardiomyocyte indivisibility.

Chapter 2: Materials and Methods

2.1 Microarrays

2.1.1 Microarray processing

One microgram of total RNA was processed through the Affymetrix GeneChip® Whole Transcript Sense Target Labeling Assay kit using Affymetrix GeneChip® Mouse Exon 1.0 ST Arrays (3/timepoint) which covers approximately 1 million exons. There are approximately four probes per exon and 40 probes per gene which allows one to analyze expression at the gene and exon level. For the exon microarrays, three hearts were pooled for each timepoint of interest (E19, 1D, 3D, 5D, 7D, 10D, adult), processed into experimental triplicates, for a total of 63 hearts analyzed over 21 chips.

Profiling was performed in duplicate per timepoint by the Genetic Analysis Facility – The Center for Applied Genomics (TCAG) at The Hospital for Sick Children. The Illumina microarray platform contains a 656 miRNA probe set (611 excluding Solexa microRNAs) based on the Sanger software, Version 12.0. These panels cover approximately 97% of the microRNAs described by the miRBase database at the time of the experiment. For the microRNA microarrays, three hearts were pooled for each timepoint of interest (E19, 1D, 3D, 5D, 7D, 10D, adult), processed into experimental duplicates, for a total of 42 hearts analyzed over 14 chips.

Data was analyzed using Affymetrix ArrayStar, DAVID, and Ingenuity Pathway Analysis. cDNA was normalized through Robust Multi-Array Average (RMA) and gene level analysis was run through a 1-way Analysis of Variance (ANOVA). MicroRNA data

was processed through a Log2 transformation and a 1-way ANOVA. Exon and microRNA expression arrays were normalized differently because of the difference in microarray platforms. Data was examined by comparing each timepoint to the following (i.e. 1 day vs. E19). All statistical results were run through the False Discovery Rate (FDR) algorithm to correct for effects introduced by multiple testing (FDR≤0.05). Post-hoc analysis was performed using Tukey's biweight function. Volcano plots were generated with mRNA and microRNAs using Affymetrix ArrayStar software or Partek software, respectively. To determine the number of significantly differentially expressed genes and microRNAs, lists were filtered at a p-value≤0.05 and ranked by fold-change.

After initial analysis and RT-qPCR confirmation, microarray data was analyzed ontologically using Ingenuity Pathway Analysis. Average-linkage hierarchical clustering and heatmaps of differentially expressed genes were generated using the Morpheus cluster program.

2.1.2 Microarray Validation

Transcripts were quantified from wild-type 129/SV-E mice hearts at embryonic day 19 and 1, 3, 4, 5, 6, 7, 10 days post-birth as well as from adult mice (6-7 weeks). RNA was isolated then DNase-treated using the Promega RQ1 RNase-Free DNase kit (Cat. # M6101) according to manufacturer's recommendation. One microgram of RNA was reverse transcribed via the New England BioLabs (NEB) M-MuLV Reverse Transcriptase System (Cat. # M0253L). cDNA was amplified using the NEB Taq DNA polymerase (Cat. # M0267L) protocol and primers designed through the University of California Santa Cruz (UCSC) Blat and supplied by Integrated DNA Technologies (IDT) (Table 1). All primers

Table 1. Primer sequences used for qPCR confirmation of microarray data

Gene	Sequence	Melting Temp (°C)
Prc1	F: 5'- CCTGTGGAGGCAATTATGACTGGA - 3' R: 5'- TCTCGGCATCATGAAGATGGAGCA - 3'	60 C
Rxrγ	F: 5'- AGAGAAGGTTTATGCCACCCTGGA- 3' R: 5'- TGGGAGTGTCTCCAATGAGCTTGA - 3'	60 C
Pln	F: 5'- AAAGTGCAATACCTCACTCGCTCG - 3' R: 5'- CAGCAGCAGACATATCAAGATGAGGC - 3'	60 C
Mad2l1	F: 5'- GTCCCAGAAAGCCATACAGGATGA - 3' R: 5'- TGAGCGTAGACGGACTTCTTCACA - 3'	60 C
Epas1	F: 5'- CTATGCCTCCCAGTTCCAGGACTA - 3' R: 5'- GGCACGTTCACCTCACAGTCATATCT - 3'	60 C
Asb15	F: 5'- TGGATTACGTCCCTCTGTGTGCAA - 3' R: 5'- AATAAGTATCTTCGCATCG - 3'	60 C
Cdk4	F: 5'- ATTGGATTGCCTCCAGAAGACGAC - 3' R: 5'- AGGCAGAGATTCGCTTATGTGGGT - 3'	60 C
Hif3α	F: 5'- AAGTTCACATACTGCGACGAGA - 3' R: 5'- CGAGTATGTTGCTCCGTTTG - 3'	55 C
Fbxw7	F: 5'- ACACGCTAACAGGACACCAGTCAT - 3' R: 5'- TCTCCAATGTGACGAGGTTTCGGA - 3'	60 C
Pfkm	F: 5'- AAAGAACAGTGGTGGCTGAAGCTG- 3' R: 5'- GCTTCCCAGACCGTTTCCTTGAA - 3'	60 C

were designed to span two separate exons (except for phospholamban (Pln), due to its small size) to prevent amplifying residual genomic DNA. Thermocycler conditions were set as follows: 1 cycle at 95°C for 1min; 35 cycles at 95°C, annealing temperature (AT), and 72°C, for 30sec each; then, 72°C for 5mins. Annealing temperature for each primer set was optimized through melting curve experiments. Ten microliters of PCR products were confirmed by size and charge electrophoresis using a 3% agarose gel in 1X Tris/Borate/EDTA buffer stained with 0.005% ethidium bromide. Amplification products were approximately 200 base pairs (bp). Gene products were analyzed and visualized throughout three independent experiments.

Transcripts were then quantified by relative Real-Time polymerase chain reaction (RT-PCR) using the Roche LightCycler® 480 Multiwell PCR System, the LC480 machine and the LightCycler® 480 SYBR Green I Master kit (Cat. # 0470751600), as per manufacturer's instruction. RNA was isolated then DNase-treated using the Promega RQ1 RNase-Free DNase kit (Cat. # M6101) according to manufacturer's recommendation. One microgram of RNA was reverse transcribed via the New England BioLabs (NEB) M-MuLV Reverse Transcriptase System (Cat. # M0253L). Reaction mix was halved to 10µL with: 1.5µL PCR-grade water, 0.5µL Forward and Reverse PCR primer (5µM), 5µL 2X Master Mix, and, 2.5µL cDNA (diluted 1:5). Annealing temperature and primer sequences may be found within Table 1. PCR primer efficiency was calculated with the slope of a standard curve of known cDNA concentrations at a standard deviation of 0.04 over 4 log quantity differences, run in technical triplicates. CT values from experimental triplicates were normalized to a calibrator (adult heart cDNA), reference

gene (Ppia), and no-template control (NTC), diluted at 1:5. RT-qPCR data confirming expression patterns is found in Figure 8.

2.2 Mouse Models

All experiments were conducted in conformity with the ethical standards set by the University of Ottawa Animal Care Committee, Animal Care and Veterinary Service, and the Canadian Council on Animal Care.

2.2.1 Wild-type Mice

Early experiments, including microarrays and initial analysis of miR-205 expression and localization, were performed using a colony originating from wild-type 129SV mice purchased from The Jackson Laboratory (Stock # 002448).

2.2.2 Cardiac-specific deletion of miR-205: MiR-205$^{fl/fl}$ αMHC^{+} = miR-205$^{-/-}$

MiR-205$^{fl/fl}$ mice were provided to our lab from Dr. Rui Yi from the University of Colorado. These mice in a BL6 background. αMHC^{Cre} mice were purchased from The Jackson Laboratory (Stock # 011038). A schematic of our breeding strategy for the generation of miR-205 cardiomyocyte-specific deletion is shown in Figure 9. Our miR-205 knockout strain was generated by crossing our miR-205$^{fl/fl}$ mice with αMHC^{+} mice to generate mice hemizygous for the miR-205 flox locus, with 50% containing the αMHC promoter locus. MiR-205 hemizygous mice with no αMHC locus were crossed with other hemizygous mice positive for αMHC. These crosses produced pups wherein one quarter were homozygous for the miR-205 floxed allele, and 50% of all pups contained the αMHC locus, resulting in some mice being miR-205$^{fl/fl}$ αMHC^{+}. For the

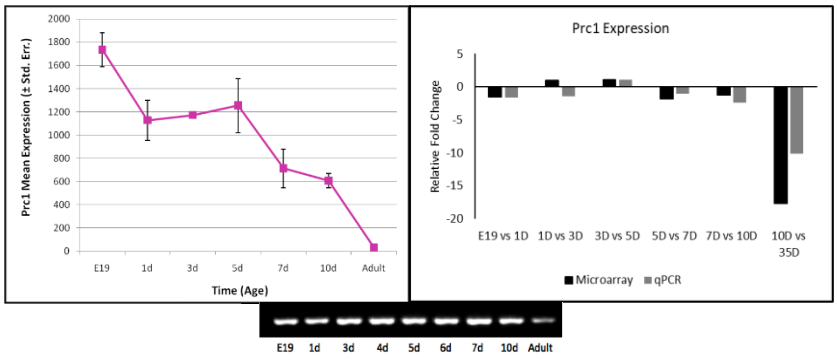
Prc1 Mean Expression (± Std. Err.)
Time (Age)
E19 1d 3d 5d 7d 10d Adult
Prc1 Expression
Relative Fold Change
E19 vs 1D
1D vs 3D
3D vs 5D
5D vs 7D
7D vs 10D
10D vs 35D
Microarray
qPCR
E19 1d 3d 4d 5d 6d 7d 10d Adult

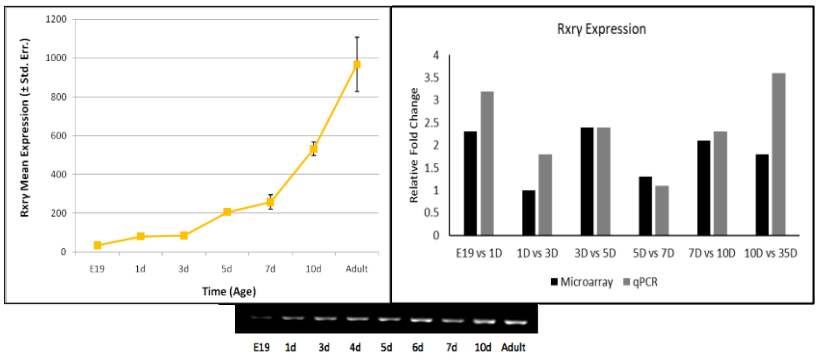
Rxry Mean Expression (± Std. Err.)
Time (Age)
E19 1d 3d 5d 7d 10d Adult
Rxry Expression
Relative Fold Change
E19 vs 1D
1D vs 3D
3D vs 5D
5D vs 7D
7D vs 10D
10D vs 35D
Microarray
qPCR
E19 1d 3d 4d 5d 6d 7d 10d Adult

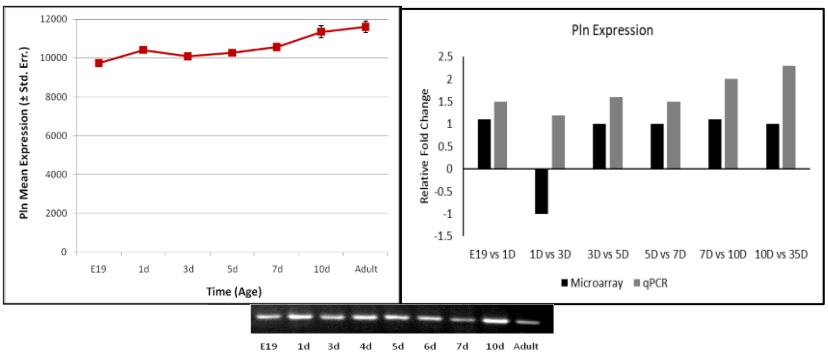
Pln Mean Expression (± Std. Err.)
Time (Age)
E19 1d 3d 5d 7d 10d Adult
Pln Expression
Relative Fold Change
E19 vs 1D
1D vs 3D
3D vs 5D
5D vs 7D
7D vs 10D
10D vs 35D
Microarray
qPCR
E19 1d 3d 4d 5d 6d 7d 10d Adult

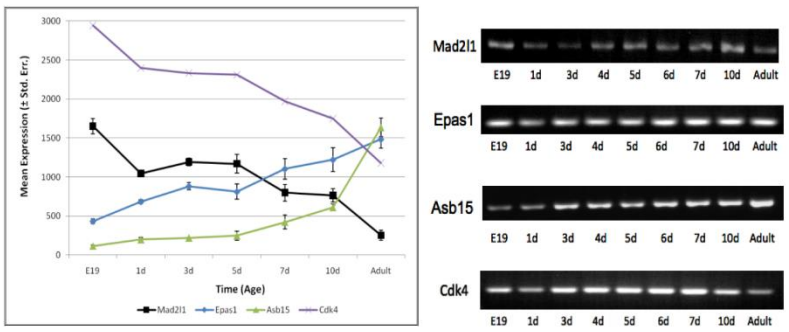
Mean Expression (± Std. Err.)
Time (Age)
E19 1d 3d 5d 7d 10d Adult
Mad2l1
Epas1
Asb15
Cdk4
Mad2l1
E19 1d 3d 4d 5d 6d 7d 10d Adult
Epas1
E19 1d 3d 4d 5d 6d 7d 10d Adult
Asb15
E19 1d 3d 4d 5d 6d 7d 10d Adult
Cdk4
E19 1d 3d 4d 5d 6d 7d 10d Adult

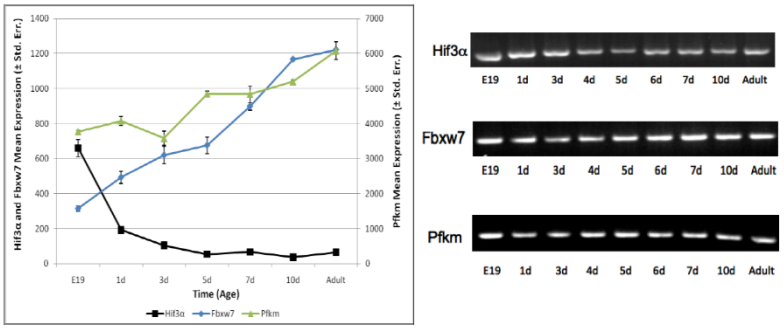
Hif3α and Fbxw7 Mean Expression (± Std. Err.)
Pfkm Mean Expression (± Std. Err.)
Time (Age)
E19 1d 3d 5d 7d 10d Adult
Hif3α
Fbxw7
Pfkm
Hif3α
E19 1d 3d 4d 5d 6d 7d 10d Adult
Fbxw7
E19 1d 3d 4d 5d 6d 7d 10d Adult
Pfkm
E19 1d 3d 4d 5d 6d 7d 10d Adult

Figure 8. RT-qPCR confirmation of microarray data. Transcripts were quantified using the Roche LightCycler® 480 Multiwell PCR System and SYBR Green I Master kit (Cat.# 0470751600), as per manufacturer's instruction. Annealing temperature and primer sequences may be found within Table 1. CT values from experimental triplicates were normalized to a calibrator (adult heart cDNA), reference gene (Ppia), and no-template control (NTC).

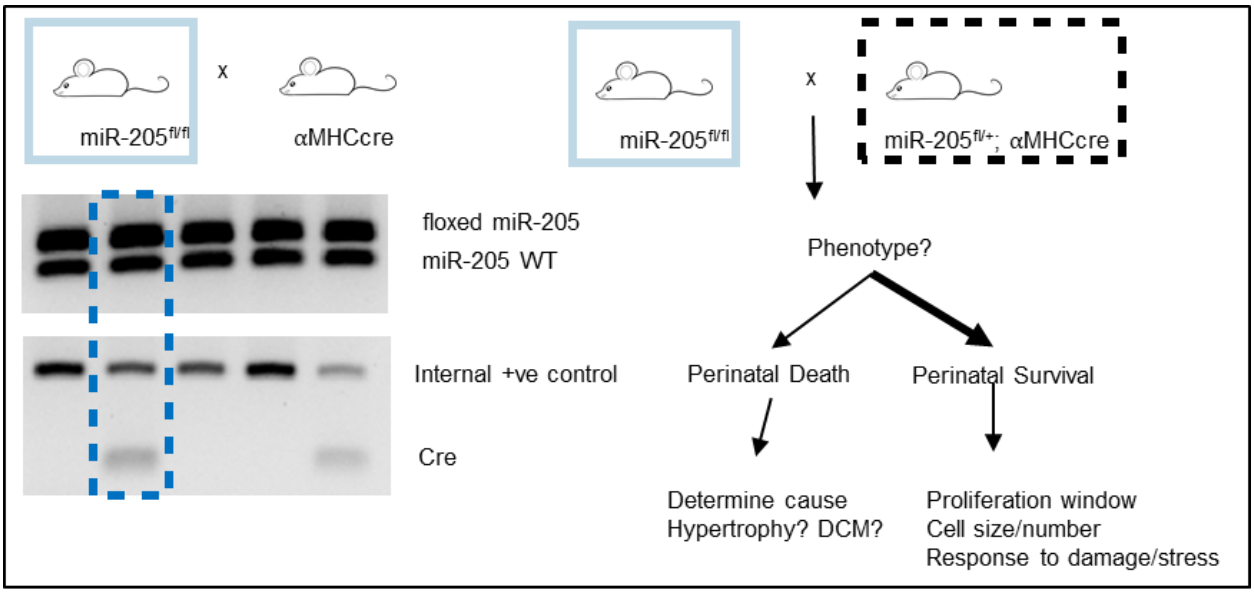

Figure 9. Schematic of the breeding strategy to generate a cardiac-specific miR 205 knockout mouse. Our miR-205 knockout strain was generated by crossing our miR-205$^{fl/fl}$ mice with αMHC^{+} mice to generate mice that are hemizygous for the miR-205 flox locus, with 50% containing the αMHC locus. Hemizygous mice with no αMHC locus were crossed with other hemizygous positive for αMHC. These crosses produced pups wherein one quarter were homozygous for the miR-205 floxed allele, and 50% of all pups contained the αMHC locus, resulting in some mice being miR-205$^{fl/fl}$ αMHC^{+}.

rest of this document, this postnatal-cardiomyocyte-specific deletion genotype (miR-205$^{fl/fl}$ αMHC^{+}) will be referred to as miR-205$^{-/-}$. Genotyping of weanlings showed that cardiac-specific deletion of miR-205 was non-lethal, and that pups were able to survive infancy. Following this, we were able to cross miR-205$^{fl/fl}$ αMHC^{-} with miR-205$^{fl/fl}$ αMHC^{+} mice to generate litters where approximately one half would possess postnatal-cardiomyocyte-specific deletion of miR-205. Littermate miR-205$^{fl/fl}$ αMHC^{-} pups were used as wild-type littermate controls in experiments from chapter 4.

2.2.3 Cardiac-specific overexpression of miR-205: αMHC^{rtTA}/miR-205$^{tetO/DOX+}$ = miR-205^{OE}

To generate a cardiac-specific inducible overexpression of miR-205, two independent mouse lines were generated and crossed with each other. A schematic of our breeding strategy for generation of a miR-205 cardiomyocyte-specific inducible overexpression model is shown in Figure 10.

The first strain is a transgenic mouse hemizygous for a reverse tetracycline transactivator (rtTA) domain downstream of an αMHC promoter. This results in a mouse that constitutively expresses rtTA in any tissue that expresses αMHC, i.e. cardiomyocytes. The rtTA protein targets a specific promoter sequence present in the second mouse strain (tetO). However, this rtTA protein requires coactivation by doxycycline to be functional, meaning that it cannot activate its promoter (whether present or not) unless doxycycline is also present.

The second strain was obtained from Dr. Rui Yi who also provided the miR-205$^{fl/fl}$ mice. This strain contains a hemizygous genetic insertion of miR-205 downstream of a

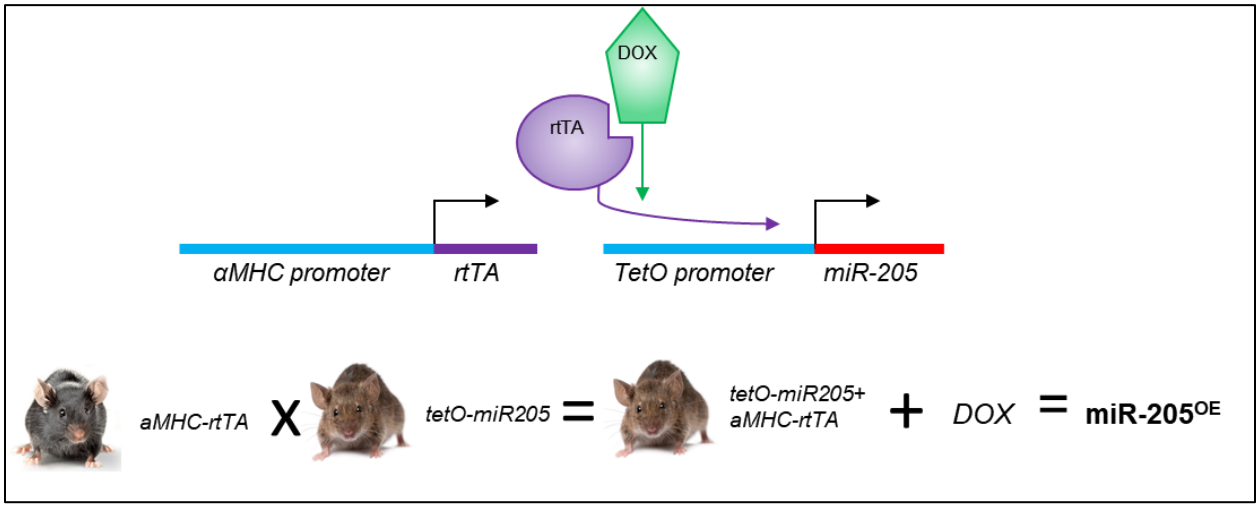

Figure 10. A 2-hit Dox-inducible system was generated to overexpress miR-205 in mice. A reverse tet-transactivator (rtTA) locus was placed under control of the αMHC promoter, while miR-205 was placed downstream of a tetO promoter. In mice that have both loci, the presence of Dox allows the rtTA to bind the TetO promoter and forces the expression of miR-205.

tet-operon. This operon contains a specific promoter targeted and activated by rtTA. When bound to the promoter via coactivation by doxycycline, rtTA forces the transcription of miR-205.

Crossing of these two strains generated offspring in which half would possess the rtTA allele, and half would possess the miR-205^{tet} allele. Mouse cardiomyocytes possessing both alleles would constitutively express miR-205 in the presence of doxycycline. For the remainder of this document, the cardiomyocyte-specific inducible overexpressor of miR-205 in the presence of doxycycline is labeled as miR-205^{OE}.

2.3 Gelatin Zymography

Each sample consists of three pooled hearts with protein extracted using a heart lysis buffer (Recipe in appendix) and run on 10% native gel containing 0.1% gelatin. Samples were loaded at the gel was run at 150V until the marker ran off the gel. Gel was washed 4x 30 min in wash buffer (Recipe in appendix) followed by a 30-minute wash in dH2O. The gel was then incubated overnight at 37°C in digestion buffer (recipe in appendix). The next day, the gel was stained with Coomassie Brilliant Blue solution for one hour followed by destaining until bands were clearly visible. Gels were then dried, mounted and captured using a regular camera.

2.4 DNA/RNA Isolation

For genotyping purposes, genomic DNA was extracted using Sigma RED Extract-n-AMP PCR kit according to manufacturers recommendations. Ear notches were placed in 40µL extraction solution (Cat. # E7526) with 10 µL tissue preparation solution (Cat. #

T3073) and incubated at 55°C for 15 minutes. Tubes were then incubated at 95°C for 10 minutes. After cooling for 1 minute, 40 µL of neutralization buffer (Cat. # N3910) was added to each tube. Follow-up PCR was performed using primers targeting flanking regions of miR-205 or other genomic transgene targets according to the manufacturer's protocol (Cat. # R4775).

RNA isolation was carried out using the TRIzol reagent method (Thermo Fisher Cat. # 15596026). All steps were performed at room temperature unless noted. Heart samples were pooled and digested in 1ML TRIzol reagent and incubated for 5 minutes. 200µL of chloroform (Sigma Cat. # 288306) was added to each tube and incubated for 3 minutes. Tubes were centrifuged at 12,000 RCF for 15 minutes at 4°C. The upper aqueous phase containing RNA was transferred to a new tube. 500µL of isopropanol (Fisher Cat. # 26181) was added to each sample and incubated for 10 minutes. Tubes were then spun at 12,000 RCF for 10 minutes at 4°C. Supernatant was discarded and the pellet was resuspended in 1mL of 75% ethanol. Tubes were spun at 7,500 RCF for 5 minutes at 4°C and supernatant was discarded. Pellets were then air dried for 5 minutes and resuspended in 50µL of RNAse-free H20. Samples were then incubated at 55°C for 10 minutes. RNA concentration was measured using a NanoDrop spectrophotometer and purity was assessed using A260/280 (A ratio of 1.9 or higher was considered pure enough for follow-up experiments).

2.5 Western Blot Analyses.

Hearts were collected from mice at specific ages (1D, 3D, 5D, 7D, 10D, and 14D) along with a tail sample to be genotyped. Hearts from mice with the same genotype were

pooled (n=3) and homogenized in heart lysis buffer (recipe in appendix) using a Polytron Homogenizer with a 7mm generator. Lysates were then rotated at 4°C for 10 minutes, then centrifuged at 12,000XG for 15 minutes. Supernatant was aliquoted into new tubes and stored at -80°C until used for SDS-PAGE sample preparation. For SDS-PAGE protein samples, Bradford protein assay was used to measure protein concentration and adjust it to 1.5µg/µL. Loading samples also consisted of 1X loading dye (Cell Signaling Cat. # 56036) and 1X DTT (Cell Signaling Cat. # 14265) and were boiled for 5 minutes (Recipe in appendix). Samples were stored at -80°C. For each western blot, 30µg total protein (20uL protein lysate sample) was loaded into 4-15% gradient SDS-PAGE gels (BioRad Cat. # 4561093) and run in a Tris-Glycine-SDS buffer at 150V for 45 minutes, or until the lane marker was near the bottom of the plates. Blotting was performed using a Transblot Turbo (BioRad Cat. # 1704150) onto 0.45um polyvinylidene difluoride (PVDF) membrane (Thermo Fisher Cat. # 88518) using manufacturers recommendations. For large or small proteins, the “high MW” or “low MW” settings were used, respectively. Membranes were then blocked for one hour in 5% bovine serum albumin (BSA), followed by overnight probing by specific antibodies diluted in 5% BSA. Membranes were briefly rinsed with tris-buffered saline (TBS) containing 0.1% Tween-20 (TBST) followed by 3 five-minute washes in TBST. The membrane was then incubated with secondary antibody diluted in 5% BSA for one hour at room temperature. Finally, another rinse with TBST and 3 five-minute washes with TBST were carried out. Blotting was visualized by electrochemiluminescence using Clarity substrate (BioRad Cat. # 1705060) on Chemidoc XRS+ (BioRad Cat. # 1708265) imaging hardware.

2.6 MiR-205 RT-qPCR

Hearts were collected from miR-205 wild-type, knockout, and overexpressing mice at 1d, 3d, 5d, 7d, and 10d until at least 3 hearts of each genotype were processed. Immediately after collection hearts were snap frozen in liquid nitrogen and stored at -80°C. Total RNA was purified using the Trizol method according to manufacturer's directions. MiR-205 was selectively reverse transcribed using ThermoFisher's Taqman miRNA Assay (ThermoFisher Cat. # A25576). As a control, U6 snRNA was also selectively reverse transcribed using the same product (Thermo Fisher Cat. # 4427975). After the RT reaction, qPCR was performed using the RT-qPCR portion of the Taqman miRNA Assay kit. Reactions were run on 96- or 384-well plates in a Roche Lightcycler 480 (Roche Cat. # 05015278001) according to Taqman manufacturer's directions.

2.7 Sectioning, Staining, Immunohistochemistry and Immunofluorescence

Hearts were collected as described in sections 2.5 and 2.6. Hearts were fixed in 10% formalin for 48 hours followed by 3x 30-minute washes in PBS and then stored in 70% ethanol. Tissue embedding (paraffin) and sectioning was performed the histology core at the University of Ottawa. Hearts were sliced in a 4-chamber view near the middle of the heart. Any H&E or Masson Trichrome staining was performed by the uOttawa histology core.

For immunofluorescent analysis, slides were submerged in xylene 3x for 5 minutes each, then 2x 10-minute washes in 100% ethanol. This was then repeated in 95% ethanol, followed by 2x 5-min washes in dH_20. Slides were then submerged in a 1ug/µL wheat germ agglutinin (WGA) (Thermo Fisher Cat. # W6748) solution for 10 minutes. Slides

were then washed in dH_20 3x for 5 minutes. Next, the slides were submerged in a 4′,6-diamidino-2-phenylindole (DAPI) solution (Sigma Cat. # 10236276001) for 5 minutes, followed by 3x 5-minute washes in dH_20. A drop of Dako mounting media (Agilent Cat. # S3023) was placed on each section and coverslips were placed on top and slides were left to dry for 1 hour. Coverslips were sealed using nail polish.

Immunohistochemistry was performed following the Cell Signaling SignalStain Boost Detection Reagent manufacturer's protocol. Slides were deparaffinized in as described in the previous paragraph, followed by citrate unmasking (Cell Signaling Cat. # 14746) in coplin jars at 90°C for 10 minutes. After the slides cooled, they were washed in dH_20 3x for 5 minutes. Slides were incubated in 3% hydrogen peroxide for 10 minutes and then washed again in dH_20 3x for 5 minutes. Slides were moved to a humidified chamber and a PAP pen (Thermo Fisher Cat. # 008899) was used to create a hydrophobic circle around the sections. Sections were blocked using 200µL of Cell Signaling Animal-Free Blocking Solution (Cell Signaling Cat. # 15019), then placed directly on the sections for 1 hour at room temperature. Blocking solution was removed and replaced with antibody diluent (Cell Signaling 8112) containing primary antibody for the protein of interest (YAP, Ki67, pH3 overnight. Antibody catalogue numbers and dilutions are provided in Table 2. The next day, slides were moved back into coplin jars and washed in dH_20 3x for 5 minutes. Slides were moved back to a humidified chamber and three drops of SignalStain Boost Detection Reagent (Cell Signaling Cat. # 8114) was placed onto the sections, followed by incubation at room temperature for 30 minutes. Slides were then washed again. DAB chromogen concentrate was diluted by diluting 30µL into 1mL of DAB Chromogen Diluent (Cell Signaling Cat. # 8059) . DAB Chromogen

Table 2. Antibody Information List

Antibody	Vendor	Catalogue #	Dilution
CDK1	Santa Cruz	8395	WB: 1:1000
P-CDK1	Santa Cruz	136014	WB: 1:1000
DICER	Cell Signaling	5325	WB: 1:1000
GAPDH	Thermo Fisher	AM4300	WB: 1:1000
Ki67	Cell Signaling	9027	IHC: 1:400
LATS1	Cell Signaling	3477	WB: 1:1000
αMHC	Abcam	50967	WB: 1:1000
MOB1	Cell Signaling	13730	WB: 1:1000
P-MOB1	Cell Signaling	8699	WB: 1:1000
MST1	Cell Signaling	3682	WB: 1:1000
pH3	Cell Signaling	9701	IHC: 1:200
PTEN	Cell Signaling	9188	WB: 1:1000
P-PTEN	Cell Signaling	9551	WB: 1:1000
Rb	Cell Signaling	9309	WB: 1:1000
P-Rb	Cell Signaling	9307	WB: 1:1000
SAV1	Cell Signaling	13301	WB: 1:1000
YAP	Cell Signaling	14074	WB: 1:1000 IHC: 1:200
P-YAP	Cell Signaling	13008	WB: 1:1000

solution was then applied to each section for up to 10 minutes, followed another 3 washes. The sections were then dehydrated by briefly (10 seconds) submerging them in 95% ethanol 2x, 100% ethanol 2x, and finally xylene 2x. Sections were then mounted using DPX mountant (Sigma 44581).

2.8 *In-situ* hybridization

For *in situ* hybridization, hearts were collected from 5-day-old wild-type mice and immediately mounted in optimal cutting temperature (OCT) compound (Agar Scientific Cat. # AGR1180) and flash frozen in liquid nitrogen. Once frozen, hearts were stored at -80°C until sectioned. Heart sectioning was performed by the Histology core at the University of Ottawa. Heart sections were defrosted at room temperature for one hour. A miR-205-specific RNA probe (Qiagen Cat. # YD00616714) was then diluted 1:200 in hybridization buffer (recipe in appendix) to a final concentration of 200ng/µL. Tubes were briefly vortexed and then denatured for 10 minutes at 70°C. Tubes were briefly spun and 300µL of probe mixture was applied onto the tissue sections on the slides. Cover slips were placed overtop and slides were incubated overnight at 65°C in a humidified chamber. The next day, coverslips were gently removed, and slides were transferred to a coplin jar. They were washed 2x for 30 minutes at 65°C in solution A (recipe in appendix), followed by 2x 30-minute washes at room temperature in 1x TBS-T.

Slides were then moved back to the humidified chamber and 300µL of 10% heat-inactivated fetal bovine serum (FBS) (Thermo Fisher Cat. # 16000044) was used to block sections for one hour at room temperature. Blocking buffer was then removed and 300 µL of anti-Dig Fab fragments (Sigma-Aldrich Cat. # 11093274910) in 10% heat-

inactivated FBS in 1x TBS-T (1µL AP + 0.9mL TBST + 0.1mL FBS). Coverslips were placed on top and incubated overnight in a humidified chamber at 4°C.

Slides were placed back into coplin jars and washed 5 times for 20 minutes in 1x TBS-T. Coverslips naturally fell from the slides after the first wash. Next, slides were incubated in NTMT solution (recipe in appendix) 2x for 10 minutes at room temperature. Slides were moved back to the humidified chamber, then stained with NBT/BCIP in NTMT at room temperature in the dark to achieve desired contrast. The reaction was stopped by two washes in distilled water. Slides were fixed in 4% paraformaldehyde (PFA) for 20 minutes, then washed in distilled water twice. Slides were then mounted with Dako mounting media (Agilent Cat. # S3023) and a coverslip, dried at room temperature, and then sealed with nail varnish.

2.9 Microscopy

All microscopy was performed on Zeiss Axio Observer with colour and fluorescent cameras. To begin, the microscope light source was centered and focused. Initial visualization was observed at 10x by eye before switching to captured video on a computer. Images were captured using either fluorescent or colour cameras. The associated Zen and AxioVision software was used to adjust objective, wavelength, exposure, and colour balance. With each experiment, these settings were adjusted for the first slide (observer was blinded to the genotype of the sample at the time of imaging) and the same parameters were used for the rest of the slides in the experiment. With each heart section, pictures of the same locations were taken for uniformity in future

quantification. Ki67 and WGA/DAPI staining was visualized at 20x magnification and pH3 was visualized at 10x magnification.

Follow-up image analysis was completed using the FIJI processing package for ImageJ. Quantification of Ki67 and pH3 was carried out by marking each positive nuclei in a given area and inputting the number into Excel. For Ki67, an area of 500µm by 500µm was counted. For pH3, the entire field of view in the microscope image was used (approx. 1cmx1cm). For quantification of cell number, WGA stained cells were counted similarly to Ki67 and pH3-positive cells above, marking each and logging the number. For these counts, an area of 200µM by 200µM was counted. For isolated cardiomyocytes, images were taken such that there were 10-50 cardiomyocytes visible, with minimal clumping and overlap of cells. Each distinct cardiomyocyte's length and width was measured. Area was calculated as length x width of cardiomyocytes. Statistical analysis was performed by comparing experimental groups to wild-type control groups using student's t-test ($p<0.05$). When comparing multiple experimental groups, one-way analysis of variance (ANOVA) was performed to test significance ($p<0.05$).

2.10 Echocardiography

Echocardiography was performed using VisualSonics Vevo 2100 preclinical echocardiography imaging system and analyzed using the associated Vevo software. Mice were anesthetized using 1L/min O_2 with 5% isofluorane for induction, and 2% isofluorane for maintenance. Once anesthetized, the chest of each mouse was initially shaved with an electric razor and then depilated using Nair cream. Mice were then placed supine on a heated pad with a nose cone providing 2% isofluorane. Conductive Redux

electrolyte cream (Thermo Fisher Cat. # PKR66) was applied to four electrodes on the heated pad and the four limbs of the mouse were secured to them using surgical tape. Aquasonic ultrasound gel (Thermo Fisher Cat. # PKR01) was applied to the chest area and the probe, secured onto a crank-controlled mount, was lowered until a beating motion was observed by the ultrasound software. The probe was then aligned in such a way that both the apex of the heart and the aortic valve could be observed, with the papillary muscle moving into frame with each beat of the heart. This precise positioning ensured that the exact same dimensions of the heart were being measured in each mouse. B-mode imaging was used to measure left ventricular systolic and diastolic diameter, length, and area. Next, the ultrasound probe was rotated 90 degrees and M-Mode imaging was used to generate a temporal reading of ventricular diameter during systole and diastole. This mode allowed for more precise measurement of ventricular diameter. Using these measurements, left ventricular (LV) volume, stroke volume, ejection fraction, fractional shortening, and ventricular mass were calculated.

Chapter 3: A rapid and efficient method for the isolation of postnatal murine cardiac myocyte and fibroblast cells

Weldrick JJ, Abdul-Ghani M, Megeney LA, Burgon PG. *Can J Physiol Pharmacol*. 2018 May;96(5):535-539. doi: 10.1139/cjpp-2017-0742. Epub 2018 Mar 13

In the cardiac research field, there were previously only 2 main strategies utilized for the isolation and culture of murine cardiomyocytes. The neonatal method involves overnight tryptic digestion of hearts, and only works on cardiomyocytes isolated from mice under 3 days of age. Otherwise, the Langendorff method involves threading of the aorta onto a perfusion apparatus to digest the heart with collagenase. This method can only be performed on adult mouse hearts due to the aortic threading being extremely difficult to impossible on young mice. This left a gap between 3 days and adulthood where individual mouse cardiomyocytes could not be isolated and studied. With inspiration from the 2 methods mentioned above, we sought to establish a novel method for cardiomyocyte isolation that could be used on mice of any age. We successfully generated an apex-perfusion-based method utilizing both trypsin and collagenase digestion of hearts. This method was used for several experiments in our lab as well as for collaborative experiments such as “Cardiotrophin 1 stimulates beneficial myogenic and vascular remodeling of the heart” by Abdul-Ghani et al. (2017). The detailed method is described in the following chapter.

3.1 Introduction

Although the medical community has made great strides in reducing the morbidity and mortality from heart disease, it remains one of the leading causes of death worldwide(Go Alan et al., 2014). Both basic and translational researchers in the cardiac

field continue to develop and refine their methods and techniques to improve our understanding and treatment of heart disease (Ackers-Johnson et al., 2016; Gao et al., 2010). Historically, two mouse cardiomyocyte (CM) isolation methods have played a critical role in advancing our general knowledge of CM biology; i) the Langendorff isolated perfused adult heart model (Bell et al., 2011) and ii) neonatal ventricle CM isolation (Vidyasekar et al., 2015). Currently, the Langendorff method is the standard robust isolation method to study adult CMs, however it can be a significant technical challenge that involves cannulation of the ascending aorta followed by retrograde perfusion of the left ventricle and coronary arteries with a Krebs/collagense buffer (Bell et al., 2011). Neonatal CMs can also be isolated from very young mice (< 3 days old) using a multiple-day protocol that involves tryptic digestion (Vidyasekar et al., 2015). These two methods are widely used for the isolation of CMs. However, these methods both have several limitations. Most importantly, these two current methods do not provide an approach that can be used to easily isolate CMs from any post-natal heart, regardless of age. Here we report a novel CM isolation strategy that allows for the isolation of CMs from murine postnatal heart regardless of age that we have successfully utilized in two recent studies (Abdul-Ghani et al., 2017; Jiang et al., 2015).

We are specifically interested in studying the perinatal heart – that is the heart during late embryonic development and neonatal development (E19 to P14), and so studying isolated CMs from these time points is critical. Isolating cells from early time points (E19 to P3) may be accomplished using the previously described neonatal method, however to conduct similar CM analysis across an aging cohort there is no consistent method for retrieving variable-aged CMs. Our goal was to develop a new approach that

utilizes the beneficial aspects of both the Langendorff (collagenase perfusion) and the neonatal (collagenase/trypsin) method of CM isolation to create a universal procedure that can be used to isolate CMs and cardiac fibroblasts from mice of any age.

3.2 Materials and Methods

All the mice were studied according to protocols approved by the Institutional Animal Care Committee in accordance with the Canadian Council on Animal Care's Guide to the Care and Use of Experimental Animals and the Animals for Research Act.

All steps were performed in a laminar flow biosafety level 2 cabinet and sterile technique was used to prevent contamination. A diagram of the perfusion apparatus is shown in Figure 11A. Perfusion tubes were cleaned with 70% ethanol for 5-10 minutes followed by several rinses with distilled water. The tubes were then filled with Perfusion Buffer (recipe in appendix A) before beginning the isolation. Injection of heparin into mice is not required.

Mice were anesthetized by injecting Avertin (0.4mg/g) intraperitoneally. Mice were then secured in surgical position using medical tape. Next, the thoracic cavity was opened to expose the heart. A syringe pump was then used to begin pumping pre-warmed (37˚C) Perfusion Buffer through the needle. A heat exchanger should be used to continue warming the solution as it is pumped (Figure 11A). For neonatal mice, we used a 30g needle with a flow rate of 2mL/min, while in fully grown adult mice we used a 26g needle with a flow rate of 4mL/min. Each of these factors (syringe size, needle gauge, and flow rate) must be adjusted based on mouse size/age. To ensure proper coronary artery perfusion, it is essential to achieve a flow rate from the needle that produces a strong, continuous flow as pictured in Figure 11B. After the perfusion buffer was flowing, the

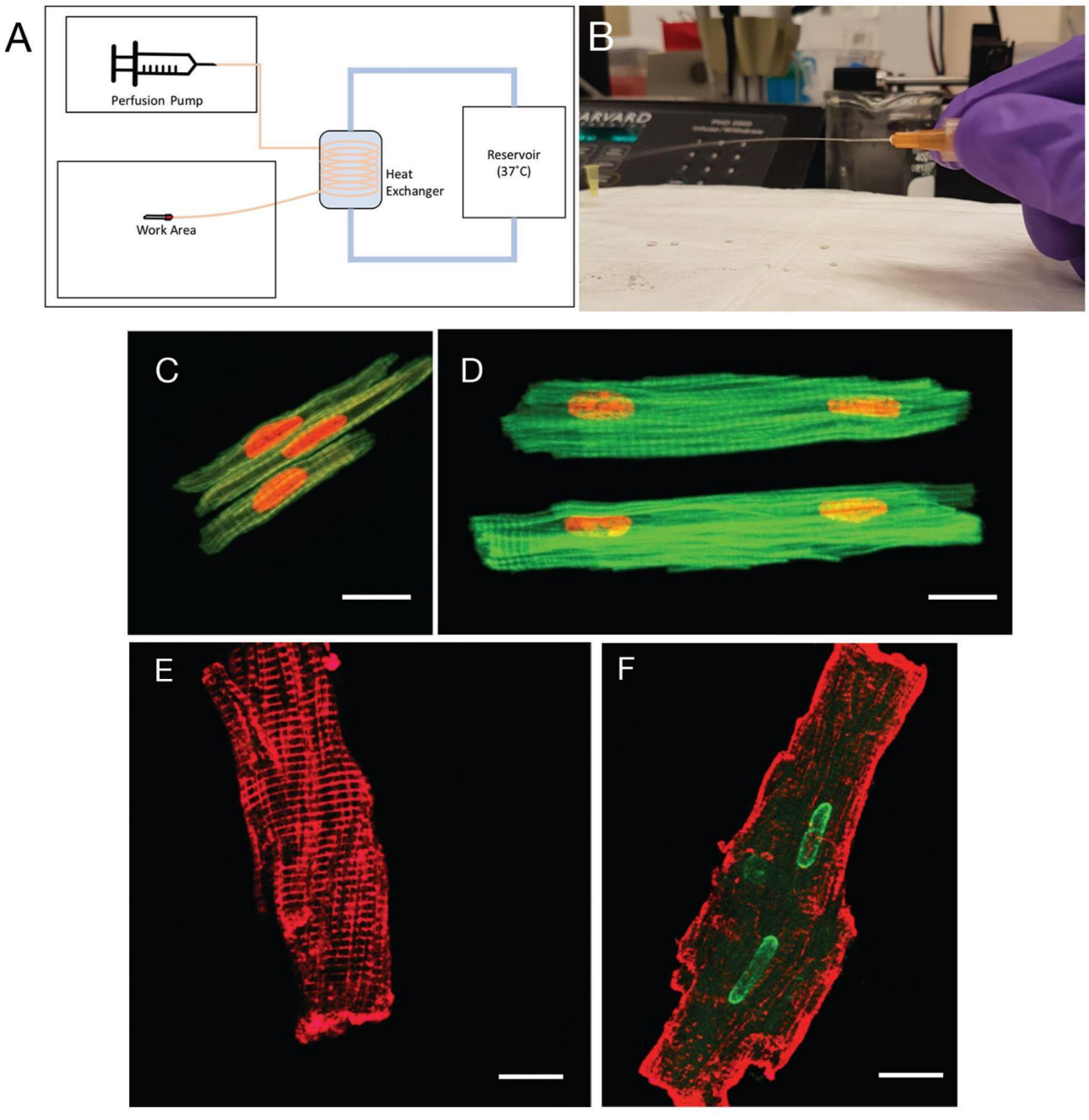
A
Perfusion Pump
Heat
Exchanger
Reservoir
(37˚C)
Work Area
B
C
D
E
F

Figure 11. Cardiomyocyte (CM) isolation perfusion apparatus and flow rate. (A) Isolation apparatus includes a syringe mounted on a syringe pump, a heat exchanger, and a tube connecting the syringe to a needle through the heat exchanger. (B) Flow rate on the syringe pump should be adjusted such that a strong, steady flow is achieved. For neonatal mice, a flow rate of2 mL/min of perfusion buffer flowing through a 30-gauge needle is sufficient. For adults, a flow rate of4 mL/min through a 26-gauge needle is sufficient. CMs isolated from a (C) 3-day-old heart and a (D) 14-day-old heart. Cells were stained with phalloidin (green) and propidium iodide (red). (E and F) CMs isolated from a 3-month-old heart stained with phalloidin (red) and lamin A/C (green). Scale bars = 10µm.

needle was inserted into the left ventricle through the apex of the heart while the right atrial appendage was severed. The mice were then perfused for 2-5 minutes, depending on mouse age (2 minutes for early neonates, 5 minutes for adults).

After perfusion, the heart was carefully removed and placed into a 15mL tube containing Stop Buffer (recipe in appendix A) and incubated at 37˚C for 10 minutes. The heart + Stop Buffer was then poured into a 60mm petri dish, and the heart was quickly minced into small (1mmx1mm) pieces. To promote dissociation of cells from the extracellular matrix (ECM), gentle trituration (10-20 times) of tissue with a wide-bore pipette (smooth edged to limit sheering) was performed. A 100µm nylon mesh filter (Fisher 352360) placed in a 50mL conical tube was then used to filter out large debris. Cells were then centrifuged at 50xG for 5 minutes to pellet CMs. When performing the isolation from adult mice (>10 weeks), tubes can be left in the bio-hood for 10-15 minutes, and CMs will settle to the bottom of the tube. At this point, the supernatant can be removed and centrifuged again at 2000xG for 5 minutes to pellet cardiac fibroblasts, which can also be cultured for use in experiments.

The CMs were then resuspended in media, and a pre-plating step was performed to remove any non-CMs in the pellet. After 2 hours of pre-plating, CMs were moved to a gelatin-coated ExCellness (01.100.100.00) plate and incubated overnight. When media (recipe in appendix A) is changed daily, CMs can live in culture for up to 24-48 hours. Alternatively, after CMs have been pelleted, they can be resuspended in 10% neutral buffered formalin and fixed for 15 minutes in suspension. Cardiomyocytes can then be gently spun down onto glass slides with a Cytospin (Fisher A78300003) and be used immediately for staining and immunofluorescence.

3.3 Results

The primary limitation for any CM isolation method is to establish the conditions by which a digestion buffer could be delivered efficiently to the coronary arteries, to break down the extracellular matrix and release intact cells from the heart. Typically, whole body fixation is accomplished by delivering fixative via the left ventricle, using a syringe or pump, such that the fixative can permeate throughout the circulatory system(Gage et al., 2012).

We used a syringe pump with a 30-gauge needle to deliver digestion buffer at a high flow rate (2ml/min) with constant pressure (Figure 11A). Using the method described, we perfused 3-day-old and 14-day-old old pup via the left ventricle for 2 minutes. The heart was excised and placed in a pre-warmed Krebs buffer containing BSA and incubated for 10 minutes at 37°C. After 10 minutes, the heart was cut into several small fragments and then gently triturated. Single cells were separated from large tissue pieces using a 100micron filter. The filtrate was then gently centrifuged (50g). The pellet was resuspended in 10% neutral-buffered formalin for 15 minutes then spun again. Afterward, the pellet was gently disrupted, and the cell suspension was spun onto a glass slide using a cytospin apparatus. The isolated CMs were stained with phalloidin (Fisher A12379)/propidium iodide (Fisher P1304MP) and visualized under a fluorescence microscope (Figure 11C&D).

To demonstrate the utility of this new method, we measured the cellular dimensions of CMs isolated from hearts that were chronically stimulated with phenylephrine (PE). PE is commonly used to induce pathological cardiac hypertrophy, and a hallmark of this organ growth is an increase in cardiac cell size (Maillet et al., 2013).

Osmotic pumps were implanted into two groups of mice, with one group being infused with saline while the other group was infused with PE for a two-week period. Using our new method for CM isolation, we have successfully isolated cells from 18 adult mouse hearts in one day. The cells were stained with a fluorescently labeled phalloidin and DAPI and were subsequently visualized with a fluorescent microscope (Figure 12A). As shown in Figure 12, CMs isolated from mice treated with PE exhibited increased cell width ($p<0.001$) and area ($p<0.001$) when compared to PBS treated mice, indicating that the PE treatment on mice caused concentric CM growth leading to pathological hypertrophy.

3.4 Discussion

The significant advantage of the method we have developed and described is that CMs can be isolated from mice or rats of any age, and processed for alterations in morphology and structure. Another advantage of this method compared to others is the duration of the isolation procedure. It is not unreasonable to expect to isolate cells from 5-7 adult hearts in an hour when working alone, not including preparation of buffers nor time spent culturing cells. This number is substantially increased when working in a pair (10-15 per hour), or when isolating from neonatal hearts as the perfusion time is reduced. Langendorff based CM isolations typically take 40-60mins per adult heart and require a specialized perfusion apparatus. Another beneficial outcome of this method is that during perfusion, all blood is evacuated from the vasculature, ensuring no erythrocyte contamination in the isolated cells without performing a red blood cell lysis step. Previous studies using perfusion in other tissues have noted that elimination of erythrocyte contamination is essential for producing high-quality images and isolated cells (Assmus et al., 2010; Chow et al., 2005; Toyota et al., 2002).

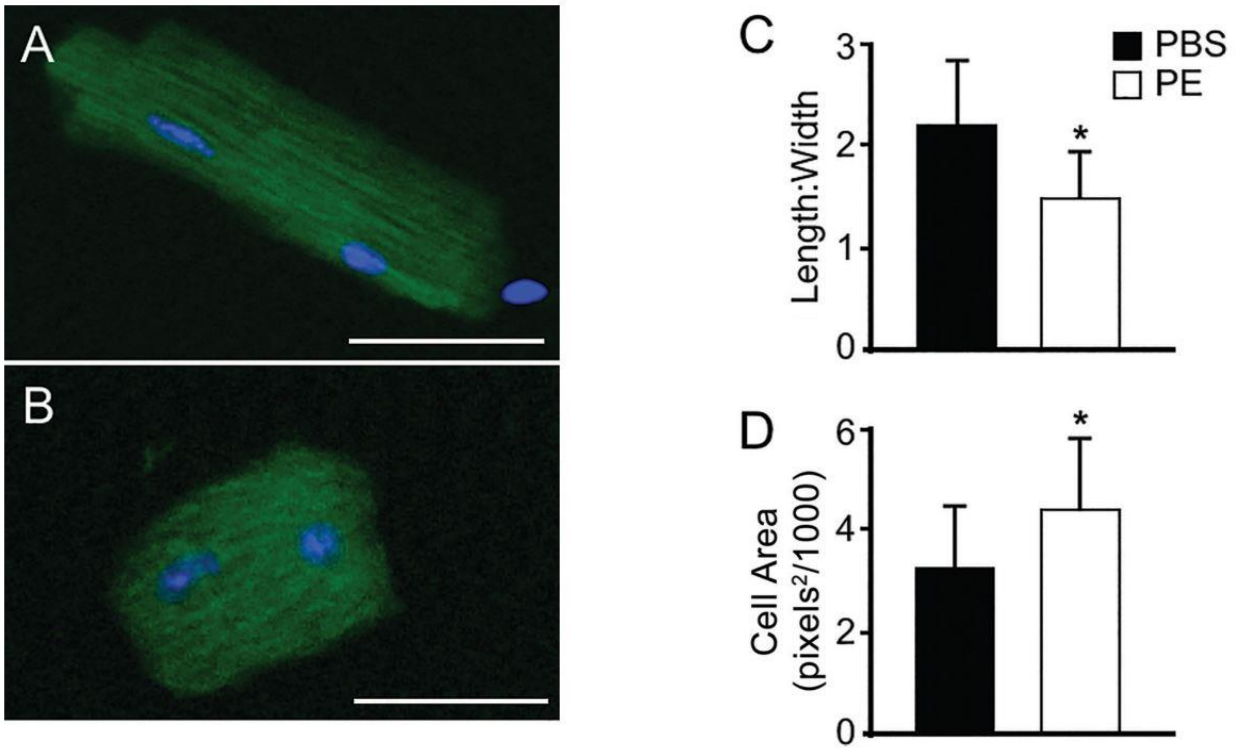

Figure 12. Isolation of cardiomyocytes (CMs) for cell measurements upon phenylephrine (PE)-treated hearts in vivo. (A and B) Representative images of PBS-treated (A) and PE-treated (B) CMs isolated using the perfusion-based method (n = 6 mice per time point). (C and D) CMs treated with PBS or PE were measured (n > 100 cells measured per group) and average length/width ratio and cell area are displayed. PE-treated cells are significantly wider and larger in area compared with PBS-treated cells. Student's t test was used to test for significant differences. *, $p < 0.001$. Scale bars = 50µm.

We have successfully cultured these freshly isolated CMs overnight and have not cultured them for long periods of time. The overnight cultures retain their rod-shaped phenotype. Long-term culturing of rodent CMs has been problematic, as adult rat CM cultured cells do not retain their phenotype over time whereas adult guinea pig ventricular myocytes retain their phenotype (Horackova and Byczko 1997; Horackova and Mapplebeck 1989).

In summation, we have now established an efficient and reproducible method for rapid CM isolation from postnatal murine hearts of any age. We envision that this method will have broad utility, allowing rapid and efficient isolation of all cell types that comprise the post-natal heart, including CMs, endothelial cells and fibroblasts. Furthermore, these cell types can be separated and studied individually using flow-assisted cell sorting (FACS). We also believe that the method can be readily scaled and adapted for the isolation of CMs from larger animal models.

Finally, this method was used for collaborative experiments such as “Cardiotrophin 1 stimulates beneficial myogenic and vascular remodeling of the heart” by Abdul-Ghani et al. (2017). Mice were treated with exogenous cardiotrophin 1, and our method was used to isolate and measure cardiomyocyte size after the induction of hypertrophy. Cardiotrophin-1-treated hearts were significantly larger than wild-type, however maintained the same length-to-width ratio. This is in contrast to PE-treated hearts which are larger, but primarily due to eccentric pathological growth.

3.5 Acknowledgements

This work was supported, in whole or in part, by Canadian Institutes of Health Research Grants to P.G.B. and L.A.M. as well as support the Heart and Stroke

Foundation of Canada Grant to P.G.B. Jonathan Weldrick was a recipient of the Queen Elizabeth II Graduate Scholarship in Science and Technology (QEII-GSST) and a University of Ottawa Excellence Scholarship.

Chapter 4: Identification and analysis of the perinatal transitional gene program

Soon after birth, cardiomyocytes cease to divide, and the subsequent increase in myocardial mass is accomplished by growth in the size of the individual cells (Brooks et al., 1998). This growth strategy is universally conserved in mammals. The mammalian heart's ability to proliferate is lost shortly after birth (Porrello et al., 2011a). However, very little information is available regarding the regulatory factors that manage the expression of growth regulators and how such factors manage the irreversible shift in cardiac cell proliferation.

Several studies have previously aimed to identify major changes occurring during this period, however these studies often suffer from a lack of temporal resolution. Most studies using two timepoints (i.e comparing 1D vs 10D or 1D vs adult) are not able to identify transient changes occurring over the course of days. We expected, and confirmed, that many important genetic alterations were being missed due to the lower resolution of previous studies. To address this issue, we executed a high-resolution microarray analysis (embryonic day 19 (E19), 1-day (1D), 3D, 5D, 7D, 10D and 35D) of the neonatal period to identify transcripts which have varying expression throughout the neonatal period.

Bioinformatic analyses using DNAStar: ArrayStar, Partek, and Ingenuity Pathway Analysis revealed valuable clustering data that was used to better characterize the neonatal transition. In parallel, we also performed microarray analysis for miRNAs expressed during the neonatal period as we hypothesized that miRNAs are a key regulator of the transitional program. By using the approach as is taken during early cardiac development, we were able to identify and characterize a neonatal transitional

program that promotes cell cycle withdrawal, and thereby inhibits cardiomyocyte proliferation to establish the adult physiologic growth program of cardiomyocytes.

4.1 Identification of the perinatal transitional period

Our first aim was to define the time-frame of the neonatal transitional program and optimal timepoints for gene expression analysis. Western blot analysis was performed on neonatal mouse hearts to analyze the expression of several key cell cycle markers. These expression profiles were used to outline the important transitional period. Through analysis of multiple timepoints, we determined the period when the transition from hyperplastic to hypertrophic cardiomyocytes begins during the neonatal period (Figure 13A).

Phosphorylated retinoblastoma protein (p-Rb) is a G1/S checkpoint marker that has been shown to be downregulated in adult cardiomyocytes (Ikeda et al., 1996; Neganova and Lako, 2008). Total Rb levels increase during the neonatal period, however the phosphorylated form is initially expressed at high levels, then sharply decreases after 5D (Figure 13A). Although Rb protein accumulates in the neonatal heart, the lack of phosphorylation leads to the inhibition of cell cycle progression. Figure 13A also demonstrates total and p-Rb expression is significantly lower in the adult heart compared to any timepoint in the neonatal period, further confirming that expression of cell cycle markers is downregulated in adult hearts.

Cyclin-Dependent Kinase 1 (CDK1) is a serine/threonine kinase directly involved in activating cell cycle progression (Malumbres et al., 2014; Woo and Poon, 2003b). Phosphorylation of CDK1 (p-CDK1) is commonly used as a marker to identify cells active in G2/M. Total CDK1 levels remain constant throughout the neonatal period and into

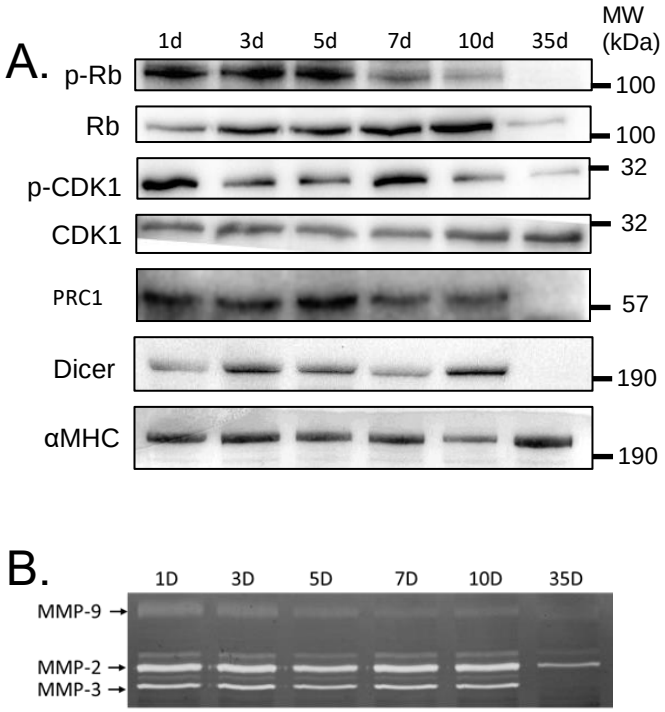

Figure 13. Cell cycle kinetics and remodeling of the neonatal heart. A) Cell cycle markers PRC1, phospho-Rb (p-Rb), and phospho-CDK1 (p-CDK1) protein expression in wild-type hearts as assessed by Western blot analysis. Dicer expression is also shown as a marker of neonatal miRNA production. Extracts from post-natal hearts were pooled (n=3 hearts and 30µg protein per lane) and fractionated by SDS-PAGE. Western blots are representative images from 3 independent experiments. B) Gelatin zymography analysis of matrix metalloproteinases in the postnatal heart shows that the heart undergoes significant remodelling in the perinatal period. Each sample consists of three pooled hearts with protein extracted and run on SDS-PAGE followed by overnight incubation at 37°C in 50mM Tris pH 7.4, 1mM CaCl, 1µM ZnCl and subsequent staining with Coomassie Brilliant Blue. Zymography shown in representative of 3 independent experiments.

adulthood (Figure 13A). We observed that p-CDK1 levels are initially high at 1D, then decrease until 7D when there is a resurgence of expression (Figure 13A). After 7D, p-CDK1 expression is reduced and nearly absent in the adult heart. Similar to Rb, there is dephosphorylation of CDK1 during the neonatal period and inhibition of proliferative signaling. The decrease in p-CDK1 levels also occurs 2 days after p-Rb levels have similarly been reduced. These observations support the contention that cardiomyocytes that have been progressing through G1/S at 3D and 5D, then rapidly initiate their final cell divisions (G2/M) in the post-natal period.

Protein Regulator of Cytokinesis 1 (PRC1) is required for the formation and pinching of the contractile ring during cytokinesis (Jiang et al., 1998). PRC1 is activated by CDKs and interacts with Anillin to mediate formation and pinching of the contractile ring in dividing cells. After the perinatal period, cardiomyocytes no longer express PRC1 and have lost the ability to divide (Jiang et al., 1998; Mollinari et al., 2002). Interesting to note is that PRC1 levels, similar to p-Rb, also peak at 5D and then decrease until absent in the adult heart (Figure 13A). This reduction in PRC1 expression likely plays a direct and important role in the lack of cytokinesis in terminally differentiated cardiomyocytes.

Finally, based on our hypothesis that non-coding miRNAs play an important role in the neonatal transition, we examined the expression of Dicer, the sole protein responsible for processing immature pre-miRNAs into mature miRNA. Dicer expression levels are variable but expressed throughout the first 10 days of life (Figure 13A), consistent with the timeframe of miRNA production. Dicer expression peaks at 3D and 10D. Notably, this increase in Dicer expression at 3D precedes the decrease in

expression of p-Rb, p-CDK1, and PRC1. In adult hearts, Dicer expression is dramatically downregulated (Figure 13A).

The perinatal heart undergoes significant remodeling in preparation for a lifetime of stress with no ability to rest or heal. Matrix metalloproteinases (MMPs) are important for heart collagen remodeling in both the perinatal stage and during heart failure (DeCoux et al., 2014). In both cases, the heart is undergoing significant changes to its morphology and thus extracellular matrix (ECM) reorganization is a critical component of cardiac hypertrophy (Borg et al., 1984). A protein gelatin zymography assay was performed on mouse perinatal heart lysates to observe where the gelatin was degraded by MMPs. A detailed description of the zymography method used is found in Methods chapter 2.3. The zymography assay indicates that throughout the neonatal period, there is extensive MMP-2, -3, and -9 activity (Figure 13B). MMP-9 activity is highest immediately after birth and decreases gradually over the neonatal period, while MMP-2 and MMP-3 remain highly active throughout the neonatal period. MMP-3 and MMP-9 show very low expression in the adult heart, while some MMP-2 activity remains. This is consistent with previous data showing that MMP-2 is expressed in nearly all cardiac cells (DeCoux et al., 2014). The results show that overall MMP activity is high to during the neonatal stages but has mostly ceased in the healthy adult heart.

From our initial western blot and zymography analyses, we were able to determine that during the first 10 days of life, the murine heart is undergoing significant changes in protein expression. At 5D post-birth, there is a transition that results in downregulation of cell cycle signaling, starting with the G1/S checkpoint marker p-Rb, followed by the G2/M marker p-CDK1. miRNA production is also very high during this period as indicated by

Dicer expression, suggesting that miRNA processing and expression is active throughout this transition. Finally, MMP activity is high postnatally, consistent with the significant ECM remodelling occurring during this period.

Based on this 10D window we identified, our next goal was to analyze expression patterns of mRNA and miRNA during this period. For microarray analysis, two additional time-points were included: E19 and 35D for pre-birth and post-adolescent comparisons, respectively.

4.2 Microarray Analysis

Microarray analysis was performed on mouse hearts from multiple time points between E19 and 35D. A detailed description of our microarray experiment is described in the Methods chapter 2.1. To mitigate time-point variation, between 9 to 18 hearts were collected from each time-point (E19, 1D, 3D, 5D, 7D, 10D, and 35D). For each time-point, three MoGene 1.0 Exon Array mRNA microarray replicates were performed with three pooled hearts for each. The MoGene 1.0 Exon array was chosen due to its ability to examine intronic splicing as well as total mRNA transcript levels. Additionally, two Solexa miRNA microarrays were run for each time-point with three pooled hearts, in parallel to the mRNA microarrays. A schematic of our experimental method is shown in Figure 14. Data was examined by comparing one timepoint to the previous (i.e. E19 versus 1D). To determine the number of significantly differentially expressed genes and miRNAs, datapoints were filtered at a p-value≤0.05 and ranked by fold-change. A fold-change threshold of 1.5, and a p-value threshold of $p<0.01$, were chosen because even small but significant changes in upstream regulators may produce large downstream global effects.

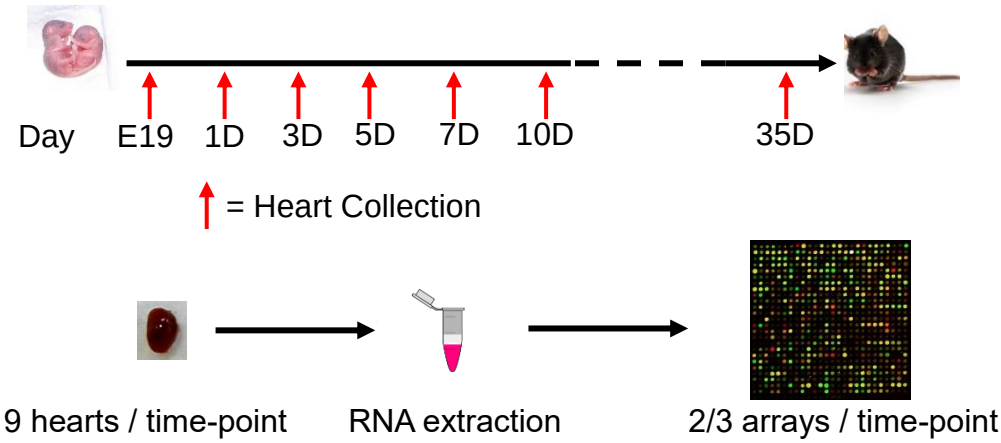

Figure 14. Experimental timeline of microarray experiment. For mRNA, a total of 63 hearts were collected and analyzed over 21 Affymetrix GeneChip Mouse Exon 1.0 ST microarray chips. Hearts were collected from each time point in E19, 1D, 3D, 5D, 7D, 10D and 35D old mice. Hearts were pooled into groups of three and RNA was extracted using the Qiagen mRNA isolation kit. One microgram of total RNA was used on each chip. For miRNA, 42 hearts were analyzed over 14 Illumina Solexa Microarray chips. Three hearts were pooled for each timepoint and processed into experimental duplicates to run on 14 chips. cDNA was normalized through Robust Multi-Array Average (RMA) and gene level analysis was run through a 1-way Analysis of Variance (ANOVA). MicroRNA data was processed through a Log2 transformation and a 1-way ANOVA.

Using these thresholds, volcano plots were created to quantify the number of mRNAs (Figure 15) or miRNAs (Figure 16) upregulated or downregulated when comparing each time point (approximately 1 million exons analyzed). Large variations in mRNA expression occur at E19 vs. 1D and 10D vs. 35D (Figure 15). Between E19 and 1D, 283 mRNAs are downregulated and 164 are upregulated. These large scale alterations have been suggested to originate from the birth process, which causes significant changes in blood pressure and oxygen levels in the heart, resulting in a massive increase in reactive oxygen species (ROS) and shear-stress response in vascular and myocardial cells (Puente et al., 2014). In each of the comparisons of 1D vs 3D, 3D vs. 5D, and 5D vs. 7D, there are only 50-100 total significantly changing genes at each time-point. Interestingly, mRNA fold-changes follow a cyclic pattern that fluctuates between upregulation and downregulation during this transition. From 7D to 10D there are 324 downregulated mRNAs, while only 75 are upregulated. From 10D to 35D there are 1129 upregulated mRNAs and 457 downregulated mRNAs. The greater time-frame and maturation between 10D and 35D also explains the high number of significantly changing genes. This cohort of mRNAs represents the maturation undergone by the adolescent heart. The large changes occurring from 7D to 10D identifies this as a critical timepoint for heart maturation, as hundreds of genes are changing in a time-span of only 3 days (Figure 15).

As expected, due to the relatively smaller number of miRNAs detected, the total number of significantly changing miRNA targets is much lower compared to the total number of altered mRNAs (Figure 16). However, there are both similar and contrasting patterns between the mRNA and miRNA data. Between E19 and 1D there are 18

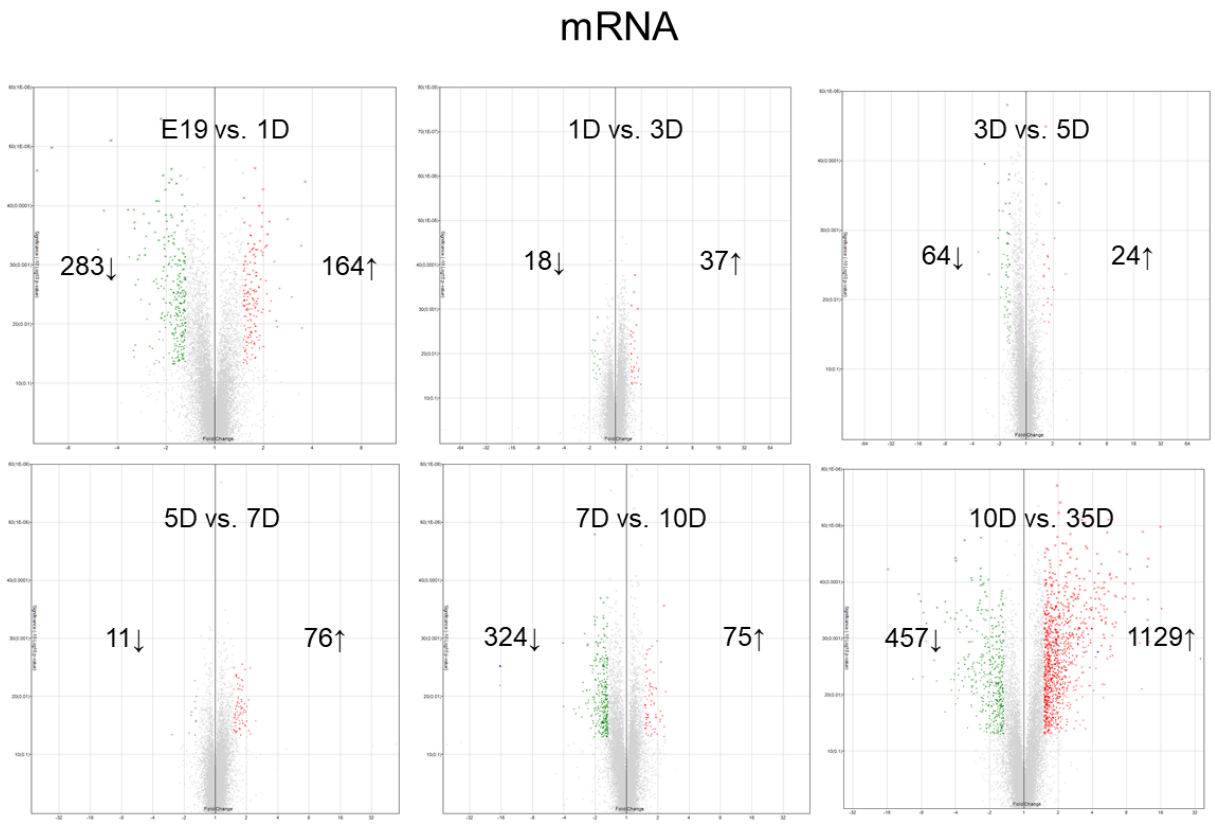

Figure 15. Microarray analysis of the perinatal heart. A) Volcano plots comparing the microarray expression of mRNA in the heart from embryonic day 19 up to adult life. RNA was run on a GeneChip Mouse Exon 1.0 ST Array. Volcano plots were generated using DNAstar: Arraystar. Coloured points fit the criteria of at least a 1.5 fold-change and $p<0.01$. Coloured points fit the criteria of at least 1.5 fold-change and $p<0.01$.

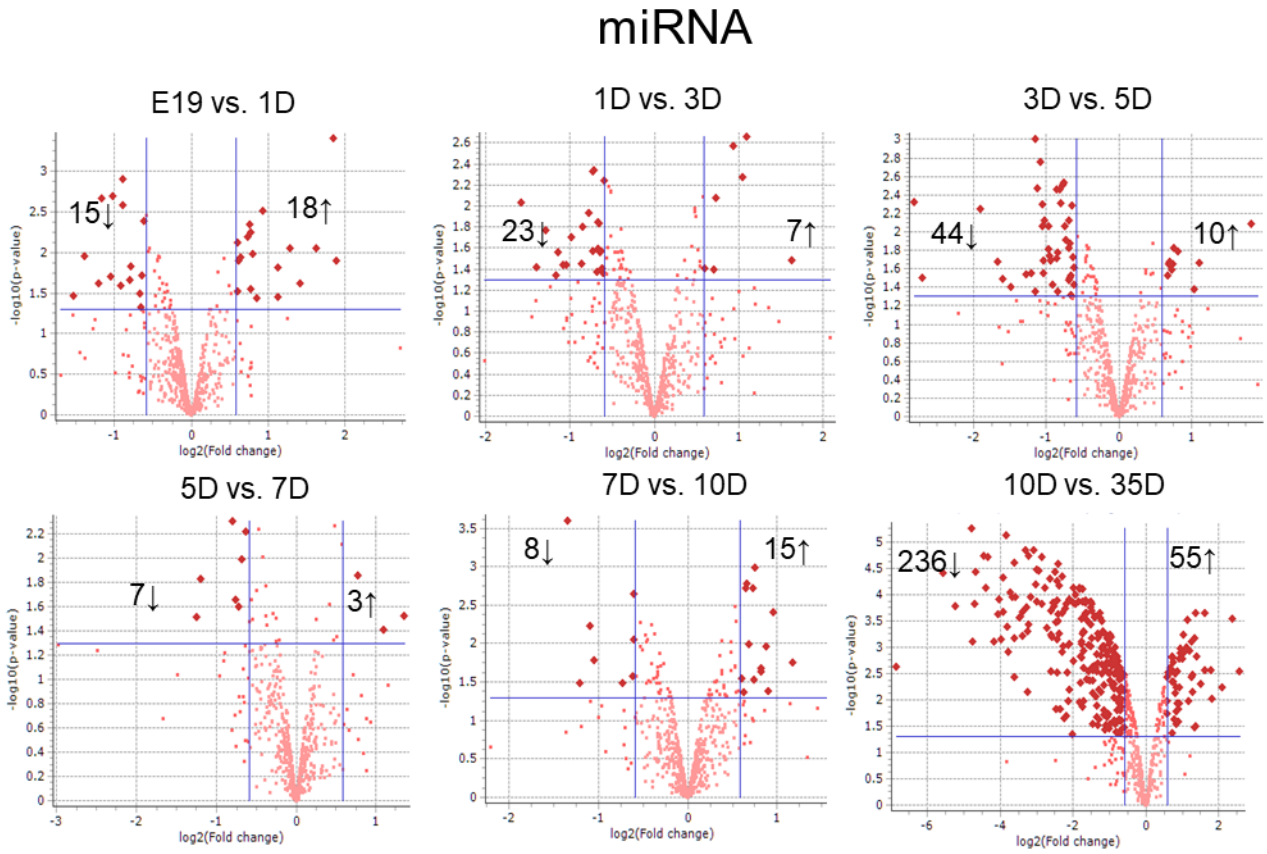

Figure 16. Microarray expression of microRNAs in the heart from embryonic day 19 up until adult life. miRNA was run on Illumina Solexa mouse microRNA analysis chip. MicroRNA data was processed through a Log2 transformation and a 1-way ANOVA. Bolded points fit the criteria of at least 1.5 fold-change and $p<0.01$. All statistical results were run through the False Discovery Rate (FDR) algorithm to correct for effects introduced by multiple testing (FDR≤0.05). Post-hoc analysis was performed using Tukey's biweight function. Volcano plots were generated using Partek software.

upregulated and 15 downregulated miRNAs. From 1D to 3D there are only 7 upregulated and 23 downregulated miRNAs. During the neonatal period, the largest number of changing miRNAs occurs from 3D to 5D, with 10 miRNAs being upregulated and 44 being downregulated. 5D hearts compared to 7D hearts only have a total of 10 changing miRNAs. Between 7D and 10D there is a total of 15 upregulated miRNAs and 8 downregulated miRNAs. Similar to the observations in the mRNA analysis, the largest number of significant changes occurs between 10D and 35D. Contrasting the mRNA expression overall increase between 10D and 35D, there are significantly more downregulated miRNAs than upregulated miRNAs during heart maturation. This agrees with the functional role of miRNA to promote degradation of mRNA transcripts. The second largest number of changing miRNAs occurs between 3D and 5D, which precedes the most significant neonatal mRNA timepoint (7D vs. 10D). Although the number of significantly changing miRNAs is lower, each miRNA is able to target many transcripts and inhibit their activity (Bartel, 2004). A few changing miRNAs can have widespread effects on multiple signaling and regulatory pathways. Our data shows that more changes are occurring in mRNA expression, but the number of changes observed in miRNA expression indicates that they are involved in the neonatal heart transitional program.

4.3 Gene Ontology

After observing significant genomic alterations throughout the neonatal period, we sought to identify co-regulated groups of genes that may be involved in regulating neonatal heart maturation. First, the microarray expression data was clustered hierarchically into groups following similar expression patterns. After hierarchical clustering, the mRNA data was categorized using gene ontology (GO) analysis (Figure

17). GO analysis was performed to identify whether there was a functional relationship between transcripts following similar expression patterns. The significant clusters identified from the GO data shown in Figure 17 were then categorized to examine the gene transcripts involved and their functional properties within the clusters (Table 3). Each significantly changing cluster has a graph with the gene expression pattern shown immediately below the cluster number. In the second column, the sub-categories within each cluster are broken down and the significantly changing genes are displayed in the third column. Finally, the p-value for each group is displayed in the fourth column.

Several patterns were identified in the clustered data such as overall increases/decreases in expression, or transient changes occurring at specific time-points. These analyses revealed many hierarchical clusters containing genes involved in the same biological functions, suggesting co-regulation by the transitional program during the neonatal period. Three major ontological processes were identified through our analysis. The first, metabolism, which includes clusters 3 and 15. Cluster 3 shows a cyclical variation in expression levels of transcripts related to oxidation-reduction process (p=6.95E-11), transport/protein transport (p=1.20E-08 and 3.50E-04, respectively) metabolic process (p=1.76E-04), fatty acid beta-oxidation (p=3.17E-04), fatty acid metabolism (p=3.30E-04), lipid metabolism (p=1.33E-03), autophagy (p=2.17E-03), 2-oxoglutarate metabolism (p=8.59E-03), and tricarboxylic acid cycle (p=0.0149). Cluster 15 shows additional changes in metabolic signaling (p=6.25E-05) and follows the opposite cyclical regulation pattern as cluster 3. The processes present in these clusters are generally related to metabolism and the transition from glycolytic to fatty-acid

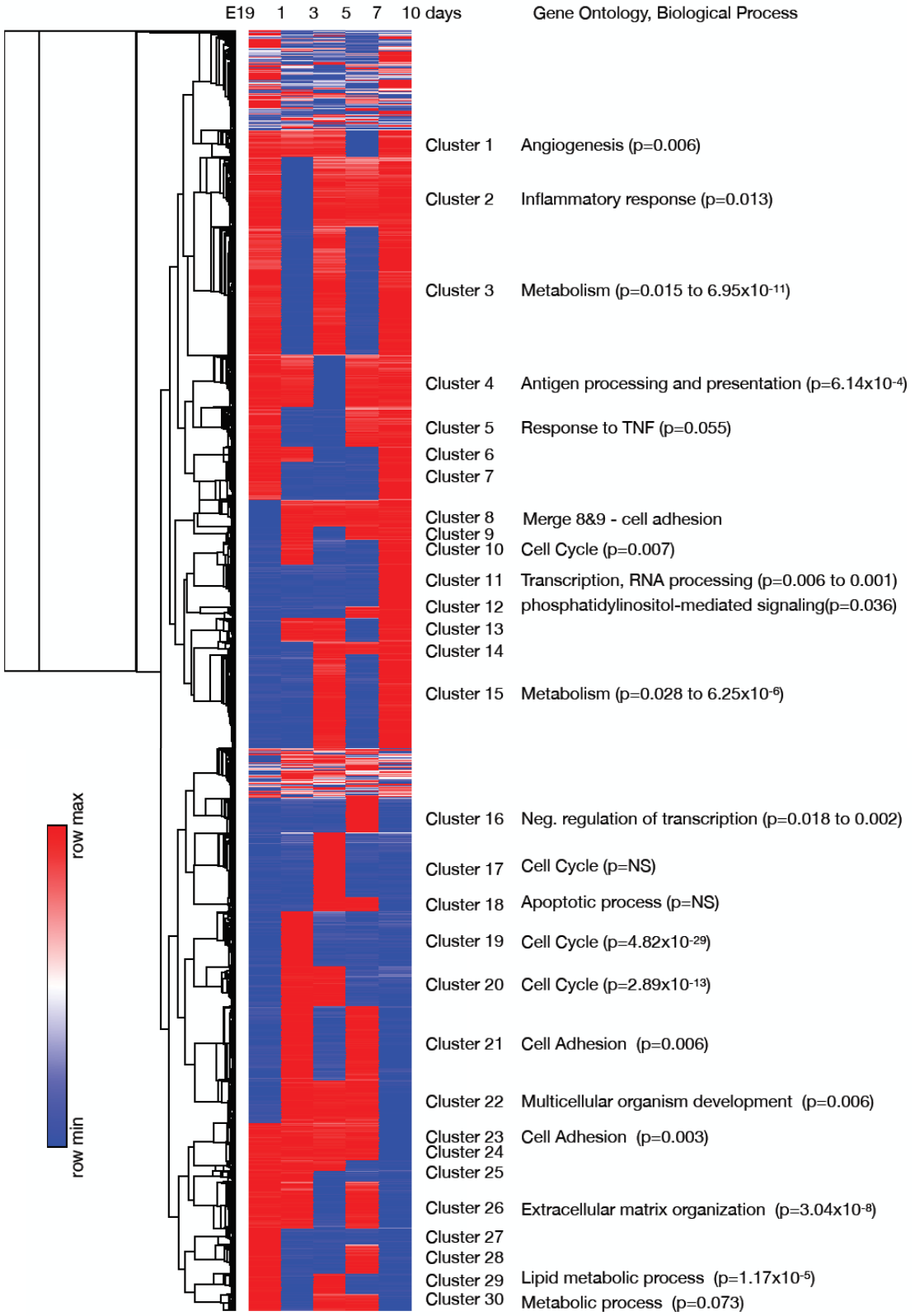
E19
1
3
5
7
10 days
Gene Ontology, Biological Process
Cluster 1
Angiogenesis (p=0.006)
Cluster 2
Inflammatory response (p=0.013)
Cluster 3
Metabolism (p=0.015 to 6.95x10-11)
Cluster 4
Antigen processing and presentation (p=6.14x10-4)
Cluster 5
Response to TNF (p=0.055)
Cluster 6
Cluster 7
Cluster 8
Merge 8&9 - cell adhesion
Cluster 9
Cluster 10
Cell Cycle (p=0.007)
Cluster 11
Transcription, RNA processing (p=0.006 to 0.001)
Cluster 12
phosphatidylinositol-mediated signaling(p=0.036)
Cluster 13
Cluster 14
Cluster 15
Metabolism (p=0.028 to 6.25x10-6)
row max
row min
Cluster 16
Neg. regulation of transcription (p=0.018 to 0.002)
Cluster 17
Cell Cycle (p=NS)
Cluster 18
Apoptotic process (p=NS)
Cluster 19
Cell Cycle (p=4.82x10-29)
Cluster 20
Cell Cycle (p=2.89x10-13)
Cluster 21
Cell Adhesion (p=0.006)
Cluster 22
Multicellular organism development (p=0.006)
Cluster 23
Cell Adhesion (p=0.003)
Cluster 24
Cluster 25
Cluster 26
Extracellular matrix organization (p=3.04x10-8)
Cluster 27
Cluster 28
Cluster 29
Lipid metabolic process (p=1.17x10-5)
Cluster 30
Metabolic process (p=0.073)

Figure 17. Microarray gene ontology analysis. Average-linkage hierarchical clustering and heat maps of differentially expressed genes were generated using Morpheus cluster program (https://software.broadinstitute.org/morpheus).

Table 3. Detailed ontological analysis of mRNA microarray data.

Cluster	GO Term	Genes	P-value
1 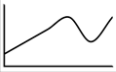	Angiogenesis	PTK2, HTATIP2, MEOX2, SRPX2, EGFL7, EFNA1, CCR2, HBEGF, PLCD1, THY1	0.005844896
2 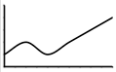	Inflammatory Response	C3AR1, CCL2, CYSLTR1, LYN, CCR1, CSF1, LY86, TLR13, CCL9, EPHX2, TLR3, PF4, CCL6, CD163, CCRL2, REL, AGTR1A, ZC3H12A, CLEC7A	0.013255114
3 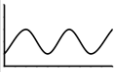	Oxidation-Reduction Process	UQCRC2, SC5D, ENOX2, EHHADH, DNAJC10, PRDX5, UQCRFS1, NDUFS7, NDUFS4, IDH3G, GPX4, NDUFS8, CREG1, SPR, PDHA1, ASPH, ACAD8, AKR7A5, HADH, NQO1, NDUFS2, NDUFS1, SDR39U1, ACADM, ACADS, CBR4, ACADL, NDUFA10, GMPR, DDO, DHDH, OGFOD1, SCCPDH, DLD, OXNAD1, 4833439L19RIK, MECR, NDUFB5, NDUFB8, NDUFB9, ALDH3A2, GLRX2, ETFDH, IDH1, ETFB, PTGR2, NDUFA9, NDUFA6, PHYH, IDH3A, MSRB2, SOD2, SDHA, ADI1, HSDL2, FOXRED1, ALKBH3	6.95E-11
	Transport	DYNC1LI1, CHMP4C, PITPNA, ACBD5, CUL3, SLC2A4, VPS13A, PITPNC1, SLC25A26, SAR1B, RAB21, SCAMP1, VTI1B, VTI1A, SLC25A32, RAB18, SLC25A38, TMEM184C, RAB10, VPS26A, CROT, ZFAND6, CLCN3, MTX2, STAM2, SNX4, KCNJ2, SLC29A1, SLC11A2, STX17, STX16, TESC, OSBPL2, TRPC6, NIPA2, NIPA1, CRAT, RAB33B, VDAC1, SLC25A12, SLC25A11, P2RX4, SLC25A13, AKTIP, FOXRED1, YIPF5, SLC25A16, UQCRC2, ENOX2, UQCRFS1, PEX7, NDUFS7, NDUFS4, AP1S2, ATP5S, NDUFS8, NDUFS2, NDUFS1, ATP5J, SNUPN, DYNLT3, NDUFA10, TIMM44, TMEM38B, ATP6V1C1, ATG4D, ATG4C, CLIC5, KPNA4, KPNA3, SNX13, KPNA1, ATG10, NDUFB5, NDUFB8, SNX14, NDUFB9, STAU2, GLRX2, TMED5, BCAP29, ABCD2, SLC25A46, ETFDH, ABCD3, EXOC6, EXOC5, ETFB, EXOC1, TMC7, NDUFA9, NDUFA6, RUFY1, MICALL1, SDHA, SLC17A5, COG6, ATP6V1E1, YKT6	1.20E-08
	Metabolic Process	COASY, GLB1L, EHHADH, ECHDC1, ARSK, ECHS1, ACAT1, ALDH3A2, AUH, FAHD1, GPHN, ALAS1, ACSL1, NT5C3, PHOSPHO2, SRR, GSTZ1, GNPAT, PDHA1, ACAD8, SUCLA2, PDHX, DLST, ACADM, GSTA4, LPGAT1, SPTLC2, ACADS, NADK, DLAT, ACADL, UGT1A10, HDHD3, NEU1, FLAD1	1.76E-04
	Fatty acid beta-oxidation	ACADM, EHHADH, ABCD2, ECHS1, ABCD3, HIBCH, HADH, ACAT1, CROT, AUH, PEX7	3.17E-04
	Fatty acid metabolic process	ACADM, ACADS, EHHADH, PRKAG1, ABHD5, AMACR, PRKAB1, ADIPOR2, ECHS1, ADIPOR1, LYPLA1, CBR4, CRAT, ACADL, ACSL1, HADH, MECR, CROT, GHR	3.30E-04
	Protein transport	ZFAND6, ATG10, CHMP4C, SNX14, STAM2, MTX2, SNX4, PPT1, PEX7, AP1S2, TMED5, STX16, BCAP29, VPS13A, EXOC6, EXOC5, SAR1B, RAB21, EXOC1, SCAMP1, TESC, RUFY1, VTI1B, TIMM44, VTI1A, RAB33B, MICALL1, COG6, ATG4D, AKTIP, RAB18, ATG4C, YIPF5, KPNA4, RAB10, KPNA3, SNX13, VPS26A, YKT6, KPNA1	3.50E-04
	Lipid metabolic Process	SC5D, CDIPT, ACP6, EHHADH, PRKAG1, ABHD5, ECHS1, PTEN, ACSL1, INSIG2, INPP5E, HADH, OMA1, IAH1, PLA2G16, ACADM, LPGAT1, SPTLC2, ACADS, PRKAB1, ADIPOR2, ADIPOR1, CIDEA, LYPLA1, CBR4, CRAT, ACADL, CHPT1, PTPN11, DGAT2, NEU1, MECR, CROT	0.00133526
	Autophagy	ATG10, ATG12, FUNDC1, EPM2A, RNF185, 1600014C10RIK, OPTN, ACBD5, VTI1A, RAB33B, LAMP1, ATG4D, MAP1LC3A, ATG4C, TMEM59, STX17, VPS13A	0.00217721
	2-Oxoglutarate metabolic process	DLST, GOT1, IDH3G, DLD, IDH1, IDH3A, GHR	0.00859905
	Tricarboxylic acid cycle	SDHA, DLST, IDH3G, IDH1, DLAT, PDHA1, SUCLA2, IDH3A	0.0149538
4 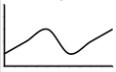	Antigen processing and presentation of exogenous peptide antigen via MHC class II	H2-EB1, UNC93B1, H2-AA, H2-AB1, TRAF6, CD74	6.13E-04
	Immune Response	FYB, ENPP1, IGK-V28, H2-AB1, CTSS, VAV1, CD74, TNFSF13B, H2-EB1, H2-AA, FAS, TRAF6, BMPR1A, CD28, LCP2	0.00659526
10 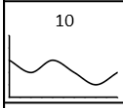	Cell cycle	CDC7, NASP, DBF4, BRCA2, PRKCD, ESCO2, CCNE2, UHRF2, KIF20B, FBXO5, USP37, LIN54, HELLS, DSCC1	0.007117464
11 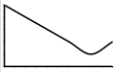	DNA-templated transcription	EID1, TAF1D, AHCTF1, TCEAL5, RLIM, STAT4, GTF2E2, TSPYL2, WBP5, TCERG1, MED29, TARDBP, TBPL1, MLLT3, POLR3G, KAT2A, PLAG1, KHDRBS3, TAF6, RCOR2, TAF5, CCNL1, PKN2, NCOA7, KLF15, SUZ12, HDAC2, RFC1, ID2, SP4, THRAP3, PSPC1, ZIK1, AKAP8, PBX3, TFB1M, TBL1X, PBX2, XRN2	0.001170222
	mRNA processing	KHDRBS3, CSTF2, SNRPD1, HNRNPM, AQR, TARDBP, THRAP3, DHX15, CPSF6, PTBP2, HNRNPH1, XRN2, 1110037F02RIK, PRPF40A	0.006486444
	Centriole replication	CEP72, SASS6, CEP135, CEP63, CENPJ	0.009831288
12 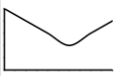	Phopsphatidylinositol-mediated signaling	PIK3C2A, GSN, OGT, IRS1	0.035756962

Cluster	GO Term	Genes	p value
15 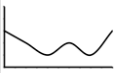	Oxidation-reduction process	HSD17B10, GMPR2, ME2, SORD, FDX1, GLUD1, ETHE1, EGLN1, PRDX3, PRDX1, PDHB, HIBADH, NDUFB2, MTHFD1, CYP39A1, AGPS, IVD, MMACHC, CH25H, DHODH, ALDH4A1, GSTO1, ERO1L, DHTKD1, RTN4IP1, HIGD1A, NQO2, ALDH6A1, GCDH, ALKBH7, NDUFA8, AIFM1, AKR1E1, BCKDHB, SDHB, L2HGDH, JMJD6, SDHC, NDUFV2, TXNRD2, MDH1	6.25E-06
	Metabolic process	BCAT2, ME2, XRCC6, ACSS2, PDHB, RNGTT, GSTM7, MTHFD1, MUT, IVD, OXCT1, GYS1, ALDH4A1, UCK2, GSTO1, DHTKD1, ACSL4, CTBS, ACSL5, GCDH, ALDH6A1, ACY1, BCKDHB, PFKP, DBT, PCX, UCKL1, PLA2G6, UGP2	0.001009087
	Protein folding	FKBP8, ERP29, FKBP3, FKBP1A, CCT2, CCT3, PPIF, TRAP1, TXNDC11, CCT4, PPIB, BAG2, ERO1L	0.028189345
16 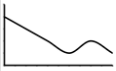	Negative regulation of transcription from RNA pol II	USP3, HCFC1, CNOT1, FOXO3, FOXP1, CDKN1C, PCGF2, SIN3B, KDM2B, SIN3A, GATA6, NEDD4, SALL1, IFT172, PER2, GATAD2A, PER1, PTCH1, RARA, ETV6, KDM5C	0.001647289
	Negative regulation of DNA-templated transcription	PTPRK, RUNX1T1, SMAD2, FOXP1, SIN3B, SIN3A, SFRP1, GATA6, SALL1, PER2, GATAD2A, PER1, PTCH1, RARA, LIMD1, KDM5B, KDM5C	0.01808314
	Uteric bud development	SFRP1, SALL1, SMAD6, SMAD2, RARA, VCAN	0.042505832
19 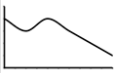	Cell cycle	KIF23, E2F1, CLSPN, E2F7, E2F8, PKMYT1, CDT1, CCNE1, RAD21, MCM7, DDX11, PAK4, INCENP, CDCA2, CDCA5, CCNA2, ASPM, CDCA3, CDC6, RBL1, SGOL1, MCM2, MCM3, UBE2C, MCM4, ECT2, MCM5, WEE1, MCM6, NCAPD2, UHRF1, TIMELESS, APITD1, CNTROB, BUB1B, NEK6, CKS1B, CHEK1, ANLN, MDC1, NCAPG2, BUB1, MKI67, WDR6, BIRC5, CENPE, PMF1, REEP4, GSG2, CDC25A, BRCA1, CENPT, CHAF1A, SMC1A, CIT, CHAF1B, USP44	4.82E-29
	Cell division	KIF23, CKS1B, ANLN, CCNE1, RAD21, NCAPG2, INCENP, BUB1, CDCA2, CDCA5, CCNA2, ASPM, CDCA3, CDC6, SGOL1, CENPE, BIRC5, PMF1, UBE2C, ECT2, REEP4, MCM5, CDC25A, WEE1, NCAPD2, APITD1, TIMELESS, CNTROB, BUB1B, CENPT, SMC1A, CIT, NEK6, USP44	1.80E-15
	Mitotic nuclear division	KIF23, ANLN, RAD21, NCAPG2, INCENP, BUB1, CDCA2, CDCA5, CCNA2, ASPM, CDCA3, CDC6, SGOL1, ESPL1, BIRC5, CENPE, PMF1, UBE2C, REEP4, CDC25A, WEE1, NCAPD2, APITD1, TIMELESS, BUB1B, CENPT, SMC1A, CIT, NEK6, USP44	2.47E-15
	DNA replication	RECQL4, GINS1, GINS2, CDC6, DTL, POLE, MCM2, MCM10, MCM3, MCM4, BRCA1, MCM5, MCM6, CDT1, PRIM1, RPA2, DNA2, MCM7, POLD1, CHAF1A, POLQ, CHAF1B	6.23E-15
	Cellular response to DNA damage	CLSPN, E2F7, CHEK1, MCM10, MEN1, RPA2, RAD21, MCM7, DDX11, MDC1, FANCG, POLQ, PALB2, FANCA, TOP2A, EXO1, MSH6, DTL, POLE, TOPBP1, RAD54L, BRCA1, DNA2, UHRF1, DCLRE1B, APITD1, TIMELESS, SFPQ, SMC1A, ABL1, CHAF1A, CHAF1B, UBE2T, BARD1	5.79E-14
	DNA repair	CLSPN, CHEK1, ANKLE1, RPA2, RAD21, MDC1, FANCG, POLQ, PALB2, FANCA, EXO1, MSH6, TRIM28, POLE, TOPBP1, RAD54L, BRCA1, DNA2, UHRF1, DCLRE1B, APITD1, SFPQ, SMC1A, ABL1, CHAF1A, CHAF1B, UBE2T, BARD1	8.32E-12
	Chromosome segregation	SGOL1, ESPL1, BIRC5, CENPE, PMF1, BRCA1, RAD21, INCENP, BUB1, CDCA2, CENPT, CDK5RAP2, TOP2A, NEK6, USP44	8.35E-09
	DNA replication initiation	CCNE1, CDC6, MCM7, TOPBP1, MCM2, MCM3, MCM10, MCM4, MCM5, MCM6	1.05E-08
	G1/S transition	CCNE1, POLE, SKP2, IQGAP3, TCF19, CDCA5, CAMK2A, CDC25A, ACVR1	0.001439932
	Protein phosphorylation	PDK1, PASK, TRIM28, STK35, PKMYT1, CHEK1, BIRC5, GSG2, WEE1, CCNE1, DDR1, HUNK, PAK4, BUB1, BUB1B, NRK, DYRK3, CIT, CSK, ABL1, CAMK2A, NEK6, ACVR1	0.006143795
	DNA unwinding for replication	MCM7, MCM2, MCM4, TOP2A, MCM6	0.006281111
	Phosphorylation	PDK1, CHKB, PASK, STK35, PKMYT1, CHEK1, GSG2, WEE1, DDR1, HUNK, PAK4, BUB1, BUB1B, DYRK3, NRK, CIT, CSK, ABL1, CAMK2A, NEK6, PRPS2, ACVR1	0.048812059
20 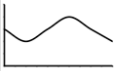	Mitotic nuclear division	NEK2, AURKA, CEP55, PTTG1, AURKB, FAM83D, SPC24, SPC25, KIF2C, NCAPH, CDCA8, BUB3, ERCC6L, CENPN, KIF11, NUF2, TPX2, CDC25C, CCNB1, CCNB2, NUP62, RCC2, SPAG5, PLK1, NSL1	2.67E-14
	Cell cycle	SPIN1, PRC1, NEK2, FOXM1, AURKA, CEP55, AURKB, PTTG1, FAM83D, SPC24, KIF2C, SPC25, CDCA8, NCAPH, CDKN2C, H2AFX, BUB3, ERCC6L, CKAP2, KIF11, DLGAP5, NUF2, TPX2, RACGAP1, CDC25C, CCNB1, CDKN1A, CCNB2, RCC2, SPAG5, PLK1, NSL1, CHTF18	2.89E-13
	Cell division	PRC1, NEK2, AURKA, CEP55, PTTG1, AURKB, FAM83D, SPC24, SPC25, KIF2C, CDCA8, NCAPH, BUB3, ERCC6L, KIF11, NUF2, TPX2, CDC25C, RACGAP1, CCNB1, CCNB2, RCC2, SPAG5, PLK1, NSL1	2.51E-11
	Chromosome segregation	KIF2C, CENPN, SPC25, KIF11, NEK2, SPAG5, NSL1, PTTG1, BUB3	0.001053769
	Mitotic sister chromatid segregation	CDCA8, PLK1, NEK2, SPAG5, NSL1, BUB3	0.001308979
	Mitotic cytokinesis	CKAP2, PLK1, KIF4, CEP55, RACGAP1, KIF20A	0.005262691

Cluster	GO Term	Genes	p value
21 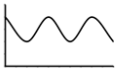	Cell adhesion	ATP1B2, TLN2, PCDH20, PTK7, EDIL3, EPHB4, CDH6, LPXN, CNTNAP1, ZYX, COL18A1, ICAM1, COL13A1, SDK2, PCDH8, NID1, PTPRU, SLAMF1, TINAG, COL5A1, CTNNA2, LAMA1, EPHA8, ITGA5, CNTN3	0.00350982
	Multicellular organism development	DCC, NANOS3, SHROOM3, EVX1, GLIS2, EDIL3, FOXO4, EPHB4, SCRIB, EPHB2, ARHGAP22, UNC5B, DDX25, SMOC1, DNER, ROBO2, AGRN, ALX4, DISC1, PHC1, COL18A1, DVL2, COL13A1, ENC1, SLIT1, CTNNA2, DLX3, NOTCH2, NOTCH1, NAV1, CATSPER3, EPHA8, SPATA18, EFNA5, NLRP14, EDA, IGSF9, TBX18, INTU	0.005692534
22 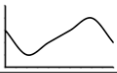	Multicellular organism development	PDGFB, JAG2, HIC1, PAQR5, SEMA5B, ANGPTL6, HOXC8, HEY1, PIWIL1, ROBO4, SEMA3B, PLXND1, CCNA1, ZBTB7B, INSM1, ARC, NES, TWF2, DLL3, FZD1, DPYSL2, MSX1, NOTCH4, BIN1, CHRD, DBN1	0.018302935
23 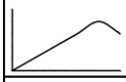	Cell adhesion	CADM4, CLSTN1, PCDH12, ITGB3, PCDH17, COL16A1, EMILIN2, CDH5, PCDH18, ISLR, COL14A1, SULF1, COL6A2, COL6A1, SPON2, THBS3, AOC3	0.002508207
26 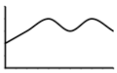	Extracellular matrix organization	RECK, COL4A2, TNXB, ADAMTSL4, ELN, NFKB2, EMILIN1, LAMA2, FBLN1, COMP, FBLN5, AGT, PDGFRA, LAMC1, FN1	3.04E-08
	Multicellular organism development	TSHZ2, TNFRSF26, TBX20, ANPEP, JAG1, EPHB3, GLI1, SEMA5A, MUSK, TNFRSF11A, UNC5C, FGF2, DCLK1, ZFP423, OBSCN, EFNB1, TBX5, MTL5, DLL1, NOTCH3, DKK3, SMO, EPHA4, ARVCF, DACT1, LRP1, EYA2, SEMA6C, SEMA6D, PDGFRA, HHAT, NGFR, LRP5	7.19E-05
29 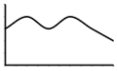	Sterol biosynthetic process	CYB5R3, CYP51, MVD, HMGCS1, MVK, DHCR24, FDFT1	1.24E-06
	Cholesterol biosynthetic process	CYB5R3, CYP51, MVD, HMGCS1, MVK, DHCR24, FDFT1	3.71E-06
	Steroid biosynthetic process	STARD3, CYB5R3, CYP51, MVD, HMGCS1, MVK, DHCR24, FDFT1	7.71E-06
	Lipid metabolic Process	CYP51, CYB5R3, SGPL1, ACOX1, MVD, LDLR, ABHD4, HMGCS1, FDFT1, PLCG2, PLCD3, MVK, DHCR24, PTDSS2, DEGS1	1.17E-05
	Steroid metabolic process	CYB5R3, CYP51, LDLR, MVD, HMGCS1, MVK, DHCR24, FDFT1	6.55E-05
	Cholesterol metabolic process	CYB5R3, CYP51, LDLR, MVD, HMGCS1, MVK, DHCR24, FDFT1	9.78E-05
	Isoprenoid biosynthetic process	MVD, HMGCS1, MVK, FDFT1	0.034445486

RNA was run on a GeneChip Mouse Exon 1.0 ST Array and analyzed via Ingenuity Pathway Analysis. Graphs in the first column were generated with Microsoft Excel using average value obtained from ontological analysis. cDNA was normalized through Robust Multi-Array Average (RMA) and gene level analysis was run through a 1-way Analysis of Variance (ANOVA). All statistical results were run through the False Discovery Rate (FDR) algorithm to correct for effects introduced by multiple testing (FDR≤0.05). Post-hoc analysis was performed using Tukey's biweight function.

β-oxidation, which the post-neonatal heart uses as its primary energy source. This fundamental shift from glycolysis to fatty acid oxidation is critical for proper heart maturation and is reflected in the significance of the relationship in ontology.

The second overarching ontology observed was related to cell cycle processes, and includes clusters 10, 11, 12, 16, 19, 22 and 20. Cluster 10 shows an overall reduction in cell cycle transcript expression (p=7.11E-03), with a slight transient increase around 5D. Cluster 11 shows a decrease in DNA-templated transcription (p=1.17E-03), mRNA processing (p=6.48E-03), and centriole replication (p=9.83E-03), likely due to cardiomyocyte cell cycle withdrawal leading to reduced transcription and centriole requirements. Cluster 12 shows a transient decrease in phosphatidylinositol-mediated signaling (p=0.0357), specifically the PI3K/PTEN pathway, which is directly involved in cell growth, proliferation, and differentiation. Cluster 16, like cluster 11, shows a decrease in RNA pol II transcription and DNA-templated transcription (p=1.65E-03 and 0.0180, respectively).

Clusters 19 and 20 are two of the most significantly changing clusters containing the most changing genes. Cluster 19 consists of cell cycle (p=4.82E-29), cell division (p=1.80E-15), mitotic nuclear division (p=2.47E-15), DNA replication (p=6.23E-15), DNA damage response (p=5.79E-14), DNA repair (p=8.32E-12), chromosome segregation (p=8.35E-09), DNA replication initiation (p=1.05E-08), G1/S transition (p=1.44E-03), protein/overall phosphorylation (p=6.14E-03 and 0.0488, respectively), and DNA unwinding for replication (p=6.28E-03). Cluster 20 shows gene regulatory changes in some similar ontologies as cluster 19 such as mitotic nuclear division (p=2.67E-14), cell cycle (p=2.89E-13), cell division (p=2.51E-11), and chromosome segregation

(p=1.05E-03). Cluster 20 also contains ontologies not found in cluster 19, related to mitotic sister chromatid segregation (p=1.31E-03) and cytokinesis (p=5.26E-03). Both cluster 19 and 20 show drastic decreases in many cell cycle-related processes. Each of these expression pathways are extremely important during embryonic heart development to generate a fully functional heart and are then rapidly downregulated after birth. In addition, both clusters show a transient increase in expression, however each cluster peaks at a different timepoint. While cluster 19 is re-expressed from 3D to 5D, cluster 20 is re-expressed from 5D to 7D. This coincides with the G1/S and G2/M checkpoint markers p-Rb and p-CDK1 expression previously shown in Figure 13, indicating that either cluster is involved in regulating different stages of the cell cycle. Important transcripts found within cluster 19 include: Wee1, Chek1, Anillin, Cdc25a, Cyclin E1, and E2F7. Notable members of cluster 20 are AurkA, AurkB, Ccnb1/2 (Cyclin B1&2), Cdc25c, Kif11, and Cdkn1a (p21).

The third major ontological process observed was related to heart growth and extracellular matrix remodelling, and includes clusters 1, 21, 23, and 26. Cluster 1 shows an increase in angiogenesis, which would be expected in the rapidly hypertrophying heart (p=5.84E-03). Clusters 21, 23, and 26 all show varying changes in cell adhesion (cluster 21: p=3.51E-03, cluster 23: p=2.51E-03), organism development (cluster 21: p=5.70E-03, cluster 26: p=7.19E-05) and extracellular matrix organization (cluster 26: p=3.04E-08). While cluster 21 shows varying expression, clusters, 23, and 26 all shown upregulation during the perinatal period, indicating an increase in regulation of cellular organization and extracellular matrix remodelling.

Several unique ontological clusters were also identified in the expression analysis. Cluster 2 shows increased inflammatory response (p=0.0132), which may result from increased ROS production after the coronary vasculature fills with more highly oxygenated blood after birth (Puente et al., 2014; Torres-Cuevas et al., 2017). Clusters 5 through 9 showed distinct expression patterns, however there was no significant relationship in ontology when tested by ANOVA. Finally, cluster 29 includes sub-ontologies related to cholesterol and steroid biosynthesis and metabolism. Cluster 29 shows cyclical expression during the perinatal period, with expression decreasing in adults. This cluster includes sterol biosynthesis (p=1.24E-06), cholesterol biosynthesis/metabolism (p=3.71E-06 and 9.78E-05, respectively), steroid biosynthesis (p=7.71E-06), lipid metabolism (p=1.17E-05), and isoprenoid biosynthesis (p=0.0344).

Based on the gene ontology data, we categorized 3 overarching ontological changes occurring as part of the neonatal transitional period: 1) A metabolic switch toward fatty acid oxidation throughout the neonatal period, 2) cardiomyocyte cell cycle withdrawal revolving around 5D, and 3) ECM remodelling peaking around 7D. For our next step, we sought to identify miRNAs that could be regulating cardiomyocyte cell cycle withdrawal during the neonatal period.

4.4 miRNA expression patterns

Given the lower number of individual miRNA identified in the expression screens, categorization through GO analysis on miRNA expression kinetics was not performed. Rather, our approach was to identify significant miRNA changes occurring over the neonatal timeframe, then further investigate the role of the specific miRNA that has been established in the literature. For our analysis, we generated miRNA expression heat maps

to identify the most significantly changing miRNAs at each time point during the perinatal period. The most significantly upregulated miRNA by 5D is miR-205, undergoing a 20-fold increase in expression over the first 5-days post-birth, followed by miR-200c and miR-141 (Figure 18A). Interestingly, miR-200c and miR-141 are both members of the miR-200 family. They are clustered together on chromosome 6 and are co-regulated by the same promoter. The miR-200 family has previously been studied in the context of cancer, where it has proven to be antiproliferative and is a promising therapeutic for inhibiting cancer cell replication (Chen and Zhang, 2017; Koutsaki et al., 2017; Lim et al., 2013; Park et al., 2008). MiR-205 is also closely associated with the miR-200 family due to its functionally similar roles, common targets, and seed sequence. The effects of global miR-205 deletion in mice was previously examined and proven to be neonatally lethal (Farmer et al., 2013). Furthermore, miR-205 has primarily been studied in the context of cancer, where it functions as a tumour suppressor (Greene et al., 2010b; Qin et al., 2013; Zhang et al., 2014). MiR-205 is able to modulate cancer cell growth, division, and maturation via it's involvement in the PI3K, Hippo and ZEB1/2 pathways (Greene et al., 2010b; Hashiguchi et al., 2017). As mentioned in Chapter 1.3, the PI3K and Hippo pathways have both been identified as essential for normal cardiac development (von Gise et al., 2012; Maillet et al., 2013; Xiao et al., 2018). Based on its transient expression, temporal correlation with the cardiomyocyte transitional program, and previous research suggesting a role in cell division, we chose to further investigate the role of miR-205 in the neonatal heart, which will be described in Chapters 5 and 6.

Many of the other significantly increasing miRNAs shown in Figure 18A were also cited in studies revolving around cancer, and more specifically, the proliferative capacity

A.

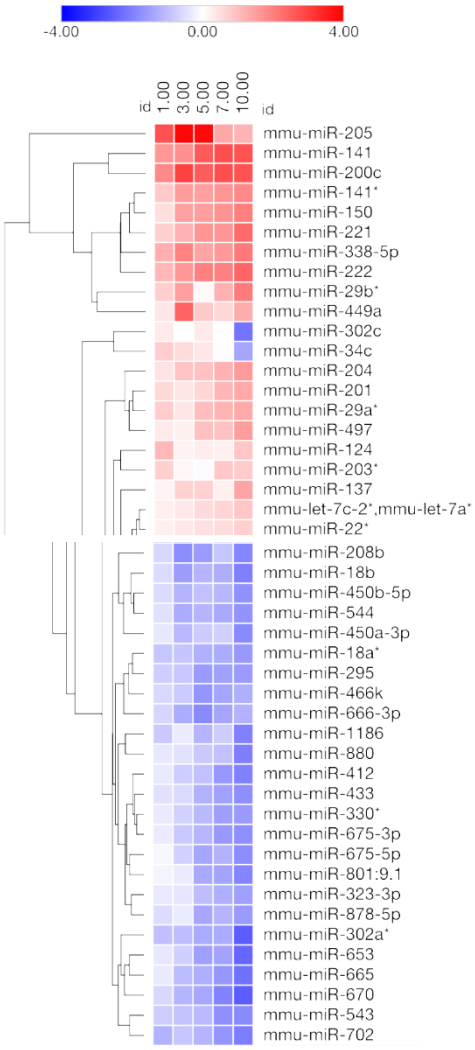
-4.00
0.00
4.00
id
1.00
3.00
5.00
7.00
10.00
id
mmu-miR-205
mmu-miR-141
mmu-miR-200c
mmu-miR-141*
mmu-miR-150
mmu-miR-221
mmu-miR-338-5p
mmu-miR-222
mmu-miR-29b*
mmu-miR-449a
mmu-miR-302c
mmu-miR-34c
mmu-miR-204
mmu-miR-201
mmu-miR-29a*
mmu-miR-497
mmu-miR-124
mmu-miR-203*
mmu-miR-137
mmu-let-7c-2*,mmu-let-7a*
mmu-miR-22*
mmu-miR-208b
mmu-miR-18b
mmu-miR-450b-5p
mmu-miR-544
mmu-miR-450a-3p
mmu-miR-18a*
mmu-miR-295
mmu-miR-466k
mmu-miR-666-3p
mmu-miR-1186
mmu-miR-880
mmu-miR-412
mmu-miR-433
mmu-miR-330*
mmu-miR-675-3p
mmu-miR-675-5p
mmu-miR-801:9.1
mmu-miR-323-3p
mmu-miR-878-5p
mmu-miR-302a*
mmu-miR-653
mmu-miR-665
mmu-miR-670
mmu-miR-543
mmu-miR-702

B.

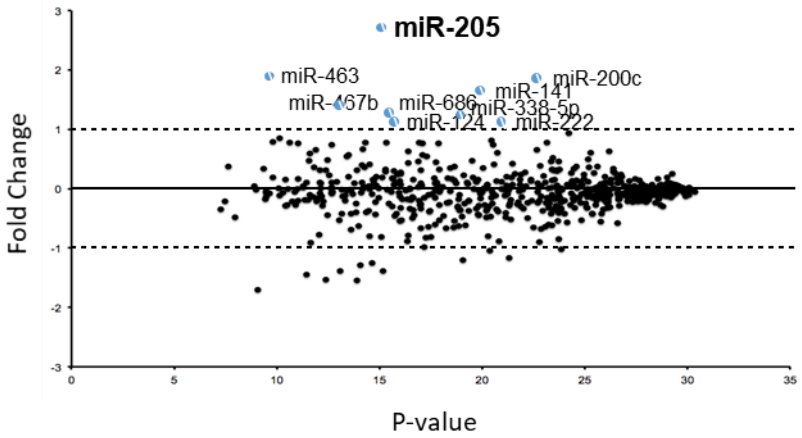
miR-205
miR-463
miR-200c
miR-141
miR-467b
miR-686
miR-338-5p
miR-124
miR-222
Fold Change
P-value
3
2
1
0
-1
-2
-3
0
5
10
15
20
25
30
35

Figure 18. miRNA microarray expression analysis. A) Heatmap data showing the expression patterns of the most significantly changing miRNAs during the neonatal period. All data was clustered hierarchically, and the most upregulated and downregulated miRNAs were selected to be displayed. Of note is miR-205 which is transiently upregulated. MiR-141 and 200c are members of a similar family and show co-regulation with miR-205. B) miRNA microarray data from Figure 16 displayed as p-value vs. fold-change at 5D. Note than miR-205 is the largest change occurring at 5D.

of cancer cells (Garofalo et al., 2012; Kwon et al., 2019; Santolla et al., 2018; Sun et al., 2019; Wang and Qin, 2018; Yong-Ming et al., 2017).

The most significantly downregulated miRNAs during the perinatal period were miR-702, miR-543, miR-670, miR-665. Of note, these miRNAs have also been implicated in several studies involving cancer and proliferative ability (Hu et al., 2018; Kim and Choi, 2012; Shi and Xu, 2016; Zhai et al., 2017).

4.5 Conclusions

Our microarray expression analyses have provided insight regarding the regulation of gene expression during the neonatal cardiac growth transition, providing a novel candidate miRNA for study. Using our temporal resolution approach, we have identified many mRNAs and miRNAs that undergo significant changes in expression post-birth. We were also able to observe an ontological expression pattern in cell cycle signaling to confirm the widespread downregulation of factors that modulate cell proliferation post-birth. Key findings include the characterization of the 3 overarching expression patterns in the neonatal heart: a metabolic switch, cell cycle inhibition, and extracellular matrix remodelling. Within the category of cell cycle regulation, there are 2 distinct clusters which show transient upregulation at 5D and 7D, respectively. Additionally, we observed the most changes occurring at the transition from embryonic to neonatal and young to adult. Most importantly, we discovered significant RNA changes centralized around 5D post-birth. Based on these observations we hypothesize that 5D post-birth is a critical transition in the developing neo-nate heart. While the focus of our research has remained on cell cycle, the other expression pathways also posit interesting avenues for

further research. Our data will continue to be an invaluable tool in future studies regarding neonatal heart development.

After analyzing mRNA expression patterns in the neonatal heart, we next sought to identify relevant miRNAs that impact this same transitional period. Since the role of miRNAs involved in cardiomyocyte proliferative capacity has not been studied in great detail, there is a lack of literature identifying a role for the miRNAs we observed changing during the neonatal period. We investigated the miRNAs to elucidate whether their role in cancer and/or cell proliferation could be extrapolated to a role in the developing heart. A key finding of our miRNA data analysis was the observation that miR-205 undergoes a significant and transient 20-fold upregulation after birth to 5D, after which it decreases by 10D, with continued reductions in the adult heart. During the perinatal period, miR-205 expression displays the greatest alteration of any detected miRNA at 5D (Figure 18B). Additionally, this expression pattern aligns with cardiomyocyte withdrawal from the cell cycle. After reviewing the literature surrounding miR-205 in cancer, we concluded that miR-205 may possess similar antiproliferative properties in the postnatal heart. Furthermore, the study of miR-205 in cancer and epidermal development has shown it can target Pten and Yap1, both of which participate in critical cell cycle regulation pathways. In the PI3K pathway, Pten is a phosphatase responsible for dephosphorylating phosphatidylinositol (3,4,5)-triphosphate (PIP3) into PIP2, resulting in inhibition of the AKT signaling pathway to inhibit cell growth and replication (Goberdhan and Wilson, 2003). In the Hippo pathway, YAP1 is the downstream transcriptional co-activator that activates a wide variety of genes to promote cell growth and division (Fa-Xing Yu, Bin Zhao, 2016; Halder and Johnson, 2010). Based on miR-205's compelling expression

profile coinciding with cell cycle withdrawal, as well as the literature supporting miR-205's antiproliferative role in the PI3K and Hippo pathways, investigation into the role of miR-205 in the inhibition of cardiomyocyte replication was warranted.

Chapter 5: Micro-RNA-205 and its role in heart maturation

To support miR-205's potential role in the cardiac transitional program, there is a large body of literature describing miR-205's role in cancer, specifically it's tumour-suppressing activity. Evidence has shown that miR-205 is highly expressed in many forms of cancer (Qin et al., 2013; W. et al., 2010), where it's overexpression is hypothesized to act as a compensatory mechanism to reduce PTEN and Hippo pathway signaling and limit cancer growth (Du et al., 2017; Zhang et al., 2014). Elevated expression of miR-205 in various forms of cancer has been associated with improved prognosis and outcome, suggesting that such a compensatory response may have anti-proliferative outcomes. Interestingly, in cancer cases where miR-205 is not present, the cancerous cells have hypermethylated the miR-205 promoter, silencing expression and thereby reducing anti-proliferative signaling (Kim et al., 2019). Finally, previous research has shown miR-205 germline-deletion causes severe developmental defects by postnatal 5D, and death before 10D (Wang et al., 2013). While the role of miR-205 has been studied in cancer, the role of miR-205 in the heart is unknown. During our screening described in Chapter 4, we observed large changes in miR-205 expression during the neonatal period (20-fold by 5D, reduced by 10D). Due to it's role described previously in cancer models (Du et al., 2017; Greene et al., 2010b, 2010a; Hashiguchi et al., 2017; Qin et al., 2013; W. et al., 2010), we hypothesized that miR-205' antiproliferative properties and targeting of Yap1/Pten (Maillet et al., 2013; Tian et al., 2015) likely plays a regulatory role in the cardiac transitional program

In Figure 19, the sequence of mature miR-205 is shown with its seed sequence highlighted in green. Below, the reversed sequence of miR-205 is matched it to

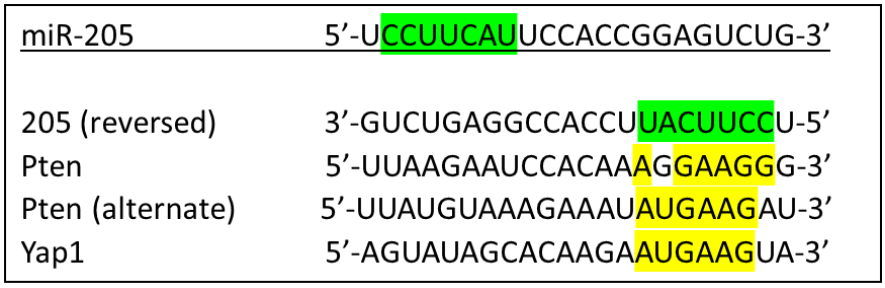

Figure 19. Pten and Yap1 as putative targets of miR-205. The full sequence of mature miR-205 is shown at the top. Regions from the 3' UTR of PTEN and YAP (miR-205 targets) are shown below. Seed sequence of miR-205 is highlighted in green, while complimentary sequences from 3' UTRs of Pten and Yap1 are highlighted in yellow.

homologous regions within the 3' untranslated regions (UTRs) of Pten and Yap1. These complimentary regions provide support on top of published data to show that miR-205 targets Pten and Yap1 (Greene et. al. 2010, Du et. al. 2017).

5.1 MicroRNA-205 expression and localization in the neonatal heart

The first step, after selecting miR-205 for further analysis, was to confirm the trend seen in the microarray. RT-qPCR was used to analyze miR-205 expression throughout the perinatal period and confirm the microarray analysis showing transient expression of miR-205 during the neonatal period (Figure 20A). All miR-205 RT-qPCR data is normalized to the expression of U6 snoRNA, which has been shown to be an appropriate non-coding RNA control (Mase et al., 2017; Peltier and Latham, 2008). Using RT-qPCR, we were also able to show that miR-205 expression is indeed coming from cardiomyocytes, as well as supporting cells (Figure 20B). Based on the literature surrounding miR-205 and it's expression in fibroblasts, we expected that there would also be miR-205 expression originating from fibroblasts in the heart (Du et al., 2017; Wang et al., 2013)

We next wanted to visualize where within the heart miR-205 was being expressed. To do this, we used an RNA probe specific for mature miR-205 to perform *in situ* hybridization. The detailed protocol for the *in situ* hybridization is found in Methods Chapter 2.8. We have demonstrated that when miR-205 expression increased dramatically at 5D, this expression originated from the epicardium (Figure 20C). The epicardium is a layer of epithelial cells that envelopes the heart. During development, the epicardium gives rise to cardiac cells, including myocytes, fibroblasts, smooth muscle cells, and endothelial cells (Singh et al., 2016). Epicardium-deficient

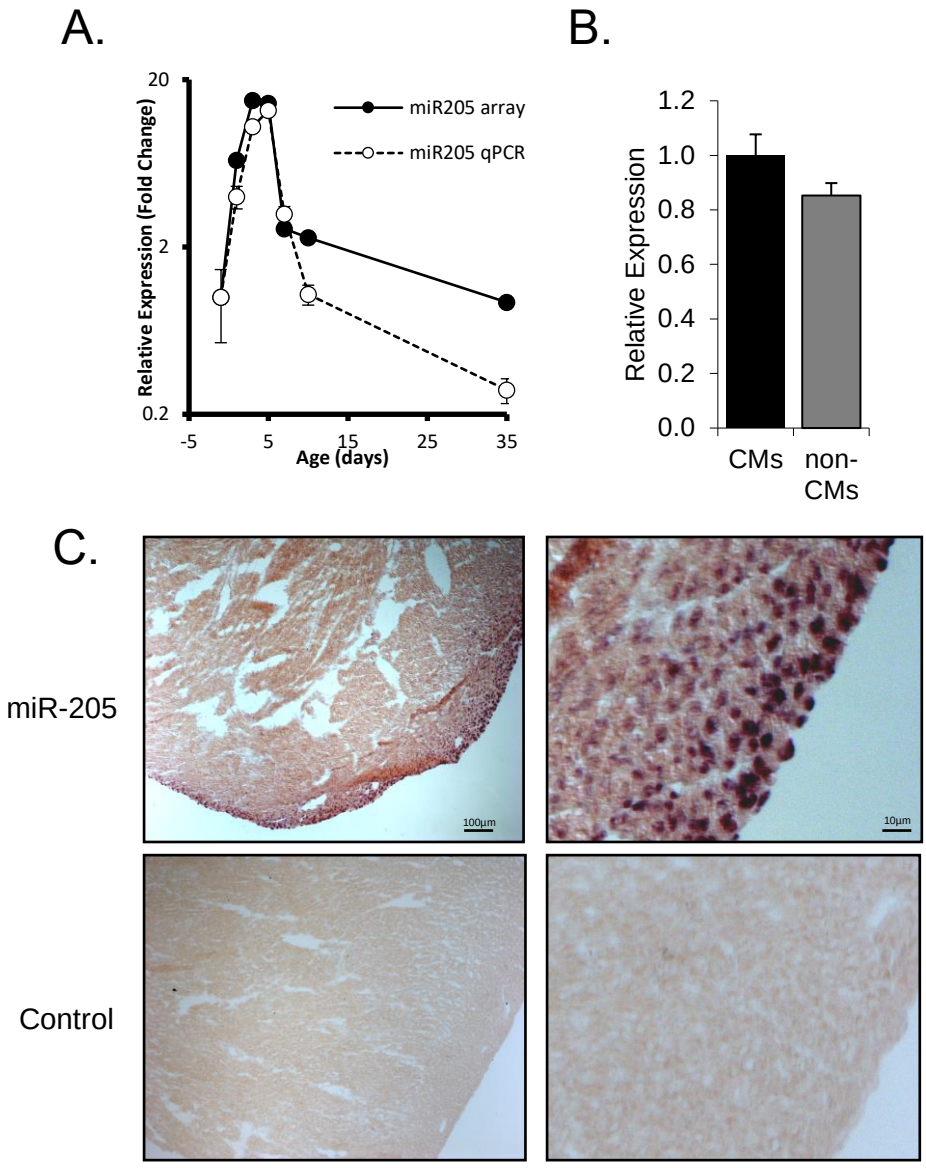

Figure 20. MiR-205 localization and cell-type specificity in the neonatal heart. A) miR-205 was identified in the microarray as having a dramatic transient increase in expression after birth (solid line). RT-qPCR was performed to confirm the trend seen in the microarray (dashed line). RT-qPCR data consists of 3 independent experiments run in triplicate. B) RT-qPCR data shows that miR-205 is expressed by both cardiomyocytes and supporting cells of the myocardium (p=0.0831). Data is presented as mean ± is presented as mean ± SEM. RT-qPCR data in A and B consists of 3 independent experiments run in triplicate. Significance was tested using student's t-test. C) In situ hybridization showing miR-205 localization to the epicardium in 5D mouse hearts. The bottom row serves as a control run in tandem with no miRNA probe. Heart sections are representative images.

hearts have been shown to have a thin myocardium and abnormalities in the ventricular walls (Singh et al., 2016). Logically, antiproliferative signaling would be strongest near the epicardium where cardiomyocytes are actively dividing. Taking into account miR-205's antiproliferative properties, it's localization near epicardium suggests a role in cardiomyocyte cell cycle withdrawal.

Previous studies have shown that there is an upregulation of fetal/perinatal genes in the heart after injury, although no replication occurs. Using samples obtained from Dr. Liu's laboratory at the University of Ottawa Heart Institute, examination of miR-205 expression levels was carried out in hearts 3D post-myocardial infarction (MI), or after 7D of transverse aortic constriction (TAC). RT-qPCR analysis showed an increase in miR-205 expression (5-7 fold) (Figure 21). After myocardial injury, fetal genes promoting replication have been shown to be expressed in the region of injury (Dirkx et al., 2013). However, there is minimal success in initiating cardiomyocyte cell division, possibly due to antiproliferative non-coding RNA signaling such as miR-205. For our studies, we have focused on the role of miR-205 in neonatal cardiomyocyte proliferation.

5.2 Generation of a postnatal cardiac-specific deletion of miR-205

In a study published by Wang et. al in 2013, gene targeting model of miR-205 was generated and characterized (Wang et al., 2013). This miR-205 global deletion model resulted in death beginning around 5.5D, which the authors hypothesized to be due to negative regulation of Pten, causing restriction of skin stem cell proliferation. The neonatal cardiac miR-205 expression suggested that the lethality of miR-205 genetic deletion model may have originated (in part) from cardiac abnormalities. Accordingly, we reached out to this group for a collaborative investigation into the role of miR-205 in the heart (Dr.

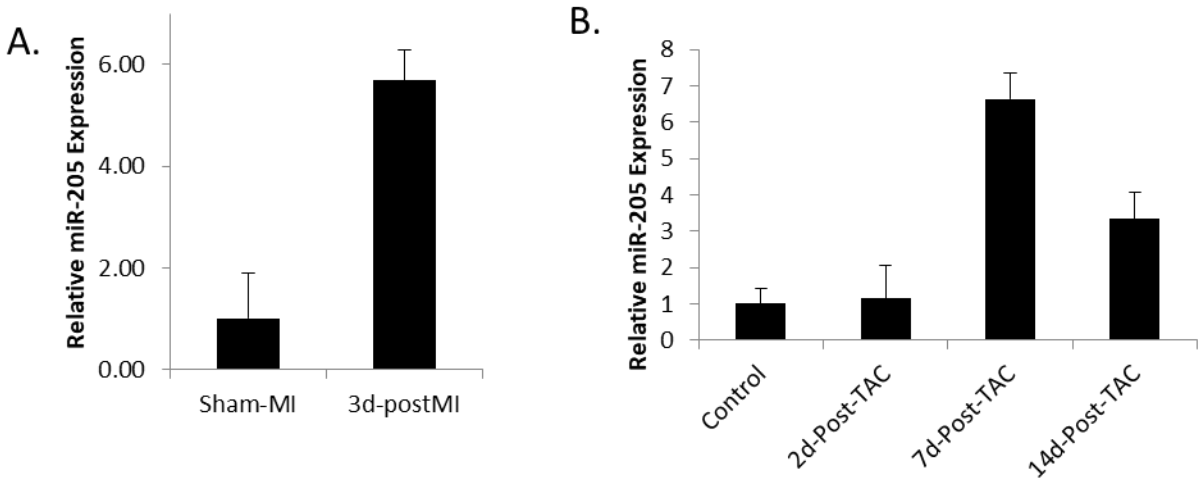

Figure 21. MiR-205 expression is upregulated after cardiac injury. A) MiR-205 undergoes a 5-fold increase in expression 3 days post-myocardial infarction. B) Preliminary data showing that miR-205 expression increases after 7 days of transverse aortic constriction (TAC), and with a reduction by 14 days of TAC. Data is presented as mean ± SEM. RT-qPCR data consists of 2 hearts pooled and run in triplicate.

Rui Yi, at the University of Colorado, provided us with a miR-205$^{K19Cre-/-}$ mouse model). This mouse strain contained a conditional deletion of miR-205 in skin fibroblasts. Using a backcross approach, we outbred the K19Cre locus and generated a miR-205$^{fl/fl}$ mouse line. To conditionally delete miR-205 from postnatal cardiomyocytes, the miR-205$^{fl/fl}$ mouse line then was bred with a αMHC-Cre mouse (JAX Stock # 011038) (Agah et al., 1997) to establish a miR-205$^{\alpha MHCCre-/-}$ mouse line. For the remainder of this chapter, our postnatal cardiac-specific deletion of miR-205 will be labeled as miR-205$^{-/-}$. A detailed explanation for the generation of miR-205$^{-/-}$ is found in Methods chapter 2.2.2 and Figure 22A. These mice survive the neonatal period in expected Mendelian ratios and are externally phenotypically normal (normal weight gain and behaviour) through to early adulthood. With no external phenotype, we sought to determine whether there were changes occurring in gene and protein expression, and whether this had any effect on heart and/or cardiomyocyte maturation and growth.

5.3 Characterization of cell cycle protein expression in miR-205$^{-/-}$ hearts

Due to the body of literature supporting a role for miR-205 in cell cycle inhibition, we performed a thorough investigation into the consequences of miR-205 deletion in the heart and whether similar disruptions in cell cycle control were evident. Specifically, we aimed to determine whether there were any gross morphologic and phenotypic changes including heart size, myocardial cell number and/or size.

Initial RT-qPCR analysis confirmed that miR-205 expression is reduced in miR-205 hearts at 5D (p=2.66E-06) and comparably low at 10D (p=0.221) (Figure 22B). For this experiment, RNA was extracted from whole hearts, including fibroblasts, which explains the residual expression of miR-205 still observed. In terms of heart mass,

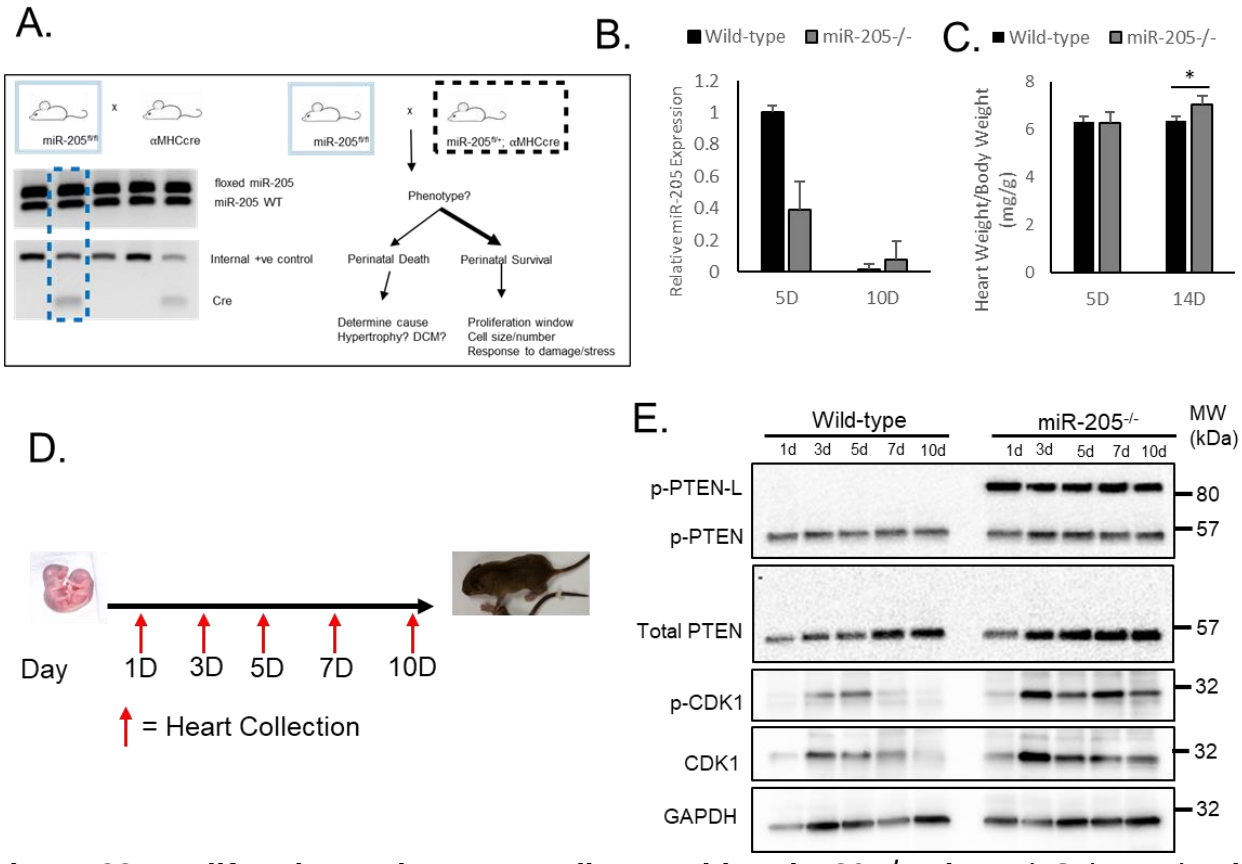

Figure 22. Proliferative pathways are disrupted in miR-205$^{-/-}$ mice. A) Schematic of the breeding strategy to generate a cardiac-specific miR-205 knockout mouse. B) RT-qPCR analysis confirming reduced miR-205 expression in the heart at 5D (p=2.66E-06) and 10D (p=0.221). RNA was extracted from whole hearts, which explains the residual expression in 5D mice. C) MiR-205$^{-/-}$ hearts are the same size as wild-type at 5D (p=0.471) and are larger by 14D post-birth (*p=0.0459). Data in B and C is presented as mean ± SEM. Significance was tested using student's t-test. RT-qPCR data represents 3 independent experiments run in triplicate. D) Schematic for the timeline of neonatal heart collection. E) Western blot analysis of PTEN and CDK1 in wild-type and miR-205$^{-/-}$ hearts. Extracts from post-natal hearts were pooled (n=3 hearts and 30µg protein per lane) and fractionated by SDS-PAGE. Western blots shown are a representative of three independent experiments. GAPDH is included as a loading control.

miR-205$^{-/-}$ hearts are comparable to wild-type at 5D (p=0.471), but by 14D miR-205$^{-/-}$ hearts are slightly but significantly larger (p=0.0459) (Figure 22C).

Similar to the microarray experiments, hearts were collected from mice at several timepoints during the neonatal period (1D, 3D, 5D, 7D, and 10D) (schematic in Figure 22D) and protein expression analysis was carried out via western blot. PTEN is a tumour-suppressor gene in the PI3K pathway responsible for regulating cell cycle and preventing unregulated growth (Goberdhan and Wilson, 2003). A schematic showing PTEN and its role in the PI3K pathway was previously shown in Figure 6 (Introduction chapter 1.3.5). PTEN protein expression levels appear higher in neonatal miR-205$^{-/-}$ hearts compared to wild-type (Figure 22E). Our data confirms miR-205's targeting of the PTEN transcript. Since p-PTEN levels are comparable in wild-type and miR-205$^{-/-}$ hearts, we hypothesize a compensatory mechanism exists to maintain PTEN phosphorylation and activity in the maturing heart.

Interestingly, miR-205$^{-/-}$ hearts express significant levels of an alternate N-terminal extended isoform of PTEN. Several translational isoforms of PTEN have been confirmed, including PTEN-L/M/N/O, with each having an increasingly longer N-terminal extension (Malaney et al., 2017). These constitutively active isoforms are produced from non-AUG translational initiation and are not well characterized, but have been shown to play a role in rRNA production, cell proliferation, and mitochondrial structure/function (Malaney et al., 2017). Our finding of increased PTEN-L in miR-205$^{-/-}$ mice suggests that miR-205 may also be responsible for repressing expression of alternate PTEN isoforms which participate in proliferative signaling.

We next sought to determine whether the increased heart weight observed in Figure 22C was due to increased cardiomyocyte proliferation. Interestingly, we also observed a marked increase in both total- and p-CDK1 expression in miR-205$^{-/-}$ hearts (Figure 22E). p-CDK1 is a G2/M checkpoint marker signifying cells actively undergoing division. This result suggests that cardiomyocytes may have increased G2/M activity which is consistent with the increased proliferative signaling up to 10D post-birth in miR-205$^{-/-}$ hearts.

5.4 MiR-205 regulates Hippo signaling by targeting Yap1

The reported miR-205 interaction with Yap1 (Du et al., 2017) suggests that this miRNA may similarly influence Hippo pathway dynamics in cardiomyocytes. The Hippo pathway is a major regulator of organ size via cell proliferation and apoptosis, and has recently been identified as playing an important role in the epicardium and heart development (Singh et al., 2016). A schematic showing the role of YAP1 in the Hippo pathway was shown previously in Figure 5 (Introduction chapter 1.3.4). Inhibition of Hippo signaling (via suppression of YAP1) leads to a reduction in epicardial cell proliferation and differentiation into mature endothelial cells (Singh et al., 2016). Alternatively, constitutive activation of YAP1 has been shown to increase heart size and cardiomyocyte number (von Gise et al., 2012). MiR-205$^{-/-}$ mice, as expected, show increased YAP1 protein expression at all neonatal timepoints (Figure 23A). By de-repressing YAP1, miR-205 deletion resulted in severe dysregulation of other members of the Hippo signaling pathway such as LATS1, p-MOB1, MST1, and SAV1 (Figure 23A). Each of these Hippo pathway proteins show increased expression in miR-205 deletion hearts throughout the neonatal period. Since activation of the upstream members of the Hippo pathway lead to

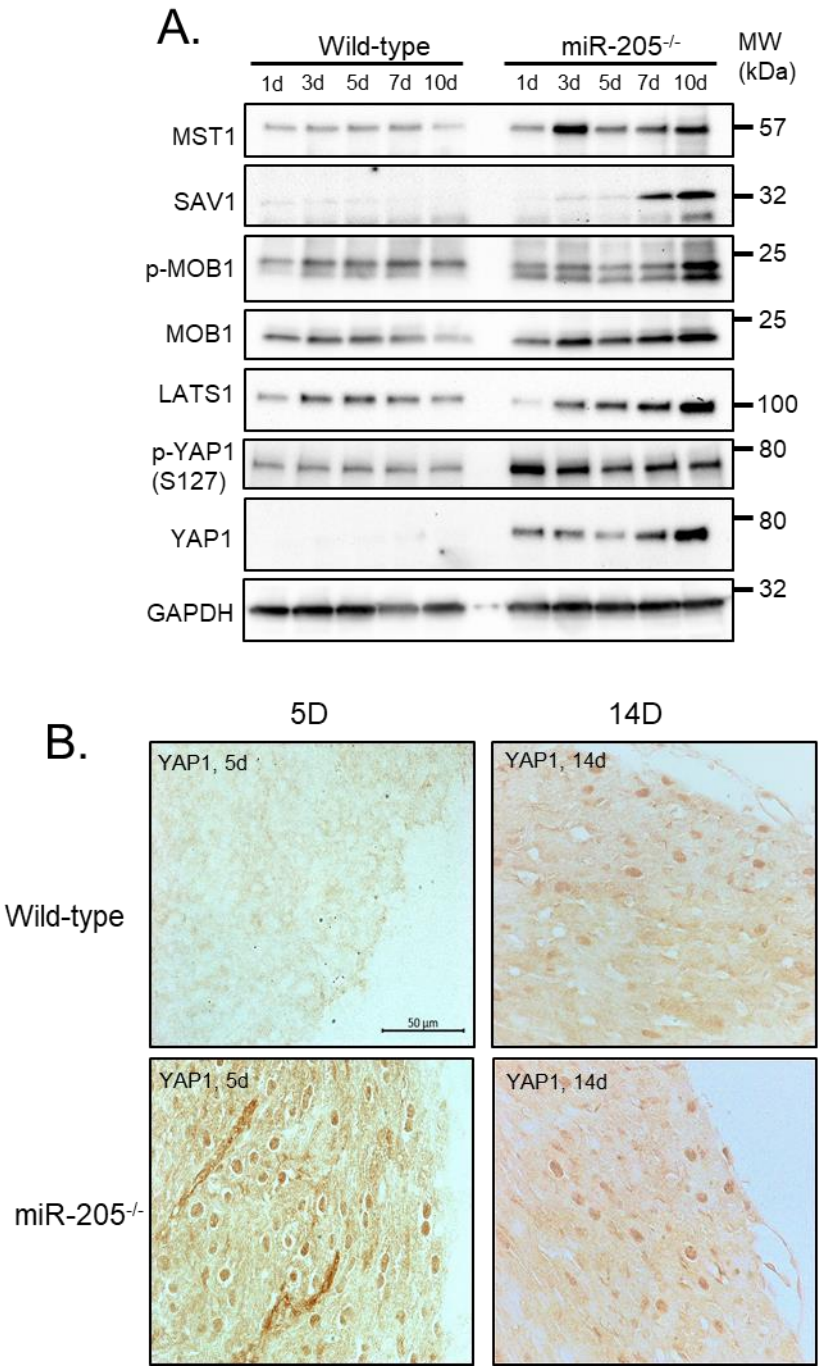
A.
Wild-type
miR-205-/-
MW (kDa)
1d 3d 5d 7d 10d
1d 3d 5d 7d 10d
MST1
SAV1
p-MOB1
MOB1
LATS1
p-YAP1 (S127)
YAP1
GAPDH
57
32
25
25
100
80
80
32
B.
5D
14D
Wild-type
miR-205-/-
YAP1, 5d
YAP1, 14d
YAP1, 5d
YAP1, 14d
50 µm

Figure 23. The Hippo pathway is disrupted in miR-205$^{-/-}$ mice. A) MiR-205 has been shown to target YAP1, further confirmed by increased YAP1 expression in miR-205$^{-/-}$. Additionally, there is upregulation of other Hippo signaling proteins. Extracts from post-natal hearts were pooled (n=3 hearts and 30µg protein per lane) and fractionated by SDS-PAGE. Western blots shown are a representative of three independent experiments. GAPDH is included as a loading control. B) Nuclear YAP1 expression is increased in miR-205$^{-/-}$ mice at 5D. Yap1 expression visualized by immunohistochemistry in 5D and 14D wild-type and miR-205$^{-/-}$ hearts. Heart sections shown are representative images.

inhibition of YAP1 activity, this is likely a compensatory response to inhibit YAP1 proliferative signaling and promote terminal differentiation of cardiomyocytes.

Next, we used immunohistochemistry to visualize YAP1 levels and localization in neonatal mice. In miR-205$^{-/-}$ mice, YAP1 is more highly expressed in the myocardium compared to wild-type mice at 5D post-birth (Figure 23B). YAP1 expression is especially prominent in the nuclei of miR-205$^{-/-}$ cardiomyocytes, where it is functionally active and can exert its proliferative effects. These observations demonstrate that the upstream Hippo pathway regulating YAP1 is active and phosphorylating YAP1, yet these alterations are not sufficient to overcome the robust increase in total YAP1 protein in the heart. At 14D, expression levels of YAP1 are similar in both wild-type and miR-205$^{-/-}$ mice.

5.5 The neonatal proliferative window is extended in miR-205$^{-/-}$ mice resulting in increased cardiomyocyte number

Based on our findings that miR-205$^{-/-}$ hearts displayed increased expression of pro-proliferative signaling proteins, we next investigated whether miR-205 deletion altered the growth/proliferative capacity of cardiomyocytes. Here, we utilized immunohistochemical analysis of Ki67 and pH3 in neonatal miR-205$^{-/-}$ hearts as a compliment to the western blot analysis of heart protein lysates. Ki67 and pH3 are commonly used markers to identify actively dividing cells when visualized by IHC (Kim et al., 2017; Scholzen and Gerdes, 2000). Ki67 and pH3 levels were similar at 5D when comparing miR-205$^{-/-}$ to wild-type ($p=0.189$ and 0.464, respectively), indicating a similar number of actively cycling cells (Figure 24 A&B). By 14D, the overall number of actively dividing cells in both miR-205$^{-/-}$ and wild-type is reduced, however miR-205$^{-/-}$ hearts possessed significantly more Ki67+ and pH3+ cardiomyocytes compared to wild-type

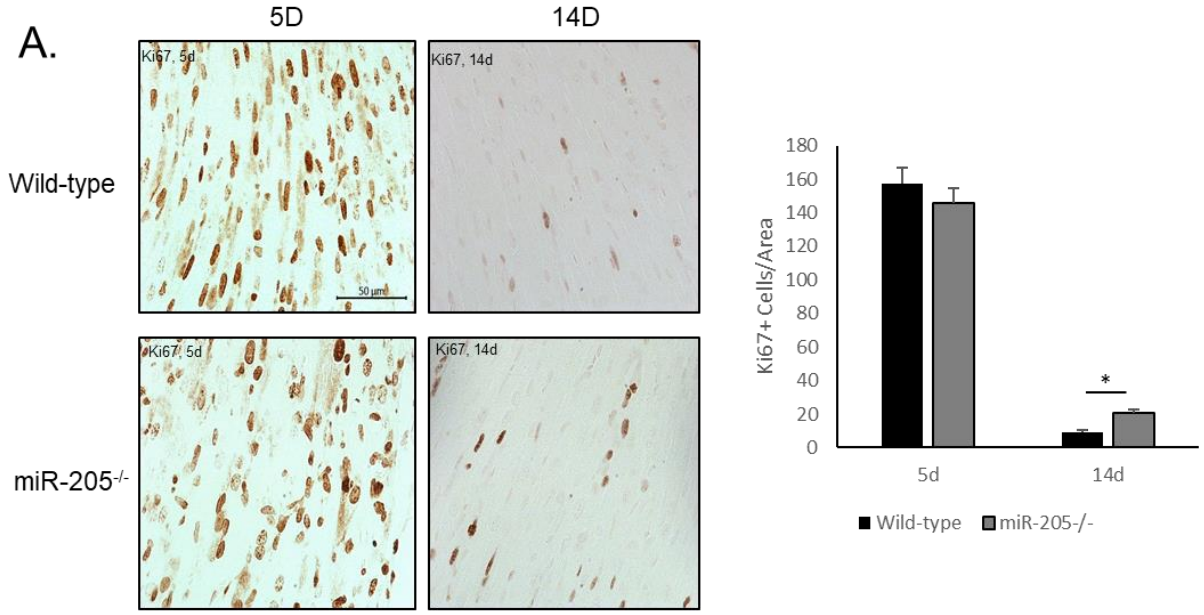
A.
5D
14D
Wild-type
miR-205-/-
Ki67, 5d
Ki67, 14d
Ki67, 5d
Ki67, 14d
50 µm
Ki67+ Cells/Area
180
160
140
120
100
80
60
40
20
0
*
5d
14d
Wild-type
miR-205-/-

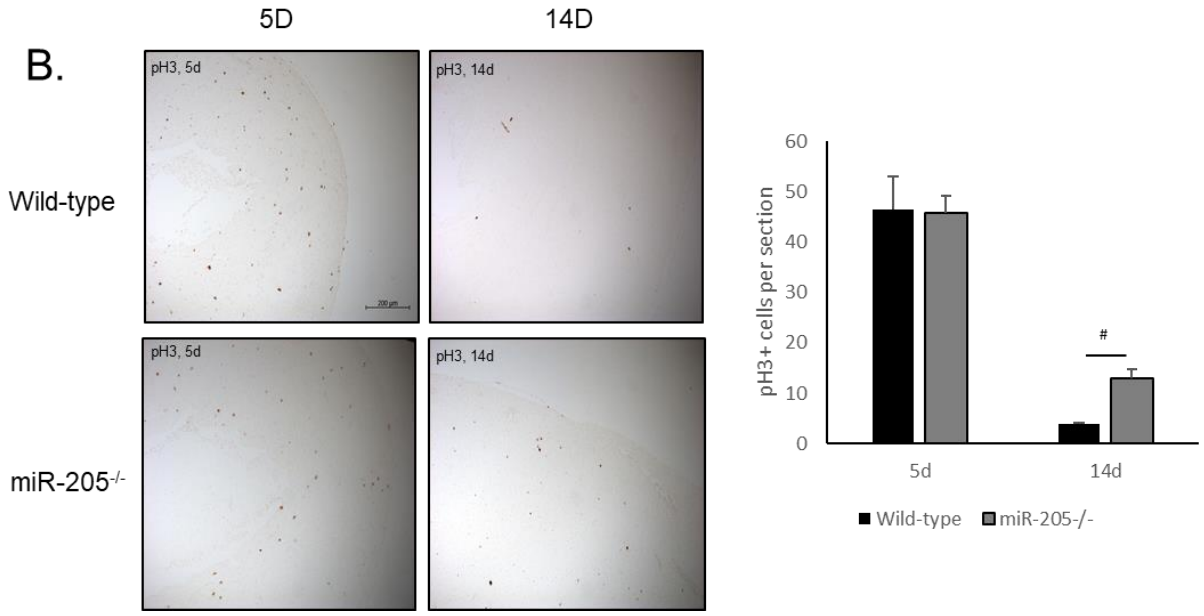
B.
5D
14D
Wild-type
miR-205-/-
pH3, 5d
pH3, 14d
pH3, 5d
pH3, 14d
200 µm
pH3+ cells per section
60
50
40
30
20
10
0
#
5d
14d
Wild-type
miR-205-/-

Figure 24. The neonatal cardiomyocyte proliferation window is expanded in miR-205$^{-/-}$ mice. A) At 5D, miR-205$^{-/-}$ and wild-type hearts show comparable numbers of Ki67+ nuclei (p=0.189). At 14D, miR-205$^{-/-}$ hearts contain significantly more Ki67+ cells (*p=7.31E-05). B) At 5D, pH3 staining levels are similar in miR-205$^{-/-}$ and wild-type hearts (p=0.464). At 14D, miR-205$^{-/-}$ hearts contain significantly increased levels of pH3 staining ($^{\#}$p=5.79E-04). Data was collected as # of positive cells per heart section. Data is presented as mean ± SEM. Significance was tested using student's t-test. Heart sections shown are representative images.

(p=7.31E-05 and 5.79E-04, respectively). These observations suggest that the cardiomyocyte proliferative window is expanded in miR-205$^{-/-}$ hearts and further imply that miR-205 may modify the cardiomyocyte cell cycle.

To monitor the impact on cardiomyocyte proliferation/total cell number, wild-type and miR-205$^{-/-}$ hearts were sectioned and stained with WGA/DAPI to outline cell membranes and label nuclei, respectively. ImageJ was used to measure and count cardiomyocytes from 5D and 14D stained heart sections. For cell number, cardiomyocytes were identified by large cell and nucleus size. Fibroblasts were identifiable by their dramatically smaller size and were omitted from cardiomyocyte cell counts. MiR-205$^{-/-}$ mice showed a similar number of cardiomyocytes at 5D compared to wild-type (p=0.161), however by 14D they possessed a significantly increased number of cardiomyocytes (p=1.58E-10) (Figure 25A). Next, using our previously published method described in Chapter 3, we isolated cardiomyocytes from wild-type and miR-205$^{-/-}$ hearts to measure cell length, width, and area. For cell measurements, cardiomyocytes were identified by their rod-shape, then ImageJ was used to measure the length and width of each identified cardiomyocyte. MiR-205$^{-/-}$ cardiomyocytes showed reduced cell length (p=2.90E-03), increased cell width (p=0.0336), and comparable cell area (p=0.207) when compared to wild-type littermate controls (Figure 25B). This data shows that the increased proliferative signaling in miR-205$^{-/-}$ hearts shown by western blot translates to increased cardiomyocyte replication and number after the neonatal period. Furthermore, the miR-205$^{-/-}$ cardiomyocytes appear to be measurably shorter and wider than wild-type cells, with more density in the extracellular matrix scaffolding of the heart.

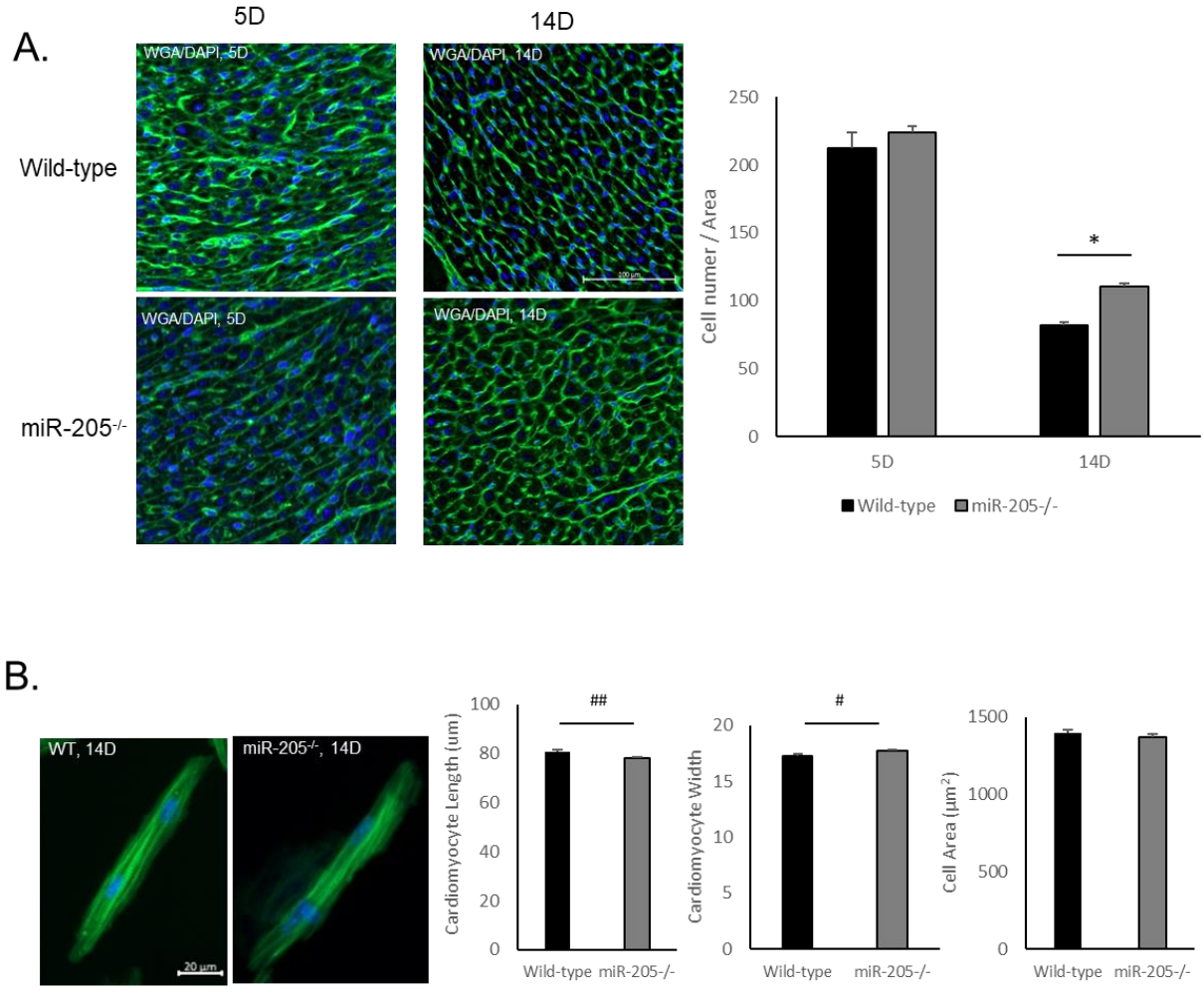

Figure 25. MiR-205$^{-/-}$ hearts have increased cell number. A) At 14D, miR-205$^{-/-}$ mice have an increased number of cells per unit as measured by wheat germ agglutinin staining (*p=1.58E-10). No difference in cell number is observed at 5 days (p=0.161). Density was calculated as number of cardiomyocytes in a 200µm x 200µm area. Heart sections are representative images. B) Isolated 14D miR-205$^{-/-}$ cardiomyocytes show reduced cell length ($^{\#\#}$p=2.90E-03), increased cell width ($^{\#}$p=0.0336), and comparable cell area (p=0.207) compared to wild-type littermate controls. All data is presented as mean ± SEM. Significance was tested using student's t-test.

5.6 Conclusions

In summary, we confirmed that miR-205 expression peaks at postnatal 5D in cardiomyocytes. Additionally, this expression originates from the epicardium, where cardiomyocyte proliferative is most active before birth. As seen with many fetal genes, miR-205 expression is also increased after cardiac injury.

We generated a miR-205$^{-/-}$ mouse model to identify the role of miR-205 during the neonatal cardiac transition. Our miR-205$^{-/-}$ model demonstrated increased heart weight by 14D post-birth (Figure 22B). This increase in weight was explained by the increased cardiomyocyte number resultant from the enhanced proliferative signaling throughout the neonatal period (p-CDK1, p-PTEN, YAP1) (Figure 22E). YAP1 expression was drastically increased in miR-205$^{-/-}$ hearts, as shown by western blot and immunohistochemistry (Figure 23). We also observed a compensatory increase in upstream Hippo pathway phosphorylation and activation (Figure 23).

We next demonstrated that miR-205$^{-/-}$ cardiomyocytes possess an expanded proliferative window (Figure 24). This resulted in increased in cardiomyocyte number in the neonatal heart (Figure 25). Additionally, these cardiomyocytes have a significant reduction in length and increased width, while maintaining an overall similar cell area (Figure 25B). By removing miR-205 regulation of the PI3K/PTEN and Hippo pathways, there was a notable increase in proliferative signaling. Overall, the deletion of miR-205 is consistent with an extended proliferative window in the neonatal period.

Given these observations, we also sought to determine whether deletion of miR-205 (and the resultant increase in cardiomyocyte number) would impact adult heart function. Preliminary experiments showed miR-205$^{-/-}$ adult mice have a heart failure

phenotype and die before 1 year of age. This premature death was investigated thoroughly, and the data is found in Figures A2 to A4. The data displayed for miR-205$^{-/-}$ adult hearts is consistent with previous studies showing that the prolonged expression of Cre recombinase under control of the αMHC promoter results in cardiac maladaptation and heart failure (Pugach et al., 2015). As such, we could not confidently determine whether the characteristics observed in our miR-205$^{-/-}$ adult mice were a result of miR-205 deletion or Cre-recombinase overexpression. The effect of miR-205 deletion in the adult heart would need to be studied using an alternative method such as a doxycycline- or tamoxifen-inducible Cre promoter to overcome the confounding effects of Cre recombinase under the control of the αMHC promoter.

Chapter 6: MiR-205 overexpression dysregulates proliferative signaling in the postnatal heart

Based on the observations in chapter 5, where miR-205 deletion resulted in cell cycle dysregulation and an expanded proliferative window, we next sought to determine the effect of miR-205 overexpression on the heart. By doing so, we aimed to further characterize the role that miR-205 plays in the neonatal heart. We generated a cardiac-specific conditional overexpression model of miR-205 and characterized its effect on the PI3K and Hippo signaling pathways.

6.1 Generation of a cardiac-specific inducible overexpressor of miR-205

As described in the Methods Chapter 2.2.3, a doxycycline (DOX)-inducible overexpression model of miR-205 was generated. This model utilizes two transgenic strains as a strategy for selectively overexpressing miR-205 in cardiomyocytes, while allowing for temporal control of expression. One mouse strain contained a reverse tet-transactivator (rtTA) locus under control of the αMHC promoter. MiR-205 was placed downstream of a tetO promoter in another strain. In offspring that possess both loci, the administration of DOX-containing water facilitates the binding of rtTA to the tetO promoter and forces the expression of miR-205 in aMHC-expressing cells (cardiomyocytes). These cardiac-specific DOX-induced overexpression mice will be referred to as miR-205^{OE} for the rest of this chapter (Figure 26A).

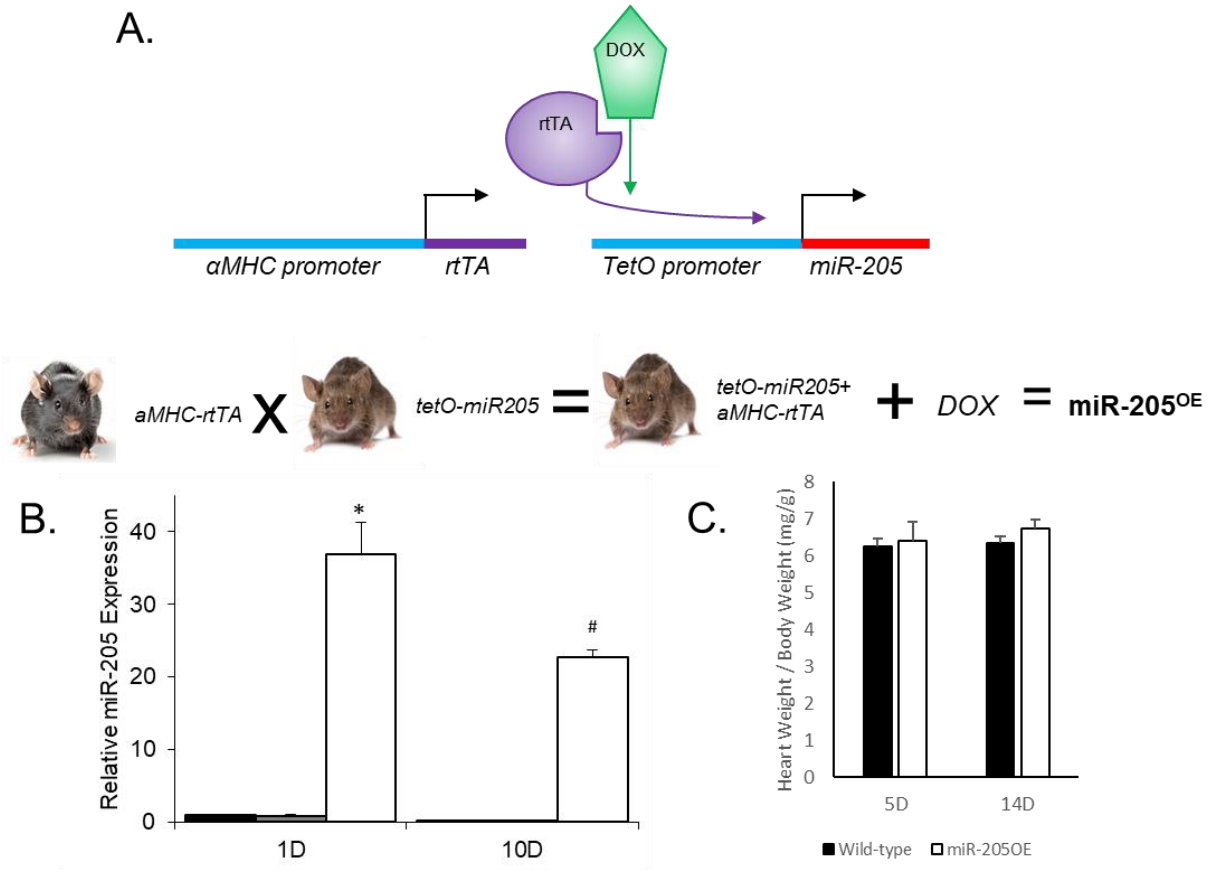

Figure 26. Generation and characterization of a cardiac-specific miR-205 overexpressing mouse. A) A 2-hit Dox-inducible system was generated to overexpress miR-205 in mice. A reverse tet-transactivator (rtTA) locus was placed under control of the αMHC promoter, while miR-205 was placed downstream of a tetO promoter. In mice that have both loci, the presence of Dox allows the rtTA to bind the TetO promoter and forces the expression of miR-205. B) RT-qPCR data confirming the upregulation of miR-205 in miR-205^{OE} cardiac tissue compared to wild-type controls at 1D (*p=7.42E-03) and 10D ($^{\#}$p=1.03E-03) (n=3 hearts per timepoint). RT-qPCR data consists of 3 independent experiments run in triplicate. C) HW/BW data shows no significant difference between miR-205^{OE} and wild-type mice at 5D (p=0.468) nor 14D (p=0.0946). Data is presented as mean ± SEM. Significance was tested using student's t-test.

6.2 Characterization of the neonatal transitional period in the miR-205^{OE} myocardium

RT-qPCR data confirmed the overexpression of miR-205 at 1D (p=7.42E-03) and 10D (p=1.03E-03) compared to wild-type, when miR-205 expression is normally low (Figure 26B). MiR-205^{OE} mice are born in expected ratios and survive the neonatal period with no noticeable phenotype. There is no significant difference in heart weight between miR-205^{OE} and littermate controls at both 5D (p=0.468) and 14D (p=0.0946) post-birth (Figure 26C).

Eight breeding pairs were established to generate a cohort of miR-205^{OE} mice. Two days before pups were expected to be born, the pregnant mice were provided with DOX water at a concentration of 2mg/mL. Hearts were collected from 1D, 3D, 5D, 7D, and 10D mice, flash frozen, and stored at -80°C until sample preparation (Figure 27A). Genotyping was performed to determine which mice contained both alleles required for overexpression. This process was repeated until at least 3 overexpressing hearts were collected from each time point. Wild-type littermate control hearts were also collected and pooled (n=3) to run alongside miR-205^{OE}. SDS-PAGE followed by western blotting was performed to analyze proliferative signaling pathways in the postnatal heart.

In our miR-205$^{-/-}$ mice, we observed an increase in protein expression of PTEN, YAP1, and a variety of other cell cycle regulators. In the miR-205 overexpression model, we anticipated that early and sustained expression of miR-205 would accelerate cardiomyocyte cell cycle withdrawal, diminishing the proliferative window. During normal cardiomyocyte cell cycle withdrawal, CDK is present throughout the neonatal period, while p-CDK1 peaks at 5D. As p-CDK levels decline, cardiomyocyte cell division is

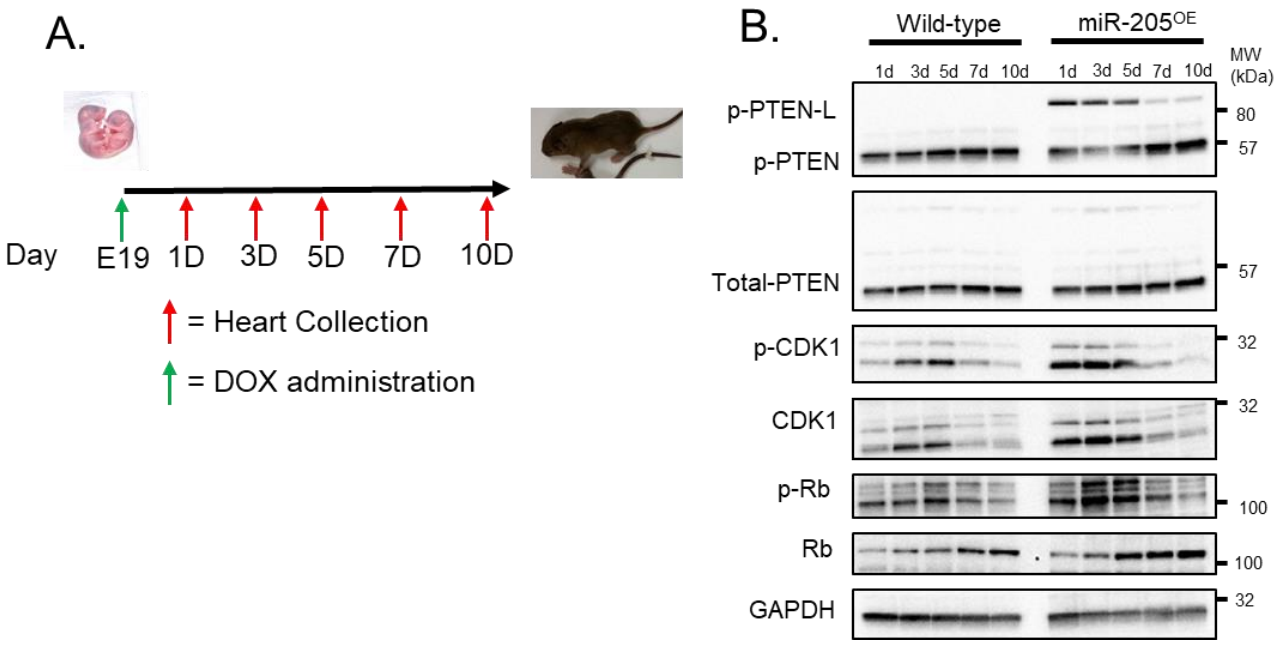

Figure 27. Cell cycle characterization of the cardiac-specific miR-205 overexpressing mouse. A) Schematic showing the timeline of DOX administration and heart collection. DOX water was provided throughout the neonatal period. B) Western blots showing dysregulated levels of cell cycle markers (p-Rb, p-CDK1) and regulators (PTEN) in wild-type and miR-205^{OE} mouse hearts. Extracts from post-natal hearts were pooled (n=3 hearts and 30µg protein per lane) and fractionated by SDS-PAGE. Western blots shown are a representative of three independent experiments. GAPDH is included as a loading control.

inhibited, and the heart's proliferative capacity is lost. In miR-205^{OE} hearts, there is an increase in both total and p-CDK1 levels early in the neonatal period (Figure 27). This indicates that miR-205 overexpression in the heart caused an unexpected increase in proliferative signaling. Interestingly, while p-CDK1 levels peak at 5D in wild-type, in miR-205^{OE} the peak occurs earlier (3D) before declining and reaching comparable levels to wild-type by postnatal 7D. Total CDK1 levels are also comparable to wild-type by 7D (Figure 27).

A similar result is observed in the Rb western blot data of Figure 27. In wild-type hearts undergoing normal cardiomyocyte cell cycle withdrawal, total Rb gradually increases over the neonatal period. Simultaneously, p-Rb levels increase until 5D, after which they reduce dramatically. Along with this reduction in p-Rb, cardiomyocyte division is halted. MiR-205^{OE} hearts show the same total Rb expression level pattern as wild-type through the neonatal period (Figure 27). In miR-205^{OE} hearts, p-Rb levels peak earlier than wild-type (3D vs. 5D), with much higher expression levels (Figure 27). At 7D post-birth, p-Rb levels in miR-205^{OE} hearts are comparable to wild-type. This result, along with the CDK1 data described above, suggests that miR-205^{OE} hearts are hyperproliferative earlier than wild-type littermates, with a similar shutdown of proliferative signaling around 5D. In wild-type hearts, there is a correlation between the reduction in p-CDK1 and p-Rb levels and cardiomyocyte indivisibility after birth. MiR-205^{OE} hearts show increased proliferative signaling compared to wild-type, which was unexpected. However, levels of p-CDK1 and p-Rb reach normal levels by 7D in miR-205^{OE} hearts. These results indicate compensatory mechanisms may exist to overcome miR-205

antiproliferative signaling to ensure enough cardiomyocytes are generated for proper function of the heart.

Finally, PTEN and p-PTEN levels appear to be quite similar when comparing wild-type and miR-205^{OE} (Figure 27B). Interestingly, there is increased expression of p-PTEN-L between 1D and 5D in miR-205^{OE} mice. In both our miR-205$^{-/-}$ and miR-205^{OE} mouse models, there is an increase in PTEN-L expression, although they do not follow the same expression patterns. In miR-205$^{-/-}$ heart, PTEN-L expression was high throughout the neonatal period, while in miR-205^{OE}, PTEN-L is most highly expressed at 1D and is mostly absent by 7D. As mentioned in Chapter 5.4, PTEN-L is a constitutively active isoform of PTEN involved in cell proliferation and differentiation. Although little is known about PTEN-L, especially in the heart, miR-205 may be involved in the regulation of the PTEN-L isoform to regulate PI3K/PTEN pathway signaling.

6.3 Hippo signaling is dysregulated in miR-205^{OE} mice

After observing an increase in YAP1 and Hippo signaling in neonatal miR-205$^{-/-}$ mice with subsequent expansion of the proliferative window, we sought to address whether overexpression of miR-205 would lead to the inverse phenotype: reduced YAP1 and Hippo signaling with a corresponding reduction in proliferative signaling. Unexpectedly, miR-205 overexpression also caused an acute increase in Hippo signaling, albeit occurring immediately after birth (Figure 28). Later in the neonatal period, levels of MST1, SAV1, p-MOB1, and LATS1 are comparable to wild-type levels by 10D. Total YAP1 protein levels were not decreased in miR-205^{OE} hearts compared to wild-type and were higher than levels seen in wild-type mice.

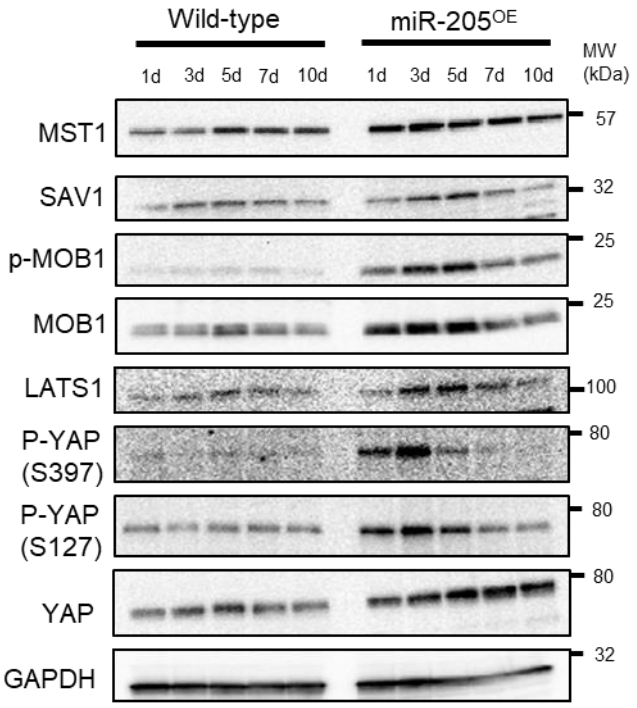

Figure 28. Hippo signaling is dysregulated during the early neonatal period in miR 205^{OE} mice. Western blots showing dysregulated Hippo signaling in wild-type and miR-205^{OE} mice. Extracts from post-natal hearts were pooled (n=3 hearts and 30µg protein per lane) and fractionated by SDS-PAGE. Western blots shown are a representative of three independent experiments. GAPDH is included as a loading control.

Although we have induced overexpression of miR-205, it seems there are separate regulatory mechanisms in place to drive expression of YAP1. It is also interesting to note the difference in p-YAP1 levels. Phosphorylation of YAP1 by LATS1 results in translocation to the cytoplasm where it is inactive. Thus, p-YAP1 is inactive YAP1. Our analysis revealed increased levels of p-YAP1 immediately after birth in miR-205^{OE} hearts (Figure 28). Although overexpression of miR-205 resulted in increased YAP1 levels, it also increased YAP1 phosphorylation. At 5D, overall YAP1 expression is increased, in both the cytoplasm and nuclei (Figure 29). By 14D, YAP1 levels in miR-205^{OE} hearts are comparable to wild-type (Figure 29). MiR-205 overexpression appears to initiate the transitional program earlier, as the increased levels of p-YAP1 suggest that cells are trying to promote terminal differentiation of the cardiomyocytes by phosphorylating YAP1 to inhibit proliferative signaling.

By overexpressing miR-205, we have disrupted the transitional program leading to dysregulation of the PTEN and Hippo pathways. These results suggest that the hearts are larger due to hyperproliferation after induction of miR-205 overexpression to compensate for the earlier cell cycle withdrawal signaling observed in Figure 27. Based on our data, the overexpressors appear to be trying to establish a normal cardiomyocyte number before transitioning to their terminally differentiated state. Our next step was to determine whether the dysregulation of proliferative signaling we observed translated into altered proliferation of postnatal cardiomyocytes.

6.4 MiR-205^{OE} hearts possess increased cardiomyocyte number by 5D post-birth

An additional cohort of miR-205^{OE} neonates was used to generate samples for immunohistochemistry and immunofluorescence. At both 5D and 14D, there is no

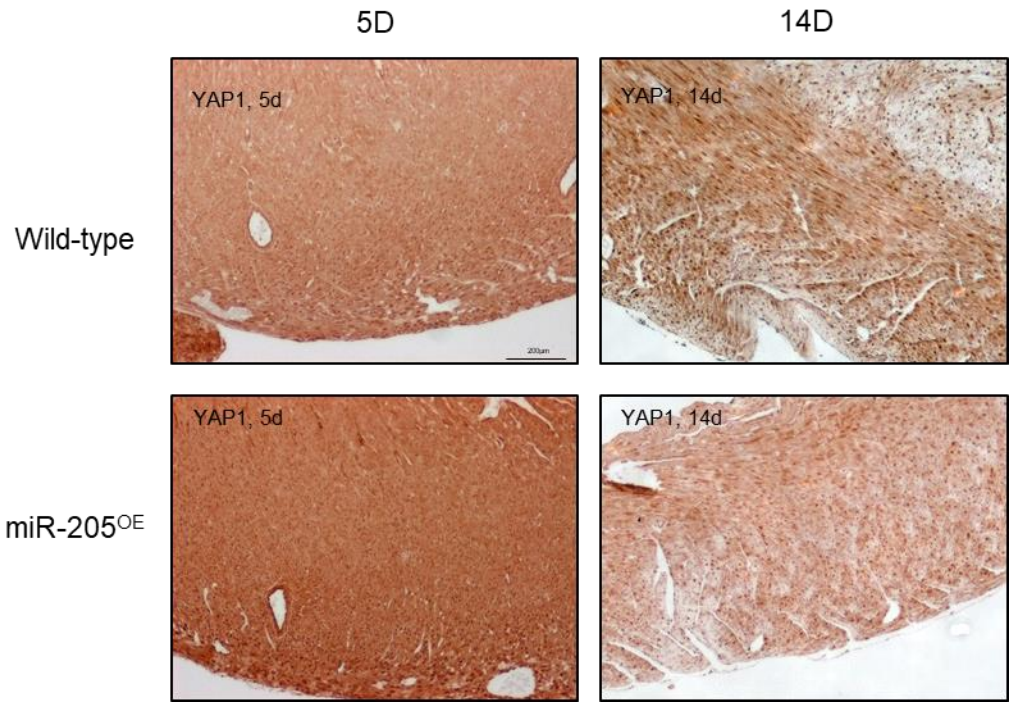

Figure 29. YAP expression and localization in miR-205^{OE} mice. Immunohistochemical view of YAP localization within 5D and 14D miR-205 overexpressors and wild-type. Increased YAP expression is observed in 5D mice with no difference in nuclear localization. At 14D, YAP levels are comparable between miR-205^{OE} and wild-type mice. Heart sections shown are representative of three independent experiments.

significant difference in Ki67 levels in the heart when comparing miR-205^{OE} mice to litter-mate controls (p=0.314 and 0.134, respectively) (Figure 30A). Similarly, there is no significant difference in pH3 staining at 5D (p=0.290) nor 14D (p=0.179) in miR-205^{OE} hearts compared to wild-type (Figure 30B). This suggests that by 5D, the expedited transitional program is over, and miR-205^{OE} hearts have similar proliferative capacity compared to wild-type at 5D.

When examining cell number in miR-205^{OE} hearts compared to wild-type, a significant increase in cell number was observed miR-205^{OE} hearts at both 5D (p=4.52E-05) and 14D (p=0.0298) (Figure 31A). This increased cell number coincides with the data in Figures 27 and 28 showing increased proliferative signaling (CDK1, p-Rb, YAP1) early during the neonatal period. By overexpressing miR-205 and expediting the transitional program, the heart establishes its cardiomyocyte number earlier than in wild-type mice. Because the transitional program was expedited, the result is an increased number of total cardiomyocytes by the end of the neonatal period. Next, cardiomyocyte size was measured using WGA/DAPI staining. MiR-205^{OE} cardiomyocytes showed no difference in length when compared to wild-type littermate controls (p=0.0785), however they exhibited reduced cell width (p=0.0332) and cell area (p=0.0261) (Figure 31B). The finding of reduced cell width contrasts with the effects of miR-205 deletion described in chapter 5, which caused cardiomyocytes to exhibit increased cell width.

The results of the overexpression model appear to show that miR-205 expression drives the transitional program in mouse neonatal hearts. When miR-205 expression is induced earlier, the hearts undergo hyperproliferation followed by earlier cell-cycle

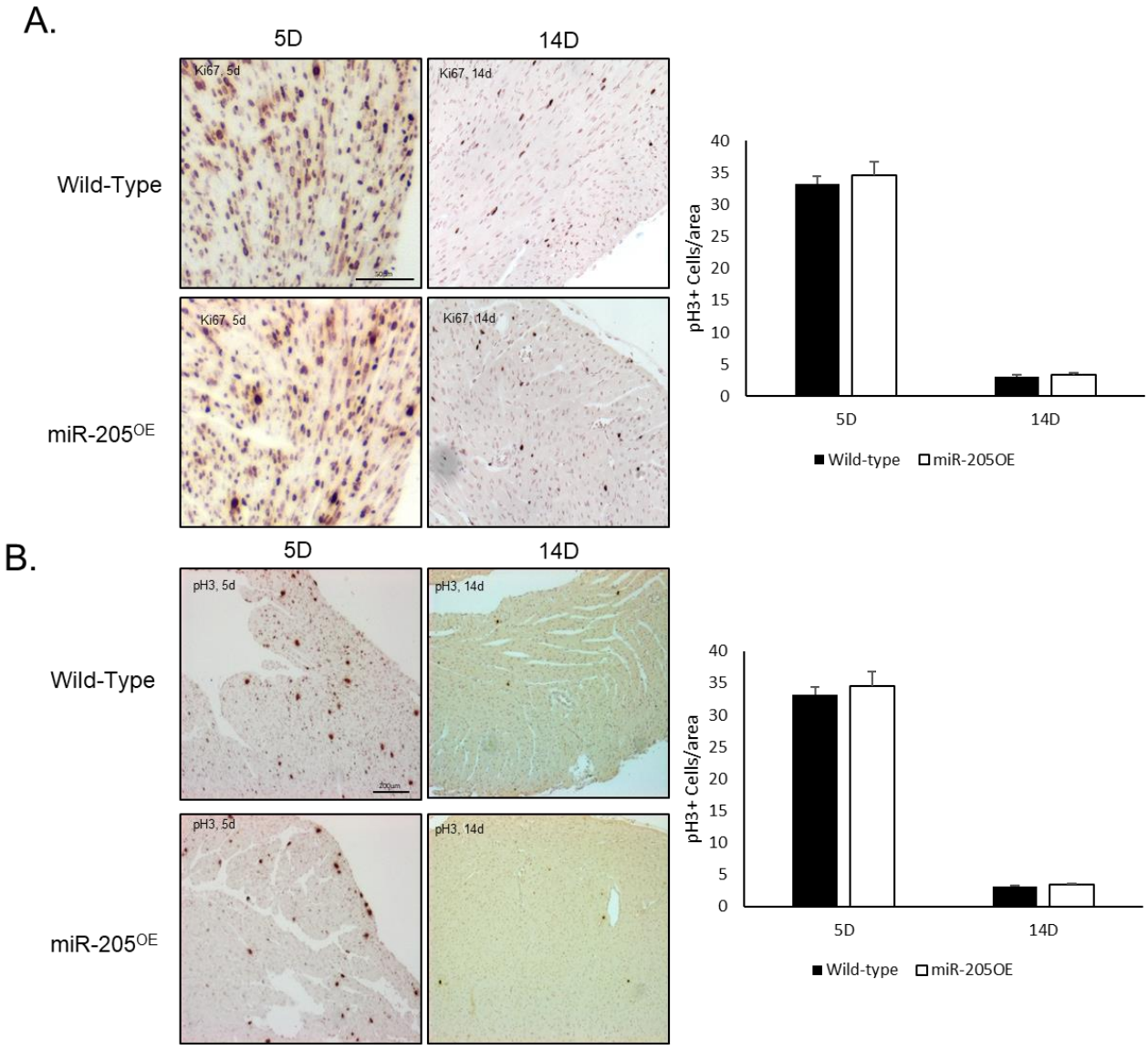

Figure 30. MiR-205 overexpression does not alter number of proliferating cells at 5D and 14D. A) Immunohistochemical analysis of cell division marker Ki67 shows that there is no significant increase or decrease in number of actively cycling cardiomyocytes at 5D (p=0.314) or 14D (p=0.134). B) Analysis of the cell division marker pH3 shows no difference in actively cycling cells at 5D (p=0.290) or 14D (p=0.179). Heart sections shown are representative images. All data is presented as mean ± SEM. Significance was tested using student's t-test.

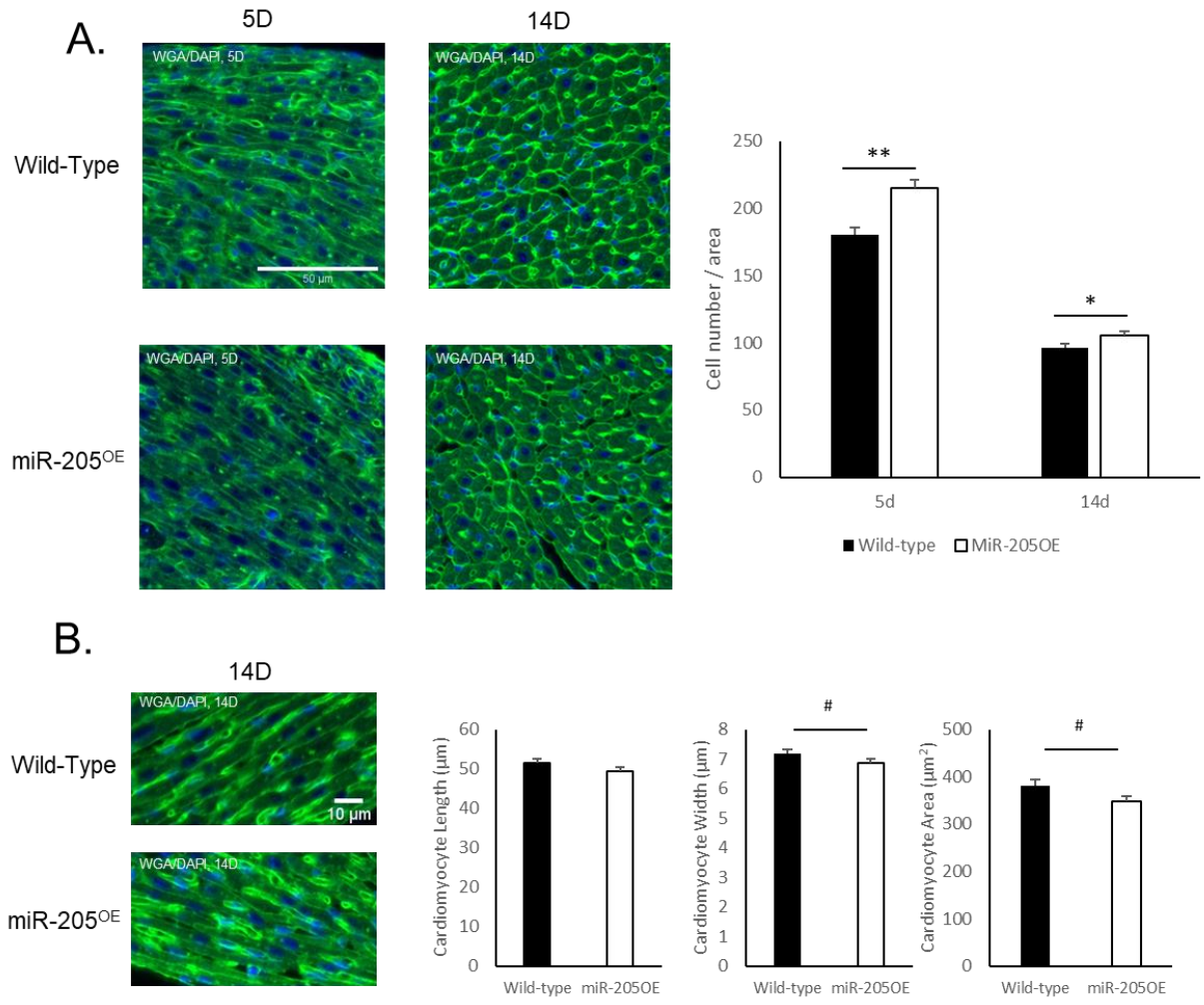

Figure 31. MiR-205^{OE} hearts contain more total cardiomyocytes at 5D and 14D. A) MiR-205^{OE} mice have an increased number of cells per unit area as measured by wheat germ agglutinin staining at 5D (**p=2.26E-05) and 14D (*p=0.0298). Density was calculated as number of cardiomyocytes in a 200µm x 200µm area. B) Cardiomyocyte measurement in heart sections indicates no significant difference in cardiomyocyte length (p=0.0785), with reduced cell width ($^{\#}$p=0.0332) and area ($^{\#}$p=0.0261) at 14D. Heart sections shown are representative images. All data is presented as mean ± SEM. Significance was tested using student's t-test.

withdrawal. The result is a heart that contains a higher number of more densely organized cardiomyocytes at 5D and 14D due to undergoing the transitional program earlier than their wild-type littermates.

6.5 Conclusions

The overexpression of miR-205 in cardiomyocytes resulted in an intriguing phenotype. Based on the miR-205 null data (Chapter 5), we expected reduced proliferative signaling and reduced cardiomyocyte division, miR-205's antiproliferative signaling appears to activate compensatory mechanisms to ensure the establishment of normal cardiomyocyte number. In miR-205^{OE} hearts, proliferative signaling by p-CDK1 and p-Rb occurs earlier and more robustly, however levels are comparable to wild-type by 7D. This early increase in proliferative signaling is further supported by a similar expression pattern observed in Hippo pathway members. Overall, the regulatory mechanisms surrounding cardiomyocyte division are dysregulated, yet compensatory mechanisms are in place to ensure enough cardiomyocytes exist to produce a functioning heart. Interestingly, miR-205^{OE} hearts appear to be healthy and normal functioning after the neonatal period, although they possess more cardiomyocytes. Dysregulation of cell cycle early in life may have long-term negative consequences on proliferative capacity and ECM integrity, and will be investigated in future studies.

Chapter 7: Discussion

In this project, we first identified the timeframe of the neonatal heart transition. We then used microarray analysis to identify significantly changing expression of mRNA and miRNA in perinatal hearts. Furthermore, our clustering and gene ontology (GO) analysis allowed us to identify significantly changing gene regulatory networks, and the transient changes they undergo. Our primary example is cell cycle mechanics, which showed 3 distinct gene expression patterns based on the cell cycle checkpoint the genes are associated with. Through our microarray analysis, we identified miR-205 as having an exceptional expression pattern with a transient 20-fold increase by 5D, returning to baseline by 10D. Further analysis showed that miR-205 was expressed primarily in cardiomyocytes near the epicardium. Using our generated miR-205$^{-/-}$ model, we showed that deletion of miR-205 results in increased postnatal heart weight and cardiomyocyte number, with an increased number of actively cycling cardiomyocytes at 14D. Individual cardiomyocytes were shorter, wider, and more densely organized in the myocardium. Based on miR-205's targeting of YAP1 and PTEN, we concluded that these phenotypical changes were caused by dysregulated Hippo and PTEN signaling. Next, we generated our miR-205^{OE} mouse model. MiR-205^{OE} hearts were similar in weight to wild-type littermate controls. However, we observed increased cardiomyocyte number at both 5D and 14D, with reduced cell width and area. MiR-205^{OE} hearts showed both increased proliferative and antiproliferative signaling, suggesting the existence of compensatory mechanisms to force cardiomyocyte replication in the context of antiproliferative signaling. Through our studies we have identified a novel role for miR-205 in the postnatal inhibition of cardiomyocyte cell division.

The neonatal period is the final critical phase for heart formation, cardiomyocyte maturation, and long-term heart homeostasis, yet the neonatal cardiac transition is not fully understood. Embryonic heart development has been studied extensively with less than day-by-day resolution of morphological changes (Brade et al., 2013; Bruneau, 2002; Moorman and Christoffels, 2003; Paige et al., 2015; Van Vliet et al., 2012; Williams et al., 2012). The primary stages of heart morphogenesis are: 1) the formation of two heart fields, 2) formation of the linear heart tube, 3) heart looping, 4) chamber development, and 5) heart cell expansion (Figure 2). Fetal cardiomyocyte specification and differentiation is orchestrated through the complex interactions of *Nkx2-5*, *Gata4/6*, *Tbx20*, and *Mef2c*, among others (Edmondson et al., 1994; Hiroi et al., 2001; Maitra et al., 2009; Xiang et al., 2016). These master transcriptional regulators mediate the expression of other key transcription factors for the heart to progress through each of these stages. Mesp1, Wnt, and Fgf signaling is involved in the earliest specification of cardiac progenitors (Marvin et al., 2001; Saga et al., 2000; Watanabe et al., 2012). Heart tube formation and looping is primarily mediated by Tbx-family transcription factors, *Mef2*, *Myocardin*, SRF, *Bmp*, *Hand1/2*, and *Irx4* (Bao et al., 1999; Desjardins and Naya, 2016; Hoogaars et al., 2007; McFadden, 2004; Tirosh-Finkel et al., 2010). Chamber morphogenesis involves regulation by Pitx2, Notch1, Bmp, Nrg1, Erbb1/2, and SRF (Bersell et al., 2009; Grego-Bessa et al., 2007; Prall et al., 2007; Sanchez-Soria and Camenisch, 2010; Schlesinger et al., 2011). Finally, heart growth via cardiomyocyte proliferation is regulated by Cyclins, CDKs, CDKIs, Meis1, the Hippo pathway, and the PI3K/Pten/AKT signaling pathway (Brooks et al., 1998; von Gise et al., 2012; Goberdhan and Wilson, 2003; Mahmoud et al., 2013; McGill and Brooks, 1995; Woo and Poon,

2003b). Developmental biologists have identified which cells contribute to the structures of the heart, and which progenitor cells they arise from. The development, proliferation, and differentiation of these cardiac progenitors is tightly regulated by *Nkx2-5*, *Gata4/6*, *Tbx20*, and *Mef2c* (Figure 1). However, this high-resolution examination of heart development during embryonic development does not continue for postnatal development. Previous studies have missed transient changes occurring in the heart when comparing 1D to 10D or adult hearts. Although these studies have provided invaluable data to the cardiac field, as we delve further into the molecular mechanisms regarding heart physiology and molecular signaling, a more detailed analysis of neonatal heart development is required. In this thesis, we have taken the first steps toward extending our in-depth knowledge of heart development into the postnatal heart.

7.1 Neonatal cardiogenomic program

During embryonic development, cardiomyocytes possess robust proliferative/regenerative capacity. After birth, the cardiac transition results in a phenotypical switch from hyperplastic growth to hypertrophic growth of myocardium, associated with an increase in binucleation index of cardiomyocytes (Soonpaa et al., 1996). Specific proteins directly involved in cytokinesis such as Anillin and Aurora kinases, are shown to be downregulated and/or improperly localized in maturing cardiomyocytes (Foglia and Poss, 2016). We have shown that Protein Regulator of Cytokinesis 1 (PRC1) is also heavily downregulated postnatally, confirming downregulation of cell cycle machinery after birth (Figure 13A). Expression of p-pRb and p-CDK1, known regulators of cell cycle checkpoint regulation, were also confirmed to be downregulated after birth (Figure 13A). Also, we observed significant Dicer1 expression

in the neonatal heart, supporting the role of miRNA biogenesis in cardiomyocyte maturation. As Dicer is the protein responsible for the processing of pre-miRNAs into mature miRNAs, the notable expression of Dicer1 indicates extensive miRNA processing during neonatal heart maturation. Due to the drastic hypertrophic growth the heart undergoes in the first 10 days of life (Figure 3), extracellular matrix remodeling is essential to generate a heart that is elastic enough to fill with enough blood, but still capable of pumping blood throughout the circulation without sustaining damage to cells. Collagen, fibronectin, and cells are reorganized by matrix metalleoproteinase (MMP) activity to regulate ECM remodeling and ensuring a structurally competent heart. We were able to show high MMP-2, -3, and -9 activity during neonatal heart development, with much lower levels in the adult heart (Figure 13B).

Through comprehensive microarray analysis, evaluating several time points post-birth, this project has achieved its goal of providing a high-resolution analysis of perinatal heart development. The microarrays for mRNA and miRNA during the perinatal period contain an immense amount of data and information. Published within an article, this data can be utilized by other researchers to examine proteins/genes of interest or discover new key regulators of neonatal heart maturation. Moreover, it is expected that this foundational analysis can be built upon in even more detailed and higher-resolution. As we have shown with miR-205, the low-resolution comparison of neonatal hearts can easily fail to identify major transient changes occurring during the neonatal period (Eulalio et al., 2012; Kou et al., 2010; Lopaschuk and Spafford, 1992; Sun et al., 2017; Talman et al., 2018). For instance, a microarray experiment comparing 1D vs. 10D would not have identified miR-205, as its levels are quite similar at 1D and 10D. The 20-fold increase in

expression at day 5 would have been missed, demonstrating the importance of high-resolution analysis during this essential developmental period. Indeed, one limitation of our study is that we only examined every 2 days, and future studies should continue the developmental approach to characterize changes that occur day-by-day or even hour-to-hour in the timespan immediately after birth. This study has shown that the physiological and molecular changes occurring as the heart begins to perform its primary function happen very rapidly, and a high-resolution approach is necessary to characterize these changes. Since the neonatal period continues to prove to be a critical point in heart development, further examination into the regulatory changes occurring in the heart could provide insight into unlocking the regenerative potential of cardiomyocytes.

Our high-resolution analysis of mRNA expression in the neonatal period elucidated many novel changes in gene ontology (GO) expression in the postnatal heart. The largest number of changes occurred between E19 vs. 1D and 10D vs. 35D (Figure 15). The large number of changes occurring between E19 and 1D compared to other timepoints demonstrates the impact that birth has on global cardiac gene expression. Also, the largest change, between 10D and 35D, was likely due to the large time scale and extensive maturation that the heart undergoes during adolescence. Other than the comparisons of pre-birth vs. post-birth and pre-adolescence vs. post-adolescence, the largest change in mRNA expression occurred between 7D and 10D (324 downregulated and 75 upregulated) (Figure 15). When performing our GO analysis, we identified many cell cycle regulatory genes being downregulated after 7D (clusters 10, 19, and 20) (Table 3). 7D post-birth is also the timepoint at which the neonatal heart has permanently lost proliferative capacity of cardiomyocytes (Porrello et al., 2011a). Interestingly, the

timepoint before this (5D vs. 7D) contains only 11 downregulated genes (Figure 15). This expression pattern can be further confirmed by clusters 11 and 16 in our gene ontology analysis, which show dramatic reductions in DNA-templated transcription, mRNA processing, and RNA pol II transcription by 7D (Table 3).

Volcano plot analysis of our microarray data allowed us to identify the number of gene expression changes occurring between each timepoint. We next sought to determine whether changes occurring over the perinatal period showed coregulation among genes with similar function. First, we used bioinformatic analysis to identify clusters of genes that followed a similar expression pattern. Next, we sought to determine whether the gene sets within each cluster shared a functional profile related to the same biological processes. Gene ontology provided a system where each gene can be classified with one or more molecular function, biological process, or cellular component. Each gene can be classified with multiple terms. Thus, we could input our dataset and identify enrichment for specific classifications. Through our GO analysis, we identified three major biological changes occurring in the neonatal heart: 1) metabolism, 2) cell cycle, and 3) heart growth and ECM remodeling (Figure 17). Other than these three, there were also several unique ontologies identified to be robustly altered.

A significant amount of research has described the metabolic changes that occur in the postnatal heart. Prior to birth, the heart resides in a hypoxic state and uses anaerobic glycolysis as its primary source of energy (Dawes et al., 1954; Lopaschuk and Spafford, 1992). As a benefit, glycolysis also provides nucleotides, amino acids, and lipids that are useful for new cell production (Heiden et al., 2009). After birth, the newborn heart is solely responsible for blood circulation, therefore energy demands increase

dramatically. With the respiratory system becoming active at birth, the heart gains access to a significantly larger supply of oxygen (Torres-Cuevas et al., 2017). With increased cardiac demand and a larger supply of oxygen, the heart switches from glycolysis to oxygen-dependent fatty acid oxidation (Onay-Besikci, 2006). Cluster 3 of our microarray analysis showed upregulation of many genes related to oxidative fatty acid metabolism. Expression of this cluster begins low and is increased by adulthood, however expression levels vary significantly during the neonatal period, showing a cyclic expression pattern. This cyclic expression pattern may represent transient regulation of fatty-acid metabolism-related gene programming via cross-talk feedback mechanisms to facilitate the metabolic transition. The metabolic transition also includes cluster 15 (oxidation-reduction, metabolism, and protein folding), which shows a similar, yet less-pronounced, pattern as Cluster 3. Expression of cluster 15 is downregulated after birth, then cycles between upregulation and downregulation between time-points, before being upregulated again by adulthood. Overall, clusters 3 and 15 show overall increase in expression of fatty-acid metabolic signaling by adulthood. The varying expression levels throughout the neonatal period demonstrate that transient regulatory changes are also occurring during the heart's metabolic transition. The two described metabolism clusters may represent interdependent transitional programs that regulate the expression of one another. Our GO analysis did not uncover a significant gene expression program change in glycolytic energy metabolism. Future research may characterize the differential expression between these metabolic clusters and why cycling of expression occurs.

The largest and most significantly changed protein ontologies were related to cell cycle kinetics (Figure 17 and Table 3), in concordance with the large body of literature

describing the downregulation of cell cycle proteins in the heart after birth (Cui et al., 2018; Porrello et al., 2013). Due to the potential of altering cardiomyocyte proliferative capacity to induce heart healing, we chose to focus our studies on cell cycle-related gene regulation. Our high-resolution analysis was able to add new depth to the understanding of the neonatal heart transition. Our data was able to identify three distinct clusters of cell cycle expression patterns within the perinatal timeframe. Each of these clusters shows a transient upregulation in expression at different postnatal time-point. In the first cluster (cluster 10), expression is initially high, then shows a decrease in expression after transient upregulation at 3D. Of the 3 cell-cycle clusters, cluster 10 shows the earliest transient upregulated activity at 3D. Cluster 10 also contains the fewest genes of the cell-cycle-related clusters, but includes notable genes such as Cdc7, Brca2, Kif20B, and Cyclin E2. The second cluster (cluster 19) contains the highest number of genes with the most significant changes occurring. This cluster shows very high initial expression which overall decreases significantly, with transient upregulation at 5D. Within cluster 19 are several important cell cycle regulatory genes such as Wee1, Chek1, Anillin, Cdc25a, Cyclin E1, and E2F7. Wee1 and Chek1 are serine/threonine kinases and key regulators of cell cycle progression by targeting and controlling checkpoint markers such as CDK1 (Mohamed et al., 2018; Porrello et al., 2011b). In concordance, we observed significant expression regulation of p-CDK1 in the postnatal heart (Figure 13). Cdc25a activation is required for progression from G1 to S phase of the cell cycle, and has been shown to activate CDK1, CDK2, and CDK4 (Sur and Agrawal, 2016). As described in Introduction Chapter 1, Anillin, Cyclin E1, and E2F7 have been shown to be heavily involved in heart

development and cardiomyocyte proliferation (Cobrinik, 2005; Engel et al., 2006; Williams et al., 2012).

The third cell cycle-related cluster (cluster 20) also contains a very large number of genes related to cell cycle regulation. After birth, expression of genes within cluster 20 increase up to 7D before being downregulated at 10D continuing into adulthood. Notable members of this cluster are PRC1, AurkA, AurkB, Cyclin B1&2, Cdc25c, Kif11, and Cdkn1a (p21). The presence of PRC1 in this cluster is notable as it supports the finding of increased PRC1 expression up until 5D and subsequent downregulation at 7D (Figure 13). Upon further investigation, the expression pattern of PRC1, shown by western blot in Figure 13, parallels the expression pattern of cluster 20. This finding helps to validate the findings of our microarray experiments, in addition to the RT-qPCR confirmation performed in Methods Chapter 2.1.2. The Aurora Kinases are serine-threonine kinases essential for mitotic entry and progression. Expression of AurkA and AurkB is associated with increased proliferative capacity (Tao et al., 2008). Cdc25c is closely related to Cdc25a describe in the previous cluster. Cdc25c phosphorylates Cyclin B and CDK1 to trigger entry into mitosis (Sur and Agrawal, 2016). Kinesin family member 11 (Kif11, also called Kinesin-5), is an essential regulator of cell cycle progression by controlling chromosome positioning, centrosome separation, and the establishment of the spindle during mitosis (Johnson et al., 2014). Finally, as described in Introduction Chapter 1, Cyclin B1/B2 and CDK inhibitor p21 are key regulators of cell cycle entry and progression (Neganova and Lako, 2008; Tane et al., 2014). Although it is well-known that proliferative signaling is downregulated after birth, our data shows that there are transient variations in expression at specific postnatal time points. Each distinct cluster related to cell cycle

dynamics shows a transient upregulation at different time-points during neonatal heart maturation. The transient upregulation identified in these cell cycle clusters, is consistent with cardiomyocytes undergoing a final round of cell division post-birth. Each cluster contains genes which represent different checkpoints within the cell cycle, and we can observe the upregulation of each checkpoint before being permanently downregulated. Although our data has identified distinct cell cycle ontology regulation, the underlying regulators of these gene expression programs remained elusive.

The third major ontology identified was related to heart growth and ECM remodelling. Cluster 1 includes several genes related to angiogenesis. This is logical because the drastic increase in heart size, as shown in Figure 3 (Introduction chapter 1.2), would require increased vascularization for the myocardium to receive sufficient oxygen for normal function. This increase in oxygenation was also important for the induction of the first major ontology identified (metabolism) and the transition to fatty-acid oxidation. Clusters 21, 23, and 26 all include genes regulating cell adhesion and extracellular matrix organization. As the heart grows during neonatal development, the ECM must adapt to accommodate for the dramatic increase in cardiomyocyte cell size, resulting in a fine balance between the myocardium being strong enough to efficiently pump blood, yet not being too rigid to fill with blood (Borg et al., 1984; Lockhart Marie , Wirrig Elaine, Phelps Aimee, 2011). Clusters 23 and 26 show upregulation, while cluster 21 shows varying expression over time ending in downregulation in the adult heart. The high expression of ECM remodelling gene programming in a number of distinct clusters identifies this as a major contributor to neonatal heart development. The large number of clusters related to ECM remodelling is important, as it signifies that this process may be

more complex than expected. It is commonly known that ECM remodelling occurs to increase heart size after birth, however the identification of such a number of clusters involved indicates that more subtle changes may be occurring in specific cell types or structures of the heart. For instance, the right ventricle is structurally, geometrically, and mechanically distinct from the left ventricle (Walker and Buttrick, 2009), and so each ventricle may express distinct temporal gene expression patterns during postnatal development. After our gene ontology analysis, we can conclude that the neonatal heart undergoes an overall increase in remodeling-related signaling, however this upregulation is multifaceted. Further research into the members of clusters 21, 23, and 26 could further elucidate more specific extracellular changes undergone by the neonatal heart.

In addition to the 3 major ontologies, our microarray analysis also identified several other unique clusters involved in neonatal heart maturation. Clusters 11 and 16 both include many genes related to mRNA synthesis and processing. Both clusters show distinct downregulation after birth, indicating reduced overall mRNA expression as the heart transitions from developmental proliferation to a hypertrophic state. Prior to birth, cardiomyocytes undergo extremely complex regulatory signaling to properly undergo cardiomyocyte specification and differentiation. Once heart morphogenesis is complete, the heart's focus turns to pumping blood. Overall, there would be a transition from expressing a wide variety of developmental genes to expressing more specific genes focused on cardiomyocyte contractility and strength, and thus an overall reduction in mRNA synthesis and processing.

Another unique cluster identified in our analysis was Cluster 2, which includes inflammatory response genes related to reactive-oxygen species (ROS) stress and

response. Prior to birth, the heart resides in a hypoxic state (Patterson and Zhang, 2010). After birth, the lungs oxygenate blood that travels to the left heart and is pumped into the systemic arterial vasculature. As a result, the myocardium is exposed to significantly increased amounts of (ROS) after birth (Torres-Cuevas et al., 2017). The increase in inflammatory response regulation identified by our microarray analysis may be explained by the increased oxygenation of blood in the postnatal heart.

7.2 miRNA gene regulation plays a role in neonatal heart maturation

Due to the large numbers of transcripts that can be targeted by each miRNA and their relatively recent discovery, the same gene ontology analysis performed for the mRNA was not performed for miRNA. A single miRNA can have hundreds of targets, and the regulation of their expression is multifaceted and poorly defined. For our analysis, we organized miRNAs such that we could identify the largest changes occurring around 5D, which we identified as the key time-point of cardiomyocyte cell cycle transition in Results Chapter 4. The single most significantly changing miRNA throughout the neonatal period was miR-205. Other significantly changing miRNAs were miR-141 and 200c, which are members of the miR-200 family clustered together on mouse chromosome 6. The other members of the miR-200 family (miR-200a, -200b, and -429) are located on chromosome 4. In support of this, our data shows similar expression patterns of miR-141 and miR-200c (Figure 18A), while the other members of the miR-200 family (miR-200a and miR-200b) did not change significantly during the neonatal period. The overexpression of miR-141 and -200c has been shown to be more effective in decreasing cell growth and migration compared to other members (Choi et al., 2016), and this may be why we only see significant regulation of miR-141/200c. As stated in Results Chapter 4, miR-205 is closely

related to the miR-200 family due to similarities in function and targets. Our microarray analysis was able to strengthen this association by identifying a similar expression pattern throughout neonatal development.

Other upregulated miRNAs during postnatal heart maturation included miR-150, miR-221, miR-338, miR-222, miR-29b, and miR449a. When investigating the literature surrounding these miRNAs, it was noted that each has been implicated in cell cycle regulation, specifically in studies regarding cancer cell proliferation (Garofalo et al., 2012; Kwon et al., 2019; Santolla et al., 2018; Sun et al., 2019; Wang and Qin, 2018; Yong-Ming et al., 2017). Although not directly related to heart development, it is significant that cell cycle regulatory miRNAs show distinct patterns in the developing heart, which loses proliferative capacity. Interestingly, the most significantly downregulated miRNAs shown (miR-702, miR-543, miR-670, miR-665) have also been implicated in cell migration, proliferation, and proliferative capacity in cancer models (Hu et al., 2018; Kim and Choi, 2012; Shi and Xu, 2016; Zhai et al., 2017). As stated previously, the literature surrounding miRNA involvement in modulating cardiomyocyte proliferation is scarce, and so the antiproliferative properties of miRNAs in cancer must be extrapolated to potential mechanisms in inhibiting cardiac growth. In particular, miR-665 has been suggested to decrease Hippo pathway signaling in cancer cells (Hu et al., 2018). With these data, we were able to identify miRNAs that may be playing a role in regulating proliferation in the neonatal heart.

As mentioned in Chapter 1.5.2, the miR-15 family has been demonstrated to be involved in neonatal cardiomyocyte maturation. The mir-15 family member miR-195 acts to regulate Chek1 expression. Through our mRNA microarray analysis we observed

significant regulatory changes in Chek1 expression (Cluster 19), however we did not observe a significant change in miR-195 expression nor any member of the miR-15 family in our miRNA analysis. While transgenic deletion of this family resulted in only a mild phenotype of increased cardiomyocyte number, while overexpression caused significant cardiac defects such as hypoplasia and ventricular-septal defects (VSDs) (Porrello et al., 2013). These data show that the deletion and overexpression of a miRNA may not cause opposite effects, likely due to compensatory mechanisms in place to oppose the action of miRNAs. This difference in phenotype between deletion and overexpression is also what we observed with miR-205.

The miR-302-367 family is expressed during embryonic heart development and has been linked to cardiomyocyte proliferation via targeting of key Hippo pathway members Mst1, Lats2, and Mob1b (Tian et al., 2015). Overexpression of the miR-302-367 cluster resulted in cardiomegaly and death by postnatal 6D due to reduced inhibitory phosphorylation of YAP1, thus promoting proliferation. In our miRNA microarray analysis, we observed a significant change in each member of the miR-302-367 family occurring over the neonatal period (Figure 32). This observation strongly supports the Hippo pathway as having a critical role in neonatal heart maturation. Based on our results regarding the role of miR-205 in Hippo pathway regulation during neonatal heart development, further research may discover that miR-302-367 is also involved in the neonatal proliferative transition.

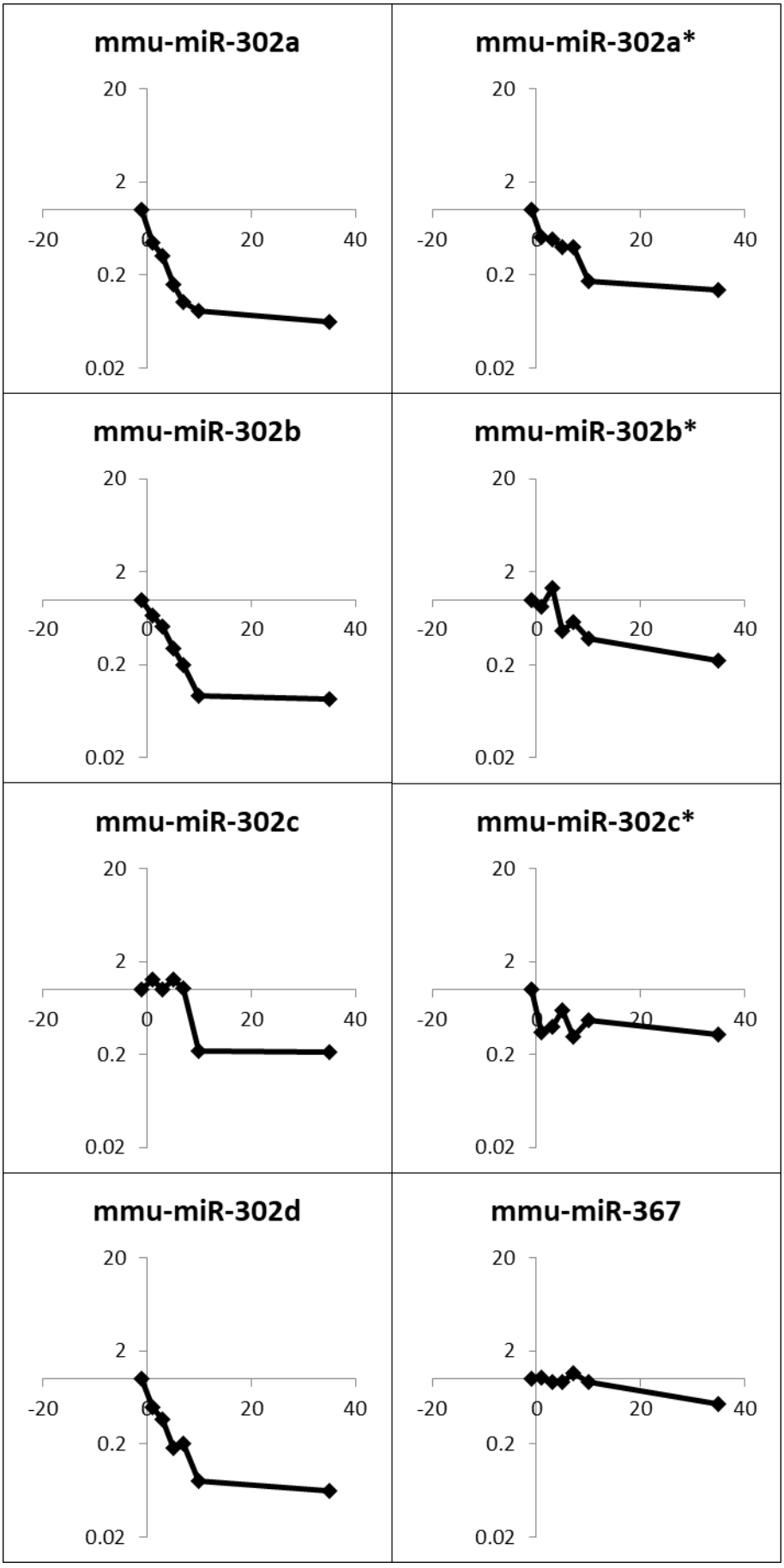
mmu-miR-302a
mmu-miR-302a*
mmu-miR-302b
mmu-miR-302b*
mmu-miR-302c
mmu-miR-302c*
mmu-miR-302d
mmu-miR-367
20
2
0.2
0.02
-20
0
20
40

Figure 32. Microarray expression profiles of the miR-302-367 family during neonatal heart development. Expression levels of each miRNA were analyzed and plotted to show their overall downregulation during the neonatal period.

In our studies, we have chosen to focus directly on the cell-cycle aspect and miRNA involvement during the neonatal cardiac transition, owing to the identified miRNA alterations and the correlated changes in cell cycle regulatory gene expression. Any injuries occurring in hearts past the neonatal period can never heal, and this is due to the inherent indivisibility of cardiomyocytes after the transition. By unraveling the mechanisms here, we begin to understand more about why these cells are unable to divide. Furthermore, entire fields of biology, including cell cycle mechanics, metabolism, response to oxidative stress, and ECM remodeling, can benefit from our microarray data. There are innumerable potential targets that could be identified and characterized in order to more fully understand their role in the neonatal heart. Additionally, by using bioinformatic pathway analysis, entire pathways and signaling mechanisms could be investigated with a holistic, systems-biology approach.

Although our microarray data provided invaluable results, the analysis is not without limitations. Since the performance of our microarray experiments, the continued development and improvement to RNA-sequencing (RNA-seq) has made it a more functional assay for the analysis of gene expression (Kukurba and Montgomery, 2015; Liang and Zeng, 2016; Wang et al., 2009). Microarray analysis is limited to detecting existing sequencing information. Thus, as new mRNAs/miRNAs are characterized, we are unable to determine whether these play a role in the neonatal heart transition. For example, identification and confirmation of many novel miRNAs has occurred since the performance of our miRNA microarray, and we are unable to analyze whether these were significantly changing in the postnatal heart. In comparison, RNA-seq can be updated as new sequence information is obtained, and retrospective analysis of transcript expression

can be performed. Furthermore, RNA-seq has proven to have improved signal-to-noise ratio, with much less likelihood of false-positive results (Kukurba and Montgomery, 2015; Liang and Zeng, 2016). Finally, RNA-seq can measure absolute levels of transcripts, while microarray analysis is performed relative to control sequences present on the microarray platform. In future high-resolution analyses of neonatal heart gene regulatory networks, RNA-seq would likely provide more in-depth and up-to-date information.

7.3 The role of miR-205 in cancer

MiR-205 is located on chromosome 1 in both mouse and human, encoded within a conserved lncRNA, 4631405K08Rik. In humans, this gene has been named miR-205 host gene (miR-205HG). Recently, a study determined that miR-205HG plays a role in repressing prostate basal cell proliferation and differentiation by targeting and blocking interferon-regulatory-factor (IRF) transcriptional activation sites in target gene promoters (Profumo et al., 2019) . Although unrelated in function, this is complementary to the antriproliferative actions of miR-205. The authors of this study have proposed the name LEADeR (Long Epithelial Alu-interacting differentiation-related RNA) for miR-205HG.

MiR-205 has been most widely studied in the context of cancer, where it is commonly used as a biological marker for a variety of cancers such as lung, bladder, pancreatic, breast, gastric, and thyroid (Fang et al., 2016; Li et al., 2017; Qin et al., 2013; Wang et al., 2018a). Notable mRNA transcript targets of miR-205 include Zeb1/2, Yap1, and Pten (Qin et al., 2013). Interestingly, studies involving miR-205 as a biomarker have also noted that increased miR-205 expression seems to have a protective role in cancer progression and prognosis (Li et al., 2017). In breast cancer, miR-205 is downregulated by Erbb2 and results in increased expression of Cyclin D1, Cyclin E, and CDK6 (Adachi

et al., 2011). In melanoma, E2F1 is inhibited by miR-205, leading to reduced E2F1- regulated Akt phosphorylation and increased p16 expression, and a resultant decrease in proliferation (Dar et al., 2011). MiR-205 has also been delivered alongside the first-line chemotherapy drug gemcitabine, where it proved to be effective in sensitizing GEM-resistant pancreatic cancer (Chaudhary et al., 2017). Co-treatment with gemcitabine and miR-205 was more efficient in reducing cancer cell proliferation than gemcitabine alone (Chaudhary et al., 2017). Ectopic expression of miR-205 in a cervical cancer line decreased proliferation, colony formation, and apoptosis by targeting insulin-like growth factor receptor 1 and forcing cell cycle arrest in G1. Knockdown of miR-205 and the YAP1 signaling axis has been shown to transform normal breast fibroblasts into cancer-associated fibroblasts (CAFs), and also promotes tubule formation and generation of human umbilical vein endothelial cells (HUVECs) (Du et al., 2017). Reintroduction of miR-205 blunts angiogenesis in CAFs and halts the metastasis of breast cancer cells *in vivo* (Du et al., 2017). Thus, miR-205 has been extensively described as a tumour suppressor (Xu et al., 2012), and based on our observed expression profile in the heart (Figure 18) we can extrapolate this antiproliferative effect into inhibition of cardiomyocyte proliferation after birth.

Other studies of miR-205 have suggested it plays a role inhibiting cancer proliferation via targeting of phosphatase and tensin homolog (PTEN) (Zhang et al., 2014). Many types of cancer rely on the epithelial-to-mesenchymal transition (EMT) to promote dedifferentiation of cells into a more proliferative state, and to become malignant (Friedmann-Morvinski and Verma, 2014) . PTEN is heavily involved in the EMT and cancerous cells generally try to reduce expression of PTEN which acts to prevent cell

division (Kohnoh et al., 2016). As previously mentioned, miR-205 is usually upregulated in cancerous cells. MiR-205 has been shown to directly target PTEN, and this interaction may play a role in preventing cancer dedifferentiation and development (Zhang et al., 2014). Together, these data suggest that increased miR-205 expression may be a compensatory response to limit cancer cell growth.

7.4 MiR-205 regulation of the Hippo pathway

In recent years, many studies have investigated the role of the Hippo pathway in heart development and regeneration. Several models for modulation of the Hippo pathway have been developed by deletion or overexpression of various pathway members at different time-points. Targeted deletion of the Yap1 gene using the Nkx2-5 promoter was shown to result in cardiac hyperplasia and early embryonic lethality (von Gise et al., 2012; Xin et al., 2011). Postnatal deletion of Yap1 using the αMHC promoter impeded neonatal heart regeneration and led to increased fibrosis after injury (Del Re et al., 2013; Xin et al., 2013). YAP1 overexpression has also been noted to increase cardiomyocyte apoptosis and cause dilated cardiomyopathy in mice (Del Re et al., 2013). Heterozygous deletion resulted in no phenotype unless the heart was injured via myocardial infarction.

Conversely, forced expression of YAP1 has been shown to stimulate cardiac regeneration and improve contractility after induced MI (Del Re et al., 2013). Overexpression has also been shown to cause hyper-proliferation of cardiomyocytes (Xin et al., 2011, 2013). Furthermore, this regenerative activity was shown to be due to the activation of embryonic proliferative gene programming. Another study using constitutively active YAP1 overexpression by βMHC increased cardiomyocyte

proliferation. Interestingly, by adulthood these overexpression mice showed normal heart size with reduced cardiomyocyte size and increased cell density/number (Xin et al., 2011). YAP1 expression has been shown to be sufficient to promote increased cell size and hypertrophic gene expression in cardiomyocytes (Del Re et al., 2013). Additionally, YAP1 expression is linked to protection from ROS-induced cell death and attenuation of phenylephrine-induced hypertrophy (Del Re et al., 2013).Transgenic deletion of intermediary Hippo pathway members such as Mst1, Sav1, and Lats1 have all also been shown to induce cardiomyocyte hyperplasia. Overexpression of Mst1 resulted in abnormal cardiac growth and dilated cardiomyopathy (Matsui et al., 2008; Yamamoto et al., 2003). Yap1 overexpression and Mst1 deletion mouse models also show similar increases in cardiomyocyte regeneration instead of fibrosis after MI (Lin et al., 2014). Through review of the literature surrounding the role of the Hippo pathway in the heart, we can conclude that regulation of YAP activity is essential for proper heart development.

As research into the role of the Hippo pathway in heart development and regeneration continues, it is evident that miRNAs play an important role in regulating Hippo signaling. For example, YAP1 has been shown to activate expression of miR-206 and subsequently increase cardiac hypertrophy (Yang et al., 2015). Moreover, inhibition of miR-206 expression attenuated this YAP1-induced hypertrophy (Yang et al., 2015). Studies have also shown that the administration of various miRNAs is able to induce cardiomyocyte proliferation *in vitro* (Eulalio et al., 2012; Torrini et al., 2019). These miRNAs include miR-590-3p, miR-199a-3p, the miR-302 family, miR-1825, miR-1248, miR-18a, miR-33b, and miR-30e (Torrini et al., 2019). Furthermore, it was shown that expression of these miRNAs was correlated with increased TEAD reporter activity. TEAD

is an essential part of the regulatory complex with YAP1, which promotes expression of proliferative genes, and has shown to be essential for heart development (Chen et al., 1994). Treatment of cells with the miRNAs mentioned above increased active YAP1 levels in the nucleus. Furthermore, knockdown of YAP1 using siRNA, while also treating with the above-mentioned miRNAs, prevented the pro-proliferative gene signaling. The importance of miRNAs in the regulation of the Hippo pathway is further emphasized by a study that demonstrated miR-199a-3p treatment was able to downregulate expression of the serine/threonine-protein kinase TAOK1 (Torrini et al., 2019). TAOK1 has been demonstrated to phosphorylate and activate MST1/2 and LATS1/2 (Boggiano et al., 2011; Plouffe et al., 2016; Poon et al., 2011). Thus, miR-199a-3p can modulate cell proliferation by affecting the Hippo pathway. Furthermore, miR-199a-3p can target F-box/WD repeat-containing protein 1A (β-TrCP), which catalyzes the ubiquitination of YAP1 and promotes its degradation (Zhao et al., 2010b).

Based on the literature surrounding the regulation of YAP1, we can conclude that miRNA regulation of YAP1 plays a critical role in controlling proliferative signaling. Although many miRNAs have been identified as playing a role in heart development via interaction with YAP1, studies have not identified miR-205, most likely due to the previously described lack of temporal resolution in experiments. MiR-205 is only transiently expressed in the heart between 3D and 7D, and so its regulation of Yap1 in the heart has not been studied.

After birth, miR-205 expression follows a distinct pattern, and the evidence shown herein strongly supports a role for miR-205 in establishing cardiomyocyte number in the neonatal heart via targeting of the Yap1 transcript. Temporally, the expression of miR-205

precedes loss of cardiomyocyte proliferative capacity. By 7D post-birth, the murine heart has achieved its final cardiomyocyte number and primarily grows via hypertrophy. MiR-205 expression sharply and significantly increases immediately before this 7D timepoint (Figure 20A). From miR-205's highly investigated role in cancer, we can deduce that these antiproliferative effects may be utilized by the neonatal heart transitional program to end cardiomyocyte proliferation. Furthermore, this strongly supports miR-205 as a regulator of the neonatal transitional program.

7.5 MiR-205 exerts an antiproliferative effect on neonatal cardiomyocytes to inhibit cell division by postnatal 5D

After confirming the expression profile for miR-205 (Figure 20A), we examined the localization of miR-205 expression. Interestingly, miR-205 is expressed in both the cardiomyocytes and supporting cells of the heart (Figure 20B). Importantly, miR-205 expression originates from the epicardium. Studies have shown that the developing heart appears to grow outward, with new cells being generated from the epicardium and being placed on top of the previous layer of cardiomyocytes (Cai et al., 2008; Zhou et al., 2008). When antiproliferative signaling begins post-birth, it is logical that it would originate from the epicardial regions where cardiomyocytes are actively proliferating. A limitation of our miR-205$^{-/-}$ mouse model is the possibility of miR-205 being secreted from neighbouring cardiac fibroblasts and having a paracrine role on cardiomyocytes. Indeed, as the global deletion model resulted in neonatal lethality (Wang et al., 2013), it is possible that deletion of miR-205 in both cardiomyocytes and supporting cells of the heart using an inducible knockout in all cardiac-lineage cell types (Hand1/2, Nkx2-5, Tbx) may have had a more significant phenotype. Our study shows that miR-205's antiproliferative signaling at 5D is

localized near the epicardium (Figure 20C). MiR-205 is likely involved in forcing cardiomyocytes to exit the cell cycle and progress toward terminal differentiation. Furthermore, research has shown that the limited regeneration that occurs in an injured adult heart arises from cardiomyocytes near the epicardium (Smits and Riley, 2014). Unlocking the proliferative potential of cardiomyocytes will likely occur at the epicardium, where the cardiomyocytes have room to expand and grow. MiR-205 expression increases after myocardial injury (Figure 21), therefore determining whether miR-205 is preventing cardiomyocyte proliferation in this circumstance would be a promising avenue for future research.

7.6 The deletion of miR-205 results in an expanded proliferative window and increased cardiomyocyte number

Our observations demonstrate that miR-205 is expressed at the precise time when cardiomyocytes stop dividing, expression is localized to regions with actively dividing cardiomyocytes, and that miR-205 has anti-proliferative properties. Taken together, this data strongly supports miR-205 having a significant role in the neonatal cardiac transitional program. Our next step was to further elucidate the role of miR-205 by examining the effect of transgenic deletion in the postnatal heart.

Based on the western blots in Figure 22E, it is clear that miR-205 deletion had an effect on several aspects of cardiomyocyte maturation. Increased levels of p-CDK1 indicates that there is increased cell growth and division signaling. As a target of miR-205, it was notable that p-PTEN expression levels did not differ significantly between wild-type and miR205$^{-/-}$, but total levels of PTEN were modestly increased, helping to confirm miR-205's targeting of the Pten transcript. Additionally, the presence of a strong, clear

band at the size corresponding to the mass of PTEN-L, suggests that miR-205 may target all PTEN transcripts, including the N-terminally extended versions such as PTEN-L and -M. Although PTEN-L levels are slightly increased in control mice, which only express αMHC-Cre (Appendix Figure 4), PTEN-L levels measured in miR-205$^{-/-}$ mice were notably higher. Very little is known regarding PTEN-L's role in the heart, but based on its interaction with miR-205 and its role in regulating Akt signaling, PTEN-L may be hypothesized to play a role in the neonatal transitional program. An updated model of the PI3K/PTEN pathway including the role of miR-205 is shown in Figure 33. By targeting the Pten transcript, miR-205 can increase the proliferative signaling of cells through multiple pathways such as the Akt/mTOR and MEK/ERK pathways. Future studies of PTEN-L's role in cell proliferation signaling should provide useful insight into the function of miR-205 in neonatal heart development.

In response to significantly increased YAP1 expression, the Hippo pathway is activated to phosphorylate YAP1 and sequester it in the cytoplasm. Although p-YAP1 levels are increased in miR-205$^{-/-}$ hearts, the overall increase in total YAP1 expression was too strong to completely inhibit proliferation. We observed robust expression of YAP1 in 5D miR-205$^{-/-}$ hearts visualized by IHC (Figure 23B). We also show that YAP1 expression was significantly higher both in the cytoplasm and the nuclei (Figure 23B), supporting the idea that the Hippo pathway activation was not sufficient to suppress YAP1 signaling in the absence of miR-205. Overall, miR-205 deletion resulted in increased YAP1 protein expression (Figure 23), which helps confirm previous studies identifying the Yap1 transcript as a target of miR-205 in EMT and cancer cell models.

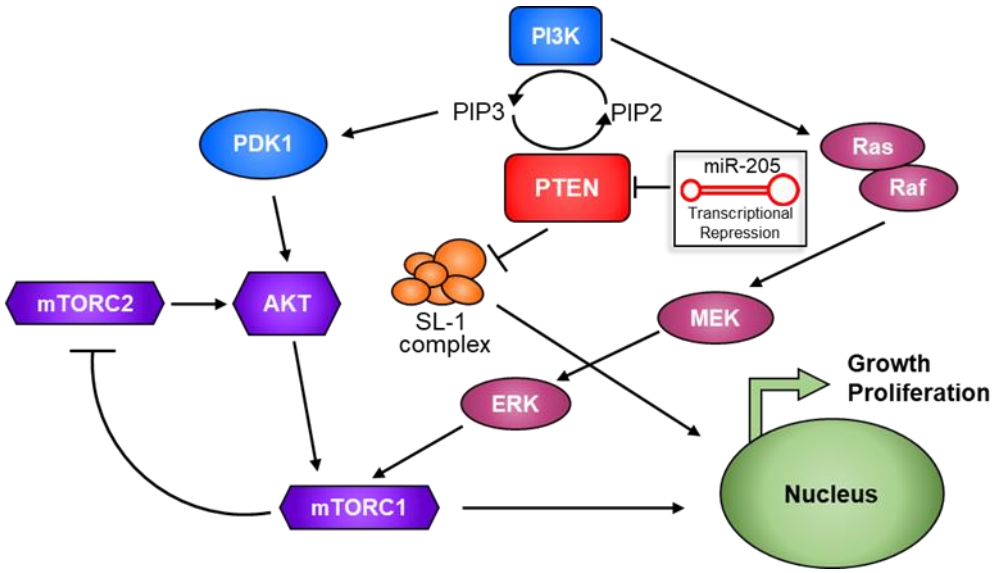

Figure 33. The PTEN/PI3K signaling pathway. PI3K and PTEN regulate PIP2 and PIP3 levels to mediate cell signaling and growth through both the AKT/mTOR and MEK/ERK pathways. PTEN is a negative regulator of cell growth by dephosphorylating PIP3 and inhibiting its pro-proliferative downstream effects.. PTEN also negatively regulates the SL1 complex responsible for ribosomal creation and function. PTEN expression is inhibited by miR-205.

By targeting key elements such as Yap1 and Pten, it is likely that miR-205 tumour suppressor functionality is involved in halting cell cycle progression. In the absence of miR-205, there is significantly increased expression of both Ki67 and pH3 at 14D (Figure 24). Both markers are actively expressed in cells that are currently undergoing mitosis. Another result of upregulated YAP1 expression was an increase in proliferative signaling as observed by increased levels of CDK1. Therefore, we can conclude that miR-205$^{-/-}$ cardiomyocytes have an expanded proliferative window as there are more actively dividing cells at 14D. While expression of these proliferative markers is still low, it is significantly higher in miR-205$^{-/-}$ mice compared to wild-type. The fact that there is a increased cardiomyocyte number in 14D miR-205$^{-/-}$ hearts further confirms that the proliferative window is expanded in miR-205$^{-/-}$ hearts (Figure 25). Furthermore, these data strongly suggest that miR-205's antiproliferative role observed in cancer models is also utilized by the transitional program to inhibit proliferative signaling of cardiomyocytes in the neonatal heart. The data provided in Results Chapter 5 strongly supports a role for miR-205 acting primarily through suppressing Yap1 in order to initiate cell cycle withdrawal and inhibit postnatal cardiomyocyte proliferation. An updated schematic of the Hippo pathway, including the transcriptional repression of Yap1 by miR-205 is displayed in Figure 34. Based on the intriguing phenotype of increased proliferation displayed by our miR-205$^{-/-}$ mice, we next sought to determine whether overexpression of miR-205 would result in reduced proliferative signaling in the heart.

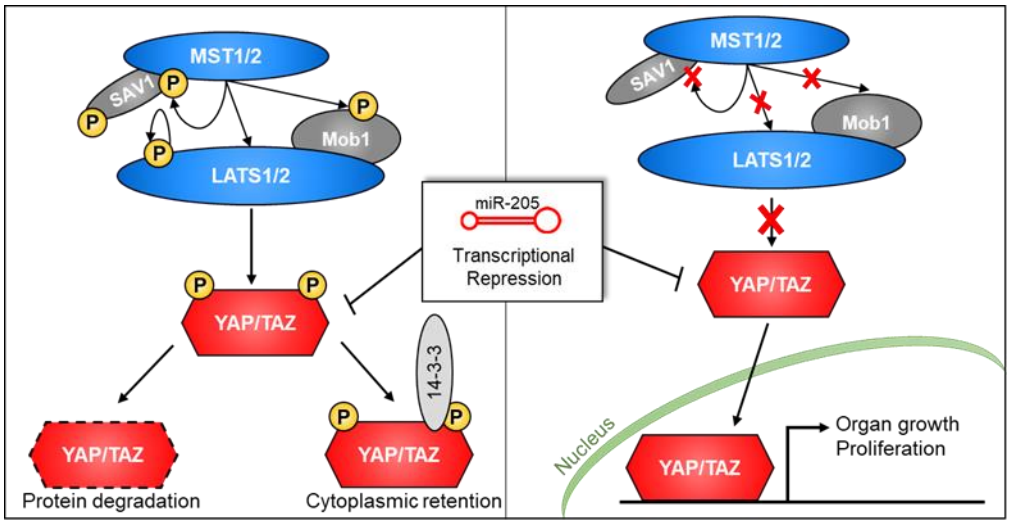

Figure 34. The Hippo pathway responsible for organ growth and cellular proliferation. When the Hippo pathway is activated (phosphorylated), it results in the phosphorylation of YAP/TAZ. Phosphorylated YAP/TAZ is sequestered in the nucleus and inactive. It is temporarily stored in the cytoplasm or degraded if necessary. When the Hippo pathway is not active (dephosphorylated), YAP/TAZ remains unphosphorylated and active, and migrates to the nucleus to regulate transcription of proliferative genes. YAP1 expression is inhibited by miR-205.

In our miR-205$^{-/-}$ mice we observed severe cardiac hypertrophy in adult mice, with up to 50% increased heart mass (Appendix Figure 1). At 10 months of age, miR-205$^{-/-}$ mice displayed significantly reduced ejection fraction and increased left ventricular mass and did not live past one year of age (Appendix Figure 2). Furthermore, these mice had worse outcome after induced cardiac injury from 9 days of transverse aortic constriction (TAC) (Appendix Figure 3). Although we initially hypothesized this to be a result of miR-205 deletion, our phenotypical data was similar to previously published data indicating that αMHC-Cre expression alone causes cardiac hypertrophy and death (Pugach et al., 2015). Because of the similarities, we could not conclude the effect of miR-205 deletion in the adult heart. Future studies into the role of miR-205 in the adult heart would use inducible overexpression models such as tamoxifen or doxycycline to avoid the prolonged expression of Cre recombinase.

In our transgenic model of miR-205 deletion, there are limitations that were taken into account when analyzing data. For example, experiments examining protein expression in postnatal mice containing αMHC-Cre with no deletion of miR-205 (αMHC-Cre-only) displayed a DNA damage phenotype. These αMHC-Cre-only mice showed increased levels of DNA-damage markers γH2AX and XRCC1 (Appendix Figure 4), demonstrating that the expression of Cre recombinase results in DNA damage even when no floxed allele is present. Furthermore, αMHC-Cre-only neonatal mice displayed significantly increased levels of p-Akt (Appendix Figure 1). P-Akt is one of the downstream effectors of the PI3K/PTEN pathway, but also participates in cell survival and apoptosis signaling in cases of DNA damage. Thus, we expected dysregulation of Akt in miR-205$^{-/-}$ mice, however since expression of αMHC-Cre alone caused dysregulation we

could not make any conclusions regarding miR-205's effect on Akt signaling. Other than DNA damage markers, αMHC-Cre expression did not have a significant impact on the expression of other proteins examined.

Finally, our analysis of the proliferative capacity of cardiomyocytes could be improved. Although our microarray and protein expression analyses were performed at many neonatal time-points, our examination of cell number, cell size, and Ki67/pH3 staining was only performed at 5D and 14D. Future investigation into cell number and proliferative capacity will examine additional time-points to further elucidate the temporal changes occurring during postnatal heart maturation. Additional methods of identifying actively cycling cells could also be utilized, such as BrdU or EdU incorporation.

7.7 Comparing and contrasting effects of miR-205 deletion and overexpression in the postnatal heart

Based on our observations in chapter 5, we hypothesized that miR-205 overexpression would result in a phenotype opposite to that of the deletion model. However, as described in chapter 6, miR-205^{OE} mice did not have reduced cell number nor impaired cardiac transition by 14D. In contrast, miR-205^{OE} hearts contained significantly more cardiomyocytes at 5D and 14D (Figure 31). From our observations, the cardiac transition still occurred, although it appeared to occur at an earlier timepoint than the knockouts and wild-types (3D vs. 5D). The earlier transition in the miR-205^{OE} hearts was characterized by higher-than-normal proliferative signaling (p-CDK1, p-Rb, p-PTEN-L) immediately after birth. It is possible that the overexpressed miR-205 is bound by circular RNAs (cDNAs), which can act as miRNA 'sponges' to inhibit the action of miRNAs (Barret & Salzman, 2016)

In wild-type mice, CDK1 expression transiently increases from 3D to 5D before dropping (Figure 27B), which is consistent with other literature showing that this is concurrent cardiomyocytes undergoing their last replication event (Sedmera and Thompson, 2011). In miR-205$^{-/-}$ mice, this same transient increase is seen, however expression is much higher and lasts much longer (up to 10D) (Figure 22). In miR-205^{OE}, p-CDK1 expression also transiently increases, but instead occurs from postnatal1D to 3D, with levels becoming comparable to that of wild-type and miR-205$^{-/-}$ hearts by 5D (Figure 27). Comparable levels of Ki67 and pH3 staining between wild-type and miR-205^{OE} mice at 5D shows that cardiomyocyte proliferative index reached a comparable level to wild-type by 5D continuing to 14D (Figure 30). The increased cell number in miR-205^{OE} mice at 5D and 14D (Figure 31) indicates that there was a period of cardiomyocyte hyperproliferation from 1D to 3D. Our miR-205^{OE} data indicates that overexpression of miR-205 results in an earlier initiation of cardiomyocyte cell cycle withdrawal. Earlier initiation results in a proliferative burst immediately after birth to establish a suitable cardiomyocyte number for heart maturation.

A similar situation exists for p-Rb. Wild-type mice have a transient increase around 5D, with expression dropping by 10D. In miR-205$^{-/-}$ mice, p-Rb is expressed at higher levels and for a longer duration, consistent with an increased proliferative window. In miR-205^{OE} mice, p-Rb levels are significantly higher than either wild-type or knockout immediately after birth, but expression still drops off after 5D and is comparable to wild-type levels by 7D. The CDK1 and p-Rb data show evidence of an expedited cardiac transitional program in miR-205^{OE} mice, with the cardiomyocytes hyperproliferating

before the antiproliferative signaling induced by miR-205 overexpression takes hold, and forces cell cycle withdrawal and terminal differentiation.

Furthermore, this suggests that there are likely molecular mechanisms in place to account for variations in gestation time. Gestation times are known to vary within a species, for example the human gestational period is on average 280 days, with a standard deviation of 16 days (Jukic et al., 2013). The typical gestation period for a mouse is 19 to 21 days (Murray et al., 2010). Once born, the heart undergoes the same changes regardless of gestational duration (within normal timeframe). Based on our data, we can predict that regardless of gestation time, the stress of birth induces the expression of the transitional program, including miR-205, and rapidly establishes the required cardiomyocyte number before becoming indivisible. The mechanisms involved in the transitional period could be further studied in the context of premature births to determine if hyperproliferative signaling is required for shorter gestational periods when cardiomyocytes have spent less time proliferating, to establish a healthy cardiomyocyte number in the heart.

In our miR-205$^{-/-}$ mice, we observed severe dysregulation of neonatal Hippo pathway signaling (Figure 23). From our overexpression data, it is evident that the Hippo-signaling pathway is also disrupted in miR-205^{OE} mice (Figure 28). As discussed previously, miR-205$^{-/-}$ mice generally show an increase in Hippo signaling compared to wild-type, however increased YAP1 expression results in increased cardiomyocyte proliferation. Coinciding with the miR-205^{OE} hyperproliferation immediately after birth, Hippo signaling follows the same pattern, with heavily increased expression immediately after birth (Figure 28). Several Hippo pathway members such as MST1, SAV1, p-MOB1,

and LATS1 are all upregulated in miR-205^{OE} hearts, especially in the first few days after birth (Figure 28). The increased Hippo signaling consequently and expectedly results in increased levels of inactive p-YAP1. However, total YAP1 levels were also increased, suggesting that compensatory mechanisms exist to drive YAP1 expression when cardiomyocyte proliferation is required for heart maturation. By stimulating the cell-cycle withdrawal gene programming, compensatory overexpression of YAP1 results in increased proliferation of cardiomyocytes immediately after birth. Especially during the first 3 days of life, miR-205^{OE} show greatly increased expression of p-YAP1.

The proliferative window in miR-205^{OE} mice is similar to wild-type, with no difference in pH3 or Ki67 staining at 5D and 14D (Figure 30). However, the resulting heart in miR-205^{OE} mice contains a larger cell number (Figure 31). The increased cell number observed at 5D and 14D is explained by the increased proliferative signaling observed very early in the neonatal period. By overexpressing miR-205, we have disrupted the neonatal transitional period, however the heart is still able to produce cardiomyocytes by undergoing a compensatory proliferative burst earlier in neonatal heart maturation.

In conclusion, miR-205^{OE} hearts display contradictory pro- and anti-proliferative signaling. We hypothesize that this pro-proliferative signaling is a compensatory response to the anti-proliferative signaling initiated by miR-205 overexpression earlier than when miR-205 would normally be expressed. The miR-205$^{-/-}$ and miR-205^{OE} models provided invaluable information about miR-205's function in the neonatal heart. By knocking down miR-205 we expanded the proliferative window and increased cardiomyocyte number, while overexpressing mir-205 expedited cell cycle withdrawal and established cardiac number sooner. Altogether our results heavily support miR-205 as a key regulator of the

neonatal transition by inhibiting PI3K and Hippo signaling to promote cardiomyocyte cell cycle withdrawal.

In the analysis of our miR-205^{OE} mice, we experienced similar limitations as our transgenic deletion experiments. Future experiments will assess proliferative capacity and cell number at additional timepoints to obtain a higher-resolution analysis of postnatal cardiomyocyte maturation. By using a DOX-inducible mouse model, we were able to circumvent confounding data caused by the mouse model. Since this model requires two alleles inherited from separate parents, we were able to use littermates as transgenic controls. Littermates included mice with either one of the two required alleles for overexpression and were also provided with DOX water. Thus, any phenotype from the presence of either allele would be observed in control mice. Supporting this, our miR-205^{OE} control mice display the same expression as wild-type mice used in miR-205$^{-/-}$ experiments.

7.8 Conclusions

MiR-205 expression is strongly and transiently upregulated during the neonatal transitional window. Through it's interaction with Yap1 and Pten, we have uncovered a novel role for miR-205 in shifting the balance from pro-proliferative signaling to pro-hypertrophic signaling. A working model of miR-205's roles in the Hippo and PI3K/PTEN pathways is presented in Figures 33 and 34, respectively. In the absence of miR-205, YAP1 expression is significantly increased, leading to increased cardiomyocyte number and larger heart size in miR-205$^{-/-}$ mice. Hippo signaling pathway activation is increased in these mice as an attempt to phosphorylate and inactivate YAP1 to inhibit cardiomyocyte proliferation. Overexpression of miR-205 resulted in an expedited

transitional period characterized by drastically increased expression of cell cycle progression markers, such as CDK1, p-Rb, during the first few days of life. Overexpression also resulted in earlier establishment of cardiomyocyte number. By 5D, miR-205^{OE} hearts contained more cardiomyocytes, however by 14D the number was comparable to wild-type. Our results indicate that miR-205 is critical for establishing a healthy cardiac environment, including cell number and cell size

The neonatal heart undergoes a remarkable transition from hyperplastic to hypertrophic growth after birth. The transition is a critical yet understudied phenomenon that results in the mammalian heart being indivisible and unable to compensate for injury or maladaptation. Along with this proliferative transition, there is a metabolic transition from glycolysis to fatty acid oxidation. Although these pathways also posit interesting avenues to explore, we have chosen to focus our efforts on the cell cycle and proliferation aspect, as it holds the most promise in discovering new mechanisms for the treatment of heart disease using pre-existing molecular mechanisms and pathways present in the heart. By uncovering the molecular mechanisms involved in locking cardiomyocytes out of the cell cycle, we can surmise new ways to unlock them, and allow the replenishment of cardiomyocytes via the division of pre-existing cardiomyocytes. Whether miR-205 antagomir treatment would be beneficial in a heart disease model would be an interesting avenue for further study. If our hypothesis is correct, then delivery of a MiR-205 antagomir may be able to reengage cardiomyocyte proliferation at times when cardiomyocyte loss impairs heart function, i.e. the most obvious application being in the post-infarct heart.

Another important experiment to support miR-205's role in proliferative capacity will be the induction of myocardial infarction in 1D and 7D miR-205$^{-/-}$ and miR-205^{OE} mice

(as in Porrello et al., 2011a) to identify whether our mouse models possess increased or reduced regeneration after injury. With further research and collaboration, we move closer toward unlocking adult cardiomyocytes from an indivisible state, allowing these cells to replenish so that the heart may heal. As a result, this research may be a first step in moving us closer to an effective treatment and cure for heart disease.

Appendix Figures

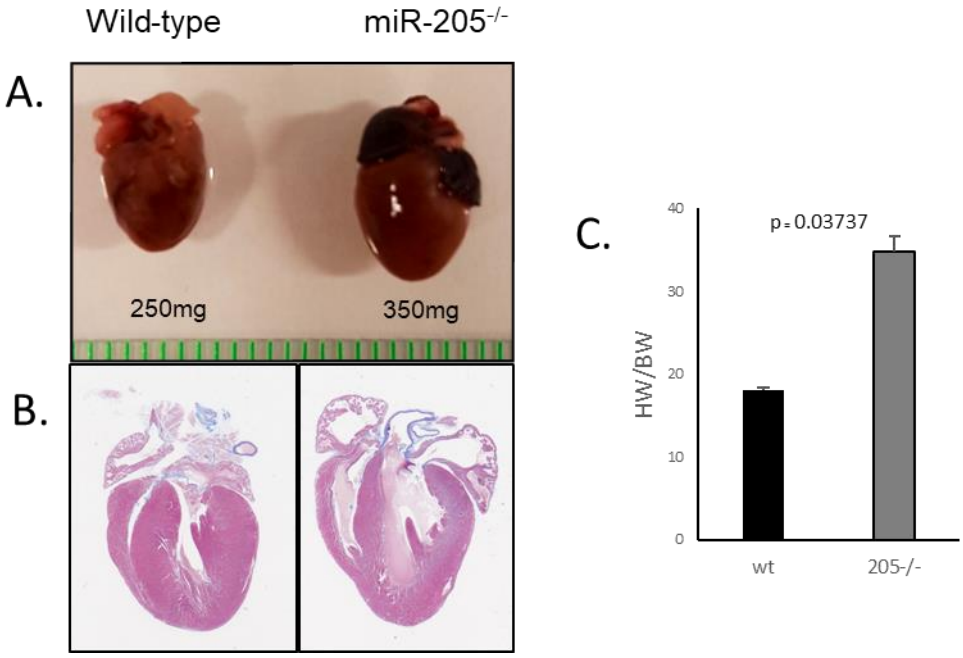

Appendix Figure 1. Phenotypic differences between wild-type and miR-205$^{-/-}$ mice. A) miR-205$^{-/-}$ hearts are 30-50% larger than wild-type littermates at 10 months of age. B) Masson Trichrome staining of the hearts from (A), showing drastic differences in heart structure. C) Heart weight and body weight were measured and compared between wild-type and miR-205 knockout mice (n=3). Significance was tested using student's t-test. Data is presented as mean ± standard deviation.

A.

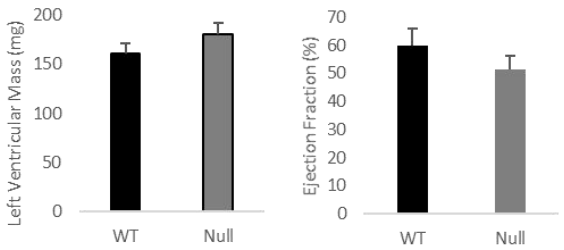

B.

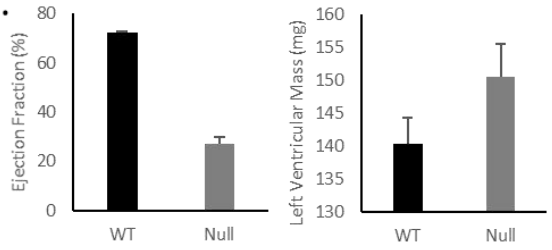

C.

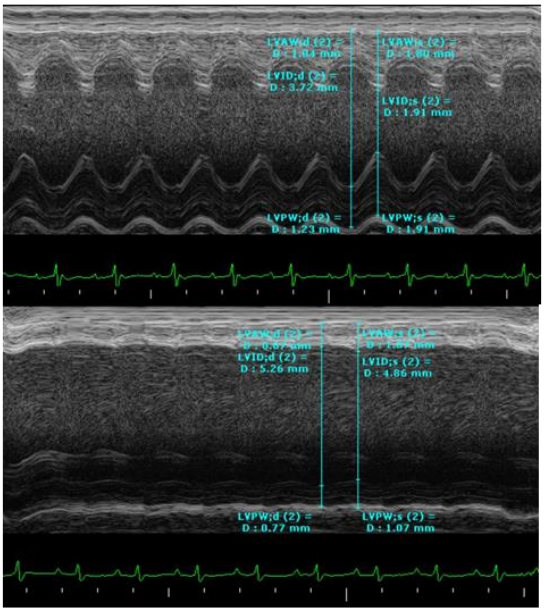

D.

	Wild-type		miR-205$^{-/-}$	
	3 month	10 month	3 month	10 month
LV Vol;d	39.4	63.8	42.0	107.8
LV Vol;s	16.2	16.0	20.9	88.9
Stroke Volume	23.2	47.8	21.2	18.9
%EF	59.5	75.2	50.8	20.7
% FS	40.3	43.9	33.1	11.4
LV Mass (AW)	166.4	175.6	180.3	198.8

E.

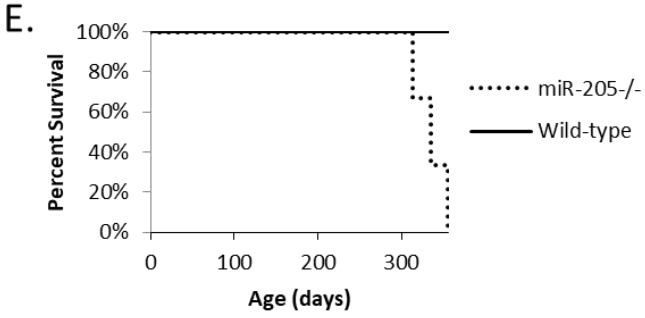

F.

Masson Trichrome, 10 months

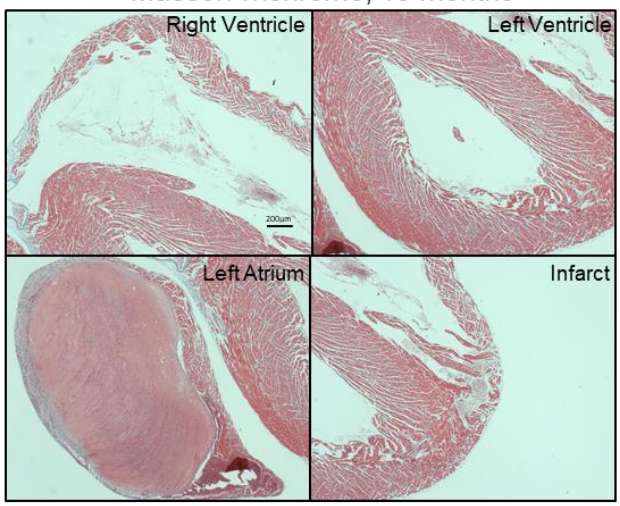

Appendix Figure 2. Aged miR-205$^{-/-}$ mice develop heart failure and die by the age of 1 year. A) At 3 months old, wild-type and miR-205$^{-/-}$ mice show little difference in terms of left ventricular mass and ejection fraction. B) By 10 months, miR-205$^{-/-}$ mice have significantly reduced ejection fraction and increased left ventricular mass. Significance was tested using student's t-test. C) Representative echocardiography M-mode images of wild-type (top) and miR-205$^{-/-}$ (bottom) hearts at 10 months of age. D) More extensive data showing differences in cardiac function in wild-type vs. miR-205$^{-/-}$ mice at 3 and 10 months. E) Survival curve of wild-type (n=3) and miR-205$^{-/-}$ (n=3) over the course of one year. F) Masson trichrome staining of a 10-month-old mouse which died without warning. Staining shows increased right ventricular volume, left ventricular hypertrophy, a blood clot in the left atrium, and an infarct at the apex of the heart. All data is presented as mean ± standard deviation.

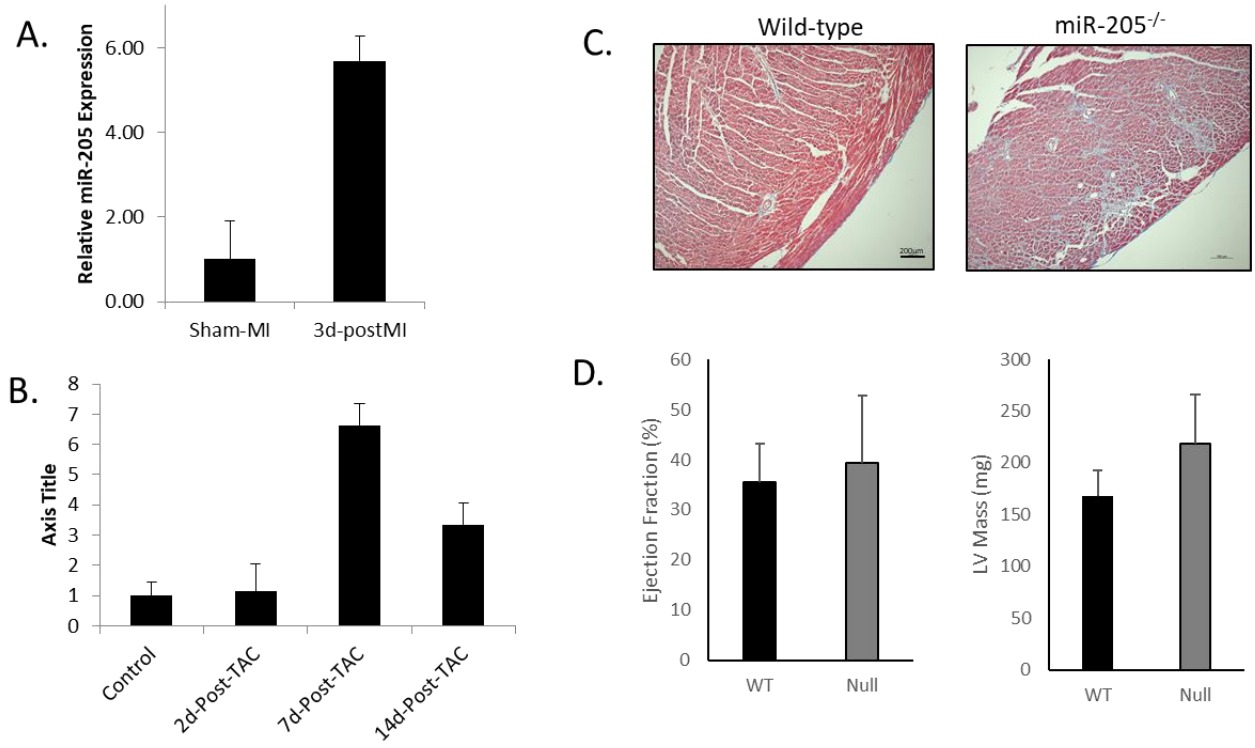

Appendix Figure 3. MiR-205 plays a role after cardiac injury. A) Preliminary RT-qPCR data showing that miR-205 expression is increased in 3-day post-MI hearts (n=2). B) RT-qPCR data showing that miR-205 expression peaks at 7d-post transverse aortic constriction (TAC)C) Masson's Trichrome staining on wild-type and miR-205$^{-/-}$ mice after 9 days of TAC. Data is presented as mean ± standard deviation. C) Echocardiography analysis shows no significant difference in ejection fraction or LV mass 9 days post-TAC.

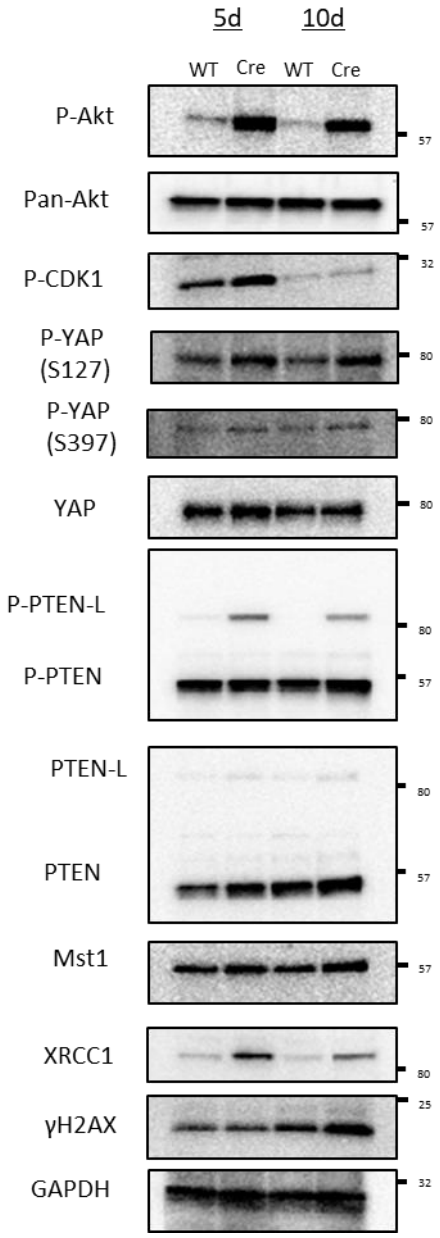

Appendix Figure 4. Western blot controls for mice expressing only αMHC-Cre. Western blot analysis comparing wild-type and αMHC-Cre expressing mice shows no major differences in p-YAP, p-PTEN, p-CDK1, or Mst1 levels at both time points. P-Akt, XRCC1, and γH2AX are all elevated when αMHC-Cre in expressed in cardiomyocytes, suggesting there is increased DNA damage causing pro-survival signaling in these hearts.

Bibliography

Abad, M., Hashimoto, H., Zhou, H., Morales, M.G., Chen, B., Bassel-Duby, R., and Olson, E.N. (2017). Notch Inhibition Enhances Cardiac Reprogramming by Increasing MEF2C Transcriptional Activity. Stem Cell Reports *8*, 548–560.

Abbas, T., and Dutta, A. (2009). p21 in cancer: intricate networks and multiple activities. Nat. Rev. Cancer *9*, 400–414.

Abdul-Ghani, M., Suen, C., Jiang, B., Deng, Y., Weldrick, J.J., Putinski, C., Brunette, S., Fernando, P., Lee, T.T., Flynn, P., et al. (2017). Cardiotrophin 1 stimulates beneficial myogenic and vascular remodeling of the heart. Cell Res. *27*, 1195–1215.

Ackers-Johnson, M., Li, P.Y., Holmes, A.P., O'Brien, S.M., Pavlovic, D., and Foo, R.S. (2016). A Simplified, Langendorff-Free Method for Concomitant Isolation of Viable Cardiac Myocytes and Nonmyocytes from the Adult Mouse Heart. Circ. Res. *119*, 909–920.

Adachi, R., Horiuchi, S., Sakurazawa, Y., Hasegawa, T., Sato, K., and Sakamaki, T. (2011). ErbB2 down-regulates microRNA-205 in breast cancer. Biochem. Biophys. Res. Commun. *411*, 804–808.

Agah, R., Frenkel, P.A., French, B.A., Michael, L.H., Overbeek, P.A., and Schneider, M.D. (1997). Gene recombination in postmitotic cells. Targeted expression of Cre recombinase provokes cardiac-restricted, site-specific rearrangement in adult ventricular muscle in vivo. J. Clin. Invest. *100*, 169–179.

Ahuja, P., Perriard, E., Pedrazzini, T., Satoh, S., Perriard, J.C., and Ehler, E. (2007a). Re-expression of proteins involved in cytokinesis during cardiac hypertrophy. Exp. Cell Res. *313*, 1270–1283.

Ahuja, P., Sdek, P., and Maclellan, W.R. (2007b). Cardiac Myocyte Cell Cycle Control in Development , Disease , and Regeneration. Physiol Rev *87*, 521–544.

Ai, D., Fu, X., Wang, J., Lu, M.-F., Chen, L., Baldini, A., Klein, W.H., and Martin, J.F. (2007). Canonical Wnt signaling functions in second heart field to promote right ventricular growth. Proc. Natl. Acad. Sci. *104*, 9319–9324.

Alao, J.P. (2007). The regulation of cyclin D1 degradation: roles in cancer development and the potential for therapeutic invention. Mol. Cancer *6*, 24.

Anderson, K.M., Anderson, D.M., McAnally, J.R., Shelton, J.M., Bassel-Duby, R., and Olson, E.N. (2016). Transcription of the non-coding RNA upperhand controls Hand2 expression and heart development. Nature *539*, 433–436.

Assmus, B., Tonn, T., Seeger, F.H., Yoon, C.H., Leistner, D., Klotsche, J., Schächinger, V., Seifried, E., Zeiher, A.M., and Dimmeler, S. (2010). Red Blood Cell Contamination of the Final Cell Product Impairs the Efficacy of Autologous Bone Marrow Mononuclear Cell Therapy. J. Am. Coll. Cardiol. *55*, 1385–1394.

Azpiazu, N., and Frasch, M. (1993). Tinman and bagpipe: Two homeo box genes that determine cell fates in the dorsal mesoderm of Drosophila. Genes Dev. *7*, 1325–1340.

Bakkers, J. (2011). Zebrafish as a model to study cardiac development and human cardiac disease. Cardiovasc. Res. *91*, 279–288.

Bao, Z.Z., Bruneau, B.G., Seidman, J.G., Seidman, C.E., and Cepko, C.L. (1999). Regulation of chamber-specific gene expression in the developing heart by Irx4. Science *283*, 1161–1164.

Barrett SP, Salzman J. Circular RNAs: analysis, expression and potential functions. Development. 2016 Jun 1;143(11):1838-47. doi: 10.1242/dev.128074. Review. PubMed PMID: 27246710; PubMed Central PMCID: PMC4920157.

Barroso-delJesus, A., Romero-Lopez, C., Lucena-Aguilar, G., Melen, G.J., Sanchez, L., Ligero, G., Berzal-Herranz, A., and Menendez, P. (2008). Embryonic Stem Cell-Specific miR302-367 Cluster: Human Gene Structure and Functional Characterization of Its Core Promoter. Mol. Cell. Biol. *28*, 6609–6619.

Bartel, D.P. (2004). MicroRNAs: genomics, biogenesis, mechanism, and function. Cell *116*, 281–297.

Beigi, F., Schmeckpeper, J., Pow-Anpongkul, P., Payne, J.A., Zhang, L., Zhang, Z., Huang, J., Mirotsou, M., and Dzau, V.J. (2013). C3orf58, a novel paracrine protein, stimulates cardiomyocyte cell-cycle progression through the PI3K-AKT-CDK7 pathway. Circ. Res. *113*, 372–380.

Bell, R.M., Mocanu, M.M., and Yellon, D.M. (2011). Retrograde heart perfusion: The Langendorff technique of isolated heart perfusion. J. Mol. Cell. Cardiol. *50*, 940–950.

Benson, D.W., Silberbach, G.M., Kavanaugh-McHugh, A., Cottrill, C., Zhang, Y., Riggs, S., Smalls, O., Johnson, M.C., Watson, M.S., Seidman, J.G., et al. (1999). Mutations in the cardiac transcription factor NKX2.5 affect diverse cardiac developmental pathways. J. Clin. Invest. *104*, 1567–1573.

Bergmann, O., Zdunek, S., Felker, A., Salehpour, M., Alkass, K., Bernard, S., Sjostrom, S.L., Szewczykowska, M., Jackowska, T., Dos Remedios, C., et al. (2015a). Dynamics of Cell Generation and Turnover in the Human Heart. Cell *161*, 1566–1575.

Bergmann, O., Zdunek, S., Felker, A., Salehpour, M., Alkass, K., Bernard, S., Sjostrom, S.L., Szewczykowska, M., Jackowska, T., Dos Remedios, C., et al. (2015b). Dynamics of Cell Generation and Turnover in the Human Heart. Cell *161*, 1566–1575.

Bernstein, E., Kim, S.Y., Carmell, M.A., Murchison, E.P., Alcorn, H., Li, M.Z., Mills, A.A., Elledge, S.J., Anderson, K. V, and Hannon, G.J. (2003). Dicer is essential for mouse development. Nat. Genet. *35*, 215–217.

Bersell, K., Arab, S., Haring, B., and Kuhn, B. (2009). Neuregulin1/ErbB4 signaling induces cardiomyocyte proliferation and repair of heart injury. Cell *138*, 257–270.

Berthet, C., and Kaldis, P. (2006). Cdk2 and Cdk4 cooperatively control the expression of Cdc2. Cell Div. *1*, 10.

Berthet, C., Klarmann, K.D., Hilton, M.B., Suh, H.C., Keller, J.R., Kiyokawa, H., and Kaldis, P. (2006). Combined loss of Cdk2 and Cdk4 results in embryonic lethality and Rb hypophosphorylation. Dev. Cell *10*, 563–573.

Bicknell, K.A., Coxon, C.H., and Brooks, G. (2004). Forced expression of the cyclin B1–CDC2 complex induces proliferation in adult rat cardiomyocytes. Biochem. J. *382*, 411–416.

Bodmer, R. (1993). The gene tinman is required for specification of the heart and visceral muscles in Drosophila. Development *118*, 719–729.

Boettger, T., Beetz, N., Kostin, S., Schneider, J., Kruger, M., Hein, L., and Braun, T. (2009).

Acquisition of the contractile phenotype by murine arterial smooth muscle cells depends on the Mir143/145 gene cluster. J. Clin. Invest. *119*, 2634–2647.

Boggiano, J.C., Vanderzalm, P.J., and Fehon, R.G. (2011). Tao-1 Phosphorylates Hippo/MST Kinases to Regulate the Hippo-Salvador-Warts Tumor Suppressor Pathway. Dev. Cell *21*, 888–895.

Bondue, A., Lapouge, G., Paulissen, C., Semeraro, C., Iacovino, M., Kyba, M., and Blanpain, C. (2008). Mesp1 acts as a master regulator of multipotent cardiovascular progenitor specification. Cell Stem Cell *3*, 69–84.

Borg, T.K., Ranson, W.F., Moslehy, F.A., and Caulfield, J.B. (1981). Structural basis of ventricular stiffness. Lab. Invest. *44*, 49–54.

Borg, T.K., Rubin, K., Lundgren, E., Borg, K., and Obrink, B. (1984). Recognition of extracellular matrix components by neonatal and adult cardiac myocytes. Dev. Biol. *104*, 86–96.

Botting, K.J., Wang, K.C.W., Padhee, M., McMillen, I.C., Summers-Pearce, B., Rattanatray, L., Cutri, N., Posterino, G.S., Brooks, D.A., and Morrison, J.L. (2012). Early origins of heart disease: low birth weight and determinants of cardiomyocyte endowment. Clin. Exp. Pharmacol. Physiol. *39*, 814–823.

Brade, T., Pane, L.S., Moretti, A., Chien, K.R., and Laugwitz, K.L. (2013). Embryonic heart progenitors and cardiogenesis. Cold Spring Harb. Perspect. Med. *3*, 1–18.

Brooks, G., Poolman, R. a, and Li, J.M. (1998). Arresting developments in the cardiac myocyte cell cycle: role of cyclin-dependent kinase inhibitors. Cardiovasc. Res. *39*, 301–311.

Brown, D.D., Martz, S.N., Binder, O., Goetz, S.C., Price, B.M.J., Smith, J.C., and Conlon, F.L. (2005). Tbx5 and Tbx20 act synergistically to control vertebrate heart morphogenesis. Development *132*, 553–563.

Bruneau, B.G. (2002). Transcriptional regulation of vertebrate cardiac morphogenesis. Circ. Res. *90*, 509–519.

Bruneau, B.G. (2013). Signaling and transcriptional networks in heart development and regeneration. Cold Spring Harb. Perspect. Biol. *5*, a008292–a008292.

Bruneau, B.G., Nemer, G., Schmitt, J.P., Charron, F., Robitaille, L., Caron, S., Conner, D.A., Gessler, M., Nemer, M., Seidman, C.E., et al. (2001). A murine model of Holt-Oram syndrome defines roles of the T-Box transcription factor Tbx5 in cardiogenesis and disease. Cell *106*, 709–721.

Buckingham, M., Meilhac, S., and Zaffran, S. (2005). Building the mammalian heart from two sources of myocardial cells. Nat. Rev. Genet. *6*, 826–835.

Cai, C.-L., Liang, X., Shi, Y., Chu, P.-H., Pfaff, S.L., Chen, J., and Evans, S. (2003). Isl1 identifies a cardiac progenitor population that proliferates prior to differentiation and contributes a majority of cells to the heart. Dev. Cell *5*, 877–889.

Cai, C.-L., Martin, J.C., Sun, Y., Cui, L., Wang, L., Ouyang, K., Yang, L., Bu, L., Liang, X., Zhang, X., et al. (2008). A myocardial lineage derives from Tbx18 epicardial cells. Nature *454*, 104–108.

Callis, T.E., Pandya, K., Hee, Y.S., Tang, R.H., Tatsuguchi, M., Huang, Z.P., Chen, J.F., Deng, Z., Gunn, B., Shumate, J., et al. (2009). MicroRNA-208a is a regulator of cardiac hypertrophy and conduction in mice. J. Clin. Invest. *119*, 2772–2786.

Carè, A., Catalucci, D., Felicetti, F., Bonci, D., Addario, A., Gallo, P., Bang, M.-L., Segnalini, P., Gu, Y., Dalton, N.D., et al. (2007). MicroRNA-133 controls cardiac hypertrophy. Nat. Med. *13*, 613–618.

Chan, R., Hardy, W.R., Laing, M.A., Hardy, S.E., and Muller, W.J. (2002). The Catalytic Activity of the ErbB-2 Receptor Tyrosine Kinase Is Essential for Embryonic Development. Mol. Cell. Biol. *22*, 1073–1078.

Chaudhary, A.K., Mondal, G., Kumar, V., Kattel, K., and Mahato, R.I. (2017). Chemosensitization and inhibition of pancreatic cancer stem cell proliferation by overexpression of microRNA-205. Cancer Lett. *402*, 1–8.

Chaudhry, H.W., Dashoush, N.H., Tang, H., Zhang, L., Wan, X., Wu, E.X., and Wolgemuth, D.J. (2004). Cyclin A2 mediates cardiomyocyte mitosis in the postmitotic myocardium. J. Biol. Chem. *279*, 35858–35866.

Chen, H. (2004). BMP10 is essential for maintaining cardiac growth during murine cardiogenesis. Development *131*, 2219–2231.

Chen, J., and Wang, D.-Z. (2012). microRNAs in cardiovascular development. J. Mol. Cell. Cardiol. *52*, 949–957.

Chen, Y., and Zhang, L. (2017). Members of the microRNA-200 family are promising therapeutic targets in cancer. Exp. Ther. Med. *14*, 10–17.

Chen, J.-F., Mandel, E.M., Thomson, J.M., Wu, Q., Callis, T.E., Hammond, S.M., Conlon, F.L., and Wang, D.-Z. (2006). The role of microRNA-1 and microRNA-133 in skeletal muscle proliferation and differentiation. Nat. Genet. *38*, 228–233.

Chen, J.-F., Murchison, E.P., Tang, R., Callis, T.E., Tatsuguchi, M., Deng, Z., Rojas, M., Hammond, S.M., Schneider, M.D., Selzman, C.H., et al. (2008). Targeted deletion of Dicer in the heart leads to dilated cardiomyopathy and heart failure. Proc. Natl. Acad. Sci. *105*, 2111–2116.

Chen, L., Fulcoli, F.G., Tang, S., and Baldini, A. (2009). Tbx1 regulates proliferation and differentiation of multipotent heart progenitors. Circ. Res. *105*, 842–851.

Chen, Z., Friedrich, G.A., and Soriano, P. (1994). Transcriptional enhancer factor 1 disruption by a retroviral gene trap leads to heart defects and embryonic lethality in mice. Genes Dev. *8*, 2293–2301.

Cheng, Y., Liu, X., Yang, J., Lin, Y., Xu, D.-Z., Lu, Q., Deitch, E.A., Huo, Y., Delphin, E.S., and Zhang, C. (2009). MicroRNA-145, a novel smooth muscle cell phenotypic marker and modulator, controls vascular neointimal lesion formation. Circ. Res. *105*, 158–166.

Chi, N.C., Shaw, R.M., De Val, S., Kang, G., Jan, L.Y., Black, B.L., and Stainier, D.Y.R. (2008). Foxn4 directly regulates tbx2b expression and atrioventricular canal formation. Genes Dev. *22*, 734–739.

Chiavacci, E., Dolfi, L., Verduci, L., Meghini, F., Gestri, G., Evangelista, A.M.M., Wilson, S.W., Cremisi, F., and Pitto, L. (2012). MicroRNA 218 mediates the effects of Tbx5a over-expression on zebrafish heart development. PLoS One *7*, e50536.

Choi, S.K., Kim, H.S., Jin, T., Hwang, E.H., Jung, M., and Moon, W.K. (2016). Overexpression of the miR-141/200c cluster promotes the migratory and invasive ability of triple-negative breast cancer cells through the activation of the FAK and PI3K/AKT signaling pathways by secreting VEGF-A. BMC Cancer *16*, 570.

Choong, O.K., Lee, D.S., Chen, C., and Hsieh, P.C.H. (2017). The roles of non-coding RNAs in cardiac regenerative medicine. Non-Coding RNA Res. *2*, 100–110.

Chow, S., Hedley, D., Grom, P., Magari, R., Jacobberger, J.W., and Shankey, T.V. (2005). Whole blood fixation and permeabilization protocol with red blood cell lysis for flow cytometry of intracellular phosphorylated epitopes in leukocyte subpopulations. Cytom. Part A *67*, 4–17.

Christoffels, V.M., Smits, G.J., Kispert, A., and Moorman, A.F.M. (2010). Development of the pacemaker tissues of the heart. Circ. Res. *106*, 240–254.

Ciemerych, M.A., Kenney, A.M., Sicinska, E., Kalaszczynska, I., Bronson, R.T., Rowitch, D.H., Gardner, H., and Sicinski, P. (2002). Development of mice expressing a single D-type cyclin. Genes Dev. *16*, 3277–3289.

Cobrinik, D. (2005). Pocket proteins and cell cycle control. Oncogene *24*, 2796–2809.

Cohen, E.D., Wang, Z., Lepore, J.J., Lu, M.M., Taketo, M.M., Epstein, D.J., and Morrisey, E.E. (2007). Wnt/beta-catenin signaling promotes expansion of Isl-1-positive cardiac progenitor cells through regulation of FGF signaling. J. Clin. Invest. *117*, 1794–1804.

Combs, M.D., and Yutzey, K.E. (2009). Heart valve development: regulatory networks in development and disease. Circ. Res. *105*, 408–421.

Compernolle, V., Brusselmans, K., Franco, D., Moorman, A., Dewerchin, M., Collen, D., and Carmeliet, P. (2003). Cardia bifida, defective heart development and abnormal neural crest migration in embryos lacking hypoxia-inducible factor-1alpha. Cardiovasc. Res. *60*, 569–579.

Cordes, K.R., Sheehy, N.T., White, M.P., Berry, E.C., Morton, S.U., Muth, A.N., Lee, T.-H., Miano, J.M., Ivey, K.N., and Srivastava, D. (2009). miR-145 and miR-143 regulate smooth muscle cell fate and plasticity. Nature *460*, 705–710.

Cordes, K.R., Srivastava, D., and Ivey, K.N. (2010). MicroRNAs in cardiac development. Pediatr. Cardiol. *31*, 349–356.

Cui, M., Wang, Z., Bassel-Duby, R., and Olson, E.N. (2018). Genetic and epigenetic regulation of cardiomyocytes in development, regeneration and disease. Development *145*, dev171983.

Dang, C. V (2012). MYC on the path to cancer. Cell *149*, 22–35.

Dar, A.A., Majid, S., de Semir, D., Nosrati, M., Bezrookove, V., and Kashani-Sabet, M. (2011). miRNA-205 suppresses melanoma cell proliferation and induces senescence via regulation of E2F1 protein. J. Biol. Chem. *286*, 16606–16614.

Davis, A.C., Wims, M., Spotts, G.D., Hann, S.R., and Bradley, A. (1993). A null c-myc mutation causes lethality before 10.5 days of gestation in homozygotes and reduced fertility in heterozygous female mice. Genes Dev. *7*, 671–682.

Dawes, B.Y.G.S., Mott, J.C., and Widdicombe, J.G. (1954). The Foetal Circulation in the Lamb. 563–587.

DeCoux, A., Lindsey, M.L., Villarreal, F., Garcia, R.A., and Schulz, R. (2014). Myocardial matrix metalloproteinase-2: inside out and upside down. J. Mol. Cell. Cardiol. *77*, 64–72.

Desjardins, C.A., and Naya, F.J. (2016). The Function of the MEF2 Family of Transcription Factors in Cardiac Development, Cardiogenomics, and Direct Reprogramming. J. Cardiovasc. Dev. Dis. *3*.

Devine, W.P., Wythe, J.D., George, M., Koshiba-Takeuchi, K., and Bruneau, B.G. (2014). Early patterning and specification of cardiac progenitors in gastrulating mesoderm. Elife *3*, 1–23.

Dirkx, E., da Costa Martins, P.A., and De Windt, L.J. (2013). Regulation of fetal gene expression in heart failure. Biochim. Biophys. Acta *1832*, 2414–2424.

Dodou, E. (2004). Mef2c is a direct transcriptional target of ISL1 and GATA factors in the anterior heart field during mouse embryonic development. Development *131*, 3931–3942.

Du, K.L., Ip, H.S., Li, J., Chen, M., Dandre, F., Yu, W., Lu, M.M., Owens, G.K., and Parmacek, M.S. (2003). Myocardin Is a Critical Serum Response Factor Cofactor in the Transcriptional Program Regulating Smooth Muscle Cell Differentiation. Mol. Cell. Biol. *23*, 2425–2437.

Du, Y.E., Tu, G., Yang, G., Li, G., Yang, D., Lang, L., Xi, L., Sun, K., Chen, Y., Shu, K., et al. (2017). MiR-205/YAP1 in activated fibroblasts of breast tumor promotes VEGF-independent angiogenesis through STAT3 signaling. Theranostics *7*, 3972–3988.

Dyer, L.A., and Kirby, M.L. (2009). The role of secondary heart field in cardiac development. Dev. Biol. *336*, 137–144.

E.G., S., C., B., A., E., L., B., F., K., L., R., R.P., H., Stanley, E.G., Biben, C., Elefanty, A., et al. (2002). Efficient cre-mediated deletion in cardiac progenitor cells conferred by a 3′UTR-ires-Cre allele of the homeobox gene Nkx2-5. Int. J. Dev. Biol. *46*, 431–439.

Edmondson, D.G., Lyons, G.E., Martin, J.F., and Olson, E.N. (1994). Mef2 gene expression marks the cardiac and skeletal muscle lineages during mouse embryogenesis. Development *120*, 1251–1263.

Engel, F.B., Schebesta, M., Duong, M.T., Lu, G., Ren, S., Madwed, J.B., Jiang, H., Wang, Y., and Keating, M.T. (2005). p38 MAP kinase inhibition enables proliferation of adult mammalian cardiomyocytes. 1175–1187.

Engel, F.B., Schebesta, M., and Keating, M.T. (2006). Anillin localization defect in cardiomyocyte binucleation. J. Mol. Cell. Cardiol. *41*, 601–612.

Engelman, J.A., Luo, J., and Cantley, L.C. (2006). The evolution of phosphatidylinositol 3-kinases as regulators of growth and metabolism. Nat. Rev. Genet. *7*, 606–619.

Eulalio, A., Mano, M., Ferro, M.D., Zentilin, L., Sinagra, G., Zacchigna, S., and Giacca, M. (2012). Functional screening identifies miRNAs inducing cardiac regeneration. Nature *492*, 376–381.

Fa-Xing Yu, Bin Zhao, and K.-L.G. (2016). Hippo Pathway in Organ Size Control, Tissue Homeostasis, and Cancer.

Fang, Z., Dai, W., Wang, X., Chen, W., Shen, C., Ye, G., and Li, L. (2016). Circulating miR-205: a promising biomarker for the detection and prognosis evaluation of bladder cancer. Tumour Biol. *37*, 8075–8082.

Farmer, D.T., Shariat, N., Park, C.Y., Liu, H.J., Mavropoulos, A., and McManus, M.T. (2013). Partially penetrant postnatal lethality of an epithelial specific MicroRNA in a mouse knockout. PLoS One *8*, e76634.

Feliers, D., Frank, M.A., and Riley, D.J. (2002). Activation of cyclin D1-Cdk4 and Cdk4-directed phosphorylation of RB protein in diabetic mesangial hypertrophy. Diabetes *51*, 3290–3299.

Firulli, A.B., McFadden, D.G., Lin, Q., Srivastava, D., and Olson, E.N. (1998). Heart and extra-embryonic mesodermal defects in mouse embryos lacking the bHLH transcription factor Hand1.

Nat. Genet. *18*, 266–270.

Fish, J.E., Wythe, J.D., Xiao, T., Bruneau, B.G., Stainier, D.Y.R., Srivastava, D., and Woo, S. (2011). A Slit/miR-218/Robo regulatory loop is required during heart tube formation in zebrafish. Development *138*, 1409–1419.

Flink, I.L., Oana, S., Maitra, N., Bahl, J.J., and Morkin, E. (1998). Changes in E2F complexes containing retinoblastoma protein family members and increased cyclin-dependent kinase inhibitor activities during terminal differentiation of cardiomyocytes. J. Mol. Cell. Cardiol. *30*, 563–578.

Foglia, M.J., and Poss, K.D. (2016). Building and re-building the heart by cardiomyocyte proliferation. Development *143*, 729–740.

Foley, A.C., and Mercola, M. (2005). Heart induction by Wnt antagonists depends on the homeodomain transcription factor Hex. Genes Dev. *19*, 387–396.

Friedmann-Morvinski, D., and Verma, I.M. (2014). Dedifferentiation and reprogramming: origins of cancer stem cells. EMBO Rep. *15*, 244–253.

Fujita, N., Sato, S., Katayama, K., and Tsuruo, T. (2002). Akt-dependent phosphorylation of p27Kip1 promotes binding to 14-3-3 and cytoplasmic localization. J. Biol. Chem. *277*, 28706–28713.

Gage, G.J., Kipke, D.R., and Shain, W. (2012). Whole Animal Perfusion Fixation for Rodents. J. Vis. Exp. 1–9.

Gao, E., Lei, Y.H., Shang, X., Huang, Z.M., Zuo, L., Boucher, M., Fan, Q., Chuprun, J.K., Ma, X.L., and Koch, W.J. (2010). A novel and efficient model of coronary artery ligation and myocardial infarction in the mouse. Circ. Res. *107*, 1445–1453.

Garg, V., Kathiriya, I.S., Barnes, R., Schluterman, M.K., King, I.N., Butler, C.A., Rothrock, C.R., Eapen, R.S., Hirayama-Yamada, K., Joo, K., et al. (2003). GATA4 mutations cause human congenital heart defects and reveal an interaction with TBX5. Nature *424*, 443–447.

Garofalo, M., Quintavalle, C., Romano, G., Croce, C.M., and Condorelli, G. (2012). miR221/222 in cancer: their role in tumor progression and response to therapy. Curr. Mol. Med. *12*, 27–33.

Gassmann, M., Casagranda, F., Orioli, D., Simon, H., Lai, C., Klein, R., and Lemke, G. (1995). Aberrant neural and cardiac development in mice lacking the ErbB4 neuregulin receptor. Nature *378*, 390–394.

Ghosh, T.K., Song, F.F., Packham, E.A., Buxton, S., Robinson, T.E., Ronksley, J., Self, T., Bonser, A.J., and Brook, J.D. (2009). Physical Interaction between TBX5 and MEF2C Is Required for Early Heart Development. Mol. Cell. Biol. *29*, 2205–2218.

Gibb, N., Lazic, S., Yuan, X., Deshwar, A.R., Leslie, M., Wilson, M.D., and Scott, I.C. (2018). Hey2 regulates the size of the cardiac progenitor pool during vertebrate heart development. Development *145*.

Gilsbach, R., Preissl, S., Grüning, B.A., Schnick, T., Burger, L., Benes, V., Würch, A., Bönisch, U., Günther, S., Backofen, R., et al. (2014). Dynamic DNA methylation orchestrates cardiomyocyte development, maturation and disease. Nat. Commun. *5*.

von Gise, a., Lin, Z., Schlegelmilch, K., Honor, L.B., Pan, G.M., Buck, J.N., Ma, Q., Ishiwata, T., Zhou, B., Camargo, F.D., et al. (2012). YAP1, the nuclear target of Hippo signaling, stimulates

heart growth through cardiomyocyte proliferation but not hypertrophy. Proc. Natl. Acad. Sci. *109*, 2394–2399.

Go Alan, S., Mozaffarian Dariush, L., Roger Véronique, J., Benjamin Emelia, D., Berry Jarett, J., Blaha Michael, S., Dai Shifan, S., Ford Earl, J., Fox Caroline, M., Franco Sheila, A., et al. (2014). Heart Disease and Stroke Statistics—2014 Update: A Report From the American Heart Association. Circulation *129*, e28–e292.

Goberdhan, D.C.I., and Wilson, C. (2003). PTEN: tumour suppressor, multifunctional growth regulator and more. Hum. Mol. Genet. *12*, R239–R248.

Goberdhan, D.C., Paricio, N., Goodman, E.C., Mlodzik, M., and Wilson, C. (1999). Drosophila tumor suppressor PTEN controls cell size and number by antagonizing the Chico/PI3-kinase signaling pathway. Genes Dev. *13*, 3244–3258.

González-Rosa, J.M., Burns, C.E., and Burns, C.G. (2017). Zebrafish heart regeneration: 15 years of discoveries. Regen. (Oxford, England) *4*, 105–123.

Gottlieb, P.D., Pierce, S.A., Sims, R.J., Yamagishi, H., Weihe, E.K., Harriss, J. V., Maika, S.D., Kuziel, W.A., King, H.L., Olson, E.N., et al. (2002). Bop encodes a muscle-restricted protein containing MYND and SET domains and is essential for cardiac differentiation and morphogenesis. Nat. Genet. *31*, 25–32.

Greco, C.M., Kunderfranco, P., Rubino, M., Larcher, V., Carullo, P., Anselmo, A., Kurz, K., Carell, T., Angius, A., Latronico, M.V.G., et al. (2016). DNA hydroxymethylation controls cardiomyocyte gene expression in development and hypertrophy. Nat. Commun. *7*, 1–15.

Green, N.K., Franklyn, J.A., Ohanian, V., Heagerty, A.M., and Gammage, M.D. (1997). Transfection of cardiac muscle: effects of overexpression of c-myc and c-fos proto-oncogene proteins in primary cultures of neonatal rat cardiac myocytes. Clin. Sci. (Lond). *92*, 181–188.

Greene, S.B., Herschkowitz, J.I., and Rosen, J.M. (2010a). The ups and downs of miR-205: identifying the roles of miR-205 in mammary gland development and breast cancer. RNA Biol. *7*, 300–304.

Greene, S.B., Gunaratne, P.H., Hammond, S.M., and Rosen, J.M. (2010b). A putative role for microRNA-205 in mammary epithelial cell progenitors. J. Cell Sci. *123*, 606–618.

Grego-Bessa, J., Luna-Zurita, L., del Monte, G., Bolós, V., Melgar, P., Arandilla, A., Garratt, A.N., Zang, H., Mukouyama, Y. suke, Chen, H., et al. (2007). Notch Signaling Is Essential for Ventricular Chamber Development. Dev. Cell *12*, 415–429.

Grishok, A., Pasquinelli, A.E., Conte, D., Li, N., Parrish, S., Ha, I., Baillie, D.L., Fire, A., Ruvkun, G., and Mello, C.C. (2001). Genes and Mechanisms Related to RNA Interference Regulate Expression of the Small Temporal RNAs that Control C . elegans Developmental Timing. *106*, 23–34.

Grote, P., Wittler, L., Hendrix, D., Koch, F., Wahrisch, S., Beisaw, A., Macura, K., Blass, G., Kellis, M., Werber, M., et al. (2013). The tissue-specific lncRNA Fendrr is an essential regulator of heart and body wall development in the mouse. Dev. Cell *24*, 206–214.

Ha, M., and Kim, V.N. (2014). Regulation of microRNA biogenesis. Nat. Rev. Mol. Cell Biol. *15*, 509–524.

Habets, P.E.M.H., Moorman, A.F.M., Clout, D.E.W., Van Roon, M.A., Lingbeek, M., Van Lohuizen, M., Campione, M., and Christoffels, V.M. (2002). Cooperative action of Tbx2 and

Nkx2.5 inhibits ANF expression in the atrioventricular canal: Implications for cardiac chamber formation. Genes Dev. *16*, 1234–1246.

Halder, G., and Johnson, R.L. (2010). Hippo signaling: growth control and beyond. Development *138*, 9–22.

Hashiguchi, Y., Kawano, S., Goto, Y., Yasuda, K., Kaneko, N., Sakamoto, T., Matsubara, R., Jinno, T., Maruse, Y., Tanaka, H., et al. (2017). Tumor-suppressive roles of ΔNp63β-miR-205 axis in epithelial-mesenchymal transition of oral squamous cell carcinoma via targeting ZEB1 and ZEB2. J. Cell. Physiol.

He, L., Thomson, J.M., Hemann, M.T., Hernando-Monge, E., Mu, D., Goodson, S., Powers, S., Cordon-Cardo, C., Lowe, S.W., Hannon, G.J., et al. (2005). A microRNA polycistron as a potential human oncogene. Nature *435*, 828–833.

Heallen, T., Morikawa, Y., Leach, J., Tao, G., Willerson, J.T., Johnson, R.L., and Martin, J.F. (2013). Hippo signaling impedes adult heart regeneration. Development *140*, 4683–4690.

Heiden, M.G. Vander, Cantley, L.C., Thompson, C.B., Mammalian, P., Exhibit, C., and Metabolism, A. (2009). Understanding the Warburg Effect : Cell Proliferation. Science (80-.). *324*, 1029.

Heineke, J., and Molkentin, J.D. (2006). Regulation of cardiac hypertrophy by intracellular signalling pathways. Nat. Rev. Mol. Cell Biol. *7*, 589.

Hiroi, Y., Kudoh, S., Monzen, K., Ikeda, Y., Yazaki, Y., Nagai, R., and Komuro, I. (2001). Tbx5 associates with Nkx2-5 and synergistically promotes cardiomyocyte differentiation. Nat. Genet. *28*, 276–280.

Holler, K.L., Hendershot, T.J., Troy, S.E., Vincentz, J.W., Firulli, A.B., and Howard, M.J. (2010). Targeted deletion of Hand2 in cardiac neural crest-derived cells influences cardiac gene expression and outflow tract development. Dev. Biol. *341*, 291–304.

Hoogaars, W.M.H., Barnett, P., Moorman, A.F.M., Christoffels, V.M., Xavier-Neto, J., Castro, R.A., Sampaio, A.C., Azambuja, A.P., Castillo, H.A., Cravo, R.M., et al. (2007). T-box factors determine cardiac design. Cell. Mol. Life Sci. *64*, 719–734.

Hu, B., Mitra, J., van den Heuvel, S., and Enders, G.H. (2001). S and G2 phase roles for Cdk2 revealed by inducible expression of a dominant-negative mutant in human cells. Mol. Cell. Biol. *21*, 2755–2766.

Hu, Y., Yang, C., Yang, S., Cheng, F., Rao, J., and Wang, X. (2018). miR-665 promotes hepatocellular carcinoma cell migration, invasion, and proliferation by decreasing Hippo signaling through targeting PTPRB. Cell Death Dis. *9*.

Huang, Y., Hickey, R.P., Yeh, J.L., Liu, D., Dadak, A., Young, L.H., Johnson, R.S., and Giordano, F.J. (2004). Cardiac myocyte-specific HIF-1alpha deletion alters vascularization, energy availability, calcium flux, and contractility in the normoxic heart. FASEB J. *18*, 1138–1140.

Hunter, M.P., Ismail, N., Zhang, X., Aguda, B.D., Lee, E.J., Yu, L., Xiao, T., Schafer, J., Lee, M.L.T., Schmittgen, T.D., et al. (2008). Detection of microRNA expression in human peripheral blood microvesicles. PLoS One *3*.

Ieda, M., Tsuchihashi, T., Ivey, K.N., Ross, R.S., Hong, T.T., Shaw, R.M., and Srivastava, D. (2009). Cardiac Fibroblasts Regulate Myocardial Proliferation through β1 Integrin Signaling. Dev. Cell *16*, 233–244.

Ieda, M., Fu, J.D., Delgado-Olguin, P., Vedantham, V., Hayashi, Y., Bruneau, B.G., and Srivastava, D. (2010). Direct reprogramming of fibroblasts into functional cardiomyocytes by defined factors. Cell *142*, 375–386.

Ikeda, M.A., Jakoi, L., and Nevins, J.R. (1996). A unique role for the Rb protein in controlling E2F accumulation during cell growth and differentiation. Proc. Natl. Acad. Sci. U. S. A. *93*, 3215–3220.

Ilagan, R., Abu-Issa, R., Brown, D., Yang, Y.-P., Jiao, K., Schwartz, R.J., Klingensmith, J., and Meyers, E.N. (2006). Fgf8 is required for anterior heart field development. Development *133*, 2435–2445.

Iso, T., Hamamori, Y., and Kedes, L. (2003). Notch signaling in vascular development. Arterioscler. Thromb. Vasc. Biol. *23*, 543–553.

Ivanovitch, K., Esteban, I., and Torres, M. (2017). Growth and Morphogenesis during Early Heart Development in Amniotes. J. Cardiovasc. Dev. Dis. *4*, 20.

Iwasaki, Y.W., Siomi, M.C., and Siomi, H. (2015). PIWI-Interacting RNA: Its Biogenesis and Functions. Annu. Rev. Biochem. *84*, 405–433.

Jiang, J., Burgon, P.G., Wakimoto, H., Onoue, K., Gorham, J.M., O'Meara, C.C., Fomovsky, G., McConnell, B.K., Lee, R.T., Seidman, J.G., et al. (2015). Cardiac myosin binding protein C regulates postnatal myocyte cytokinesis. Proc. Natl. Acad. Sci. U. S. A. *112*, 9046–9051.

Jiang, W., Jimenez, G., Wells, N.J., Hope, T.J., Wahl, G.M., Hunter, T., and Fukunaga, R. (1998). PRC1: a human mitotic spindle-associated CDK substrate protein required for cytokinesis. Mol. Cell *2*, 877–885.

Johnson, K., Moriarty, C., Tania, N., Ortman, A., DiPietrantonio, K., Edens, B., Eisenman, J., Ok, D., Krikorian, S., Barragan, J., et al. (2014). Kif11 dependent cell cycle progression in radial glial cells is required for proper neurogenesis in the zebrafish neural tube. Dev. Biol. *387*, 73–92.

Jukic, A.M., Baird, D.D., Weinberg, C.R., McConnaughey, D.R., and Wilcox, A.J. (2013). Length of human pregnancy and contributors to its natural variation. Hum. Reprod. *28*, 2848–2855.

Julien Sage (2004). Cyclin C Makes an Entry into the Cell Cycle. Dev. Cell *6*, 607–616.

Kang, M.J., Kim, J.S., Chae, S.W., Koh, K.N., and Koh, G.Y. (1997). Cyclins and cyclin dependent kinases during cardiac development. Mol. Cells *7*, 360–366.

Kango-Singh, M., and Singh, A. (2009). Regulation of organ size: Insights from the drosophila hippo signaling pathway. Dev. Dyn. *238*, 1627–1637.

Karra, R., Knecht, A.K., Kikuchi, K., and Poss, K.D. (2015). Myocardial NF-κB activation is essential for zebrafish heart regeneration. Proc. Natl. Acad. Sci. U. S. A. *112*, 2–7.

Kelly, R.G. (2012). The Second Heart Field (Elsevier Inc.).

Kikuchi, K., Holdway, J.E., Major, R.J., Blum, N., Dahn, R.D., Begemann, G., and Poss, K.D. (2011). Retinoic Acid Production by Endocardium and Epicardium Is an Injury Response Essential for Zebrafish Heart Regeneration. Dev. Cell *20*, 397–404.

Kim, B.-M., and Choi, M.Y. (2012). Non-canonical microRNAs miR-320 and miR-702 promote proliferation in Dgcr8-deficient embryonic stem cells. Biochem. Biophys. Res. Commun. *426*, 183–189.

Kim, E.S., Choi, J.Y., Hwang, S.J., and Bae, I.H. (2019). Hypermethylation of miR-205-5p by IR

Governs Aggressiveness and Metastasis via Regulating Bcl-w and Src. Mol. Ther. - Nucleic Acids *14*, 450–464.

Kim, G.H., Samant, S.A., Earley, J.U., and Svensson, E.C. (2009). Translational control of FOG-2 expression in cardiomyocytes by microRNA-130a. PLoS One *4*, e6161.

Kim, J.-Y., Jeong, H.S., Chung, T., Kim, M., Lee, J.H., Jung, W.H., and Koo, J.S. (2017). The value of phosphohistone H3 as a proliferation marker for evaluating invasive breast cancers: A comparative study with Ki67. Oncotarget *8*, 65064–65076.

Kitajima, S., Takagi, A., Inoue, T., and Saga, Y. (2000). MesP1 and MesP2 are essential for the development of cardiac mesoderm. Development *127*, 3215–3226.

Klattenhoff, C.A., Scheuermann, J.C., Surface, L.E., Bradley, R.K., Fields, P.A., Steinhauser, M.L., Ding, H., Butty, V.L., Torrey, L., Haas, S., et al. (2013). Braveheart, a long noncoding RNA required for cardiovascular lineage commitment. Cell *152*, 570–583.

Kohnoh, T., Hashimoto, N., Ando, A., Sakamoto, K., Miyazaki, S., Aoyama, D., Kusunose, M., Kimura, M., Omote, N., Imaizumi, K., et al. (2016). Hypoxia-induced modulation of PTEN activity and EMT phenotypes in lung cancers. Cancer Cell Int. *16*, 33.

Kopen, R. (2002). Notch: a membrane-bound transciption factor. J. Cell Sci. *115*, 1095–1097.

Koshiji, M., Kageyama, Y., Pete, E.A., Horikawa, I., Barrett, J.C., and Huang, L.E. (2004). HIF-1alpha induces cell cycle arrest by functionally counteracting Myc. EMBO J. *23*, 1949–1956.

Kotch, L.E., Iyer, N. V, Laughner, E., and Semenza, G.L. (1999). Defective vascularization of HIF-1alpha-null embryos is not associated with VEGF deficiency but with mesenchymal cell death. Dev. Biol. *209*, 254–267.

Kou, C.Y.-C., Lau, S.L.-Y., Au, K.-W., Leung, P.-Y., Chim, S.S.-C., Fung, K.-P., Waye, M.M.-Y., and Tsui, S.K.-W. (2010). Epigenetic regulation of neonatal cardiomyocytes differentiation. Biochem. Biophys. Res. Commun. *400*, 278—283.

Koutsaki, M., Libra, M., Spandidos, D.A., and Zaravinos, A. (2017). The miR-200 family in ovarian cancer. Oncotarget *8*, 66629–66640.

Krenning, G., Zeisberg, E.M., and Kalluri, R. (2010). The origin of fibroblasts and mechanism of cardiac fibrosis. J. Cell. Physiol. *225*, 631–637.

Kukurba, K.R., and Montgomery, S.B. (2015). RNA Sequencing and Analysis. Cold Spring Harb. Protoc. *2015*, 951–969.

Kuo, C.T., Morrisey, E.E., Lu, M.M., Parmacek, M.S., Leiden, J.M., Anandappa, R., Sigrist, K., and Soudais, C. (2007). GATA4 transcription factor is required for ventral morphogenesis and heart tube formation. Genes Dev. *11*, 1048–1060.

Kwon, C., Han, Z., Olson, E.N., and Srivastava, D. (2005). MicroRNA1 influences cardiac differentiation in Drosophila and regulates Notch signaling. Proc. Natl. Acad. Sci. U. S. A. *102*, 18986–18991.

Kwon, J.J., Factora, T.D., Dey, S., and Kota, J. (2019). A Systematic Review of miR-29 in Cancer. Mol. Ther. Oncolytics *12*, 173–194.

Lagger, G., O'Carroll, D., Rembold, M., Khier, H., Tischler, J., Weitzer, G., Schuettengruber, B., Hauser, C., Brunmeir, R., Jenuwein, T., et al. (2002). Essential function of histone deacetylase 1 in proliferation control and CDK inhibitor repression. EMBO J. *21*, 2672–2681.

Laugwitz, K.-L., Moretti, A., Caron, L., Nakano, A., and Chien, K.R. (2007). Islet1 cardiovascular progenitors: a single source for heart lineages? Development *135*, 193–205.

Laumonier, T., and Menetrey, J. (2016). Muscle injuries and strategies for improving their repair. J. Exp. Orthop. *3*, 15.

Lavine, K.J., Yu, K., White, A.C., Zhang, X., Smith, C., Partanen, J., and Ornitz, D.M. (2005). Endocardial and epicardial derived FGF signals regulate myocardial proliferation and differentiation in vivo. Dev. Cell *8*, 85–95.

Lavine, K.J., White, A.C., Park, C., Smith, C.S., Choi, K., Long, F., Hui, C.C., and Ornitz, D.M. (2006). Fibroblast growth factor signals regulate a wave of Hedgehog activation that is essential for coronary vascular development. Genes Dev. *20*, 1651–1666.

Leach, J.P., Heallen, T., Zhang, M., Rahmani, M., Morikawa, Y., Hill, M.C., Segura, A., Willerson, J.T., and Martin, J.F. (2017). Hippo pathway deficiency reverses systolic heart failure after infarction. Nature *550*, 260–264.

Li, J.M., and Brooks, G. (1999). Cell cycle regulatory molecules (cyclins, cyclin-dependent kinases and cyclin-dependent kinase inhibitors) and the cardiovascular system. Potential targets for therapy? Eur. Heart J. *20*, 406–420.

Li, J.-H., Sun, S.-S., Li, N., Lv, P., Xie, S.-Y., and Wang, P.-Y. (2017). MiR-205 as a promising biomarker in the diagnosis and prognosis of lung cancer. Oncotarget *8*, 91938–91949.

Liang, H., and Zeng, E. (2016). RNA-Seq Experiment and Data Analysis. Methods Mol. Biol. *1366*, 99–114.

Liberatore, C.M., Searcy-Schrick, R.D., and Yutzey, K.E. (2000). Ventricular expression of tbx5 inhibits normal heart chamber development. Dev. Biol. *223*, 169–180.

Lien, C.L., Wu, C., Mercer, B., Webb, R., Richardson, J.A., and Olson, E.N. (1999). Control of early cardiac-specific transcription of Nkx2-5 by a GATA-dependent enhancer. Development *126*, 75–84.

Lim, Y.-Y., Wright, J.A., Attema, J.L., Gregory, P.A., Bert, A.G., Smith, E., Thomas, D., Lopez, A.F., Drew, P.A., Khew-Goodall, Y., et al. (2013). Epigenetic modulation of the miR-200 family is associated with transition to a breast cancer stem-cell-like state. J. Cell Sci. *126*, 2256–2266.

Lin, Q., Schwarz, J., Bucana, C., and Olson, E.N. (1997). Control of mouse cardiac morphogenesis and myogenesis by transcription factor MEF2C. Science *276*, 1404–1407.

Lin, Z., Von Gise, A., Zhou, P., Gu, F., Ma, Q., Jiang, J., Yau, A.L., Buck, J.N., Gouin, K.A., Van Gorp, P.R.R., et al. (2014). Cardiac-specific YAP activation improves cardiac function and survival in an experimental murine MI model. Circ. Res. *115*, 354–363.

Liu, J., and Kipreos, E.T. (2000). Evolution of cyclin-dependent kinases (CDKs) and CDK-activating kinases (CAKs): differential conservation of CAKs in yeast and metazoa. Mol. Biol. Evol. *17*, 1061–1074.

Liu, J., Bressan, M., Hassel, D., Huisken, J., Staudt, D., Kikuchi, K., Poss, K.D., Mikawa, T., and Stainier, D.Y.R. (2010). A dual role for ErbB2 signaling in cardiac trabeculation. Development *137*, 3867–3875.

Liu, N., Bezprozvannaya, S., Williams, A.H., Qi, X., Richardson, J.A., Bassel-Duby, R., and Olson, E.N. (2008). microRNA-133a regulates cardiomyocyte proliferation and suppresses smooth

muscle gene expression in the heart. Genes Dev. *22*, 3242–3254.

Lockhart Marie , Wirrig Elaine, Phelps Aimee, W.A. (2011). Extracellular Matrix and Heart Development. Birth Defects Res A Clin Mol Teratol. *91*, 535–550.

Lopaschuk, G.D., and Spafford, M.A. (1992). Differences in myocardial ischemic tolerance between 1- and 7-day-old rabbits. Can J Physiol Pharmacol *70*, 1315–1323.

Lozano, R., Naghavi, M., Foreman, K., Lim, S., Shibuya, K., Aboyans, V., Abraham, J., Adair, T., Aggarwal, R., Ahn, S.Y., et al. (2012). Global and regional mortality from 235 causes of death for 20 age groups in 1990 and 2010: A systematic analysis for the Global Burden of Disease Study 2010. Lancet *380*, 2095–2128.

Maddika, S., Ande, S.R., Wiechec, E., Hansen, L.L., Wesselborg, S., and Los, M. (2008). Akt-mediated phosphorylation of CDK2 regulates its dual role in cell cycle progression and apoptosis. J. Cell Sci. *121*, 979–988.

Maehama, T., and Dixon, J.E. (1998). The tumor suppressor, PTEN/MMAC1, dephosphorylates the lipid second messenger, phosphatidylinositol 3,4,5-trisphosphate. J. Biol. Chem. *273*, 13375–13378.

Mahmoud, A.I., Kocabas, F., Muralidhar, S. a, Kimura, W., Koura, A.S., Thet, S., Porrello, E.R., and Sadek, H. a (2013). Meis1 regulates postnatal cardiomyocyte cell cycle arrest. Nature *497*, 249–253.

Maillet, M., Van Berlo, J.H., and Molkentin, J.D. (2013). Molecular basis of physiological heart growth: Fundamental concepts and new players. Nat. Rev. Mol. Cell Biol. *14*, 38–48.

Maitra, M., Schluterman, M.K., Nichols, H.A., Richardson, J.A., Lo, C.W., Srivastava, D., and Garg, V. (2009). Interaction of Gata4 and Gata6 with Tbx5 is critical for normal cardiac development. Dev. Biol. *326*, 368–377.

Malaney, P., Uversky, V.N., and Davé, V. (2017). PTEN proteoforms in biology and disease. Cell. Mol. Life Sci. *74*, 2783–2794.

Malliaras, K., Zhang, Y., Seinfeld, J., Galang, G., Tseliou, E., Cheng, K., Sun, B., Aminzadeh, M., and Marbán, E. (2013). Cardiomyocyte proliferation and progenitor cell recruitment underlie therapeutic regeneration after myocardial infarction in the adult mouse heart. EMBO Mol. Med. *5*, 191–209.

Malumbres, M., Cycle, C., Woo, R.A., Poon, R.Y.C., Manuscript, A., Liu, J., and Kipreos, E.T. (2014). Cyclin-dependent kinases. Genome Biol. *15*, 122.

Manning, B.D., and Toker, A. (2017). AKT/PKB Signaling: Navigating the Network. Cell *169*, 381–405.

Marvin, M.J., Di Rocco, G., Gardiner, A., Bush, S.M., and Lassar, A.B. (2001). Inhibition of Wnt activity induces heart formation from posterior mesoderm. Genes Dev. *15*, 316–327.

Mase, M., Grasso, M., Avogaro, L., D'Amato, E., Tessarolo, F., Graffigna, A., Denti, M.A., and Ravelli, F. (2017). Selection of reference genes is critical for miRNA expression analysis in human cardiac tissue. A focus on atrial fibrillation. Sci. Rep. *7*, 41127.

Matsui, Y., Nakano, N., Shao, D., Gao, S., Luo, W., Hong, C., Zhai, P., Holle, E., Yu, X., Yabuta, N., et al. (2008). Lats2 is a negative regulator of myocyte size in the heart. Circ. Res. *103*, 1309–1318.

Di Mauro, V., and Catalucci, D. (2017). The importance of being ncRNAs: from bit players as “junk DNA” to rising stars on the stage of the pharmaceutical industry. Ann. Transl. Med. *5*, 147.

Di Mauro, V., Barandalla-Sobrados, M., and Catalucci, D. (2018). The noncoding-RNA landscape in cardiovascular health and disease. Non-Coding RNA Res. *3*, 12–19.

McFadden, D.G. (2004). The Hand1 and Hand2 transcription factors regulate expansion of the embryonic cardiac ventricles in a gene dosage-dependent manner. Development *132*, 189–201.

McGill, C.J., and Brooks, G. (1995). Cell cycle control mechanisms and their role in cardiac growth. Cardiovasc. Res. *30*, 557–569.

Meyer, D., and Birchmeier, C. (1995). Multiple essential functions of neuregulin in development. Nature *378*, 386–390.

Mirra, P., Raciti, G.A., Nigro, C., Fiory, F., D’Esposito, V., Formisano, P., Beguinot, F., and Miele, C. (2015). Circulating miRNAs as intercellular messengers, potential biomarkers and therapeutic targets for Type 2 diabetes. Epigenomics *7*, 653–667.

Mjaatvedt, C.H., Nakaoka, T., Moreno-Rodriguez, R., Norris, R.A., Kern, M.J., Eisenberg, C.A., Turner, D., and Markwald, R.R. (2001). The outflow tract of the heart is recruited from a novel heart-forming field. Dev. Biol. *238*, 97–109.

Mohamed, T.M.A., Ang, Y.-S., Radzinsky, E., Zhou, P., Huang, Y., Elfenbein, A., Foley, A., Magnitsky, S., and Srivastava, D. (2018). Regulation of Cell Cycle to Stimulate Adult Cardiomyocyte Proliferation and Cardiac Regeneration. Cell *173*, 104-116.e12.

Mollinari, C., Kleman, J.-P.P., Jiang, W., Schoehn, G., Hunter, T., and Margolis, R.L. (2002). PRC1 is a microtubule binding and bundling protein essential to maintain the mitotic spindle midzone. J Cell Biol *157*, 1175–1186.

Mollova, M., Bersell, K., Walsh, S., Savla, J., Das, L.T., Park, S.-Y., Silberstein, L.E., Dos Remedios, C.G., Graham, D., Colan, S., et al. (2013). Cardiomyocyte proliferation contributes to heart growth in young humans. Proc. Natl. Acad. Sci. U. S. A. *110*, 1446–1451.

Montgomery, R.L., Davis, C.A., Potthoff, M.J., Haberland, M., Fielitz, J., Qi, X., Hill, J.A., Richardson, J.A., and Olson, E.N. (2007). Histone deacetylases 1 and 2 redundantly regulate cardiac morphogenesis, growth, and contractility. Genes Dev. *21*, 1790–1802.

Montgomery, R.L., Potthoff, M.J., Haberland, M., Qi, X., Matsuzaki, S., Humphries, K.M., Richardson, J.A., Bassel-Duby, R., and Olson, E.N. (2008). Maintenance of cardiac energy metabolism by histone deacetylase 3 in mice. J. Clin. Invest. *118*, 3588–3597.

Moorman, A.F.M., and Christoffels, V.M. (2003). Cardiac chamber formation: development, genes, and evolution. Physiol. Rev. *83*, 1223–1267.

Moretti, A., Caron, L., Nakano, A., Lam, J.T., Bernshausen, A., Chen, Y., Qyang, Y., Bu, L., Sasaki, M., Martin-Puig, S., et al. (2006). Multipotent Embryonic Isl1+ Progenitor Cells Lead to Cardiac, Smooth Muscle, and Endothelial Cell Diversification. Cell *127*, 1151–1165.

Mori, A.D., Zhu, Y., Vahora, I., Nieman, B., Koshiba-Takeuchi, K., Davidson, L., Pizard, A., Seidman, J.G., Seidman, C.E., Chen, X.J., et al. (2006). Tbx5-dependent rheostatic control of cardiac gene expression and morphogenesis. Dev. Biol. *297*, 566–586.

Morton, S.U., Scherz, P.J., Cordes, K.R., Ivey, K.N., Stainier, D.Y.R., and Srivastava, D. (2008). microRNA-138 modulates cardiac patterning during embryonic development. Proc. Natl. Acad.

Sci. U. S. A. *105*, 17830–17835.

Moya, I.M., and Halder, G. (2018). Hippo–YAP/TAZ signalling in organ regeneration and regenerative medicine. Nat. Rev. Mol. Cell Biol.

Muller, C.W., and Herrmann, B.G. (1997). Crystallographic structure of the T domain-DNA complex of the Brachyury transcription factor. Nature *389*, 884–888.

Munshi, N. V, McAnally, J., Bezprozvannaya, S., Berry, J.M., Richardson, J.A., Hill, J.A., and Olson, E.N. (2009). Cx30.2 enhancer analysis identifies Gata4 as a novel regulator of atrioventricular delay. Development *136*, 2665–2674.

Murray, S.A., Morgan, J.L., Kane, C., Sharma, Y., Heffner, C.S., Lake, J., and Donahue, L.R. (2010). Mouse gestation length is genetically determined. PLoS One *5*, e12418.

Myers, M.P., Pass, I., Batty, I.H., Van der Kaay, J., Stolarov, J.P., Hemmings, B.A., Wigler, M.H., Downes, C.P., and Tonks, N.K. (1998). The lipid phosphatase activity of PTEN is critical for its tumor supressor function. Proc. Natl. Acad. Sci. *95*, 13513–13518.

Neganova, I., and Lako, M. (2008). G1 to S phase cell cycle transition in somatic and embryonic stem cells. J. Anat. *213*, 30–44.

Ogura, T. (2007). Tbx5 Specifies the Left/Right Ventricles and Ventricular Septum Position During Cardiogenesis. Cardiovasc. Dev. Congenit. Malformations Mol. Genet. Mech. *5*, 75–77.

Onay-Besikci, A. (2006). Regulation of cardiac energy metabolism in newborn. Mol. Cell. Biochem. *287*, 1–11.

Ota, A., Tagawa, H., Karnan, S., Tsuzuki, S., Karpas, A., Kira, S., Yoshida, Y., and Seto, M. (2004). Identification and characterization of a novel gene, C13orf25, as a target for 13q31-q32 amplification in malignant lymphoma. Cancer Res. *64*, 3087–3095.

Paige, S.L., Plonowska, K., Xu, A., and Wu, S.M. (2015). Molecular regulation of cardiomyocyte differentiation. Circ. Res. *116*, 341–353.

Paradis, A.N., Gay, M.S., and Zhang, L. (2014). Binucleation of cardiomyocytes: the transition from a proliferative to a terminally differentiated state. Drug Discov. Today *19*, 602–609.

Park, S., Gaur, A., … E.L.-G.&, and 2008, U. (2008). The miR-200 family determines the epithelial phenotype of cancer cells by targeting the E-cadherin repressors ZEB1 and ZEB2. Genesdev.Cshlp.Org 894–907.

Parsons, L.M., Hartley, L., Lyons, I., Li, R., Robb, L., Andrews, J.E., and Harvey, R.P. (2007). Myogenic and morphogenetic defects in the heart tubes of murine embryos lacking the homeo box gene Nkx2-5. Genes Dev. *9*, 1654–1666.

Pasumarthi, K.B.S., and Field, L.J. (2002). Cardiomyocyte cell cycle regulation. Circ. Res. *90*, 1044–1054.

Pasumarthi, K.B.S., Nakajima, H., Nakajima, H.O., Soonpaa, M.H., and Field, L.J. (2005). Targeted expression of cyclin D2 results in cardiomyocyte DNA synthesis and infarct regression in transgenic mice. Circ. Res. *96*, 110–118.

Patterson, A.J., and Zhang, L. (2010). Hypoxia and fetal heart development. Curr. Mol. Med. *10*, 653–666.

Peltier, H.J., and Latham, G.J. (2008). Normalization of microRNA expression levels in

quantitative RT-PCR assays: identification of suitable reference RNA targets in normal and cancerous human solid tissues. RNA *14*, 844–852.

Pilny, J. (1975). The amount of contractile matter per myocardial cell nucleus in the rat during postnatal ontogenesis. II. Folia Morphol. (Warsz). *23*, 342–346.

Plouffe, S.W., Meng, Z., Lin, K.C., Lin, B., Hong, A.W., Chun, J. V, and Guan, K.-L. (2016). Characterization of Hippo Pathway Components by Gene Inactivation. Mol. Cell *64*, 993–1008.

Poon, C.L.C., Lin, J.I., Zhang, X., and Harvey, K.F. (2011). The Sterile 20-like Kinase Tao-1 Controls Tissue Growth by Regulating the Salvador-Warts-Hippo Pathway. Dev. Cell *21*, 896–906.

Porrello, E.R., and Olson, E.N. (2014). A neonatal blueprint for cardiac regeneration. Stem Cell Res. *13*, 556–570.

Porrello, E.R., Mahmoud, A.I., Simpson, E., Hill, J.A., Richardson, J.A., Olson, E.N., and Sadek, H.A. (2011a). Transient Regenerative Potential of the Neonatal Mouse Heart. *331*, 1078–1081.

Porrello, E.R., Johnson, B.A., Aurora, A.B., Simpson, E., Nam, Y.-J., Matkovich, S.J., Dorn, G.W. 2nd, van Rooij, E., and Olson, E.N. (2011b). MiR-15 family regulates postnatal mitotic arrest of cardiomyocytes. Circ. Res. *109*, 670–679.

Porrello, E.R., Mahmoud, A.I., Simpson, E., Johnson, B.A., Grinsfelder, D., Canseco, D., Mammen, P.P., Rothermel, B.A., Olson, E.N., and Sadek, H.A. (2013). Regulation of neonatal and adult mammalian heart regeneration by the miR-15 family. Proc. Natl. Acad. Sci. U. S. A. *110*, 187–192.

Potthoff, M.J., and Olson, E.N. (2007). MEF2: a central regulator of diverse developmental programs. Development *134*, 4131–4140.

Prall, O.W.J., Menon, M.K., Solloway, M.J., Watanabe, Y., Zaffran, S., Bajolle, F., Biben, C., McBride, J.J., Robertson, B.R., Chaulet, H., et al. (2007). An Nkx2-5/Bmp2/Smad1 Negative Feedback Loop Controls Heart Progenitor Specification and Proliferation. Cell *128*, 947–959.

Profumo, V., Forte, B., Percio, S., Rotundo, F., Doldi, V., Ferrari, E., Fenderico, N., Dugo, M., Romagnoli, D., Benelli, M., et al. (2019). LEADeR role of miR-205 host gene as long noncoding RNA in prostate basal cell differentiation. Nat. Commun. *10*, 307.

Puente, B.N., Kimura, W., Muralidhar, S.A., Moon, J., Amatruda, J.F., Phelps, K.L., Grinsfelder, D., Rothermel, B.A., Chen, R., Garcia, J.A., et al. (2014). The oxygen-rich postnatal environment induces cardiomyocyte cell-cycle arrest through DNA damage response. Cell *157*, 565–579.

Pugach, E.K., Richmond, P.A., Azofeifa, J.G., Dowell, R.D., and Leinwand, L.A. (2015). Prolonged Cre expression driven by the alpha-myosin heavy chain promoter can be cardiotoxic. J. Mol. Cell. Cardiol. *86*, 54–61.

Qian, L., Huang, Y., Spencer, C.I., Foley, A., Vedantham, V., Liu, L., Conway, S.J., Fu, J.D., and Srivastava, D. (2012). In vivo reprogramming of murine cardiac fibroblasts into induced cardiomyocytes. Nature *485*, 593–598.

Qin, A.Y., Zhang, X.W., Liu, L., Yu, J.P., Li, H., Emily Wang, S.Z., Ren, X.B., and Cao, S. (2013). MiR-205 in cancer: An angel or a devil? Eur. J. Cell Biol. *92*, 54–60.

Quaife-Ryan, G.A., Sim, C.B., Porrello, E.R., and Hudson, J.E. (2016). Resetting the epigenome for heart regeneration. Semin. Cell Dev. Biol. *58*, 2–13.

Qyang, Y., Martin-Puig, S., Chiravuri, M., Chen, S., Xu, H., Bu, L., Jiang, X., Lin, L., Granger, A., Moretti, A., et al. (2007). The Renewal and Differentiation of Isl1+ Cardiovascular Progenitors Are Controlled by a Wnt/β-Catenin Pathway. Cell Stem Cell *1*, 165–179.

Rana, M.S., Christoffels, V.M., and Moorman, A.F.M. (2013). A molecular and genetic outline of cardiac morphogenesis. Acta Physiol. *207*, 588–615.

Rao, P.K., Toyama, Y., Chiang, H.R., Gupta, S., Bauer, M., Medvid, R., Reinhardt, F., Liao, R., Krieger, M., Jaenisch, R., et al. (2009). Loss of cardiac microRNA-mediated regulation leads to dilated cardiomyopathy and heart failure. Circ. Res. *105*, 585–594.

Del Re, D.P., Yang, Y., Nakano, N., Cho, J., Zhai, P., Yamamoto, T., Zhang, N., Yabuta, N., Nojima, H., Pan, D., et al. (2013). Yes-associated protein isoform 1 (Yapl) promotes cardiomyocyte survival and growth to protect against myocardial ischemic injury. J. Biol. Chem. *288*, 3977–3988.

Reddy, B.V.V.G., and Irvine, K.D. (2008). The Fat and Warts signaling pathways : new insights into their regulation , mechanism and conservation. *2838*, 2827–2838.

Ren, B., Cam, H., Takahashi, Y., Volkert, T., Terragni, J., Young, R.A., and Dynlacht, B.D. (2002). E2F integrates cell cycle progression with DNA repair, replication, and G(2)/M checkpoints. Genes Dev. *16*, 245–256.

Risebro, C.A., Smart, N., Dupays, L., Breckenridge, R., Mohun, T.J., and Riley, P.R. (2006). Hand1 regulates cardiomyocyte proliferation versus differentiation in the developing heart. Development *133*, 4595–4606.

van Rooij, E., and Olson, E.N. (2007). microRNAs put their signatures on the heart. Physiol. Genomics *31*, 365–366.

van Rooij, E., Sutherland, L.B., Qi, X., Richardson, J.A., Hill, J., and Olson, E.N. (2007). Control of stress-dependent cardiac growth and gene expression by a microRNA. Science *316*, 575–579.

van Rooij, E., Quiat, D., Johnson, B.A., Sutherland, L.B., Qi, X., Richardson, J.A., Kelm, R.J.J., and Olson, E.N. (2009). A family of microRNAs encoded by myosin genes governs myosin expression and muscle performance. Dev. Cell *17*, 662–673.

Rotini, A., Martinez-Sarra, E., Pozzo, E., and Sampaolesi, M. (2018). Interactions between microRNAs and long non-coding RNAs in cardiac development and repair. Pharmacol. Res. *127*, 58–66.

Rutenberg, J.B., Fischer, A., Jia, H., Gessler, M., Zhong, T.P., and Mercola, M. (2006). Developmental patterning of the cardiac atrioventricular canal by Notch and Hairy-related transcription factors. Development *133*, 4381–4390.

Saga, Y., Miyagawa-Tomita, S., Takagi, A., Kitajima, S., Miyazaki, J. i, and Inoue, T. (1999). MesP1 is expressed in the heart precursor cells and required for the formation of a single heart tube. Development *126*, 3437–3447.

Saga, Y., Kitajima, S., and Miyagawa-Tomita, S. (2000). Mesp1 expression is the earliest sign of cardiovascular development. Trends Cardiovasc. Med. *10*, 345–352.

Sanchez-Soria, P., and Camenisch, T.D. (2010). ErbB signaling in cardiac development and disease. Semin. Cell Dev. Biol. *21*, 929–935.

Santolla, M.F., Lappano, R., Cirillo, F., Rigiracciolo, D.C., Sebastiani, A., Abonante, S., Tassone,

P., Tagliaferri, P., Di Martino, M.T., Maggiolini, M., et al. (2018). miR-221 stimulates breast cancer cells and cancer-associated fibroblasts (CAFs) through selective interference with the A20/c-Rel/CTGF signaling. J. Exp. Clin. Cancer Res. *37*, 94.

Schlesinger, J., Schueler, M., Grunert, M., Fischer, J.J., Zhang, Q., Krueger, T., Lange, M., Tönjes, M., Dunkel, I., and Sperling, S.R. (2011). The cardiac transcription network modulated by gata4, mef2a, nkx2.5, srf, histone modifications, and microRNAs. PLoS Genet. *7*.

Schneider, V.A., and Mercola, M. (2001). Wnt antagonism initiates cardiogenesis in Xenopus laevis. Genes Dev. *15*, 304–315.

Scholzen, T., and Gerdes, J. (2000). The Ki-67 protein: from the known and the unknown. J. Cell. Physiol. *182*, 311–322.

Sdek, P., Zhao, P., Wang, Y., Huang, C.J., Ko, C.Y., Butler, P.C., Weiss, J.N., and MacLellan, W.R. (2011). Rb and p130 control cell cycle gene silencing to maintain the postmitotic phenotype in cardiac myocytes. J. Cell Biol. *194*, 407–423.

Sedmera, D., and Thompson, R.P. (2011). Myocyte proliferation in the developing heart. Dev. Dyn. *240*, 1322–1334.

Shi, C., and Xu, X. (2016). MiR-670-5p induces cell proliferation in hepatocellular carcinoma by targeting PROX1. Biomed. Pharmacother. *77*, 20–26.

Siddiqi, S., and Sussman, M.A. (2014). The heart: mostly postmitotic or mostly premitotic? Myocyte cell cycle, senescence, and quiescence. Can. J. Cardiol. *30*, 1270–1278.

Sim, C.B., Ziemann, M., Kaspi, A., Harikrishnan, K.N., Ooi, J., Khurana, I., Chang, L., Hudson, J.E., El-Osta, A., and Porrello, E.R. (2015a). Dynamic changes in the cardiac methylome during postnatal development. FASEB J. *29*, 1329–1343.

Sim, C.B., Ziemann, M., Kaspi, A., Harikrishnan, K.N., Ooi, J., Khurana, I., Chang, L., Hudson, J.E., El-Osta, A., and Porrello, E.R. (2015b). Dynamic changes in the cardiac methylome during postnatal development. FASEB J. *29*, 1329–1343.

Singh, A., Ramesh, S., Cibi, D.M., Yun, L.S., Li, J., Li, L., Manderfield, L.J., Olson, E.N., Epstein, J.A., and Singh, M.K. (2016). Hippo Signaling Mediators Yap and Taz Are Required in the Epicardium for Coronary Vasculature Development. Cell Rep. *15*, 1384–1393.

Singh, R., Hoogaars, W.M., Barnett, P., Grieskamp, T., Sameer Rana, M., Buermans, H., Farin, H.F., Petry, M., Heallen, T., Martin, J.F., et al. (2012). Tbx2 and Tbx3 induce atrioventricular myocardial development and endocardial cushion formation. Cell. Mol. Life Sci. *69*, 1377–1389.

Smits, A.M., and Riley, P.R. (2014). Epicardium-Derived Heart Repair. J. Dev. Biol. *2*, 84–100.

Soonpaa, M.H., Kim, K.K., Pajak, L., Franklin, M., and Field, L.J. (1996). Cardiomyocyte DNA synthesis and binucleation during murine development. Am. J. Physiol. *271*, H2183-9.

Soonpaa, M.H., Koh, G.Y., Pajak, L., Jing, S., Wang, H., Franklin, M.T., Kim, K.K., and Field, L.J. (1997). Cyclin D1 overexpression promotes cardiomyocyte DNA synthesis and multinucleation in transgenic mice. J. Clin. Invest. *99*, 2644–2654.

Staley, B.K., and Irvine, K.D. (2012). Hippo signaling in Drosophila: Recent advances and insights. Dev. Dyn. *241*, 3–15.

Di Stefano, V., Giacca, M., Capogrossi, M.C., Crescenzi, M., and Martelli, F. (2011). Knockdown of cyclin-dependent kinase inhibitors induces cardiomyocyte re-entry in the cell cycle. J. Biol.

Chem. *286*, 8644–8654.

Stine, Z.E., Walton, Z.E., Altman, B.J., Hsieh, A.L., and Dang, C. V (2015). MYC, Metabolism, and Cancer. Cancer Discov. *5*, 1024–1039.

Sun, X., Han, Q., Luo, H., Pan, X., Ji, Y., Yang, Y., Chen, H., Wang, F., Lai, W., Guan, X., et al. (2017). Profiling analysis of long non-coding RNAs in early postnatal mouse hearts. Sci. Rep. *7*, 1–14.

Sun, X., Zhang, C., Cao, Y., and Liu, E. (2019). miR-150 Suppresses Tumor Growth in Melanoma Through Downregulation of MYB. Oncol. Res. *27*, 317–323.

Sur, S., and Agrawal, D.K. (2016). Phosphatases and kinases regulating CDC25 activity in the cell cycle: clinical implications of CDC25 overexpression and potential treatment strategies. Mol. Cell. Biochem. *416*, 33–46.

Talman, V., Teppo, J., Pöhö, P., Movahedi, P., Vaikkinen, A., Tuuli Karhu, S., Trošt, K., Suvitaival, T., Heikkonen, J., Pahikkala, T., et al. (2018). Molecular atlas of postnatal mouse heart development. J. Am. Heart Assoc. *7*.

Tane, S., Ikenishi, A., Okayama, H., Iwamoto, N., Nakayama, K.I., and Takeuchi, T. (2014). CDK inhibitors, p21(Cip1) and p27(Kip1), participate in cell cycle exit of mammalian cardiomyocytes. Biochem. Biophys. Res. Commun. *443*, 1105–1109.

Taneja, P., Zhu, S., Maglic, D., Fry, E.A., Kendig, R.D., and Inoue, K. (2011). Transgenic and knockout mice models to reveal the functions of tumor suppressor genes. Clin. Med. Insights. Oncol. *5*, 235–257.

Tao, X., Chon, H.S., Fu, S., Kavanagh, J.J., and Hu, W. (2008). Update on aurora kinase inhibitors in gynecologic malignancies. Recent Pat. Anticancer. Drug Discov. *3*, 162–177.

Terkeltaub, R., Johnson, R., and Halder, G. (2014). The two faces of Hippo: targeting the Hippo pathway for regenerative medicine and cancer treatment. Nat. Rev. Drug Discov. *13*, 63–79.

Tian, J., An, X., and Niu, L. (2017). Role of microRNAs in cardiac development and disease (Review). Exp. Ther. Med. *13*, 3–8.

Tian, Y., Liu, Y., Wang, T., Zhou, N., Kong, J., Chen, L., Snitow, M., Morley, M., Li, D., Petrenko, N., et al. (2015). A microRNA-Hippo pathway that promotes cardiomyocyte proliferation and cardiac regeneration in mice. Sci. Transl. Med. *7*, 279ra38.

Timmers, C., Sharma, N., Opavsky, R., Maiti, B., Wu, L., Wu, J., Orringer, D., Trikha, P., Saavedra, H.I., and Leone, G. (2007). E2f1, E2f2, and E2f3 control E2F target expression and cellular proliferation via a p53-dependent negative feedback loop. Mol. Cell. Biol. *27*, 65–78.

Tirosh-Finkel, L., Zeisel, A., Brodt-Ivenshitz, M., Shamai, A., Yao, Z., Seger, R., Domany, E., and Tzahor, E. (2010). BMP-mediated inhibition of FGF signaling promotes cardiomyocyte differentiation of anterior heart field progenitors. J. Cell Sci. *123*, e1–e1.

Torres-Cuevas, I., Parra-Llorca, A., Sánchez-Illana, A., Nuñez-Ramiro, A., Kuligowski, J., Cháfer-Pericás, C., Cernada, M., Escobar, J., and Vento, M. (2017). Oxygen and oxidative stress in the perinatal period. Redox Biol. *12*, 674–681.

Torrini, C., Cubero, R.J., Dirkx, E., Braga, L., Ali, H., Prosdocimo, G., Gutierrez, M.I., Collesi, C., Licastro, D., Zentilin, L., et al. (2019). Common Regulatory Pathways Mediate Activity of MicroRNAs Inducing Cardiomyocyte Proliferation. Cell Rep. *27*, 2759-2771.e5.

Toyota, E., Fujimoto, K., Ogasawara, Y., Kajita, T., Shigeto, F., Matsumoto, T., Goto, M., and Kajiya, F. (2002). Dynamic changes in three-dimensional architecture and vascular volume of transmural coronary microvasculature between diastolic- and systolic-arrested rat hearts. Circulation *105*, 621–626.

Trivedi, C.M., Min, M.L., Wang, Q., and Epstein, J.A. (2008). Transgenic overexpression of Hdac3 in the heart produces increased postnatal cardiac myocyte proliferation but does not induce hypertrophy. J. Biol. Chem. *283*, 26484–26489.

Tsai, S.-Y., Opavsky, R., Sharma, N., Wu, L., Naidu, S., Nolan, E., Feria-Arias, E., Timmers, C., Opavska, J., de Bruin, A., et al. (2008). Mouse development with a single E2F activator. Nature *454*, 1137–1141.

Tzahor, E. (2007). Wnt/beta-catenin signaling and cardiogenesis: timing does matter. Dev. Cell *13*, 10–13.

Tzahor, E., and Lassar, A.B. (2001). Wnt signals from the neural tube block ectopic cardiogenesis. Genes Dev. *15*, 255–260.

Ueno, S., Weidinger, G., Osugi, T., Kohn, A.D., Golob, J.L., Pabon, L., Reinecke, H., Moon, R.T., and Murry, C.E. (2007). Biphasic role for Wnt/beta-catenin signaling in cardiac specification in zebrafish and embryonic stem cells. Proc. Natl. Acad. Sci. *104*, 9685–9690.

Vara, D., Bicknell, K.A., Coxon, C.H., and Brooks, G. (2003). Inhibition of E2F abrogates the development of cardiac myocyte hypertrophy. J. Biol. Chem. *278*, 21388–21394.

Ventura, A., Young, A.G., Winslow, M.M., Lintault, L., Meissner, A., Erkeland, S.J., Newman, J., Bronson, R.T., Crowley, D., Stone, J.R., et al. (2008). Targeted deletion reveals essential and overlapping functions of the miR-17 through 92 family of miRNA clusters. Cell *132*, 875–886.

Verzi, M.P., McCulley, D.J., De Val, S., Dodou, E., and Black, B.L. (2005). The right ventricle, outflow tract, and ventricular septum comprise a restricted expression domain within the secondary/anterior heart field. Dev. Biol. *287*, 134–145.

Vidyasekar, P., Shyamsunder, P., Santhakumar, R., Arun, R., and Verma, R.S. (2015). A simplified protocol for the isolation and culture of cardiomyocytes and progenitor cells from neonatal mouse ventricles. Eur. J. Cell Biol. *94*, 444–452.

Vincent, S.D., Mayeuf-Louchart, A., Watanabe, Y., Brzezinski, J.A., Miyagawa-Tomita, S., Kelly, R.G., and Buckingham, M. (2014). Prdm1 functions in the mesoderm of the second heart field, where it interacts genetically with Tbx1, during outflow tract morphogenesis in the mouse embryo. Hum. Mol. Genet. *23*, 5087–5101.

Vincentz, J.W., Barnes, R.M., and Firulli, A.B. (2011). Hand factors as regulators of cardiac morphogenesis and implications for congenital heart defects. Birth Defects Res. Part A - Clin. Mol. Teratol. *91*, 485–494.

Van Vliet, P., Wu, S.M., Zaffran, S., and Pucéat, M. (2012). Early cardiac development: A view from stem cells to embryos. Cardiovasc. Res. *96*, 352–362.

W., R., B., B., L., G., J., A., A., F., Z., G., T., N., R., S., D., Y., and J., X. (2010). Identification of a new microRNA expression profile as a potential cancer screening tool. Clin. Investig. Med. *33*, E124–E132.

Waldo, K.L., Kumiski, D.H., Wallis, K.T., Stadt, H.A., Platt, D.H., and Kirby, M.L. (2001). Conotruncal myocardium arises from a secondary heart field. Development *128*, 3179–3188.

Walker, L.A., and Buttrick, P.M. (2009). The right ventricle: biologic insights and response to disease. Curr. Cardiol. Rev. *5*, 22–28.

Wamstad, J.A., Alexander, J.M., Truty, R.M., Shrikumar, A., Li, F., Eilertson, K.E., Ding, H., Wylie, J.N., Pico, A.R., Capra, J.A., et al. (2012). Dynamic and Coordinated Epigenetic Regulation of Developmental Transitions in the Cardiac Lineage. Cell *151*, 206–220.

Wang, Y., and Qin, H. (2018). miR-338-3p targets RAB23 and suppresses tumorigenicity of prostate cancer cells. Am. J. Cancer Res. *8*, 2564–2574.

Wang, D., Zhang, Z., O'Loughlin, E., Wang, L., Fan, X., Lai, E.C., and Yi, R. (2013). MicroRNA-205 controls neonatal expansion of skin stem cells by modulating the PI(3)K pathway. Nat. Cell Biol. *15*, 1153–1163.

Wang, D.Z., Chang, P.S., Wang, Z., Sutherland, L., Richardson, J.A., Small, E., Krieg, P.A., and Olson, E.N. (2001). Activation of cardiac gene expression by myocardin, a transcriptional cofactor for serum response factor. Cell *105*, 851–862.

Wang, H., Peng, R., Wang, J., Qin, Z., and Xue, L. (2018a). Circulating microRNAs as potential cancer biomarkers: the advantage and disadvantage. Clin. Epigenetics *10*, 59.

Wang, J., Greene, S.B., Bonilla-Claudio, M., Tao, Y., Zhang, J., Bai, Y., Huang, Z., Black, B.L., Wang, F., and Martin, J.F. (2010). Bmp Signaling Regulates Myocardial Differentiation from Cardiac Progenitors Through a MicroRNA-Mediated Mechanism. Dev. Cell *19*, 903–912.

Wang, J., Cao, J., Dickson, A.L., and Poss, K.D. (2015). Epicardial regeneration is guided by cardiac outflow tract and Hedgehog signalling. Nature *522*, 226–230.

Wang, J., Liu, S., Heallen, T., and Martin, J.F. (2018b). The Hippo pathway in the heart: pivotal roles in development, disease, and regeneration. Nat. Rev. Cardiol. *15*, 672–684.

Wang, Z., Wang, D.-Z., Pipes, G.C.T., and Olson, E.N. (2003). Myocardin is a master regulator of smooth muscle gene expression. Proc. Natl. Acad. Sci. *100*, 7129–7134.

Wang, Z., Gerstein, M., and Snyder, M. (2009). RNA-Seq: a revolutionary tool for transcriptomics. Nat. Rev. Genet. *10*, 57–63.

Watanabe, Y., Miyagawa-Tomita, S., Vincent, S.D., Kelly, R.G., Moon, A.M., and Buckingham, M.E. (2010). Role of mesodermal FGF8 and FGF10 overlaps in the development of the arterial pole of the heart and pharyngeal arch arteries. Circ. Res. *106*, 495–503.

Watanabe, Y., Zaffran, S., Kuroiwa, A., Higuchi, H., Ogura, T., Harvey, R.P., Kelly, R.G., and Buckingham, M. (2012). Fibroblast growth factor 10 gene regulation in the second heart field by Tbx1, Nkx2-5, and Islet1 reveals a genetic switch for down-regulation in the myocardium. Proc. Natl. Acad. Sci. *109*, 18273–18280.

Weiss, A., and Leinwand, L.A. (1996). The mammalian myosin heavy chain gene family. Annu. Rev. Cell Dev. Biol. *12*, 417–439.

Wienholds, E., Koudijs, M.J., van Eeden, F.J.M., Cuppen, E., and Plasterk, R.H.A. (2003). The microRNA-producing enzyme Dicer1 is essential for zebrafish development. Nat. Genet. *35*, 217–218.

Williams, S.D., Zhu, H., Zhang, L., Bernstein, H.S., Eulalio, A., Mano, M., Ferro, M.D., Zentilin, L., Sinagra, G., Zacchigna, S., et al. (2012). Epigenetic regulation of neonatal cardiomyocytes differentiation. Circ. Res. *13*, 670–679.

Wittig, J., and Münsterberg, A. (2016). The Early Stages of Heart Development: Insights from Chicken Embryos. J. Cardiovasc. Dev. Dis. *3*, 12.

Woo, R.A., and Poon, R.Y.C. (2003a). Cyclin-Dependent Kinases and S Phase Control in Mammalian Cells. *2*, 316–324.

Woo, R.A., and Poon, R.Y.C. (2003b). Cyclin-dependent kinases and S phase control in mammalian cells. Cell Cycle *2*, 316–324.

Wu, L., Timmers, C., Maiti, B., Saavedra, H.I., Sang, L., Chong, G.T., Nuckolls, F., Giangrande, P., Wright, F.A., Field, S.J., et al. (2001). The E2F1-3 transcription factors are essential for cellular proliferation. Nature *414*, 457–462.

Xiang, F.L., Guo, M., and Yutzey, K.E. (2016). Overexpression of Tbx20 in adult cardiomyocytes promotes proliferation and improves cardiac function after myocardial infarction. Circulation *133*, 1081–1092.

Xiao, Y., Hill, M.C., Zhang, M., Martin, T.J., Morikawa, Y., Wang, S., Moise, A.R., Wythe, J.D., and Martin, J.F. (2018). Hippo Signaling Plays an Essential Role in Cell State Transitions during Cardiac Fibroblast Development. Dev. Cell *45*, 153-169.e6.

Xin, M., Small, E.M., Sutherland, L.B., Qi, X., McAnally, J., Plato, C.F., Richardson, J.A., Bassel-Duby, R., and Olson, E.N. (2009). MicroRNAs miR-143 and miR-145 modulate cytoskeletal dynamics and responsiveness of smooth muscle cells to injury. Genes Dev. *23*, 2166–2178.

Xin, M., Kim, Y., Sutherland, L.B., Qi, X., McAnally, J., Schwartz, R.J., Richardson, J.A., Bassel-Duby, R., and Olson, E.N. (2011). Regulation of insulin-like growth factor signaling by Yap governs cardiomyocyte proliferation and embryonic heart size. Sci. Signal. *4*, ra70.

Xin, M., Kim, Y., Sutherland, L.B., Murakami, M., Qi, X., McAnally, J., Porrello, E.R., Mahmoud, A.I., Tan, W., Shelton, J.M., et al. (2013). Hippo pathway effector Yap promotes cardiac regeneration. Proc. Natl. Acad. Sci. *110*, 13839–13844.

Xu, Y., Brenn, T., Brown, E.R.S., Doherty, V., and Melton, D.W. (2012). Differential expression of microRNAs during melanoma progression: miR-200c, miR-205 and miR-211 are downregulated in melanoma and act as tumour suppressors. Br. J. Cancer *106*, 553–561.

Yamamoto, S., Yang, G., Zablocki, D., Liu, J., Hong, C., Kim, S.-J., Soler, S., Odashima, M., Thaisz, J., Yehia, G., et al. (2003). Activation of Mst1 causes dilated cardiomyopathy by stimulating apoptosis without compensatory ventricular myocyte hypertrophy. J. Clin. Invest. *111*, 1463–1474.

Yang, Y., Del Re, D.P., Nakano, N., Sciarretta, S., Zhai, P., Park, J., Sayed, D., Shirakabe, A., Matsushima, S., Park, Y., et al. (2015). miR-206 Mediates YAP-Induced Cardiac Hypertrophy and Survival. Circ. Res. *117*, 891–904.

Yang, Y., Wang, H., Ma, Z., Hu, W., and Sun, D. (2018). Understanding the role of mammalian sterile 20-like kinase 1 (MST1) in cardiovascular disorders. J. Mol. Cell. Cardiol. *114*, 141–149.

Yang, Z., Wu, L., Zhu, X., Xu, J., Jin, R., Li, G., and Wu, F. (2013). MiR-29a modulates the angiogenic properties of human endothelial cells. Biochem. Biophys. Res. Commun. *434*, 143–149.

Yarden, Y., and Sliwkowski, M.X. (2001). Untangling the ErbB signalling network. Nat. Rev. Mol. Cell Biol. *2*, 127–137.

Yi, R., Qin, Y., Macara, I.G., and Cullen, B.R. (2003). Exportin-5 mediates the nuclear export of pre-microRNAs and short hairpin RNAs. Genes Dev. *17*, 3011–3016.

Yong-Ming, H., Ai-Jun, J., Xiao-Yue, X., Jian-Wei, L., Chen, Y., and Ye, C. (2017). miR-449a: a potential therapeutic agent for cancer. Anticancer. Drugs *28*, 1067–1078.

Yoshizumi, M., Lee, W.S., Hsieh, C.M., Tsai, J.C., Li, J., Perrella, M.A., Patterson, C., Endege, W.O., Schlegel, R., and Lee, M.E. (1995). Disappearance of cyclin A correlates with permanent withdrawal of cardiomyocytes from the cell cycle in human and rat hearts. J. Clin. Invest. *95*, 2275–2280.

Yuan, X., and Braun, T. (2017). Multimodal Regulation of Cardiac Myocyte Proliferation. Circ. Res. *121*, 293–309.

Zaffran, S., and Frasch, M. (2002). Early signals in cardiac development. Circ. Res. *91*, 457–469.

Zaffran, S., and Kelly, R.G. (2012). New developments in the second heart field. Differentiation *84*, 17–24.

Zaffran, S., Kelly, R.G., Meilhac, S.M., Buckingham, M.E., and Brown, N.A. (2004). Right ventricular myocardium derives from the anterior heart field. Circ. Res. *95*, 261–268.

Zhai, F., Cao, C., Zhang, L., and Zhang, J. (2017). miR-543 promotes colorectal cancer proliferation and metastasis by targeting *KLF4*. Oncotarget *8*, 59246–59256.

Zhang, G., Hou, X., Li, Y., and Zhao, M. (2014). MiR-205 inhibits cell apoptosis by targeting phosphatase and tensin homolog deleted on chromosome ten in endometrial cancer ishikawa cells. BMC Cancer *14*, 440.

Zhang, W., Chen, H., Wang, Y., Yong, W., Zhu, W., Liu, Y., Wagner, G.R., Payne, R.M., Field, L.J., Xin, H., et al. (2011). Tbx20 transcription factor is a downstream mediator for bone morphogenetic protein-10 in regulating cardiac ventricular wall development and function. J. Biol. Chem. *286*, 36820–36829.

Zhang, Y., Matsushita, N., Eigler, T., and Marbán, E. (2013). Targeted MicroRNA Interference Promotes Postnatal Cardiac Cell Cycle Re-Entry. J. Regen. Med. *2*, 2.

Zhao, B., Li, L., Lei, Q., and Guan, K. (2010a). The Hippo – YAP pathway in organ size control and tumorigenesis : an updated version. 862–874.

Zhao, B., Li, L., Tumaneng, K., Wang, C.-Y., and Guan, K.-L. (2010b). A coordinated phosphorylation by Lats and CK1 regulates YAP stability through SCF(beta-TRCP). Genes Dev. *24*, 72–85.

Zhao, Y., Samal, E., and Srivastava, D. (2005). Serum response factor regulates a muscle-specific microRNA that targets Hand2 during cardiogenesis. Nature *436*, 214–220.

Zhao, Y., Ransom, J.F., Li, A., Vedantham, V., von Drehle, M., Muth, A.N., Tsuchihashi, T., McManus, M.T., Schwartz, R.J., and Srivastava, D. (2007). Dysregulation of Cardiogenesis, Cardiac Conduction, and Cell Cycle in Mice Lacking miRNA-1-2. Cell *129*, 303–317.

Zhou, B., Ma, Q., Rajagopal, S., Wu, S.M., Domian, I., Rivera-Feliciano, J., Jiang, D., Von Gise, A., Ikeda, S., Chien, K.R., et al. (2008). Epicardial progenitors contribute to the cardiomyocyte lineage in the developing heart. Nature *454*, 109–113.

Zhou, Y., Kim, J., Yuan, X., and Braun, T. (2011). Epigenetic modifications of stem cells: A paradigm for the control of cardiac progenitor cells. Circ. Res. *109*, 1067–1081.

Curriculum Vitae

Mr. Jonathan James Weldrick
Correspondence language: English

Degrees

2013/9 - present: **PhD, Cellular and Molecular Medicine, University of Ottawa**
Transferred to PhD from Masters
Area of Research: Neonatal heart development
Research Disciplines: Genetics, Molecular Biology, Biochemistry
Supervisors: Dr. Lynn Megeney, 2018/6 - present; Dr. Patrick Burgon, 2013/9 - present
2013/6**: Honours Specialization, Medical Science, University of Western Ontario**

Recognitions

2018/4: **ASBMB Experimental Biology 2018 Travel Award** - $1,000 (USD)
2017/9 - 2018/8: **Queen Elizabeth II Graduate Scholarship in Science and Technology** - $15,000 (CAD)
2017/9 - 2018/8: **University of Ottawa Excellence Scholarship** - $10,000 (CAD)
2016/9: **Dr. Grant Pierce Young Investigator Award Best Oral Presentation** - $1,000 (CAD) - International Academy of Cardiovascular Science North American Section
2016/5: **Servier Award for the Best Basic Science Oral Presentation** - $500 (CAD)
2015/7 - 2017/6: **University of Ottawa Cardiac Endowment Fund at the Heart Institute ($40,000)**
2015/1: 2017/8 - **Doctorate Admission Scholarship** - $18,000 (CAD)
2013/9: 2014/12 - **Master's Admission Scholarship** - $10,000 (CAD)
2010/5: 2013/5 - **Graduation with Honours**
2009/9: 2010/5 - **The Western Scholarship of Distinction** - $1,500 (CAD)
2009/9: 2013/5 - **Queen Elizabeth II Aiming for the Top Scholarship** - $14,000 (CAD)

Research Funding History

2017/9 - 2018/8: **Queen Elizabeth II Graduate Scholarship in Science and Technology**

- Competitive application for $15,000 CAD over one year

2015/7 - 2017/6: **University of Ottawa Cardiac Endowment Fund at the Heart Institute**

- Competitive application for $40,000 CAD over two years

Publications

Peer-reviewed Journal Articles

1. Cattin, M.-E., Deeke, S.A., Dick, S.A., Verret-Borsos, Z.J.A., Tennakoon, G., Gupta, R., Mak, E., Roeske, C.L., **Weldrick, J.J.**, Megeney, L.A., and Burgon, P.G. (2018). Expression of murine muscle-enriched A-type lamin-interacting protein (MLIP) is regulated by tissue-specific alternative transcription start sites. *Journal of Biological Chemistry*. 293, 19761–19770.

2. Lee, H.W., Ahmad, M., **Weldrick, J.J.**, Wang, H.-W., Burgon, P.G., and Leenen, F.H.H. (2018). Effects of exercise training and TrkB blockade on cardiac function and BDNF-TrkB signaling post-myocardial infarction in rats. *American Journal of Physiology - Heart and Circulatory Physiology*. 315, H1821–H1834.

3. **Weldrick, J.J.**, Abdul-Ghani, M., Megeney, L.A., and Burgon, P.G. (2018). A rapid and efficient method for the isolation of postnatal murine cardiac myocyte and fibroblast cells. *Canadian Journal of Physiology and Pharmacology*. 96, 535–539.

4. Abdul-Ghani, M., Suen, C., Jiang, B., Deng, Y., **Weldrick, J.J.**, Putinski, C., Brunette, S., Fernando, P., Lee, T.T., Flynn, P., Leenen, F.H.H., Burgon, P.G., Stewart, D.J., and Megeney, L.A. (2017). Cardiotrophin 1 stimulates beneficial myogenic and vascular remodeling of the heart. *Nature: Cell Research*. 27, 1195–1215.

5. Cattin, M.E., Wang, J., **Weldrick, J.J.**, Roeske, C.L., Mak, E., Thorn, S.L., DaSilva, J.N., Wang, Y., Lusis, A.J., and Burgon, P.G. (2015). Deletion of MLIP (Muscle-enriched A-type Lamin-interacting Protein) leads to cardiac hyperactivation of akt/mammalian target of rapamycin (MTOR) and impaired cardiac adaptation. *Journal of Biological Chemistry*. 290, 26699–26714.

Conference Publications

1. (2018). Micro-RNA-205 Regulates Heart Size Through Direct Modulation of the Hippo Pathway. Experimental Biology 2018, San Diego, United States
   - **Travel award from The American Society for Biochemistry and Molecular Biology.**

2. (2017). Identification & Characterization of a Transitional Program That Controls Cell Cycle Arrest in the Developing Heart. University of Ottawa Heart Institute Research Day 2016, Ottawa, Canada

3. (2016). Identification and characterization of a miRNA cohort initiated transitional program that controls cell cycle arrest of the perinatal heart. Annual Meeting of the

North American Section of the International Academy of Cardiovascular Sciences, Sherbrooke, Canada

- **Grant Pierce Young Investigator Award for best oral presentation by a graduate student.**

4. (2016). Identification and characterization of a miRNA cohort initiated transitional program that controls cell cycle arrest of the perinatal heart. University of Ottawa Heart Institute 29th Research Day, Ottawa, Canada

- **Servier Award for Best Oral Presentation**

5. Identification and Characterization of a miRNA Cohort Initiated Transitional Program That Controls Cell Cycle Arrest of the Perinatal Heart. Jonathan J Weldrick, Patrick G. Burgon. Basic Cardiovascular Sciences Scientific Sessions. BCVS. 2015

6. (2015). Identification & Characterization of a Transitional Program That Controls Cell Cycle Arrest in the Developing Heart. University of Ottawa Heart Institute Research Day 2015, Ottawa, Canada

7. (2014). Elucidating the Role of an Uncharacterized Amniotic Gene. University of Ottawa Heart Institute 27th Annual Research Day, Ottawa, Canada

Event Administration

2017/3 Session Chair, 5th International Ottawa Heart Conference: Inflammation in Cardiometabolic Disease, Ottawa, ON

Committee and Volunteer Activities

2016/10 - 2018/1 Committee Member, Cellular and Molecular Medicine Graduate Student Council

- Heart Institute Rep as well as Advances in Biomedical Research Seminar Series Rep

2016/10 - 2018/1 - Committee Member, Advances in Biomedical Research Seminar Series
2011/9 - 2012/12 - Volunteer, Alzheimer's Society of London and Middlesex
2011/9 - 2012/12 - Volunteer Tutor, London Urban Services Organization